



Karmel Beringui de Oliveira da Silva

Air quality monitoring in the state of Rio de Janeiro, Brazil, through pollution and ecotoxicological biomonitoring assessments

Tese de Doutorado

Thesis presented to the Programa de Pós-graduação em Química of PUC-Rio in partial fulfillment of the requirements for the degree of Doutor em Química.

Advisor: Prof^a. Adriana Gioda

Coadvisor: Dr^a. Rachel Ann Hauser-Davis

Rio de Janeiro

April 2022



Karmel Beringui de Oliveira da Silva

Air quality monitoring in the state of Rio de Janeiro, Brazil, through pollution and ecotoxicological biomonitoring assessments

Thesis presented to the Programa de Pós-graduação em Química of PUC-Rio in partial fulfillment of the requirements for the degree of Doutor em Química. Approved by the Examination Committee:

Prof.^a Adriana Gioda

Advisor

Departamento de Química - PUC-Rio

Dr.^a Rachel Ann Hauser-Davis

Coadvisor

Fiocruz

Prof. Wilson Thadeu Valle Machado

UFF

Prof.^a Maria de Fátima Andrade

USP

Prof. Ricardo Henrique Moreton Godoi

UFPR

Prof. José Marcus de Oliveira Godoy

Departamento de Química - PUC-Rio

Dr. Alex Ruben Huaman De La Cruz

Pesquisador Autônomo

Rio de Janeiro, April 20th, 2022

All rights reserved. The total or partial reproduction of the work without authorization from the university, the author and the supervisor is prohibited.

Karmel Beringui de Oliveira da Silva

Holds a Chemistry degree from the Rural Federal University of Rio de Janeiro (2017) and M.Sc. Degree in Chemistry from the Pontifical Catholic University of Rio de Janeiro (2019).

Bibliographic data

Silva, Karmel Beringui de Oliveira da

Air quality monitoring in the state of Rio de Janeiro, Brazil, through pollution and ecotoxicological biomonitoring assessments / Karmel Beringui de Oliveira da Silva ; advisor: Adriana Gioda ; coadvisor: Rachel Ann Hauser-Davis. – 2022.

255 f. : il. color. ; 30 cm

Tese (doutorado)–Pontifícia Universidade Católica do Rio de Janeiro, Departamento de Química, 2022.

Inclui bibliografia

1. Química – Teses. 2. Biomonitoramento. 3. Ecotoxicologia. 4. Qualidade do ar. 5. Tillandsia. I. Gioda, Adriana. II. Hauser-Davis, Rachel Ann. III. Pontifícia Universidade Católica do Rio de Janeiro. Departamento de Química. IV. Título.

CDD: 540

Acknowledgements

To God for the gift of life, for enabling me to face the challenges, and for protection at all times.

To my parents, Neusa and Reinaldo, for the incentive to reach higher achievements. To my sister, Kamila, for her unconditional support. To my boyfriend, Erick, for encouraging me to continue in graduate school and listening to my complaints. To everyone for their eventual participation in the plant sampling.

To Prof^a. Adriana Gioda for the opportunity to join the Laboratory of Atmospheric Chemistry (from portuguese, *Laboratório de Química Atmosférica* – LQA).

To Dr^a. Rachel Ann Hauser-Davis for making me part of the Hauser-Davis Research Group and helping me plan and execute the project in an area other than my domain.

To Prof^a. Tatiana Dillenburg Saint Pierre and Prof. José Marcus de Oliveira Godoy for the collaboration allowing the use of the infrastructure of their laboratories.

To Elizanne Porto de Sousa Justo for her partnership in the daily life at LQA, in managing LQA's Instagram, for collaborating on various papers, and for conversations about the challenges of the PhD.

To the scientific initiation students, Maria Vitória Rocha and Felipe Melo Dias, who collaborated in the biomonitoring execution.

To Rafael Christian Chávez Rocha and Rodrigo Araújo Gonçalves for their help with the chemical analyses.

To INEA for the collaboration by providing air pollution data and help in plant sampling. And to SMAC for providing meteorological and air pollution data.

To Apple and Google for making urban mobility data available

To PUC-Rio and Fiocruz for the physical structure that made the experiments possible.

To CNPq for the PhD scholarship that made it possible for me to dedicate myself exclusively to this project.

To FAPERJ for funding the projects that financed the experiments.

This study was financed in part by the Coordenação de Aperfeiçoamento de Pessoal de Nível Superior - Brasil (CAPES) - Finance Code 001

Abstract

Silva, Karmel Beringui de Oliveira; Gioda, Adriana (Advisor); Hauser-Davis Rachel Ann (Coadvisor); **Air quality monitoring in the state of Rio de Janeiro, Brazil, through pollution and ecotoxicological biomonitoring assessments.** Rio de Janeiro, 2022. 255 p. Tese de Doutorado – Departamento de Química, Pontifícia Universidade Católica do Rio de Janeiro.

The intense growth of urban centers has caused a considerable increase in atmospheric pollutant emission, which can lead to human health and ecosystem risks. The air quality monitoring network in Brazil is limited, covering not even half of the states. Biomonitoring employing plants is, thus, an alternative to increase the monitored areas and still allow the ecotoxicological evaluations concerning air pollution exposure. In this sense, this study sought to evaluate the air quality of the metropolitan region of Rio de Janeiro using official atmospheric pollutant concentration data and biomonitoring efforts aiming to investigate oxidative stress in the bromeliad species used as biomonitors. During the social isolation period established as a contingency measure against the spread of the coronavirus, air quality was improved overall, although ozone concentrations increased relative to the previous year and the period preceding the lockdown. This change was attributed to an urban mobility reduction of up to 85%. The biomonitoring assessments indicate that the main elements taken up by the plants were those related to vehicular traffic. The correlation of these elements with oxidative stress biomarkers indicate that air pollution exposure represents a risk to local ecosystems. *Tillandsia stricta* and *Tillandsia usneoides* displayed similar behavior regarding metal accumulation, albeit presenting different detoxification processes. Although Rio de Janeiro has one of the most widespread air quality monitoring networks, studies aimed to assess the environmental air pollution impacts are required, considering that the state is home to important and endangered Atlantic Forest remnants. In additions, vehicular emission control can contribute to air pollution reduction, considering that this is one of the main pollutant sources.

Keywords

Biomonitoring, Ecotoxicology, Air quality, *Tillandsia*

Resumo

Silva, Karmel Beringui de Oliveira; Gioda, Adriana (Orientadora); Hauser-Davis Rachel Ann (Coorientadora); **Monitoramento da qualidade do ar no estado do Rio de Janeiro, Brasil, através da avaliação da poluição e do biomonitoramento ecotoxicológico**. Rio de Janeiro, 2022. 255 p. Tese de Doutorado – Departamento de Química, Pontifícia Universidade Católica do Rio de Janeiro.

O intenso crescimento dos centros urbanos provocou aumento considerável da emissão de poluentes atmosféricos, conferindo destaque à poluição atmosférica. A qualidade do ar de uma determinada região pode ser afetada por fatores como tipos e quantidades de fontes de emissão, meteorologia e topografia, o que confere complexidade para essa área de estudo. Os principais poluentes legislados no Brasil são SO₂, NO₂, CO, O₃ e o material particulado (MP). Dentre esses, o MP pode ser considerado como uma das mais importantes classes de poluentes devido sua composição heterogênea, que pode causar efeitos adversos à saúde e ao meio ambiente.

O monitoramento dos poluentes atmosféricos para fins de fiscalização pode ser realizado utilizando métodos padronizados que incluem equipamentos capazes de determinar a concentração dos poluentes em tempo real. No Rio de Janeiro, as principais redes de monitoramento da qualidade do ar pertencem ao Instituto Estadual do Meio Ambiente (INEA) e à prefeitura do Rio de Janeiro, que dispõem de estações automáticas em diversas regiões da cidade e do estado. Entretanto, o monitoramento tradicional da poluição atmosférica demanda altos investimentos para compra e manutenção desses equipamentos, diminuindo as áreas passíveis de monitoramento. O biomonitoramento, por sua vez, que utiliza organismos vivos para avaliar mudanças ambientais, é considerado uma abordagem adequada para ampliar as áreas monitoradas e avaliar os impactos causados pela poluição.

Assim, o objetivo deste estudo foi avaliar a qualidade do ar no Rio de Janeiro através do biomonitoramento ativo utilizando *Tillandsia usneoides* e *Tillandsia stricta* como biomonitores, investigando o estresse oxidativo causado pela exposição aos metais. Considerando o efeito das fontes de emissão na qualidade do ar, buscou-se também avaliar a qualidade do ar no Rio de Janeiro durante os primeiros meses da

pandemia de COVID-19, quando a mobilidade urbana foi alterada consideravelmente. Nessa avaliação foi considerada ainda a influência das condições meteorológicas por meio da comparação com dados obtidos para os mesmos períodos do ano anterior.

O biomonitoramento ativo foi realizado entre julho de 2019 e novembro de 2020 em cinco locais do Rio de Janeiro com diferentes características quanto a emissão de poluentes: Ramos, Urca, Niterói, Duque de Caxias e Santa Cruz. As plantas foram removidas de um local rural e instaladas nos locais de monitoramento em julho de 2019 e coletadas em outubro de 2019, janeiro e novembro de 2020. A avaliação do estresse oxidativo foi realizada através da quantificação dos biomarcadores Metalotioneína (MT), Glutathione Reduzida (GSH), H_2O_2 e Peroxidação Lipídica, medida pela concentração de malondialdeído (MDA). Para avaliar a fração biodisponível dos metais presente no tecido das plantas foi realizada distribuição subcelular através do procedimento de purificação da metalotioneína, que fornece três frações nas quais os elementos foram quantificados por espectrometria de massas com plasma indutivamente acoplado (ICP-MS), bem como a quantificação dos metais totais realizada em extratos ácidos dos tecidos das plantas.

Na avaliação da qualidade do ar durante a pandemia, os dados de concentração de NO_2 , SO_2 , CO e O_3 e variáveis meteorológicas foram fornecidos pelo INEA para março e abril de 2020 e usados para avaliar mudanças na qualidade do ar em comparação com o ano anterior e a contribuição das condições meteorológicas. A prefeitura do Rio de Janeiro forneceu dados de CO, O_3 e PM_{10} e variáveis meteorológicas para o período entre março e setembro que foram usados para uma avaliação que considerou o impacto das medidas de distanciamento social na qualidade do ar através do acompanhamento desde o primeiro decreto de restrição até a abertura econômica total. Nos dois casos, os dados foram submetidos a testes estatísticos e análises temporais.

O biomonitoramento da qualidade do ar indicou que os principais elementos encontrados nos biomonitores foram Fe, Na, K, Ca, Mg and Al. Elementos relacionados ao tráfego veicular, como Pb, Cr, Cu and V também foram encontrados em concentrações expressivas. A *T. usneoides* apresentou maiores concentrações em comparação com a *T. stricta*, entretanto, o enriquecimento das duas espécies em relação

à amostra de referência foi similar, indicando que ambas são adequadas para o biomonitoramento. Duque de Caxias e Santa Cruz apresentaram os maiores enriquecimentos, o que pode estar relacionado com a contribuição das emissões industriais.

A avaliação da distribuição subcelular dos metais demonstrou que Cr, Co, Cu, Cd, Mn, Ni, Se and Zn foram encontrados na fração termoestável da purificação da metalotioneína, o que indica que as plantas estão em processo de destoxificação desses elementos. A *T. stricta* apresentou maiores percentuais da fração não biodisponível, o que indica que essa espécie é mais resistente aos efeitos tóxicos causados pelos metais. Foi observado ainda que em períodos secos a absorção das plantas é menor, devido ao metabolismo ácido das crassuláceas (CAM), que favorece o controle hídrico em condições de baixa umidade mantendo as organelas responsáveis pelas trocas gasosas fechadas durante o dia, período no qual se registram maiores concentrações de poluentes.

Os biomarcadores de estresse oxidativo indicaram que as duas espécies estão em condições semelhantes de estresse oxidativo, pois suas concentrações não apresentaram diferença significativa entre as espécies na maioria dos casos. As correlações entre os biomarcadores indicaram que a principal função da GSH é no sistema antioxidante, embora em alguns caso ela tenha atuado auxiliando a MT na destoxificação de metais. As correlações de H₂O₂ com MT e GSH indicam que a exposição de metais estimula a produção de espécies reativas de oxigênio (ROS), como H₂O₂, cuja concentração pode ser regulada pela ação da GSH, entretanto, a correlação com MDA indica que o sistema antioxidante não está sendo eficiente na prevenção do estresse oxidativo.

A avaliação da qualidade do ar durante a pandemia revelou que a redução de até 85 % na mobilidade urbana foi a principal responsável pela melhora da qualidade do ar, principalmente nos primeiros meses de isolamento social. Foi registrada diminuição na concentração dos poluentes primários e aumento da concentração de O₃, um poluente secundário. Esse mesmo comportamento também foi registrado em outras cidades ao redor do mundo e é atribuído aos complexos processos de formação de ozônio, que dependem da concentração de alguns poluentes primários. Embora as

concentrações de ozônio tenham aumentando, o índice de qualidade do ar durante a pandemia foi melhor do que em períodos com a rotina normal das cidades. A contribuição das condições meteorológicas não apresentou muita influência, uma vez que se mostrou semelhante ao mesmo período do ano anterior.

A avaliação da qualidade do ar no Rio de Janeiro revelou que as emissões veiculares são as principais fontes de poluentes atmosféricos, e que a mudança no fluxo de veículos pode melhorar a qualidade do ar, embora empreendimentos industriais também apresentem expressiva contribuição. A poluição urbana pode causar desequilíbrio ambiental, uma vez que a vegetação está em constante exposição. Pode-se destacar ainda que o estado do Rio de Janeiro abriga importantes remanescentes de mata atlântica, o que demanda constante fiscalização visando a garantia da preservação ambiental.

Palavras Chave

Biomonitoramento; Ecotoxicologia, Qualidade do Ar; *Tillandsia*

Table of Contents

1	Introduction	27
1.1.	Particulate matter	27
1.2.	Gaseous Pollutants	28
1.3.	Atmospheric Biomonitoring	28
1.4.	Oxidative Stress	30
1.5.	Oxidative stress biomarkers	31
1.6.	Rio de Janeiro Metropolitan Region	32
1.7.	Research hypothesis and layout of this thesis	33
2	Objectives	35
2.1.	General objectives	35
2.2.	Specific Objectives	35
3	Material and Methods	36
3.1.	Literature review of particulate matter sampled in Rio de Janeiro	36
3.1.1.	Search for papers	36
3.1.2.	Data arrangement	37
3.2.	Effect of partial lockdown on air quality in the city of Rio de Janeiro	38
3.2.1.	Study Area	38
3.2.2.	Air Quality and Meteorological data	39
3.2.3.	Mobility data	43
3.2.4.	Data analysis	43
3.3.	Air quality assessment in first weeks of COVID-19 pandemic	44
3.3.1.	Study area	44
3.3.2.	Air quality data	44
3.3.3.	Meteorological data	46
3.3.4.	Statistical analyses	47
3.3.5.	Air Quality Index (AQI)	47

3.3.6. Hybrid Single-Particle Lagrangian Integrated Trajectory	49
3.4. Active atmospheric biomonitoring	49
3.4.1. Study area	49
3.5. Metal quantification	52
3.6. Subcellular distribution of metals in atmospheric biomonitors	52
3.6.1. Metallothionein purification and determination	53
3.6.2. Subcellular metal quantification	53
3.7. Oxidative stress biomarkers in atmospheric biomonitors	54
3.7.1. Reduced glutathione purification and quantification	54
3.7.2. Hydrogen peroxide purification and quantification	54
3.7.3. Lipid peroxidation quantification	55
3.8. Association between oxidative stress biomarkers and metals	55
3.9. Data analysis of metal and ecotoxicological data	56
4 Assessment of concentration and inorganic composition of particulate matter sampled in Rio de Janeiro state	58
Abstract	58
4.1. Introduction	59
4.2. International air quality standards	64
4.3. Brazilian legislation	65
4.4. Sampling of particulate matter	68
4.4.1. Sample Sites	68
4.4.2. PM sampling	68
4.5. Particulate matter concentration	69
4.5.1. Results of the first diagnosis of the air quality monitoring network in Brazil	69
4.5.2. Influence of the 2016 Olympic Games on PM concentration	70
4.5.3. Results of air quality studies conducted in the state of Rio de Janeiro	72
4.6. Influence of meteorological parameters on the concentration of particulate matter	77
4.7. Particulate matter chemical characterization	79

4.7.1. Ionic characterization	80
4.7.2. Elementary characterization	80
4.7.3. Quality Control	81
4.8. Interpretation of the PM chemical composition data	83
4.8.1. Enrichment Factor	83
4.8.2. Marine contribution to the PM composition	84
4.9. Particulate matter acidity	85
4.10. Elemental composition of particulate matter	86
4.10.1. Average concentration of elements in PM	86
4.10.2. Enrichment Factor of the PM collected in Rio de Janeiro	92
4.11. Ionic composition of particulate matter	93
4.11.2. Evaluation of the marine contribution in the PM composition	94
4.11.3. Assessment of the acidity of particulate matter	96
4.12. Conclusion	96
5 Assessment of air quality changes during COVID-19 partial lockdown in a Brazilian metropolis: from lockdown to economic opening of Rio de Janeiro, Brazil	99
5.1. Introduction	100
5.2. Material and Methods	102
5.3. Results	102
5.3.1. Mobility profile	102
5.3.2. Pollutant concentration distribution	103
5.3.3. Air pollutant time variation	107
5.3.4. Carbon Monoxide monthly concentration	113
5.3.5. Ozone monthly concentration	114
5.3.6. Particulate matter monthly concentration	115
5.3.7. CO, O ₃ and PM ₁₀ diurnal and weekly cycle	116
5.3.8. Time average with satellite data	118
5.4. Conclusions	119

6	Time Variation of atmospheric pollutants in first weeks of COVID-19 lockdown in a Brazilian metropolis	122
6.1.	Introduction	123
6.2.	Material and Methods	123
6.3.	Results	124
6.3.1.	Weekly overview	124
6.3.2.	Hourly overview	126
6.3.3.	Conclusion	128
7	Effects of the first weeks of the COVID-19 partial lockdown on air quality in Rio de Janeiro, Brazil	129
7.1.	Introduction	130
7.2.	Material and Methods	132
7.3.	Results	132
7.3.1.	Pollutant concentrations and Brazilian air quality standards	132
7.3.2.	Air Quality Index (AQI)	136
7.3.3.	Statistical analysis of meteorological parameters	137
7.3.4.	Correlation between pollutants and meteorological parameters	139
7.3.5.	Pollution roses	141
7.4.	Conclusions	148
8	Pollutant source assignment through atmospheric metal biomonitoring in a tropic urban center	150
8.1.	Introduction	151
8.2.	Materials and methods	152
8.3.	Results and discussion	152
8.3.1.	Elemental concentrations	152
8.3.2.	Exposure to reference ratio (ER)	156
8.3.3.	Enrichment Factor	160
8.3.4.	Source assignment by metal correlation	162
8.4.	Conclusion	164

9	Subcellular metal distribution and detoxification in atmospheric biomonitors in a Brazilian metropolis	166
9.1.	Introduction	167
9.2.	Material and Methods	169
9.3.	Results	169
9.3.1.	MT content in <i>Tillandsia usneoides</i> and <i>Tillandsia stricta</i>	169
9.3.2.	Metal and metalloid determinations	171
9.3.3.	Metal detoxification	177
9.3.4.	Potentially protective essential metal effects	180
9.4.	Conclusions	181
10	Oxidative stress investigation in atmospheric biomonitoring plants exposed in a large Brazilian metropolis	184
10.1.	Introduction	185
10.2.	Materials and Methods	186
10.3.	Results and discussion	186
10.3.1.	GSH content in <i>Tillandsia</i> species	186
10.3.2.	H ₂ O ₂ content in <i>Tillandsia</i> species	188
10.3.3.	MDA content in <i>Tillandsia</i> species	189
10.3.4.	Correlation between biomarkers	191
10.4.	Conclusion	195
11	Subcellular heat-stable metalloprotein assessments employing the bioanalytical SEC-HPLC-ICP-MS technique	197
11.1.	Introduction	197
11.2.	Material and Methods	198
11.3.	Results and discussion	199
11.4.	Conclusion	204
12	Conclusion	205
13	References	207

14	Appendix A – Published papers	233
15	Appendix B - Published papers in the scope of this thesis	234
16	Appendix E - Participation in Congress	236
17	Supplementary Material – 1	237
18	Supplementary Material – 2	241
19	Supplementary Material – 3	248

List of Figures

Figure 3.1 Map with the location of the sampling sites used in the studies with PM carried out in the state of Rio de Janeiro. Software QGIS, Data source: Brazilian Institute of Geography and Statistics - IBGE, Institute of Applied Economic Research - Ipea, IHO Sea Area.....	37
Figure 3.2 Rio de Janeiro city map with air quality monitoring stations highlighted. Black line indicates cities boundaries.	39
Figure 3.3 Timeline (2020) with main measures taken by Rio de Janeiro state government to control the spread of coronavirus and easing measures after cases number starts to decrease	42
Figure 3.4 Timeline (2020) with opening stages adopted by city hall of Rio de Janeiro city	43
Figure 3.5 Locations of air quality monitoring station and emission sources (industrial district and roads). Itaguaí (Monte Serrat station, MS), Duque de Caxias (São Luiz station, SL), and Rio de Janeiro (Manguinhos station (MG) and Santa Cruz, (Largo do Bodegão station, LB).	46
Figure 3.6 Atmospheric biomonitoring sampling site locations in the Metropolitan Region of Rio de Janeiro, southeastern Brazil.	50
Figure 3.7 (a) <i>Tillandsia usneoides</i> washed with ultrapure water and divided into 10 g samples; (b) <i>Tillandsia stricta</i> washed with ultrapure water and divided into individual weighing 15-20 g.	51
Figure 4.1 Average PM concentrations for stations near the 2016 Olympic and Paralympic Games sites (CA - Campo dos Afonsos, GE - Gericinó, LB - Leblon, MR - Maracanã, UR - Urca, LG - Lagoa, RB - Recreio dos Bandeirantes, EG - Engenho de Dentro and CP – Copacabana).....	71
Figure 4.2 Average concentration of PM found in the studies conducted in the state of Rio de Janeiro and the limit established by CONAMA in the resolutions of 1990 and 2018. *Corresponds to the concentration of PM _{2.5-10}	74
Figure 5.1 Difference between daily concentration in 2020 and the averaged concentration in 2019 of three pollutants for the same period (the black line is	

the mean of all stations and the blue lines are concentration at each station).
 104

Figure 5.2 Time variation of the concentrations of CO (ppm) at Bangu (BG),
 Campo Grande (CG), Centro (CT), Copacabana (CP), and Tijuca (TJ) stations
 in 2019 and 2020..... 108

Figure 5.3 Time variation of the concentrations of O₃ (µg m⁻³) at Bangu (BG),
 Campo Grande (CG), Centro (CT), Copacabana (CP), and Tijuca (TJ) stations
 in 2019 and 2020..... 109

Figure 5.4 Time variation of the concentrations of PM₁₀ (µg m⁻³) at Bangu (BG),
 Campo Grande (CG), Centro (CT), Copacabana (CP), and Tijuca (TJ) stations
 in 2019 and 2020..... 110

Figure 5.5 CO, O₃ and PM₁₀ data distribution for the period between March and
 September of 2019 and 2020 112

Figure 5.6 Time average map plotted with satellite data obtained by
 Giovanni/NASA for CO and aerosol from March to September, 2020. Source:
<https://giovanni.gsfc.nasa.gov> 119

Figure 6.1 Weekly concentrations for SO₂, NO, O₃ and CO between March 1st
 and April 12th 2019 and 2020 in all monitoring sites (LB – Largo do Bodegão,
 MG – Manguinhos, MS – Monte Serrat and SL – São Luiz). 124

Figure 6.2 Weekly concentrations for SO₂, NO, O₃ and CO between March 1st
 and April 12th 2020 splited according to lockdown decree. (LB – Largo do
 Bodegão, MG – Manguinhos, MS – Monte Serrat and SL – São Luiz). 125

Figure 6.3 Hourly concentrations for SO₂, NO, O₃ and CO between March 1st
 and April 12th 2019 and 2020 in all monitoring sites. (LB – Largo do Bodegão,
 MG – Manguinhos, MS – Monte Serrat and SL – São Luiz). 126

Figure 7.1 Boxplot with the distribution of the concentrations of SO₂, NO₂, and
 O₃ (µg m⁻³) and CO (ppm) for Largo do Bodegão (LB, Rio de Janeiro),
 Manguinhos (MG, Rio de Janeiro), São Luiz (SL, Duque de Caxias) and Monte
 Serrat (MS, Itaguaí) stations in the three periods: 1) March 1st to April 12nd,
 2019, 2) March 1st to 15th, 2020 classified as “before lockdown” and 3) March

16th to April 12nd, 2020 classified as “lockdown”. The boxes cover the 1st quartile to the 3rd quartile. The lines in the boxes represent the median values. 133

Figure 7.2 Pollution rose plot to show the relation between wind direction and pollutant concentrations at Largo do Bodegão monitoring station: (a) SO₂ and (b) NO₂. Before: March 1st to 15th, 2020 and during: March 16th to April 12nd, 2020. 142

Figure 7.3 Pollution roses plot to show the relation between wind direction and pollutant concentrations at Manguinhos monitoring station: (a) SO₂, (b) NO₂, (c) CO and (d) O₃. Before: March 1st to 15th, 2020 and during: March 16th to April 12nd, 2020..... 145

Figure 7.4 Pollution roses plot to show the relation between wind direction and pollutant concentrations at Monte Serrat monitoring station: (a) SO₂, (b) NO₂ and (c) O₃. Before: March 1st to 15th, 2020 and during: March 16th to April 12nd, 2020. 145

Figure 7.5 Pollution roses plot to show the relation between wind direction and pollutant concentrations at São Luiz monitoring station: (a) SO₂, (b) NO₂, (c) CO and (d) O₃. Before: March 1st to 15th, 2020 and during: March 16th to April 12nd, 2020..... 147

Figure 8.1 Boxplot of metals detected in *T. usneoides* and *T. stricta* sampled in October, 2019 at all monitoring sites. Differences between species exposed at the same site are indicated by * for p < 0.05, ** for p < 0.01 and *** for p < 0.001. 154

Figure 8.2 Boxplot of metals detected in *T. usneoides* and *T. stricta* sampled in January, 2020 at all monitoring sites. Differences between species exposed at the same site are indicated by * for p < 0.05, ** for p < 0.01 and *** for p < 0.001 155

Figure 8.3 Boxplot of metals detected in *T. usneoides* and *T. stricta* sampled in November, 2020 at all monitoring sites. Differences between species exposed at the same site are indicated by * for p < 0.05, ** for p < 0.01 and *** for p < 0.001 156

Figure 8.4 Spearman's correlations obtained between metals determined in <i>T. usneoides</i> from all sampling sites	163
Figure 8.5 Spearman's correlations obtained between metals determined in <i>T. stricta</i> from all sampling sites	164
Figure 9.1 <i>Tillandsia stricta</i> and <i>Tillandsia usneoides</i> metallothionein (MT) concentrations ($\mu\text{mol g}^{-1}$ f.w.) per sampling date (1: October 2019, 2: January 2020, and 3: November 2020). The horizontal lines within the box plots display the medians, the upper line indicates the 75 th quartile and the lower line, the 25 th quartile. The whiskers indicate the maximum and minimum ranges, with vertical lines extending from the 10 th to the 90 th percentile, and the dots represents outlier values.	170
Figure 9.2 Subcellular metal distribution of metals in <i>T. usneoides</i> and <i>T. stricta</i> exposed at industrial sites.	173
Figure 9.3 Subcellular metal distribution of metals in <i>T. usneoides</i> and <i>T. stricta</i> exposed at urban sites (Ramos and Urca).....	174
Figure 9.4 Subcellular metal distribution of metals in <i>T. usneoides</i> and <i>T. stricta</i> exposed at urban and port region (Niterói).....	175
Figure 10.1 <i>Tillandsia stricta</i> and <i>Tillandsia usneoides</i> Reduced Glutathione (GSH) concentration ($\mu\text{mol g}^{-1}$) per sampling (1: October 2019, 2: January 2020, and 3: November 2020) The p-value < 0.05 obtained for comparison between species is represented by *	187
Figure 10.2 <i>Tillandsia stricta</i> and <i>Tillandsia usneoides</i> Hydrogen Peroxide (H_2O_2) concentration ($\mu\text{mol g}^{-1}$) per sampling (1: October 2019, 2: January 2020, and 3: November 2020) The p-value < 0.05 obtained for comparison between species is represented by *	189
Figure 10.3 <i>Tillandsia stricta</i> and <i>Tillandsia usneoides</i> Malondialdehyde (MDA) concentration ($\mu\text{mol g}^{-1}$) per sampling (1: October 2019, 2: January 2020, and 3: November 2020).....	190
Figure 10.4 Correlation between oxidative stress biomarkers determined in <i>Tillandsia usneoides</i> exposed in MRRJ and removed in three periods (1:	

October 2019, 2: January 2020, and 3: November 2020) The p-value significance is represented by * for $p < 0.05$	193
Figure 10.5 Correlation between oxidative stress biomarkers determined in <i>Tillandsia stricta</i> exposed in MRRJ and removed in three periods (1: October 2019, 2: January 2020, and 3: November 2020) The p-value significance is represented by * for $p < 0.05$	194
Figure 11.1 Chromatogram obtained for GSH, MT and a mixture of standards (BSA, Ferritin, GSH and MT) used to calibrate the separation column.....	199
Figure 11.2 Spectra obtained by SEC-HPLC-ICP-MS for GSH, MT and a mixture of standards (BSA, Ferritin, GSH and MT) used to calibrate the separation column.	200
Figure 11.3 Metal bound protein observed by SEC-HPLC-ICP-MS in <i>T. stricta</i> and <i>T. usneoides</i> exposed in Duque de Caxias.....	201
Figure 11.4 Metal bound protein observed by SEC-HPLC-ICP-MS in <i>T. stricta</i> and <i>T. usneoides</i> exposed in Niterói.	202
Figure 11.5 Metal bound protein observed by SEC-HPLC-ICP-MS in <i>T. stricta</i> and <i>T. usneoides</i> exposed in Ramos.	203
Figure 11.6 Metal bound protein observed by SEC-HPLC-ICP-MS in <i>T. stricta</i> and <i>T. usneoides</i> exposed in Santa Cruz.	203
Figure 11.7 Metal bound protein observed by SEC-HPLC-ICP-MS in <i>T. stricta</i> and <i>T. usneoides</i> exposed in Urca.....	204
Figure 14.1 Beringui, Karmel et al. Avaliação da concentração e composição inorgânica do material particulado coletado no estado do Rio de Janeiro. Química Nova. 2021, v. 44, n. 6 described in chapter 3.	233
Figure 14.2 Beringui, Karmel et al. Studies in Engineering and Exact Sciences, 2022, v 3., n 1, 95 – 106 described in chapter 5.	233
Figure 14.3 Beringui et al. Air quality, Atmosphere & Health, nov 2021, described in chapter 6.	233
Figure 15.1 Beringui, K. et. al, Atmospheric Metal Biomonitoring Along a Highway Near Atlantic Rainforest Environmental Protection Areas in Southeastern Brazil. Bull Environ Contam Toxicol 107, 84–91 (2021)	234

Figure 15.2 De La Cruz, A.R.H. et al. Biomonitoring of Potentially Toxic Elements in Two Polluted Areas from Lurigancho-Chosica Using the genus <i>Tillandsia latifolia</i> and <i>T. purpurea</i> as Biomonitor. <i>Bull Environ Contam Toxicol</i> 107, 69–76 (2021).	234
Figure 15.3 Justo, Elizanne P. S. et al. Assessment of Atmospheric PM10 Pollution Levels and Chemical Composition in Urban Areas near the 2016 Olympic Game Arenas. <i>Journal of the Brazilian Chemical Society</i> . 2020, v. 31, n. 5	235
Figure 15.4 Adriana Gioda, et. al (2021): A Review on Atmospheric Analysis Focusing on Public Health, Environmental Legislation and Chemical Characterization, <i>Critical Reviews in Analytical Chemistry</i>	235
Figure 18.1 Mobility variability measured by Apple and Google from March,2020 to September,2020	242
Figure 18.2 Spearman correlation between pollutants and meteorological parameter recorded from March to September, 2019 and 2020	247
Figure 19.1 Concentrations and AQI classes comparison regarding NO ₂ daily average in Largo do Bodegão, Manguinhos, Monte Serrat and São Luiz for March and April of 2019 and 2020	248
Figure 19.2 Concentrations and AQI classes comparison regarding O ₃ daily average in Manguinhos, Monte Serrat and São Luiz for March and April of 2019 and 2020	249
Figure 19.3 Concentrations and AQI classes comparison regarding SO ₂ daily average in Manguinhos and Monte Serrat for March and April of 2019 and 2020	250
Figure 19.4 Daily concentrations (ppm) and AQI classes for CO in Manguinhos and São Luiz from March 1st to April 12, 2019 and 2020.	251
Figure 19.5 Pearson correlation matrix with hierarchical cluster analysis grouping parameters for data obtained between March 1 st and April 12 nd , 2019 and 2020	253
Figure 19.6 Backward trajectories calculated by Hysplit Model for the period between March 1st and April 12nd.....	254

List of Tables

Table 3.1 Sampling station descriptions.....	40
Table 3.2 Characteristics of the air quality atmospheric station belonging to INEA, located in the Rio de Janeiro metropolitan region.....	45
Table 3.3 - Air Quality Index (AQI) range and air classification according to index values	48
Table 3.4 Characteristics of atmospheric biomonitoring sites located in the metropolitan region of Rio de Janeiro	50
Table 4.1 Air Quality Standards of the Brazilian legislation (CONAMA)	67
Table 4.2 Concentration range of TSP ($\mu\text{g m}^{-3}$), of metallic elements (ng m^{-3}) and ions ($\mu\text{g m}^{-3}$) in particles sampled in Hi-Vol in the state of Rio de Janeiro between 1995 and 2011.....	88
Table 4.3 Concentration range of PM ₁₀ ($\mu\text{g m}^{-3}$), of metallic elements (ng m^{-3}) and ions ($\mu\text{g m}^{-3}$) in particles sampled in Hi-Vol in the state of Rio de Janeiro	89
Table 4.4 Concentration range of PM _{2.5} ($\mu\text{g m}^{-3}$), metallic elements (ng m^{-3}) and ions ($\mu\text{g m}^{-3}$) in particles collected in Hi-Vol in Rio de Janeiro state between 1998 and 2009.	90
Table 4.5 MP _{2.5} concentration range ($\mu\text{g m}^{-3}$), metal elements (ng m^{-3}), and ions ($\mu\text{g m}^{-3}$) in particles sampled in Hi-Vol in Rio de Janeiro state between 2010 and 2016	91
Table 5.1 Variations in monthly concentrations of pollutants, expressed as percentage, comparing 2019 and 2020.....	111
Table 5.2 Results of the comparison between pairs of months (2019 vs 2020) when no statistical variations were observed in the concentration of the pollutants.	113
Table 8.1 Enrichment to reference ratios (ER) calculated for elements determined in <i>T. stricta</i> sampled at all three sampling sites.....	158
Table 8.2 Enrichment to reference ratios (ER) calculated for elements determined in <i>T. usneoides</i> sampled at all three sampling sites.....	159

Table 8.3 Enrichment factor in relation to soil composition calculated for <i>T.stricta</i> sampled at all sites in three sampling campaigns considering Fe concentration as standardization factor.....	160
Table 8.4 Enrichment factor in relation to soil composition calculated for <i>T.usneoides</i> sampled at all sites in three sampling campaigns considering Fe concentration as standardization factor.....	161
Table 9.1 Measured and certified concentrations and recovery of standard reference material (SRM 1515 and SRM 1547) determined by ICP-MS.....	172
Table 9.2 – Associations between MT and metal and metalloids for <i>T. usneoides</i> and <i>T. stricta</i> determined by Spearman correlation coefficients (rho).	178
Table 9.3. Significant associations between essential and toxic metals and metalloids for <i>T. usneoides</i> and <i>T. stricta</i> and their respective Spearman correlation coefficients (rho).	180
Table 9.4. Molar ratios between essential and toxic elements in <i>T. usneoides</i> and <i>T. stricta</i>	180
Table 10.1 Spearman's correlation ($p < 0.05$) between total metal content of Tillandsias and oxidative stress biomarkers.....	195
Table 17.1 Automatic (A) and semi-automatic (S) stations of INEA's air quality monitoring system with TSP and PM ₁₀ concentration data used for the 1st Diagnosis of the air quality monitoring network in Brazil.....	238
Table 17.2 TSP concentrations obtained by the monitoring network of the state of Rio de Janeiro (INEA) between 2000 and 2012. Data available in the first diagnosis of the air quality monitoring network in Brazil.....	239
Table 17.3 PM ₁₀ concentrations obtained by the monitoring network of the state of Rio de Janeiro (INEA) between 2000 and 2012. Data available in the 1st Diagnosis of the air quality monitoring network in Brazil.....	240
Table 18.1 Descriptive statistic (Mean \pm standard deviation and largest and smallest value of meteorological data obtained for five monitoring station in 2019 and 2020.	243

Table 18.2 CO monthly average concentration \pm standard deviation (ppm) and data range obtained for all monitoring station between March and September of 2019 and 2020.	244
Table 18.3. O ₃ monthly average concentration \pm standard deviation ($\mu\text{g m}^{-3}$) and data range obtained for all monitoring station between March and September of 2019 and 2020.....	245
Table 18.4 PM ₁₀ monthly average concentration \pm standard deviation ($\mu\text{g m}^{-3}$) and data range obtained for all monitoring station between March and September of 2019 and 2020.....	246
Table 19.1 Weekly average of meteorological parameters and Mann Withney results. Considering one site, values at each column with the same letter do not differ statistically ($p < 0.05$).....	252

List of Equations

Equation 3.1 Air Quality Index formula.....	48
Equation 3.1 Expression for ICP-MS Limit of Detection calculation.....	82
Equation 3.2 Expression for ICP-MS Limit of Quantification calculation	82
Equation 3.3 Expression for Ionic Chromatograph Limit of Detection calculation	83
Equation 3.4 Expression for Ionic Chromatograph Limit of Quantification calculation	83
Equation 3.5 Expression for Limit of Detection of method calculation	83
Equation 3.6 Expression for Limit of Quantification of method calculation....	83
Equation 3.7 Enrichment formula calculation	84
Equation 3.8 Ca ²⁺ Non sea salt contribution estimation.....	85
Equation 3.9 Mg ²⁺ Non sea salt contribution estimation	85
Equation 3.10 K ⁺ Non sea salt contribution estimation	85
Equation 3.11 SO ₄ ²⁻ Non sea salt contribution estimation.....	85
Equation 3.12 Cl ⁻ Non sea salt contribution estimation	85

List of Abbreviations

ABNT – Brazilian Association of Standards and Techniques

AQI – Air Quality Index

BSA – Bovine Serum Albumin

BTEX – benzene/toluene/ethylbenzene/xylene

CAM – Crassulacean acid metabolism

CET-Rio – Traffic Engineering Company of Rio de Janeiro

COI – International Olympic Committee

CONAMA – *National Environment Council*

CRM – Certified reference materials

Detran – Rio de Janeiro State Traffic Department

EE – Extraction efficiency

EF – Enrichment factor

ER – Exposure to reference ratio

FAAS – Flame atomic absorption spectrometry

FS – Final standard

GR – Glutathione reductase

GSH – Reduced Glutathione

GSSG – Oxidizing Glutathione

HCA – Hierarchical Cluster Analysis

HYSPLIT – Hybrid Single-Particle Lagrangian Integrated Trajectory

IC – Ion chromatography

ICP-MS – Inductively Coupled Plasma Mass Spectrometry

ICP OES – Inductively coupled plasma optical emission spectrometry

IEMA – Institute of Energy and Environment

IF – Insoluble fraction

INEA – Environment State Institute

INMETRO – Brazilian National Institute of Metrology, Quality and Technology

INMET – National Institute for Meteorology

IS – Intermediate standards

LOD – Limits of detection

LOQ – Limits of quantification
MMA – Ministry of Environment
MRC – Metropolitan Region of Campinas
MRRJ – Metropolitan Region of Rio de Janeiro
MT – Methallothionein
MDA – Malondialdehyde
NDIR – Non-dispersive infrared spectrophotometry
nss – non- sea salt
P – Pressure
PAH – Polycyclic aromatic hydrocarbons
PM – Particulate matter
PRONAR – National Air Quality Control Program
RH – relative humidity
RF – rainfall
ROS – Reactive oxygen specie
SFU – Stacked filter unit
SMAC – Municipal Secretary of the Environment
SR – Solar radiation
T – temperature
TLF – Thermolabile fraction
TOC – total organic carbon analyzer
TRS – Total Reduced Sulfur
TSF – Thermostable fraction
TSP –Total Suspended Particles
USEPA – United States Environmental Protection Agency
UV – Ultraviolet
VOCs – Volatile organic compounds
WS – Wind speed
WD – Wind direction
WHO – World Health Organization
XRF – X-ray fluorescence

1 Introduction

Environmental pollution is a theme increasingly in the spotlight in recent decades (Omidvarborna et al., 2018). Continued industrialization leads to increased urbanization and population growth, resulting in significantly increased emissions of air pollutants (Bahino et al., 2018; Mateus et al., 2013; Santos et al., 2017). Thus, air pollution can be considered one of the major environmental concerns, as it affects the environment and human and environmental health (Bahino et al., 2018; Gulia et al., 2015)

Atmospheric pollution is influenced by several variables, as meteorological conditions, topographic characteristics and emission sources. However, variations in only one variable may represent changes in air quality, which may pose risks to the population and ecosystems or contribute to lower levels of pollutants (Cruz et al., 2020; Ochoa-Hueso et al., 2017). Fuel combustion may be considered the main emission source of gaseous pollutants and particulate matter in urban centers (Villanueva et al., 2016).

1.1. Particulate matter

Particulate matter (PM) represents one of the most important classes of air pollutants, mainly due to the high heterogeneity of its composition (De Paula et al., 2015; Gioda and Amaral et al., 2011; Kim et al., 2015). The impacts caused by these particles are observed on human health, ecosystems, visibility, and climate processes (Alves, 2005; Gieré e Querol, 2010; Masiol et al., 2015; Pope et al., 1989).

Particle size can influence their residence time in the atmosphere. The coarser fraction can remain suspended for hours to days, preferably depositing itself near emission sources through dry deposition. The fine fraction can remain suspended for up to weeks, and can be transported to other regions until they settle out. The ultrafine particles remain suspended for minutes or hours. Due to their small diameter, they tend to undergo nucleation or coagulation processes to form larger particles (Al-Thani et al., 2018). The dry deposition of the particles is locally important, because it

contributes to the improvement of air quality, but it is the wet deposition, which occurs by the action of rain, that contributes to pollutant removal on a larger scale, because it also removes gaseous pollutants (Grantz et al., 2003; Pöschl, 2005).

1.2. Gaseous Pollutants

Some gaseous substances as SO₂, CO, NO₂ and O₃ are considered criteria pollutants, along with particulate matter. According to United States Environmental Protection Agency (USEPA), they represent risk to public health and environment (Guo et al., 2017; Sulaymon et al., 2021). SO₂ is a sulfur oxidation product found as impurity in fuels. This gas may act as precursor of secondary PM, producing SO₄²⁻, which may contribute to acid deposition (Cruz et al., 2020; Fioletov et al., 2015; Sulaymon et al., 2021). NO₂ is a result of internal combustion in engines (Cruz et al., 2020; Sulaymon et al., 2021). CO is formed by the incomplete combustion (partial oxidation) of hydrocarbons, the main fossil fuel constituents (Cruz et al., 2020), and O₃ is a secondary pollutants produced by complex reaction in the atmospheric using primary pollutants as precursors (Geraldino et al., 2020; Gioda et al., 2018).

1.3. Atmospheric Biomonitoring

Biomonitoring consists of using living organisms to assess pollution, as they can provide information about the bioavailability of various pollutants (AL-Alam et al., 2019; Conti and Cecchetti, 2001; Santos et al., 2017). Biomonitors are the species used for biomonitoring, which remain exposed continuously in the monitored area, interacting directly with the emitted pollutants. (AL-Alam et al., 2019; Figueiredo et al., 2007). In comparison with traditional atmospheric monitoring, biomonitoring has lower costs and is, therefore, an alternative to traditional methods. In addition, it allows the understanding of how organisms react to prolonged exposure to atmospheric contaminants (Caballero-Segura et al., 2014; Chaligava et al., 2020; Figueiredo et al., 2007).

The most commonly employed organisms for biomonitoring are plants, due to their wide geographic distribution, easy collection, and immobility (Falla et al., 2000). Different plants can accumulate toxic substances from the atmosphere, such as metals or organic compounds (AL-Alam et al., 2019; Gioda et al., 2021; Monna et al., 2017). Plants, however, can act as air pollution filters due to their ability to remove

pollutants from the atmosphere by gaseous exchange, absorbing substances present in the air through dry or wet deposition of particulate material (Janhäll, 2015; Xie et al., 2018).

Epiphytic plants are the most suitable organisms for atmospheric biomonitoring, as they obtain water and nutrients through gas exchange rather than through their root system (Techato et al., 2014; Wannaz et al., 2006). They can be found on the tops of trees or even on inert surfaces used only as support. Although they obtain nutrients only through gas exchange, they can develop roots that help sustain and fix them to surfaces (Santos et al., 2017).

Biomonitoring can be classified into two major groups: bioindicators, comprising species sensitive to pollutant exposure in such a way that they will initially present impairment of physiological functions that will later lead to morphological damage, and may even cause death, and bioaccumulators, consisting of species resistant to pollutants in such a way that they can accumulate in plant tissues, and can be determined and quantified later by chemical analyses (Falla et al., 2000; Mahapatra et al., 2019; Rai, 2016b).

Bioaccumulators can be used in passive or active biomonitoring. The passive approach consists of obtaining information by collecting species endemic to the monitoring region. The active approach, conversely, consists of transplanting species removed from unpolluted or low-polluted sites to another area for monitoring (Falla et al., 2000; Szczepaniak and Biziuk, 2003). Active biomonitoring is used in most studies involving air pollution, mainly because it allows greater control over the exposure time. In addition, this approach results in lower variations due to intrinsic organism variability (Bargagli, 2016; Monna et al., 2017).

Atmospheric biomonitoring was initiated in the 70s, using lichens, mosses, and bark as biomonitors, due to their wide distribution (Gioda et al., 2021; Szczepaniak and Biziuk, 2003). Another group of species prominent in atmospheric biomonitoring consist of *Tillandsias*. These belong to a genus of the *Tillandsioideae* subfamily, family *Bromeliaceae* (Pignata et al., 2002). They are epiphytic plants, totally independent from the soil, displaying slow growth and a high capacity to obtain nutrients from the atmosphere (Pignata et al., 2002; Techato et al., 2014). These plants use the Crassulacean Acid Mechanism (CAM) through which photosynthesis results in a more efficient conversion of water, also resulting in lower transpiration rates, leading to lower stoma density (Techato et al., 2014). Water and nutrient absorption takes place

through trichomes that cover the stem and leaf surfaces, which are also responsible for the protection against UV rays and dissection (Monna et al., 2017).

In addition to allowing for inferences regarding the degree of pollution in a given area, biomonitoring using plants can be used to assess the deleterious effects of pollutants on these organisms, such as morphological, physiological, and biochemical damage (Mahapatra et al., 2019; Rai, 2016b). Depending on PM composition, these compounds can cause damage to crops, forests, and ornamental plants, either through deposition or root absorption. Besides morphological effects visible to the naked eye, such as changes in color and size, exposure to PM can also cause damage at the cellular level, one of the main deleterious effects being oxidative stress, observed when there is an imbalance between oxidant species and antioxidant defenses in the cells (Daresta et al., 2015; Rai, 2016a; Shahid et al., 2017).

1.4.Oxidative Stress

Plants exposed to high concentrations of metallic elements are subject to the uptake of these elements, which can cause dyshomeostasis by the uptake of toxic elements or excessive uptake of essential metals, which can lead to oxidative stress (Rai, 2016b; Shahid et al., 2017). To recover homeostasis or reach tolerable levels of these chemical species, plants have defense mechanisms that remove the metals through complexation with specific ligands and activation of the antioxidant system (Santosa, 2016; Tripathi et al., 2015).

Continuous exposure to pollutants causes increased production of reactive oxygen species (ROS), reactive molecules that have one unpaired electron. The antioxidant system is responsible for maintaining the balance between production and consumption of these species; however, in polluted conditions, this system may not perform its function efficiently and the body is subjected to oxidative stress conditions, caused by the excess of ROS. Under these conditions it is possible to verify cellular modifications, such as membrane and DNA damage, protein degradation, enzyme inactivation, and lipid peroxidation. These physiological alterations can compromise the growth, development, and reproduction of organisms (Mansour et al., 2020; Nakazato et al., 2018a; Rai, 2016b). The oxidative stress condition may be assessed by investigation of several biomarkers, such as certain proteins and oxidative stress

endpoints. These include reduced glutathione (GSH), metallothionein (MT), hydrogen peroxide (H_2O_2) and lipid peroxidation, which will be further described in Chapter 8.

1.5.Oxidative stress biomarkers

Biomarkers can be assessed to evaluate the effects of pollutant exposure. These consist of biological parameters whose measurements indicate biochemical, cellular, or physiological changes (Mansour et al., 2020; Viarengo et al., 1997). Defense biomarkers are those that act to prevent oxidative stress, while damage biomarkers are those that reveal the deleterious effects caused to organisms (Mansour et al., 2020).

Metal element detoxification mechanisms developed by various animal and plant species are based on the complexation of metal ions by specific ligands, which can be applied as metal oxidative stress markers (Mahapatra et al., 2019; Mansour et al., 2020). Metallothionein (MT) is a thermally stable, cysteine-rich, low molecular weight (6 - 7 kDa) protein produced by animals, plants and bacteria (Li et al., 2018; Mahapatra et al., 2019). Cysteine is an amino acid that contains thiol groups, which makes MT rich in sulfur, allowing it to complex with several metals (Oaten et al., 2017). The ability of MT to complex metallic elements contributes to decreasing metal concentrations down to physiological levels, contributing to metal detoxification and reduced oxidative stress resulting from metal exposure (Santosa, 2016; Tripathi et al., 2015). Due to its important role in the antioxidant system, MT has been widely employed in ecotoxicological studies (Li et al., 2018).

To prevent damage caused by excess ROS, one of the main cellular defense mechanisms is the antioxidant system, which acts in preventing ROS formation. One of the main non-enzymatic antioxidants is glutathione, a low molecular weight tripeptide containing a sulfhydryl functional group, responsible for its water solubility. It is an abundant metabolite in plants and widely distribution in different tissues (Gill et al., 2013; Hasanuzzaman et al., 2017). One of its main functions comprises ROS and methylglycol detoxification and the modulation of antioxidant enzymes (Edwards et al., 2000; Hasanuzzaman et al., 2017; Liedschulte et al., 2010).

Glutathione can be found in cells at millimolar concentrations, in both its reduced form (GSH) and oxidized form (GSSG), when two molecules are joined by a sulfur bond (Edwards et al., 2000; Gill et al., 2013). Glutathione reductase (GR) is an enzyme

that performs the conversion of GSSG to GSH, which occurs in oxidative stress situations. In addition, GSH/GSSG ratio maintenance is necessary for adequate protein performance. Thus, both GR and GSH can be employed as oxidative stress biomarkers (Gill et al., 2013; Hasanuzzaman et al., 2017).

Hydrogen peroxide (H_2O_2) is one of the ROS produced in normal physiological processes, such as photosynthesis and respiration. This compound can be formed by the two-step reduction of O_2 , through the formation of a superoxide (step 1) followed by the action of a reducing enzyme (step 2) (Cuypers et al., 2016; Niu and Liao, 2016). The main H_2O_2 source in plants is glycolate oxidation during photosynthesis, although pathogen exposure stimulates its production, contributing to rapid concentration increases (Hossain et al., 2015).

The longer lifetime of H_2O_2 (1 ms), compared to that of other ROS, associated with its small size, allows for this molecule to cross membranes, diffusing molecular damage and acting in the oxidation of the thiol groups of enzymes, in addition to participating in the formation of OH^\cdot radicals (Barbosa et al., 2014). Given the fact that exposure to toxic substances alters H_2O_2 concentrations, it can also be applied as an oxidative stress biomarker (Caverzan et al., 2016). Furthermore, associations between its concentrations and GSH levels can also be considered, as this tripeptide is one of the antioxidants that acts in preventing the formation of this chemical species (Niu and Liao, 2016).

Other deleterious effects can be observed in organisms under oxidative stress. Lipid peroxidation of cell membranes, for example, leads to decreased cell membrane fluidity and selectivity (Mansour et al., 2020; Taïbi et al., 2016). Protein carbonylation is another common effect observed in organisms exposed to metals (Cuypers et al., 2016). Both physiological processes can be stimulated by the presence of ROS and can, therefore, be considered oxidative stress biomarkers (Taïbi et al., 2016).

1.6. Rio de Janeiro Metropolitan Region

The Rio de Janeiro metropolitan region was established in 1974 through Federal Complementary Law n °14/1973, after the merger between the state of Rio de Janeiro and the state of Guanabara (Margut et al., 2017). Over the years, its composition has been altered through the insertion and removal of municipalities. Since 2013 it is formed by 21 cities, which together represent 12 % of the state's territory and

concentrate 75 % of the population. (IPEA, 2018; Margut et al., 2017). It is considered the second largest metropolis in Brazil in terms of territory and has the highest population proportion among the country's metropolitan regions. (IPEA, 2018).

The industrialization of the state of Rio de Janeiro was consolidated in the 1940s, when industries were installed in the municipality of Rio de Janeiro, in addition to municipalities in the *baixada fluminense* such as Duque de Caxias and Nova Iguaçu and those located beyond the Guanabara Bay, such as Niterói and São Gonçalo (IPEA, 2015). As of the 2000s, the state's economic scenario stood out due to the installation of large industrial enterprises, such as the *Companhia Siderúrgica do Atlântico* in Santa Cruz, in the western zone of Rio de Janeiro, and the *Complexo Petroquímico do Rio de Janeiro*, in Itaboraí (IPEA, 2015).

To help drain the production of these industrial enterprises, the state needed to modernize and expand its ports (Port of Itaguaí and Port of Rio de Janeiro), as well as invest in the construction and expansion of the highways that connected the enterprises to the ports. In addition, the increase in production contributed to a higher turnover of ships in the port areas (IPEA, 2015).

The concentration of the largest industrial complexes in municipalities of the metropolitan region attracts commercial enterprises that contribute to population concentration. Thus, the characteristics of the pollutants emitted in this area of the state differ from the others (IPEA, 2015).

1.7. Research hypothesis and layout of this thesis

Plants respond to exposure to pollutants and can be used to gain information about environmental changes, so they could be used to assess the ecological risk caused by exposure to air pollutants in urban centers. Developing knowledge about the defense mechanisms of Tillandsias, epiphytic plants, can lead to inferences about the impact of atmospheric pollution on ecosystems and, subsequently, make a correlation with the effects on human health.

This PhD thesis is presented in an article-based format, in which the “Results and Discussion” section comprises an adaptation of articles already published, submitted, or still in the process of being written (Chapter 4 – 11). In order to follow the standard for final papers, the “Materials and Methods” section is described in Chapter 3 and includes the methodology employed for all written articles. Thus, in

chapters where the results are described, the reader will find the corresponding methodology section in Chapter 3.

2 Objectives

2.1. General objectives

Assess the air quality of the metropolitan region of Rio de Janeiro through the temporal variation of the concentrations of legislated pollutants and atmospheric biomonitoring for ecotoxicological evaluation.

2.2. Specific Objectives

- Perform a literature review of the studies on concentration and composition of particulate matter collected in the state of Rio de Janeiro in the last 40 years.
- Assess the variation of PM₁₀, CO and O₃ concentration in the city of Rio de Janeiro reported from the beginning of the COVID-19 pandemic until the end of the economic opening, considering the meteorological influence.
- Evaluate the air quality in the metropolitan region of Rio de Janeiro through the concentrations of CO, NO₂, SO₂ and O₃ recorded at locations under the influence of industrial and vehicular emissions in the first month of social isolation due COVID-19 pandemic.
- Investigate the daily and hourly variation of air pollutants reported in the metropolitan region of Rio de Janeiro in the first month of the partial lockdown.
- Using *Tillandsia usneoides* and *Tillandsia stricta* to perform active atmospheric biomonitoring of metals in regions with different emission profiles for source attribution.
- Explore subcellular metal distribution and metal associations to metallothionein in two *Tillandsia* species exposed in industrial, urban, and port areas in the metropolitan region of Rio de Janeiro, Southeastern Brazil.
- Assess oxidative stress in atmospheric biomonitors exposed to urban pollution in a Brazilian metropolis.
- Apply the SEC-HPLC-ICP-MS technique to investigate the association of metals and oxidative stress biomarkers in *Tillandsias* exposed to air pollution in Rio de Janeiro.

3 Material and Methods

Since this thesis is based on article format for the presentation of section “Results and Discussion”, the material and methods will be presented here and omitted from the respective articles.

3.1.Literature review of particulate matter sampled in Rio de Janeiro

The following description of methods refers to chapter 4, page 58.

3.1.1. Search for papers

A literature search was carried out using Google Scholar and SciFinder. We considered all published articles whose study areas were within the state of Rio de Janeiro and that presented data on particulate matter concentration, elemental concentration, and ionic concentration.

For the search, the keywords used were: particulate matter, PM, aerosol, atmospheric pollution, air pollution, air Quality, Chemical composition, Rio de Janeiro. The same procedure was carried out using the terms in English and in Portuguese.

We found 30 articles published between 1999 and 2020, which presented PM data collected between 1968 and 2017, mainly using large volume samplers for sampling. A total of 28 cities from the state of Rio de Janeiro were considered in this review, however, most of the studies focused on the city of Rio de Janeiro or its metropolitan region. Figure 3.1 presents the location of all PM sampling sites reported in the studies considered in the literature review.

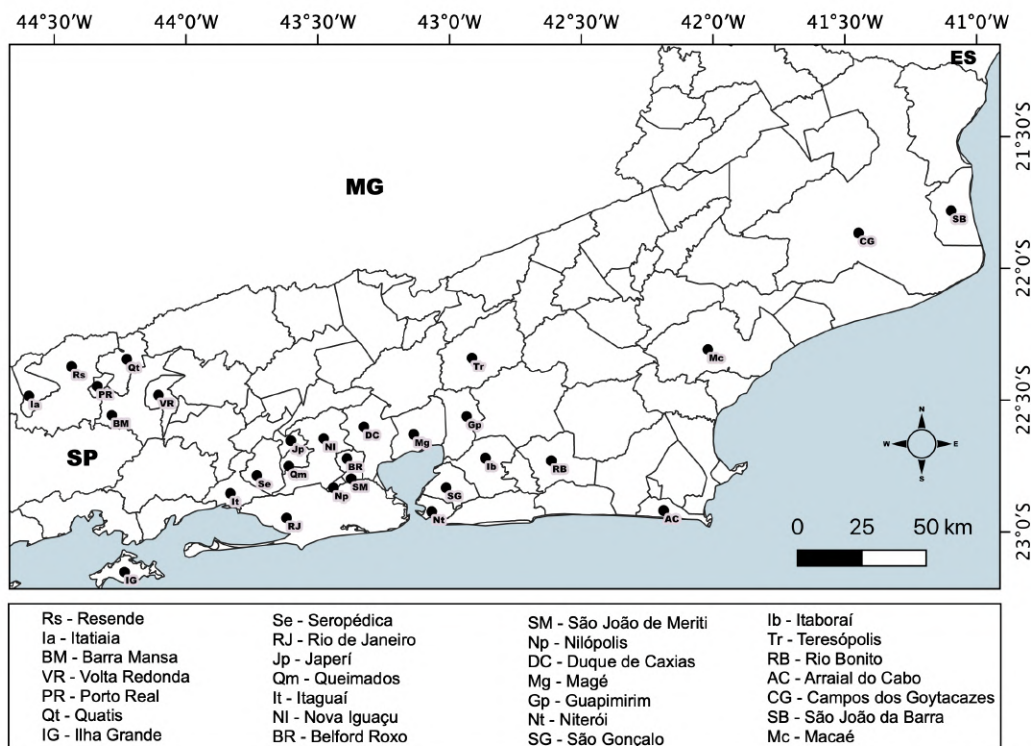


Figure 3.1 Map with the location of the sampling sites used in the studies with PM carried out in the state of Rio de Janeiro. Software QGIS, Data source: Brazilian Institute of Geography and Statistics - IBGE, Institute of Applied Economic Research - Ipea, IHO Sea Area

3.1.2. Data arrangement

The software Excel was applied to summarize the data presented in all papers considered. In a spreadsheet were recorded for each study: the size of the particulate matter sampled, the sampling periods, the sites of sampling, the type of sampling, the number of samples, the PM concentration range, the average concentration of PM, and the concentration range of the particulate matter components.

Subsequently, the data were serialized according to particulate size (PTS, PM₁₀ and PM_{2.5}) and then organized chronologically. The average of PM concentrations were plotted in a bar graph, in which the limits established by the legislation current in the sampling period (Resolution CONAMA 03/1990) and in the updated legislation were added (Resolution CONAMA 491/2018).

The particulate matter composition data were also organized chronologically. In separate tables by PM size the concentration ranges of metallic elements and ions were presented.

To further explore the discussion on the ionic composition of particulate matter, the concentrations reported in the studies were used to make the non-marine contribution calculation (nss – non sea salt), using the ratios between ions in seawater. In addition the acidity of the particles was explored using the ratios between cations and anions.

3.2.Effect of partial lockdown on air quality in the city of Rio de Janeiro

The following description of methods refers to chapter 5, page 99.

3.2.1. Study Area

Rio de Janeiro is a coastal city with an estimated population of more than 6.7 million inhabitants and more than 75 % of its territory is urbanized (IBGE, 2020). One of the main sources of pollution in the city is vehicle traffic, as it has a fleet of more than 2.5 million cars, including light vehicles, motorcycles, cargo vehicles, and municipal transport buses (Detran, 2020). In this study, five air quality monitoring stations will be considered. Copacabana, located in the southern zone, Tijuca, in the northern zone, Bangu and Campo Grande in the western zone, and Centro, located in the central region of the city. Figure 3.2 presents the location of monitoring stations and Table 3.1 presents characteristics of neighborhoods where monitoring stations are located.

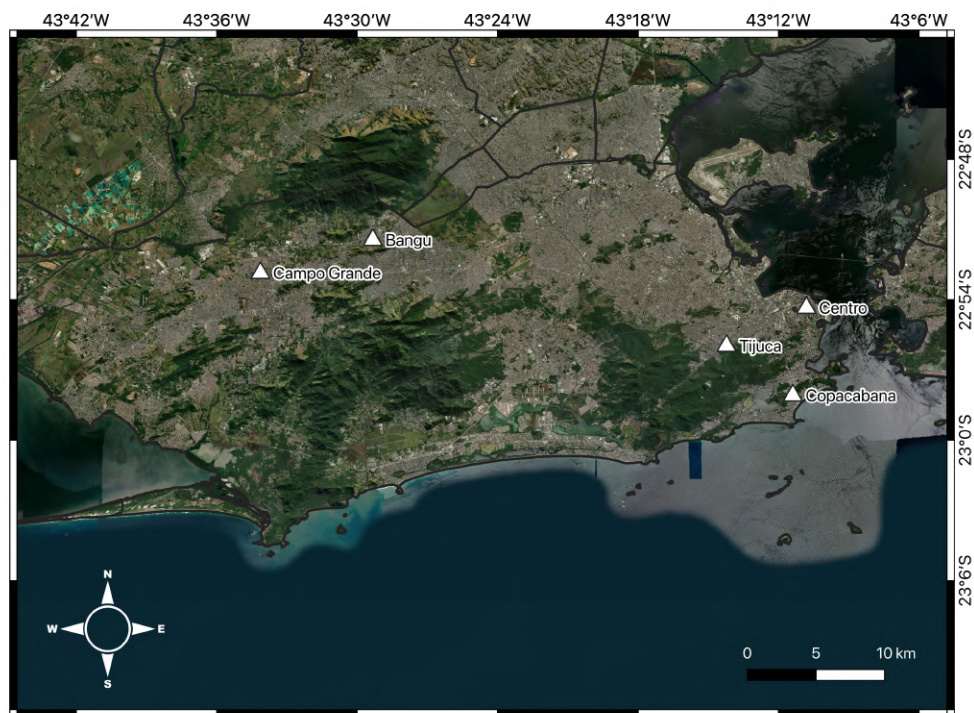


Figure 3.2 Rio de Janeiro city map with air quality monitoring stations highlighted. Black line indicates cities boundaries.

3.2.2. Air Quality and Meteorological data

Data of regulated pollutant concentrations were made available online by the Municipal Environment Department of Rio de Janeiro city SMAC (from Portuguese, Secretaria Municipal do Meio Ambiente). For this study, the concentrations of PM_{10} ($\mu g\ m^{-3}$), CO (ppm), and O_3 ($\mu g\ m^{-3}$) obtained at five air quality monitoring stations between March and September for the years 2019 and 2020 will be considered. Pollutants are sampled following the standard methodology established by Brazilian law (CONAMA, 2018; MMA, 2019).

The configuration of the SMAC air quality monitoring network detects CO by Non-dispersive infrared spectrophotometry (NDIR) technology using an Ecotech 9830 Serinus 30 series; O_3 by non-dispersive ultraviolet (UV) absorption technology through Ecotech 9810 Serinus 10 series; and PM_{10} by β -ray attenuation through Met One BAM 1020. Data for CO and O_3 were obtained at 10-minutes intervals, while PM_{10} at 1-hour intervals. They were organized on a sheet as a continuous hourly average after

evaluation of anomalous values. The equipment was calibrated periodically according to manufacturer instructions.

Table 3.1 Sampling station descriptions

Station	Pollutants	Surrounding characteristics
Bangu	CO, O ₃ and PM ₁₀	Lowland areas and land with slopes that exceed 500 m. The occupation of the soil is with residences, forest and mineral exploration areas. Located near Brazil Avenue, an important road that crosses the city.
Campo Grande	CO, O ₃ and PM ₁₀	Land with elevations up to 200 m. It is predominantly occupied by residential and commercial buildings, but it also has areas of vegetation, industrial enterprises and rural activity.
Centro	CO, O ₃ and PM ₁₀	Lowlands and part of Guanabara Bay. Hills with a slope of up to 100 m and land occupation with buildings that shelter the financial and commercial center of the city. Near streets with intense vehicle flux and under influence of Brazil Avenue.
Copacabana	CO, O ₃ and PM ₁₀	Beach and hills with slopes of 100 to 400 m. High population density that occupies high altitude buildings. Intense vehicle traffic on main streets, including public transport buses.
Tijuca	CO, O ₃ and PM ₁₀	Flat land and hills with a slope of up to 500 m. The occupation of the soil is with residence and commercial enterprises, predominantly of buildings, and forest areas. Intense traffic on streets, mainly in the morning and in the evening.

To assist in the interpretation of the atmospheric pollution data, the meteorological variables (wind speed - WS, wind direction - WD, pressure – P, solar radiation – SR, rainfall - RF, temperature - T, and relative humidity - RH) measured in each of the monitoring stations will be considered.

Online hourly data for each pollutant and meteorological parameters from SMAC (from Portuguese, Secretaria Municipal do Meio Ambiente) were used. The data were organized into daily, hourly, and monthly averages. It was also evaluated pollutant concentrations over weekdays.

Nasa's Giovanni online application was used to visualize remote sensing data obtained for aerosol throughout the *Combined Dark Target and Deep Blue AOD at 0.55 micron for land and ocean* dataset and CO “*Multispectral CO Surface Mixing Ratio (Daytime/Descending)*”. A time average map (March 2020 – September 2020) was plotted to evaluate pollutants trends and transportation. For this analysis the period considered was divided into three short periods according to pollutants variation measured by surface data: March – April (strict lockdown), May – June (social isolation relaxation), and July – September (economic opening).

Pollutant concentrations variation was evaluated considering changes in routine activities in Rio de Janeiro city after the lockdown and opening decrees. A timeline with the main measures taken by the government of Rio de Janeiro state is presented in Figure 3.3, and the opening stages adopted by the city hall of Rio de Janeiro city are presented in Figure 3.4.

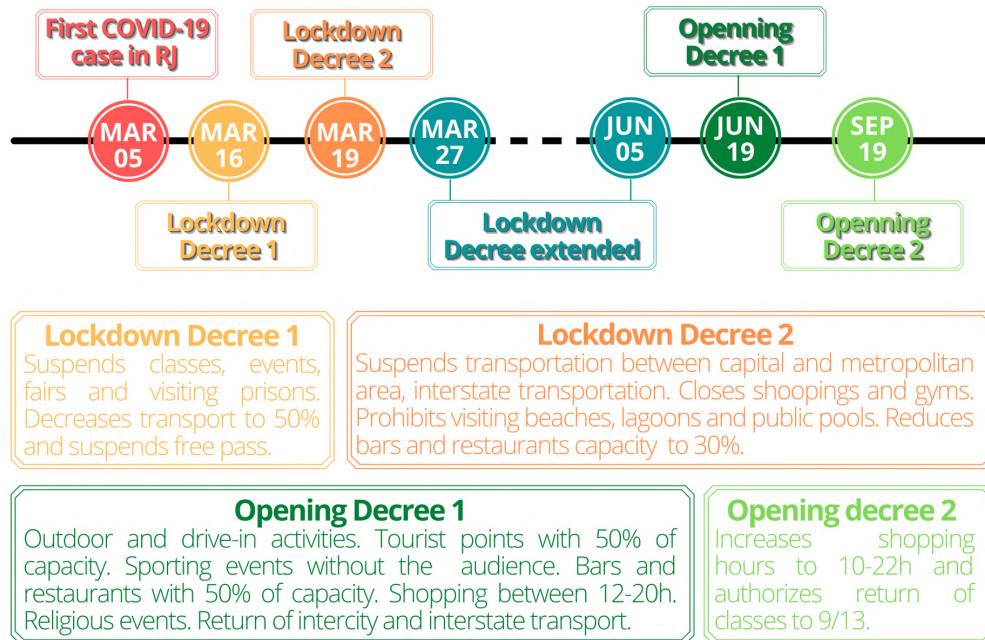


Figure 3.3 Timeline (2020) with main measures taken by Rio de Janeiro state government to control the spread of coronavirus and easing measures after cases number starts to decrease

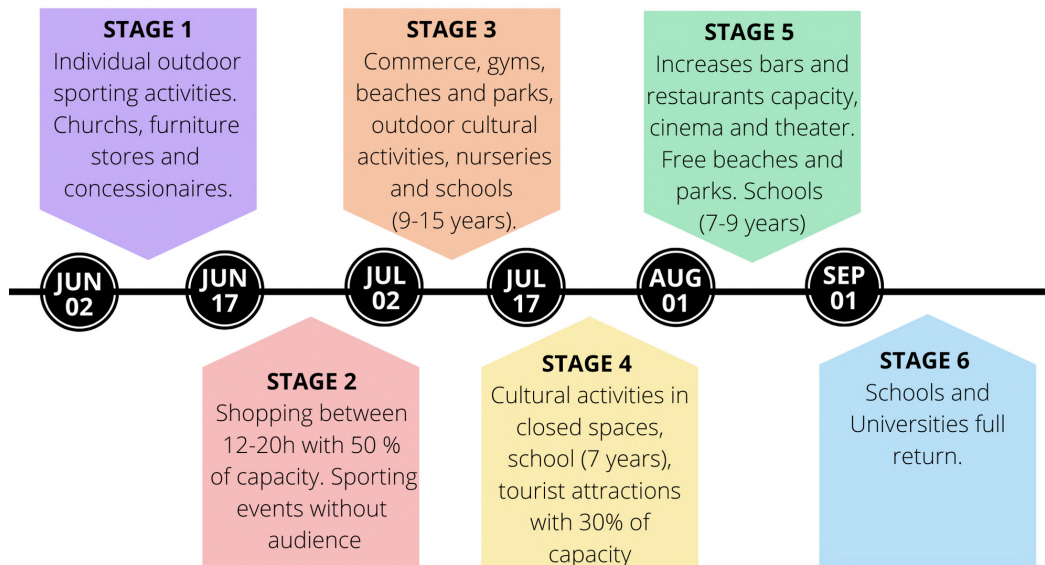


Figure 3.4 Timeline (2020) with opening stages adopted by city hall of Rio de Janeiro city

3.2.3. Mobility data

According to Chapin and Roy 2021, one of the effects of COVID-19 was mobility reduction. Using mobility data provided by Apple they build an application to show mobility variation and confirmed cases of COVID-19 which could be used by researchers to evaluate pandemic effects. While their application is limited to local regions, a similar evaluation may be done with the Apple database.

Mobility data provided by Apple (<https://covid19.apple.com/mobility>) and Google (<https://www.google.com/covid19/mobility/>) companies, available online since the pandemic beginning, was used as an indication of emission changes. Apple provide data since January 13th, while Google since February 15th. Both datasets were evaluated until September 30th. Apple dataset considers that the first day presents 100 % of mobility and the following days are a variation from it. Google mobility dataset represents the variation in mobility compared to the first day.

For comparison proposes, it was considered average data for all of Brazil, for Rio de Janeiro state and Rio de Janeiro city, the focus of this study.

3.2.4. Data analysis

The software R throughout R Studio was used for data analysis. The Openair package was employed to make pollutants and mobility time variation plots, the

ggplot2 package to make kernel density analysis, and ggcorrplot to obtain correlation matrices. Shapiro-Wilk test was applied to test data normality and Wilcoxon-Mann-Whitney test to compare months from 2020 and 2019.

3.3. Air quality assessment in first weeks of COVID-19 pandemic

The following description of methods refers to chapter 6 and 7 from page 122.

3.3.1. Study area

The study was performed in the metropolitan region of Rio de Janeiro (MRRJ), Brazil. Four air quality and meteorology monitoring stations located in urban and industrial areas with a large circulation of vehicles were selected. Two of these stations were located in Rio de Janeiro City (Manguinhos, MG and Largo do Bodegão, LB), the third is in Duque de Caxias City (São Luiz, SL) and the fourth in Itaguaí City (Monte Serrat, MS). The characteristics and location of the sampling sites are show in Table 3.2 and Figure 3.5.

3.3.2. Air quality data

To evaluate the impact of the partial lockdown on the air quality in the MRRJ, four regulated pollutants (CO, O₃, NO₂, and SO₂) concentrations obtained by automatic air quality monitoring stations belonging to INEA (form Portuguese, Instituto Estadual do Ambiente) between March 1st and April 12nd, 2019 and 2020 were evaluated. To verify changes caused by quarantine, the 2020 period was divided in two: 1) March 1st to 15th, 2020 classified as “before lockdown” and 2) March 16th to April 12th, 2020.

Pollutants were measured according to the methodologies described in the Technical Guide for Monitoring Air Quality, published by the Ministry of Environment. (MMA, 2019) Sulfur dioxide (SO₂) was monitored by the ultraviolet (UV) fluorescence methods, nitrogen dioxide (NO₂) was measured by the chemiluminescence method, carbon monoxide (CO) was measured by infrared method and tropospheric ozone (O₃) was measured by the infrared method absorption of ultraviolet light. Data were obtained each 15-minute interval by the automatic monitoring stations, calibrated monthly, using standard methods and types of equipment (Horiba, Japan and Ecotech,

Australia). The values were organized in 1-hour data means for each day including nighttime observations.

Table 3.2 Characteristics of the air quality atmospheric station belonging to INEA, located in the Rio de Janeiro metropolitan region.

Sampling site	Characteristics	Pollutants	Meteorological parameters	Coordinates
São Luiz (SL) – Duque de Caxias	Located at 500 m away from a road with intense flow of light and heavy vehicles and near to unpaved roads, 10 km away from Duque de Caxias Petrochemical Complex.	SO ₂ , NO ₂ , O ₃ , and CO	WS, WD, T, RH, RF, SR, AP	-22,784550°, -43,286388°
Manguinhos (MG) – Rio de Janeiro	Located at 500 m from two roads with intense flow of light and heavy vehicles, an oil refinery, FIOCRUZ research center, and a community.	SO ₂ , NO ₂ , O ₃ , and CO	WS, WD, T, RH, RF, SR, AP	-22.884198°, -43.242592°
Santa Cruz – Largo do Bodegão (LB) – Rio de Janeiro	Intense flow of light and heavy vehicles, 5 km from the Santa Cruz Industrial District, Sepetiba Bay, and Itaguaí Port Complex.	SO ₂ and NO ₂	WS, WD, T	-22,927140°, -43,694727°
Monte Serrat (MS) – Itaguaí	Moderate flow of light and heavy vehicles, 6 km from the Industrial District of Santa Cruz and the Itaguaí Port Complex.	SO ₂ , NO ₂ , and O ₃	WS, WD, T	-22,874843°, -43,770067°

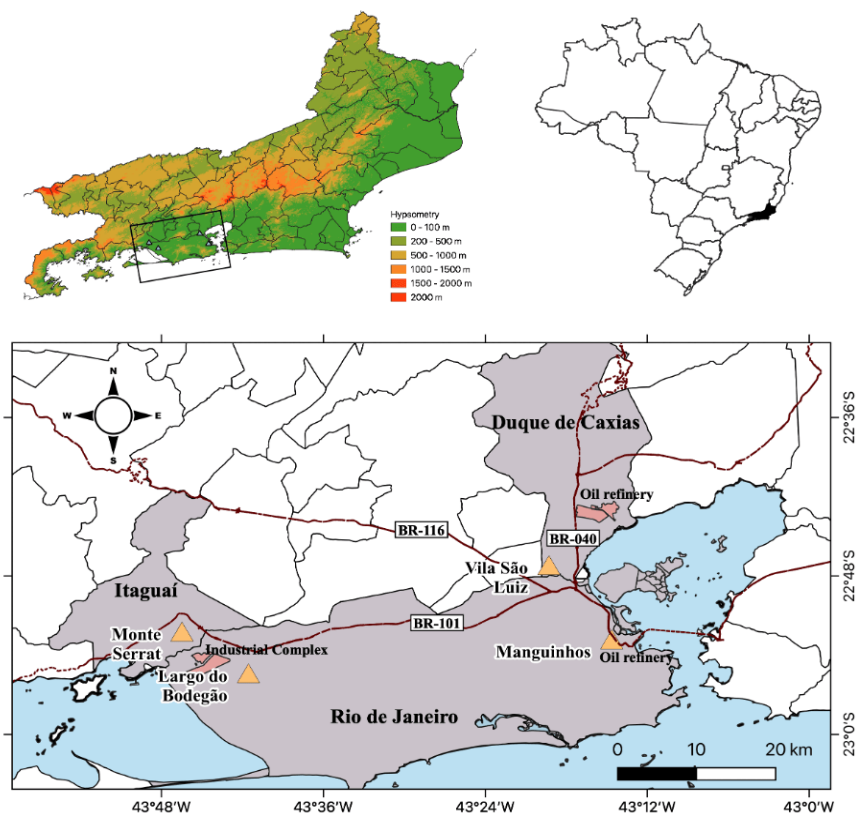


Figure 3.5 Locations of air quality monitoring station and emission sources (industrial district and roads). Itaguaí (Monte Serrat station, MS), Duque de Caxias (São Luiz station, SL), and Rio de Janeiro (Manguinhos station (MG) and Santa Cruz, (Largo do Bodegão station, LB).

3.3.3. Meteorological data

Rainfall (RF, in mm), temperature (T, in °C), solar radiation (SR, in $W m^{-2}$), relative humidity (RH, in %), atmospheric pressure (AP, in mbar), wind speed (WS, in $m s^{-1}$), and wind direction (WD, in °) were used in the study. The meteorological variables were monitored every 15 min by automated analyzers (Met One Instruments, TX, USA) at surface meteorological stations located on the sampling sites installed at a height of 10 m above the ground. The values were organized in 1-hour data means. However, the meteorological data used in the statistical analyses were averages of 24 h.

3.3.4. Statistical analyses

The *Mann Withney* test two-tailed with a confidence level of 95 % was applied to statistically verify the mean values from different periods for the meteorological variables of each of the four studied sites assuming different variances. For data collected in 2020, all sites were evaluated weekly (W), with the first two weeks (W1 and W2) corresponding to before the partial lockdown (March 1st-15th), whereas the following four weeks (W3, W4, W5, and W6) denoting during the partial lockdown period (March 16th-April 12th). The language and Environment for Statistical Computing R was applied for some statistical analysis. (R CoreTeam, 2019) Correlation matrices were used to evaluate the degree of relationship between regulated pollutant concentrations (NO₂, SO₂, O₃, and CO) against meteorological variables. *Pearson* correlations were considered for $p < 0.05$ and the Bryman and Cramer criterion was used to assess the intensity of the correlations (Bryman and Cramer, 2004). As this evaluation included many variables, a Hierarchical Cluster Analysis (HCA) was carried out in order to group variable. The package Openair was applied to make the correlation plots associated with cluster (Carslaw and Ropkins, 2012).

Pollution roses were elaborated to evaluate the predominant direction of the pollutant concentrations measured in the monitoring stations. Hourly data of wind direction and speed correlated with the hourly data of each pollutant concentration were used to build them. The pollution rose shows the frequency distribution of a specific pollutant on a wind intensity, in classes, for each wind direction. The roses help identifying the direction associated with higher or lower concentrations. (Munn, 1969) The function pollutionRose was used via the R package openair (Carslaw and Ropkins, 2012).

3.3.5. Air Quality Index (AQI)

To standardize and simplify the air quality assessment, the computation of the Air Quality Index (AQI) was carried out for each pollutant, according to the Equation 3.1 following the recommendations of the Brazilian Ministry of Environment (MMA, 2019). Depending on the index obtained, the air quality score could be ranked with Good, Regular, Poor, Very Poor, or Terrible.

$$AQI = I_{ini} + \frac{I_{fin} - I_{ini}}{C_{fin} - C_{ini}} \times (C - C_{ini})$$

Equation 3.1 Air Quality Index formula

where, I_{ini} is a value that corresponds to the initial concentration of the range, I_{fin} is a value that corresponds to the final concentration of the range, C_{ini} is the initial concentration of the range in which the measured concentration is located, C_{fin} is the final concentration of the range in which the measured concentration is located and C is the measured pollutant concentration.

According to CONAMA Resolution 491/2018, (from Portuguese, *Conselho Nacional do Meio Ambiente*) (CONAMA, 2018) the concentration values that classify quality as "Good" are the values recommended by the World Health Organization as being the safest for human health for short-term exposure and are related to the final standards of air quality. The other AQI ranges represent different levels of health effects associated with increased pollution. The daily AQIs are calculated based on the 24-hour average concentration of SO_2 , daily average 1-hour maximum concentration for NO_2 and the daily average 8-hour maximum concentrations for CO and O_3 . According to the Brazilian legislation and Brazilian air quality guideline the ranges of AQI values related to air quality can be classified into five classes as presented in Table 3.3.

Table 3.3 - Air Quality Index (AQI) range and air classification according to index values

Class	Range	Air classification	Color identification
I	0 – 40	Good	Green
II	41 – 41	Moderate	Yellow
III	81 – 120	Poor	Orange
IV	121 – 200	Very poor	Red
V	201 – 400	Terrible	Purple

3.3.6. Hybrid Single-Particle Lagrangian Integrated Trajectory

To evaluate air mass origins, a Hybrid Single-Particle Lagrangian Integrated Trajectory (HYSPLIT) model implemented by Air Resources Laboratory-NOAA was used to simulate and cluster backward trajectories for the period between March 1st and April 12th, 2020. (Rolph et al., 2017; Stein et al., 2015) The simulation was done directly on the site of the Air Resources Laboratory-NOAA considering 120 h for backward trajectories of one day of each week.

3.4. Active atmospheric biomonitoring

The following description of methods refers to chapters 8, 9, 10 and 11, from the page 150.

3.4.1. Study area

The biomonitoring assessments was carried out in the Metropolitan Region of Rio de Janeiro (MRRJ) between July 2019 and November 2020. Five sampling sites with different characteristic were chosen, namely two industrial sites: Santa Cruz and Duque de Caxias, two urban sites: Ramos and Urca, and one urban and ship port site: Niterói. Figure 3.6 displays the sampling sites in more detail and Table 3.4 presents sampling sites characteristics.

Table 3.4 Characteristics of atmospheric biomonitoring sites located in the metropolitan region of Rio de Janeiro

Sampling site	Characteristics
Santa Cruz	Intense flow of light and heavy vehicles, 1,5 km from the Santa Cruz Industrial District, Sepetiba Bay, and Itaguaí Port Complex.
Duque de Caxias	Located at 2 km away from a road with intense flow of light and heavy vehicles and near to unpaved roads, 500 m away from Duque de Caxias Petrochemical Complex.
Ramos	Located on the margins of avenida brasil, the most important avenue in the city of Rio de Janeiro, 1 km from the galeão air base and international airport and 5 km from the manguinhos refinery.
Urca	A residential neighborhood in the southern part of the city of Rio de Janeiro, 5 km from the marina, under the strong influence of the sea breeze and the movement of boats.
Niterói	Located 200 meters from one of the accesses to the Rio-Niterói bridge, which connects to the city of Rio de Janeiro, and 250 meters from the port area of Niterói.

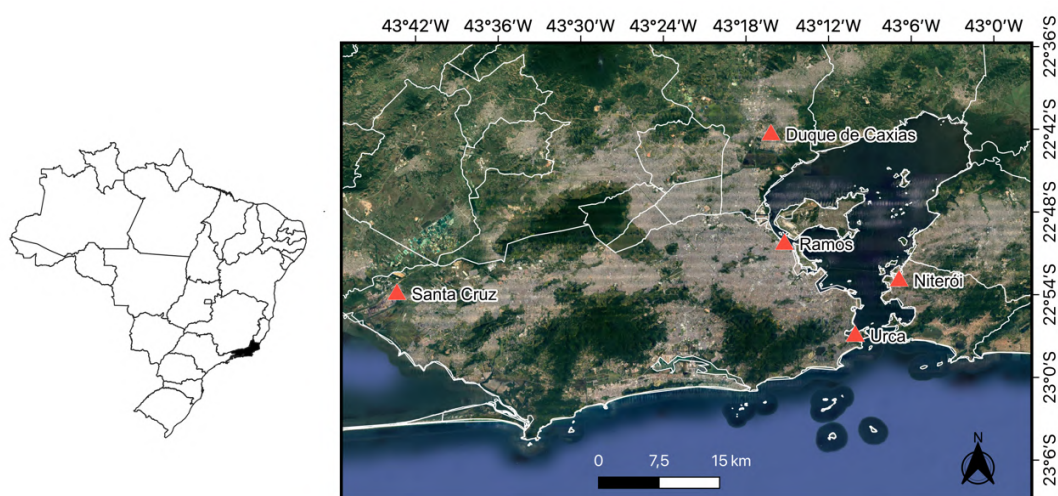


Figure 3.6 Atmospheric biomonitoring sampling site locations in the Metropolitan Region of Rio de Janeiro, southeastern Brazil.

An active biomonitoring approach was applied. *Tillandsia usneoides* and *Tillandsia stricta* were collected in Seropédica, RJ, a rural area with reduced air pollution sources, and washed with ultrapure water to remove particles deposited on leaf surfaces. *T. usneoides* were divided into 10 g samples, while *T. stricta* were divided into individuals weighing 15 – 20 g. Figure 3.7 presents *Tillandsia* species applied as atmospheric biomonitors.



Figure 3.7 (a) *Tillandsia usneoides* washed with ultrapure water and divided into 10 g samples; (b) *Tillandsia stricta* washed with ultrapure water and divided into individual weighing 15-20 g.

A total of 40 samples of each *Tillandsia* species were installed in July 2019 at each sampling site, placed on trees, and fixed using nylon thread. Samplings were performed in October 2019, January 2020, and November 2020, removing three to five plants each time. After each sampling, the unwashed plants were stored inside plastic bags at -20 °C until processing for MT and metal determinations.

Topsoil and deep soil samples were collected for determination of the elemental composition necessary for calculation of the enrichment factor, which is an approach to assess the contribution of anthropogenic sources to air pollutant emissions. At each of the monitoring sites five surface soil samples were collected with the aid of adhesive paper in the dimensions of 30 x 30 cm. In the laboratory, the particles that adhered to the adhesive were removed and homogenized, forming a composite sample. The deep soil was collected 20 cm from the surface. Five soil samples were collected and later homogenized to form a composite sample. These samples were stored under refrigeration for later chemical analysis.

3.5. Metal quantification

The following description of methods refers to chapters 8, page 146.

The analyses to determine the metals in the samples were carried out in partnership with the spectrometry laboratory of PUC-Rio (LABSPECTRO). The total metal content in plant tissue and soil samples was performed after acid decomposition. For trace element extraction, 200 mg of fresh mass of plants or soil were weighed into polypropylene tubes, to which 3 mL of HNO₃ (65 %) was subsequently added. After heating at 100 °C for 4 h, the samples were diluted with ultrapure water to complete the volume of 30 mL and then set aside for elemental quantification by Inductively Coupled Plasma Mass Spectrometry (ICP-MS) (Nexlon 300X, Perkin Elmer and 7500ce, Agilent). A ¹⁰³Rh solution (40 µg L⁻¹) was applied as internal standard. External calibration was performed using multielement standards at six different concentrations for quantitative metal and metalloid determinations.

The multi-element standards were prepared at different concentrations for certain groups of elements. Standard ranging from 1 µg L⁻¹ a 80 µg L⁻¹ for PE 29 (Al, Ag, As, Ba, Be, Bi, Ca, Cd, Co, Cr, Cs, Cu, Fe, Ga, In, K, Li, Mg, Mn, Na, Ni, Pb, Rb, Se, Sr, Tl, V, U, Zn), PE 12 (B, Ge, Mo, Nb, P, Re, S, Si, Ta, Ti, W, Zr) and Sn; from 50 µg L⁻¹ to 1000 µg L⁻¹ from PE 5 (Ca, Fe, K, Mg, Na); from 0.2 µg L⁻¹ to 20 µg L⁻¹ from PE 17 (Ce, Dy, Er, Eu, Gd, Ho, La, Lu, Nd, Pr, Sm, Sc, Tb, Th, Tm, Y, Yb); from 1 µg L⁻¹ to 20 µg L⁻¹ for Hg; from 0.5 µg L⁻¹ to 15 µg L⁻¹ for Au µg L⁻¹ and from 10 µg L⁻¹ to 800 µg L⁻¹ for Br µg L⁻¹.

The operational conditions of ICP-MS Nexlon were 1100 W radiofrequency power, 15 L min⁻¹ Ar flow rate to the plasma, 1.0 L min⁻¹ auxiliary gas flow rate and 1.06 L min⁻¹ for nebulizer gas flow rate. The operational conditions of ICP-MS 7500ce were 1500 W radiofrequency power, 1.0 L min⁻¹ Ar flow rate to the plasma, 0.15 L min⁻¹ auxiliary gas flow rate and for nebulizer pump with 0.10 RPS.

3.6. Subcellular distribution of metals in atmospheric biomonitors

The following description of methods refers to chapters 9, page 166.

3.6.1. Metallothionein purification and determination

The analyses for quantification of oxidative stress biomarkers in the samples were carried out in partnership with the Laboratory for Environmental Health Assessment and Promotion (LAPSA) of the Oswaldo Cruz Institute located at Fiocruz – RJ. The MT purification process results in three subcellular fractions and was performed according to Erk et al. (2002). Briefly, 200 mg of each plant tissue were manually homogenized in a Tris-HCl buffer (pH 8.6) containing β -mercaptoethanol and phenyl-methyl-sulphonyl-fluoride for 1 min, using a glass dounce homogenizer, and then, centrifuged at 20,000 x g at 4 °C for 60 min. The resulting supernatants (termed the thermolabile fraction – TLF) were separated from the precipitates (termed the insoluble fraction – IF) and heated at 70 °C for 10 minutes. Another centrifugation step was performed at 20,000 x g and 4 °C for 30 min to obtain the final thermostable fraction (TSF) containing MT and bioavailable metals.

MT determinations followed the procedure established by Viarengo et al. (1997). Briefly, an EDTA (4.0 mmol L^{-1}) solution containing HCl (1.0 mmol L^{-1}), and 5,5-dithiobis-2-nitrobenzoic acid (0.43 mmol L^{-1}) prepared in NaCl (2.0 mmol L^{-1}) and phosphate buffer (pH 8.0) was added to the TSF. After 30 min incubation in the dark, MT concentrations were quantified by UV-Vis spectrophotometry at 405 nm. This quantification is based on Elman's reaction, where a thiol group in the MT cleaves the sulfur bond present in the DTNB (5,5-dithiobis-2-nitrobenzoic acid), producing an ion that is yellow in a neutral-alkaline solution. The external analytical curve was prepared with reduced glutathione (GSH) standard. The stoichiometrical conversion between GSH and MT concentrations is MT:GSH of 20:1.

3.6.2. Subcellular metal quantification

During the MT purification process, 100 μL aliquots of each obtained fraction (IF, TLF, and TSF) were reserved for bioavailable metal quantifications. An acid digestion of each aliquot was performed using HNO_3 at 100 °C for 4 h. After cooling down, the samples were diluted with ultrapure water to 10 mL and analyzed for elemental determinations by ICP-MS, employing the US EPA method 6020B (US EPA, 2014). The same procedure was applied to two standard reference materials, SRM 1515 – Apple Leaves and SRM 1547 – Peach Leaves, following previously standardized conditions applied by Beringui et al. (2021a) and Monteiro et al. (2019). A ^{103}Rh

solution ($40 \mu\text{g L}^{-1}$) was applied as internal standard. External calibration was performed using multielement standards at six different concentrations for quantitative metal and metalloid determinations.

The limits of quantification (LOQ) for each investigated element were calculated according to the Brazilian National Institute of Metrology, Quality and Technology (INMETRO, 2016).

3.7. Oxidative stress biomarkers in atmospheric biomonitors

The following description of methods refers to chapter 10, page 184.

3.7.1. Reduced glutathione purification and quantification

The GSH purification procedure was applied in 300 mg of wet plant. After homogenization with 800 μL of buffer sodium phosphate 0.1 mol L^{-1} (pH 6.5) containing sucrose (0.25 mol L^{-1}) and EDTA (1.0 mmol L^{-1}), the extracts were centrifuged at 13,500 RPM and $4 \text{ }^\circ\text{C}$ for 30 minutes and the supernatant used to GSH quantification.

A solution of DTNB (0.25 mmol L^{-1}) prepared in sodium phosphate buffer 0.10 mol L^{-1} (pH 8.0) was added to an aliquot of final extract followed by incubation in the dark for 15 minutes, and then spectrophotometric quantification in 412 nm.

The analytical curve was prepared using a stock solution of GSH 10 mmol L^{-1} to prepare standard solution with concentration varying from 30 to $300 \mu\text{mol L}^{-1}$.

3.7.2. Hydrogen peroxide purification and quantification

This analysis follows the procedure proposed by Alexieva et al. (2001). The purification was performed in 100 mg of wet plants and homogenization with 300 μL of trichloroacetic acid 0.10 % m/v. After centrifugation at $10,000 \times g$ and $4 \text{ }^\circ\text{C}$ for 15 minutes, the supernatant were used for quantification.

A potassium phosphate buffer 0.10 mol L^{-1} (pH 7.5) and KI solution (1 mol L^{-1}) was added to an aliquot of the final extract followed by incubation in the dark for 1 h and then quantification in 390 nm.

The analytical curve were prepared using a stock solution of H_2O_2 1.0 mmol L^{-1} to prepare standard solution with concentration varying from 1.0 to $10 \mu\text{mol L}^{-1}$.

3.7.3. Lipid peroxidation quantification

This procedure follows the TBARS assay (Abcam, 2019). The homogenization was performed in 100 mg of wet plants with RIPA buffer, prepared with Tris-HCl (0.05 mol L⁻¹ a pH 7.5), NaCl (0.15 mol L⁻¹), Triton x-100 (1 % m/v), sodium dodecyl sulfate (3.5 mmol L⁻¹) and sodium deoxycholate (24 mmol L⁻¹). After homogenization, extract was centrifuged at 1,600 x g and 4 °C for 10 minutes and the supernatant reserved for quantification procedure.

A solution of thiobarbituric acid 0.53 %, prepared in a solution 1:1 of acetic acid 10 % and NaOH 0.35 mol L⁻¹ with pH 4.1, and trichloroacetic acid 10 % were added to an aliquot of the final extract followed by heating at 90 °C for 1 h and then ice bath for 10 minutes to stop the reaction and centrifugation at 1,600 x g and 4 °C for 10 minutes. This final supernatant was used for malondialdehyde spectrophotometric quantification at 535 nm.

The analytical curve were prepared using a stock solution of malondialdehyde 100 µmol L⁻¹ to prepare standard solution with concentration varying from 0.5 to 50 µmol L⁻¹.

3.8. Association between oxidative stress biomarkers and metals

The following description of methods refers to chapters 11, page 197

This association is performed by coupling ICP-MS and HPLC, size-exclusion chromatography column to separate protein and peptides. Thus, it is possible to observe associations between the biomolecules and metal elements by superimposing the chromatogram and the spectrum.

In order to standardize the amount of proteins inject, the total protein in the TSF obtained from TM purification was quantified, following the proceed proposed by Peterson (1977). Two reagents were prepared for addition to an aliquot of the TSF. Reagent A: Na₂CO₃ 0.02 mol L⁻¹, KNaC₄H₄O₆ 0.02 mol L⁻¹, CuSO₄ 5H₂O 0.01 mol L⁻¹, NaOH 0.8 mol L⁻¹ e sodium dodecyl sulfate 10%; Reagent B: Follin Ciocalteau 1,6 %. After reagents addition, samples were incubated in the dark for 30 minutes and then quantified at 750 nm.

The analytical curve was prepared using a stock solution of bovine serum albumin 2 mg mL^{-1} to prepare standard solution with concentration varying from 10 to $70 \text{ } \mu\text{g mL}^{-1}$.

After quantification of total proteins, an aliquot of TSF Fraction of MT purification corresponding to $40 \text{ } \mu\text{g}$ of protein was used to prepare $20 \text{ } \mu\text{L}$ of solution to be injected into the HPLC. The 20 mmol L^{-1} Tris-HCl buffer pH 7.4 is used as eluent and detection is done by a UV/Vis detector at 254 and 280 nm. A Superdex™ - 75 ($10 \times 300 \times 13$) m separating column (GE Healthcare®, Sweden) was used with a flow rate of 0.6 mL min^{-1} , allowing optimal resolution between 3 and 87 kDa.

The isotopes monitored in ICP-MS were: Al, As, Cd, Co, Cr, Cu, Fe, Ge, Hg, La, Mn, Mo, Ni, Pb, Rb, Sb, Se, Sn, Ti, V, Zn.

Column calibration was performed with Bovine Serum Albumin (BSA) (67 kDa, Zn determination), MT-I (7kDa Cd determination) and GSH (0.3 kDa Cu determination) following the same procedure adopted by Lavradas et al., 2016.

3.9.Data analysis of metal and ecotoxicological data

The following description of methods refers to chapters 8, 9, 10 and 11, page 146.

The R software was used for all statistical assessments (R CoreTeam, 2019). The Shapiro-Wilk test was first applied to verify data normality. As the data were non-normally distributed, the Mann-Whitney test was applied to verify statistical differences between the two employed *Tillandsia* species sampled at the same site and between the same species at the different sampling sites. Spearman's correlation test was applied to evaluate correlation between total metal concentrations, metals in the three different purified fractions, MT concentrations and between biomarkers and total metal concentration with biomarkers. Only significant ($p < 0.05$) and moderate to strong ($\rho > 0.40$) correlations were considered, following the classification proposed by Bryman and Cramer (2004).

The packages `xlsx` for importing dataset (Dragulescu and Arendt, 2020), `ggplot2` was applied for graphic design (WickhamHaddley, 2016), `tidyr` for data arrangement (WickhamHadley and Girlich, 2022), `dplyr` and `reshape2` (WickhamHadley, 2007; WickhamHadley et al., 2022) for data manipulations, `RColorBrewer` for color palettes

selection (Neuwirth, 2014), Hmisc for Spearman correlation (Miscellaneous and Yes, 2021), and ggpubr for statistical differences (Kassambara, 2020).

To evaluate the accumulation of metals in the tissue of the biomonitors after the exposure period, the enrichment to reference ratio (ER) was calculated, following the same procedure adopted by Beringui and Huamán De La Cruz and et al., 2021; De La Cruz Alex Rubén H. et al., 2020. This parameter consists of the ratio between the concentration of the analyte in the plant after exposure and in the sample reserved before transplanting. According to Fartei $0.75 < ER < 1.25$ indicate normal conditions, $1.25 < ER < 1.75$ indicate accumulation, and $ER > 1.75$, severe accumulation.

The enrichment factor (EF) relative to soil was calculated to verify the contribution of anthropogenic sources. The EF was calculated according to the expression proposed by Olmez et al., 1985 that consists of the ratio of the analyte and a reference element (e.g. Fe and Al) found in the sample divided by the ratio in the soil. According to Wen et al., 2007 for atmospheric particles $EF < 1$ indicates no enrichment; $1 < EF < 3$ consists in low enrichment; $3 < EF < 5$, moderate enrichment; $5 < EF < 25$, high enrichment, and $EF > 25$, very high enrichment.

4 Assessment of concentration and inorganic composition of particulate matter sampled in Rio de Janeiro state

Karmel Beringui^a, Maria Fernanda C. Quijano^a, Elizanne P. S. Justo^a, Luciana Maria Baptista Ventura^{a,b} e Adriana Gioda^a

^aDepartamento de Química, Pontifícia Universidade Católica do Rio de Janeiro, 22451-900 Rio de Janeiro – RJ, Brasil

^bInstituto Estadual do Ambiente, 20081-312 Rio de Janeiro – RJ, Brasil

Corresponding author: Adriana Gioda - agioda@puc-rio.br

Published: Química Nova, V. 44, N. 6 (2021), 737 - 754

Abstract

Cities urbanization and modernization increase emission sources, contributing to particulate matter (PM) composition heterogeneity and enhance the risk to human health and environment. This paper intends to survey the studies on particulate matter carried out in the state of Rio de Janeiro. The sampling of PM is generally made using Hi-Vol samplers to collect particles in fiberglass filter during 24 h every 6 days. Spectrometric techniques are used for elemental determination and ion chromatography for water-soluble species. The Environmental State Institute (INEA) is responsible for air quality monitoring in RJ. After 30 years, air quality standards have become more stringent and have included new pollutants. The highest PM concentrations were found in urban and industrial sites and the lowest in places away from urban activities or near the coast. Over the years, PM concentrations near steel complexes reduced even below the limits and varied at other places, remaining above the limits. Nitrate and sulfate were the main ionic compounds, and Fe, Al and Zn were the major elements in PM samples. It was also found Ni, V, Cd, Pb and Cu. Although

air quality monitoring is efficient, it still needs to be improved to help reduce the environmental impact.

Keywords: atmospheric pollution; particulate matter; chemical composition.

4.1. Introduction

Particulate matter (PM) consists of liquid or solid particles suspended in air that are up to 100 μm in diameter (Seinfeld et al., 1998). The term aerosol is used to refer to the colloidal suspension of liquids or solids in a gas. In the context of air quality assessment, however, the term particulate matter is more appropriate, as it refers only to suspended particles.

All particulate matter suspended in air is called Total Suspended Particles (TSP), but PM can be classified according to the aerodynamic diameters of the solids. Aitken nuclei, also called, ultrafine particles or nanoparticles ($\text{PM}_{0.1}$), are those with diameters smaller than 0.1 μm . Solids with diameters less than 2.5 μm form the $\text{PM}_{2.5}$ and correspond to the fine fraction of particulate matter. Particles with diameters less than 10 μm form the PM_{10} , while those with diameters between 2.5 and 10 μm correspond to the coarse fraction of the particulate matter (AlvesCélia A., 2005; Kim et al., 2015; Lenzi and Fávero, 2008; Morales et al., 1998; Sanderson et al., 2014).

PM pollution is considered one of the main environmental problems in recent decades. Due to the importance of this pollutant, its concentrations can be used to assess the air quality of a given region (Gioda and Amaral and et al., 2011; He et al., 2017; Spencer and Van Heyst, 2019). To deal with the challenge of environmental pollution, many studies have sought to understand its formation, composition, and transport, among other factors that have allowed air quality limits to be set. Once the intrinsic characteristics of particles were established through studies conducted since the 1980s, research focused then on the evaluation of the effects on human health, the ecosystem, and climate change (Fuzzi et al., 2015; Gioda et al., 2016).

Since the 1990s, some studies have sought to assess the impacts of PM on human health, although the majority of research has evolved to the chemical characterization and impact on climate (Fuzzi et al., 2015). The suspended particles act in important climatic processes, such as: i) participation in cloud formation, because they act as condensation nuclei, which leads to rainfall; ii) contribution to the

Earth's albedo, absorbing or reflecting the radiation incident on the surface of the planet; and iii) action in the ocean-troposphere exchange through marine *spray* and soil resuspension (Al-Thani et al., 2018; Fuzzi et al., 2015; Gioda and Amaral and et al., 2011; Lenzi and Fávero, 2008; Pöschl, 2005; Ventura et al., 2018).

PM can come from different emission sources, whether natural (marine spray, natural forest fires, volcanic emissions, vegetation emissions, and desert sandstorms) or anthropogenic (vehicular emissions, biomass or fuel burning, and industrial activities). PM can have primary origin, when directly emitted into the atmosphere, or secondary origin, when the primary pollutants react, producing new substances (Alves., 2005; Fuzzi et al., 2015; Spencer and Van Heyst, 2019). Primary particles tend to form the coarse fraction of the particulate material, because they are produced by the mechanical fragmentation of the larger ones; while secondary particles make up, mainly, the finest fraction, because they are formed by nucleation and condensation processes followed by chemical reactions (Alves., 2005; Seinfeld and Pandis, 2006).

Coarse particles can be removed from the atmosphere by dry deposition derived from the action of gravity. Thus, due to the greater mass and velocity of fall, the deposition occurs close to the emission sources. Fine particles, which are removed mainly by rainfall, have a longer residence time in the atmosphere and can therefore be deposited far from the emission source (Al-Thani et al., 2018; Grantz et al., 2003; Pöschl, 2005). Wet deposition, the main process for removing particles from the atmosphere, can occur through two processes: i) rainout or in-cloud, which consists in the formation of clouds through the nucleation of fine particles; ii) and washout or below-cloud that results from the action of raindrops that carry the suspended particles below the clouds, removing them from the atmosphere (Seinfeld and Pandis, 2006).

The main concern about air pollution is due to the damage that pollutants can cause to human health, especially in a scenario of continuous rise of emissions and the expansion of urbanization (Gulia et al., 2015; Mateus et al., 2013; Santos et al., 2017). This concern, however, is not recent and has been recorded in history from older times. There are, for example, records of popular protests against the use of coal since the Middle Ages in the United Kingdom, while in Paris there was a ban on the emission of nauseating fumes in the earlier fourteenth century. The intensification of coal use after the Industrial Revolution highlighted air pollution. There are records of several cases of sulfurous haze in London since the 17th century, which led to the development of air pollution control measures in the 19th century (Alves, 2005). One

of the most important episodes of air pollution occurred in London in 1952 (The Big Smoke), when a dark fog spread over the city and weather conditions made it difficult to disperse (Bell et al., 2004). During the fog, 4,000 deaths directly related to particle exposure and 100,000 cases of illness related to the episode were reported (Ware et al., 1981). Similar episodes occurred in Donora, and New York in the USA. Since these events, more stringent legislation has been developed to control air pollution. These laws are periodically revised in order to guarantee the air quality. Associated with the pollution control actions, technological advances have contributed to the improvement of air quality (Calef and Goble, 2007; Giles et al., 2011; Landrigan, 2017).

Despite the concern about air quality and the advances achieved in recent decades, according to the World Health Organization (WHO), 91 % of the world's population lives in cities where PM_{2.5} concentrations exceed the recommended annual limit of 10 µg m⁻³. As a result, about 4.2 million people die annually as a result of exposure to air pollution (WHO, 2020). As the particle diameter decreases, the penetration ability into the respiratory system increases, and it can reach the lung alveoli where the PM components can be transferred to the bloodstream (Atkinson et al., 2010; Fajersztajn et al., 2017; Kim et al., 2015; Löndahl et al., 2006).

In recent decades, studies aimed at evaluating the impacts of PM on human health are predominant. These studies seek to verify the association between exposure to PM and the development of several diseases, as well as to evaluate the impact in different population groups, such as children, young people, the elderly, and professionals who work exposed to air pollution (Fajersztajn et al., 2017; Hamra et al., 2014; Kisku et al., 2013; Paulo et al., 1998; Saldiva et al., 1995). Some research conducted in different parts of the world shows that temporary or continuous exposure to PM can be associated with respiratory and cardiovascular diseases and cancer (Cepeda et al., 2017; Fajersztajn et al., 2017; Gioda and Amaral et al., 2011; Hays et al., 2011; Kim et al., 2015; Lin et al., 2005; Mateus et al., 2013; Song and Gao, 2011). Children may be more seriously affected, as it has been found that maternal exposure to high levels of PM can lead to low birth weight, prematurity, increased fetal mortality, and impaired lung development, including irreversible deficits (Guaita et al., 2011; Kim et al., 2015; Mölter et al., 2013; Pope et al., 1989). Together with children, the elderly complete the group of those most susceptible to respiratory diseases caused by

exposure to PM, because in childhood the immune system is not fully developed and in the elderly it is already weakened (Fuzzi et al., 2015; Kim et al., 2015).

Although fine particles attract most attention due to their effects on human health, coarse particles can cause damage to ecosystems, since their components can be absorbed into the soil or directly by plants (Datta et al., 2016; Rai, 2016b). The impact on the environment depends on the composition and the surface on which PM is deposited, since its components can act as nutrients or pollutants (Gioda and Amaral et al., 2011; Grantz et al., 2003). In an ecosystem, living organisms are in constant interaction with abiotic elements, and some studies show that plants can act as pollution filters, since they remove pollutants from the environment (Baldauf, 2017; Chen et al., 2016a; Escobedo et al., 2011; Rai, 2016b). However, these substances when absorbed by plants can cause damage such as blocking stomata, organelles responsible for gas exchange, or compromising physiological processes such as photosynthesis or protein production (Rai, 2016b).

Besides altering the composition of the soil on which it is deposited, PM can also contribute to the acidification of soil or aquatic ecosystems, and can cause damage to buildings and monuments (Al-Thani et al., 2018; González and Aristizábal, 2012). The change in pH can be harmful to the endemic species of a given habitat or even lead to their death (Wu and Zhang, 2018). Acid deposition occurs both wet and dry. In the wet mode, particles containing SO_4^{2-} and NO_3^- form cloud condensation nuclei, giving rise to acid rain through the reaction between these ions and water molecules. Dry acidification occurs when particles containing strong acid ions are deposited on surfaces with a high percentage of moisture, which causes the formation of the corresponding acids (González and Aristizábal, 2012).

The heterogeneity in composition and spatial distribution of PM depends on meteorological variables, topography, emission sources and particle morphology (Gioda and Amaral and et al., 2011; Gulia et al., 2015; Kim et al., 2015). The heterogeneity is more pronounced near the emission sources, because as transport away from the sources occurs, the tendency is for greater homogeneity due to atmospheric processes (Fuzzi et al., 2015). The longer residence time of fine particles in the atmosphere makes them more susceptible to compositional changes along transport, which can make source attribution more difficult (Fuzzi et al., 2015; Mateus and Gioda, 2017).

The main components of PM are carbon compounds, in their different forms (organic, inorganic and elemental) (Pöschl, 2005). In addition to these, water-soluble species represent about 30% of the particle composition (Shen et al., 2009). Metallic elements and polycyclic aromatic hydrocarbons (PAH) are usually found in trace levels in PM, and contribute to the increase of particle toxicity, both for human health and for the ecosystem (Al-Thani et al., 2018; Bilos et al., 2001; Kim et al., 2015; Song and Gao, 2011). The fine PM fraction, especially, can also have other toxic organic components, because in the process of formation of these particles the volatile organic compounds (VOCs) are transferred from the gaseous phase to the particulate phase and undergo reactions. VOCs are emitted from natural sources, such as plants, or anthropogenic sources, such as the burning of fossil fuel (Fuzzi et al., 2015; Sousa et al., 2016). In addition to chemicals, biological material is also part of the composition of PM. Biogenic particles are made up of cell fragments, pollen, and spores (Kim et al., 2015; Pöschl, 2005).

The state of Rio de Janeiro was the pioneer to establish air quality monitoring in 1967 and, therefore, presents the largest historical series of atmospheric monitoring data, in addition to the largest quantity of pollutants monitored per station (IEMA, 2014; Ventura and Ramos and Gioda and et al., 2019). Atmospheric monitoring in the state is responsibility of the State Environmental Institute (from Portuguese, *Instituto Estadual do Ambiente* - INEA), which has 84 air quality monitoring stations and, through environmental licensing, receives data from stations operated by companies with significant polluting potential (Instituto Estadual do Ambiente, 2020).

Most studies conducted in Rio de Janeiro related to PM air pollution follow the standards established by the Brazilian Association of Standards and Techniques (from portuguese, *Associação Brasileira de Normas e Técnicas* - ABNT), which presents the same procedure recommended by international environmental agencies for PM sampling. Thus, the particles are collected using high volume air samplers (Hi-Vol). After chemical treatment, the elemental composition is determined by techniques such as flame atomic absorption spectrometry (FAAS), X-ray fluorescence (XRF) Inductively coupled plasma optical emission spectrometry (ICP OES) and inductively coupled plasma mass spectrometry (ICP-MS). The ionic composition has been determined by ion chromatography (IC), the elemental carbon composition by total organic carbon analyzer (TOC) and the PAH concentration by gas chromatography-mass spectrometry (GC-MS) (Gioda and Amaral and et al., 2011; Gioda et al., 2004,

2013; Godoy. et al., 2009; Loyola et al., 2012; Maia et al., 2014; Mariani and Mello, 2007; Mateus and Gioda, 2017; Nascimento et al., 2011; Paulino et al., 2014, 2010; Quiterio, 2004, 2005; Sella et al., 2006; Soluri et al., 2007; Toledo et al., 2008).

Considering the importance of particulate matter for air quality assessment, this article aims to carry out a literature review of studies on the concentration, size and chemical composition of particulate matter (TSP, PM₁₀ and PM_{2.5}) sampled in the state of Rio de Janeiro, since studies in this area were started in 1981 until the most recent studies referring to data obtained in 2017.

4.2. International air quality standards

Given the importance of PM and its effects on human health and the environment, some international institutions set limits for the daily and annual average concentration of PM₁₀ and PM_{2.5}. The World Health Organization (WHO), based on epidemiological studies, provides recommended guidelines on air quality standards for pollutants that pose a risk to the population's health, aiming to reduce their impact. For PM_{2.5}, the WHO recommends air quality standards for the fine fraction, 25 µg m⁻³ and 10 µg m⁻³ for the daily and annual average concentration, respectively. For the coarse PM fraction, the daily and annual limits are 50 µg m⁻³ and 20 µg m⁻³, respectively (WHO, 2005). The United States Environmental Protection Agency (USEPA) sets daily limits of 35 µg m⁻³ and 150 µg m for PM_{2.5} and PM₁₀, respectively. There is no recommended value for the annual average of PM₁₀, but for PM_{2.5} the limit is 12 µg m⁻³ (USEPA, 2016). The Environment Directorate General of the European Commission sets for PM_{2.5} only the annual limit of 25 µg m⁻³. For PM₁₀, on the other hand, daily limits are set at 50 µg m⁻³, and annual limits at 40 µg m⁻³ (DG Environment Standards, 2008). These limits set by the most important environmental agencies in the world are used as reference for the development of national air quality standards in several countries.

The composition of PM is important to estimate the impacts caused, so some international agencies have inserted into their air quality standards limits for the concentration of some substances in particulate matter. The USEPA sets a limit of 0.5 µg m⁻³ for Pb, and the limits of 0.5 µg m⁻³- 6 ng m⁻³- for As, 5 ng m⁻³ for Cd, and 20 ng m⁻³ for Ni. Although air quality standards exist for only a few elements, many studies

have been conducted that attempt to provide a broader chemical characterization of particulate matter.

4.3. Brazilian legislation

In Brazil, the concern with air quality began in the 1970s, during a period of intense industrial growth. The first Brazilian legislation that established air quality standards in Brazil was *Portaria Minter 231/1976*, which considered the pollutants: Particulate Matter, SO₂, CO and Photochemical Oxidants. In the 1980s there was an increase in the automobile fleet, which encouraged the National Council on the Environment (from Portuguese, *Conselho Nacional do Meio Ambiente* - CONAMA) to create CONAMA Resolution 18/1986, which aimed to control vehicle emissions. Subsequently, the need arose for a national air pollution control program, so in 1989 CONAMA created the National Air Quality Control Program (from portuguese, *Programa Nacional de Controle da Qualidade do Ar* - PRONAR), through Resolution 05/1989. PRONAR aimed at sustainable development through the development of control instruments, such as the establishment of emission limits, air quality standards, and emission inventories of sources. After the creation of PRONAR, the *Portaria Minter 231/1976* was revoked by CONAMA Resolution 003/1990, which, besides maintaining the standards already established, included other pollutants, considering more recent scientific information. This resolution established air quality standards for TSP, PM₁₀, SO₂, CO, NO₂, and smoke.

Resolution 003/1990 considered two concentration values for each pollutant: i) primary standard, above which the pollutant could cause health risk and ii) secondary standard, below which minimal effects to health and the environment are expected. This resolution remained in force for almost 30 years without revision, although scientific studies already pointed out the importance of monitoring other pollutants, in addition to the reduction of emission limits. Despite the scientific evidence, the standards that remained in force for decades in Brazil were very outdated in relation to standards recommended by the WHO and established by the USEPA. Regarding PM, the Brazilian legislation recommended the monitoring of TSP and PM₁₀, and considered as air quality standards concentrations much higher than the agencies. The most recent WHO and USEPA documents, which are from 2005, already included

PM_{2.5} and presented PM₁₀ concentrations up to three times lower than the Brazilian legislation.

The publication of scientific data and revisions made by international environmental agencies with the establishment of more restrictive limits stimulated the revision of the Brazilian legislation. After a long period of elaboration, in 2018, Resolution 003/1990 was replaced by CONAMA Resolution 491/2018 which presents more restrictive standards and includes new pollutants, such as MP_{2.5} and Pb in TSP (CONAMA 491, 2018; "CONAMA 3, 1990). This document was elaborated based on the reference values recommended in 2005 by the WHO. Three intermediate air quality standards (IS) and one final standard (FS) were established, which should be adopted sequentially, with the FS being equivalent to the values suggested by the WHO. The creation of the ISs was necessary due to the large difference between the old standards and the final standards foreseen in Resolution 491/2018. Such values are intended to allow state environmental agencies and emission officials to adjust to the new, more restrictive, air quality standards. As of the date of enactment of Resolution 491/2018 the IS-1 was adopted and the progression between the IS to the FS should occur according to emission control plans prepared by state environmental agencies. So far none of them have disclosed the planning to make the progression between the ISs nor the deadline for adopting the FS.

With the update of the air quality standards, the Brazilian legislation now presents limits for the three PM fractions. The 2005 WHO guide no longer sets limits for TSP, so the values for TSP were not changed in Resolution 491/2018. The limits for PM₁₀ were greatly reduced (by 20 % to 30 %) compared to FS. This gap between the values of the two resolutions can be attributed to the long time without occurrence of standards update.

Although there is a law that sets standards for air quality, the national monitoring network is quite small. According to the Institute of Energy and Environment (IEMA), in 2018 only 9 federal units, out of 27, had programs for air quality monitoring, which are managed by state agencies, except for Bahia, where monitoring is carried out by private companies (IEMA, 2020). Besides the reduced number of monitoring stations, the data issued by the environmental agencies reveal that not all the standards established in the law are monitored in all the stations. Many present discontinuity in operation, besides the low representativeness of the data, which compromises the diagnosis of air pollution (IEMA, 2014).

The Table 4.1 presents the air quality standards established by the CONAMA resolutions of 1990 and 2018. The new resolution includes limits for PM_{2.5}, particles that pose a greater risk to health due to their greater ability of penetration in the respiratory system and greater relationship with anthropogenic emissions. In addition, it can be verified that, for the first time, the legislation considers the composition of the particles when establishing Pb concentration limits in TSP in specific areas, according to the characteristics of the emission sources. The need for monitoring this parameter must be defined by the competent environmental agency. The USEPA was the pioneer agency in establishing standards for Pb concentration in particulate matter, establishing, in 1978, a concentration of 1.5 $\mu\text{g m}^{-3}$. Over the years, the standard for Pb was revised, reaching the current value of 0.5 $\mu\text{g m}^{-3}$, which was used by CONAMA as a reference for the new resolution on air quality standards in Brazil.

Table 4.1 Air Quality Standards of the Brazilian legislation (CONAMA)

Atmospheric pollutants	Period	RE 491/2018				RE 003/1990	
		IS-1 ($\mu\text{g m}^{-3}$)	IS-2 ($\mu\text{g m}^{-3}$)	IS-3 ($\mu\text{g m}^{-3}$)	FS ($\mu\text{g m}^{-3}$)	S 1° ($\mu\text{g m}^{-3}$)	S 2° ($\mu\text{g m}^{-3}$)
TSP	24 h	-	-	-	240	240	150
	Annual ^a	-	-	-	80	80	60
PM ₁₀	24 h	120	100	75	50	150	-
	Annual ^b	40	35	30	20	50	-
PM _{2.5}	24 h	60	50	37	25	-	-
	Annual ^b	20	17	15	10	-	-
NO ₂	1 h	260	240	220	200	320	190
	Annual ^b	60	50	45	40	100	100
SO ₂	24 h	125	50	30	20	365	100
	Annual ^b	40	30	20	-	80	40
CO	8 h ^c	-	-	-	10,000 ^e	10,000 ^e	-
	1 h ^c	-	-	-	-	40,000 ^f	-
O ₃	8 h ^c	140	130	120	100	-	-
	1 h ^c	-	-	-	-	160	-
Smoke	24 h	120	100	75	50	150	100
	Annual ^b	40	35	30	20	60	40
Pb	Annual ^d	-	-	-	0,5	-	-

^a Annual Geometric Mean/ Annual Arithmetic ^bMean/ ^cMaximum Daily Moving Average/ ^dMeasured at TSP ^e9 ppm/^f35 ppm.

4.4. Sampling of particulate matter

4.4.1. Sample Sites

In the state of Rio de Janeiro, studies on the concentration and composition of PM in cities²⁸ have already been carried out (Azevedo and Moreira, 1999; Azevedo et al., 2002; Gioda et al., 2004, 2016; Godoy et al., 2009; Justo et al., 2020; Loyola et al., 2006, 2009, 2012; Maia et al., 2014; Mariani and Mello, 2007; Mateus and Gioda, 2017; Mateus et al., 2020; Miranda et al., 2012; Nascimento et al., 2011; Paulino et al., 2010, 2014; Quijano et al., 2019; Quiterio et al., 2006; Quiterio et al., 2004, 2005; Rainho et al., 2014; Rainho et al., 2013; Sella et al., 2006; Soluri et al., 2007; Toledo et al., 2008; Ventura et al., 2017, 2018). Most of these were carried out in the metropolitan region, mainly in the city of Rio de Janeiro and in the municipalities of Baixada Fluminense. Figure 2.1 shows the location of the municipalities in the state of Rio de Janeiro in which studies on PM have already been carried out.

4.4.2. PM sampling

INEA performs atmospheric monitoring of gas concentrations such as SO₂, NO₂, O₂, CO, of particulate matter (TSP, PM₁₀ and PM_{2.5}) and some organic compounds such as benzene, toluene, ethylbenzene, meta, ortho, and para-xylenes, and total hydrocarbons (IEMA, 2014). It has two types of stations: (i) automatic monitoring system, in which sampling and analysis occurs in real time, every 5 seconds; this approach can be used for PM₁₀, MP_{2.5}, SO₂, NO₂, CO, O₃, benzene/toluene/ethylbenzene/xylene (BTEX) and Total Reduced Sulfur (TRS); ii) manual or semi-automatic monitoring system, those in which after being sampled, the sample is taken to the laboratory where it is analyzed; this approach can be applied for several air pollutants, as well as automatic monitoring, however, INEA uses it only for smoke, TSP, PM₁₀ and PM_{2.5}. After the validation of the PM concentration data, the filters containing the particles are not used by INEA, so they can be made available to research groups interested in chemical characterization of PM.

Some research groups have equipment similar to that used by INEA, which allows them to sample PM in areas of interest for their studies, including those in which there is no monitoring station of the state environmental agency. The PM sampling is performed using high volume samplers (Hi-Vol) following the Brazilian standard

methods (ABNT-NBR 9547 for TSP, ABNT-NBR 13412 for PM₁₀ and PM_{2.5}) that are in accordance with the detection method suggested by the USEPA. This equipment draws air at a constant flow rate (1.1 - 1.7 m³ min⁻¹), passing it through an *inlet* that selects the size of the particles to be retained on glass fiber, quartz, or Teflon® filters. Samples are taken continuously for 24 h every six days.

The mass of PM collected is determined by gravimetry, weighing the filters before and after sampling under controlled humidity (20 – 30 % ± 5%) and temperature (20 - 25 °C ± 2 °C) conditions. Dividing the weight by the product of flow rate and sampling time gives the concentration in masses of particles per sampled air volume (µg m⁻³).

Another way to sample PM is to use a stacked filter unit (SFU) system, which consists of one support for more than one filter, allowing it to be used to collect different particle sizes separately. In this case membranes with different porosities are used to sample the PM. The first membrane has larger pores to allow the passage of smaller particles, which will be retained in subsequent membranes with lower porosity. Like the Hi-Vol, the SFU uses a pump to aspirate air at a constant flow rate and a fixed sampling time (Hopke et al., 1997). This type of sampling allows the ratio between two particle sizes to be obtained and will inform which particles contribute most to the PM concentration. In addition, some studies use the ratio between particle sizes to characterize a particular region (Brook et al., 1997; Godoy et al., 2009; Soluri et al., 2007).

4.5. Particulate matter concentration

4.5.1. Results of the first diagnosis of the air quality monitoring network in Brazil

The first diagnosis of the air quality monitoring network in Brazil was prepared by the Institute for Energy and Environment and published in 2018 (IEMA, 2014). This report aimed to: i) disseminate the information and data generated by the existing monitoring networks in all Brazilian federal units under the responsibility of public or private power; ii) use such information to encourage discussion on the revision of PRONAR; iii) identify the difficulties in monitoring and propose alternatives for obtaining resources. This document gathered air quality monitoring data from the

Distrito Federal, Espírito Santo, Minas Gerais, Paraná, Rio de Janeiro, Bahia, São Paulo, Rio Grande do Sul, and Sergipe.

For the state of Rio de Janeiro it was considered data on particulate matter (TSP and PM₁₀), SO₂, NO₂, O₃ and CO sampled by INEA between 2000 and 2012 in 18 municipalities of the state. Table 17.1 presents the INEA stations that presented data for particulate matter and Tables 17.2 and 17.3 present the averages by municipality for TSP and PM₁₀, respectively. The averages of particulate concentrations were calculated using only the data considered representative.

The results presented in the diagnosis show that in many stations there was discontinuity of monitoring or data that were not considered representative, which is a problem for the efficient air quality evaluation. For both particle sizes, the municipalities of Rio de Janeiro and Volta Redonda were the ones that presented the most complete data series. Although Volta Redonda hosts important industrial enterprises, lower concentrations of TSP and PM₁₀ were found than in Rio de Janeiro. São Gonçalo and Belford Roxo, municipalities of the Baixada Fluminense (lowland), presented the highest concentrations of TSP, all of them above the annual limit established by CONAMA. São João de Meriti and Nova Iguaçu, also in Baixada Fluminense, had the highest concentrations of PM₁₀. The lowest concentrations of TSP and PM₁₀ were observed in the cities in the north of the state, in medium Paraíba (except Volta Redonda), in Guapimirim, Itaboraí, and Itaguaí.

In addition to the evident gap in Brazilian legislation, which remained in force between 1990 and 2018, it is apparent from the above that there has been little progress in air quality monitoring in Brazil, even in Rio de Janeiro, a pioneering state in atmospheric monitoring. The main barriers to this advancement were the low number of professionals involved, resulting in precarious monitoring coverage, and the lack of resources. Given this, in the 2018 document, it is argued that government agencies do not give due importance to air quality monitoring.

4.5.2. Influence of the 2016 Olympic Games on PM concentration

The city of Rio de Janeiro hosted the 2016 Olympic and Paralympic Games, which took place between August 5 and September 18 (Ventura et al., 2019). Since the Sydney Olympics in 2000, the International Olympic Committee (COI) has shown more concern about monitoring air quality, so monitoring some air pollutants, such as PM_{2.5},

has become one of the priorities of the regional committees (Ventura et al., 2019). Hosting such a mega event can lead to increased emissions, so increasing emission control measures and shutting down some activities in order to reduce traffic during events are practices that contribute to better air quality (De La Cruz et al., 2019). Due to the COI's encouragement of air quality monitoring and the hosting of a large event such as the Olympic Games, some studies have been conducted to assess the air quality before, during, and after this event. Figure 4.1 presents the average PM concentrations obtained in studies conducted at stations near the Olympic Games areas before, during, and after the event.

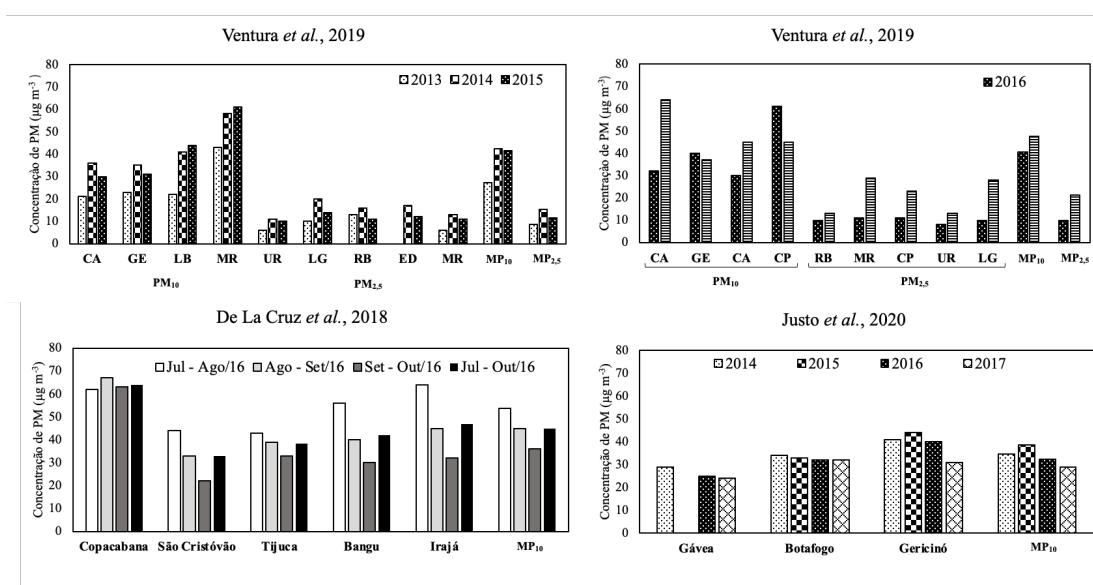


Figure 4.1 Average PM concentrations for stations near the 2016 Olympic and Paralympic Games sites (CA - Campo dos Afonsos, GE - Gericinó, LB - Leblon, MR - Maracanã, UR - Urca, LG - Lagoa, RB - Recreio dos Bandeirantes, EG - Engenho de Dentro and CP – Copacabana)

Justo et al. (2020) observed the highest concentrations of PM_{10} in 2014 in Gávea and Botafogo, having been attributed to the works related to the 2014 World Cup in both locations. In 2015, the highest concentrations were observed in the neighborhood of Gericinó, being attributed to the works of the Deodoro Olympic Park, located 300 m from the sampling site. Concentrations above the WHO limit ($20 \mu g m^{-3}$) occurred during the event, which took place during the dry season, which may have compromised the dispersion or removal of pollutants. The lower averages in 2017 may be attributed to the closure of construction sites.

In the study carried out by Ventura et al. (2019) in the years prior to the Olympic Games, PM_{10} concentrations were below the CONAMA limit and similar to those found in other large South American cities, with a similar degree of development to the city of Rio de Janeiro. The increase of $PM_{2.5}$ in the Barra da Tijuca region can be attributed to the construction works of the Bus Rapid Transit system. The higher concentrations observed in 2014 were attributed to emissions generated by construction, since in 2015, after the inaugurations, concentrations decreased.

Ventura et al. (2019) showed that only at the stations near the Copacabana Olympic region, PM_{10} concentrations were higher than the annual CONAMA limit in force during the Olympic Games period ($50 \mu\text{g m}^{-3}$). The concentrations observed in Rio de Janeiro were similar to those observed in Athens, Greece, in 2004 and much lower than those observed in Beijing, China, in 2008. Furthermore, these concentrations were similar to those recorded in the month of August in the previous three years. For $PM_{2.5}$ annual concentrations were lower than in previous years, which was attributed to the modifications in the city traffic with the implementation of the bus corridor and bus rapid transit.

De La Cruz et al. (2019) presented results similar to those of Ventura, Luciana M.B. e Ramos e Gioda e et al. (2019) regarding PM_{10} , because they recorded that only in Copacabana the concentrations were higher, exceeding the CONAMA limit. Bezerra et al. (2018) observed that the Air Quality Index showed lower values in 2016, which indicates that there has been an improvement in air quality. The authors attributed such improvement to restrictions on vehicular traffic.

Tsuruta et al. (2018) observed lower PM_{10} during the Olympic period, which was attributed to the decrease in vehicular flow due to the vacation period in schools and universities. Evaluation of the years prior to the event showed similar concentrations between 2011 and 2015, some violations of the CONAMA limit were observed between 2013 and 2015.

4.5.3. Results of air quality studies conducted in the state of Rio de Janeiro

The average concentrations of particulate matter (TSP, PM_{10} and $PM_{2.5}$) are shown in Figure 4.2. There is great variation in the average concentrations of the three particle sizes at the different sites evaluated. In addition, the range of the data at all

sites evaluated was pronounced, which indicates that such sites have different characteristics and variation in the amount or type of emission source.

In 10 of the 17 TSP evaluations, the averages observed were higher than the annual limit established by CONAMA ($80\mu\text{g m}^{-3}$). The highest average TSP levels were found by Loyola et al. (2009) in a bus station in Duque de Caxias and by Azevedo et al. (2002) in Campos do Goytacazes during the sugarcane burning period.

The lowest average concentrations of TSP were observed by Quiterio et al. (2006) in Ilha Grande, an environmental preservation area located 3 km from the mainland, where there is no car traffic. Loyola et al. (2006) found similar concentrations in the Médio Paraíba region. Although in this region there is industrial activity, the authors attributed the low TSP concentrations to industrial emission control measures imposed by INEA, then called FEEMA (from Portuguese, *Fundação Estadual de Engenharia e do Meio Ambiente*), because a reduction in PTS concentration from 245 to $66\mu\text{g m}^{-3}$ was observed from 1995 to 2004. This reduction in PTS concentration can also be seen by comparison with the average found by Gioda et al. (2004) in Volta Redonda.

The evaluation of the variation trend of the TSP concentration over the years allowed us to verify that in the city of Rio de Janeiro there was a decrease between 1997 and 2009, in such a way that the annual average became lower than the limit established by CONAMA (Azevedo and Moreira, 1999; Loyola et al., 2012). Also in Santa Cruz, an industrial district of Rio de Janeiro, there was a reduction in the concentration of PTS to levels below the CONAMA limit (MateusVinicius Leonel et al., 2013; Quiterio et al., 2004). In Seropédica there was maintenance in the concentrations of TSP, even considering the averages obtained by Gioda et al. (2016) for a long period of evaluation (33 years). Gioda et al. (2016) found lower TSP concentrations in Duque de Caxias than Loyola et al. (2009) but it should be noted that in the first case the study was conducted over a period of more than 30 years, which may contribute to a lower mean value than the second study whose sampling was conducted at a bus station. Although the studies show large differences that compromise the comparison, both found concentrations below the CONAMA limit.

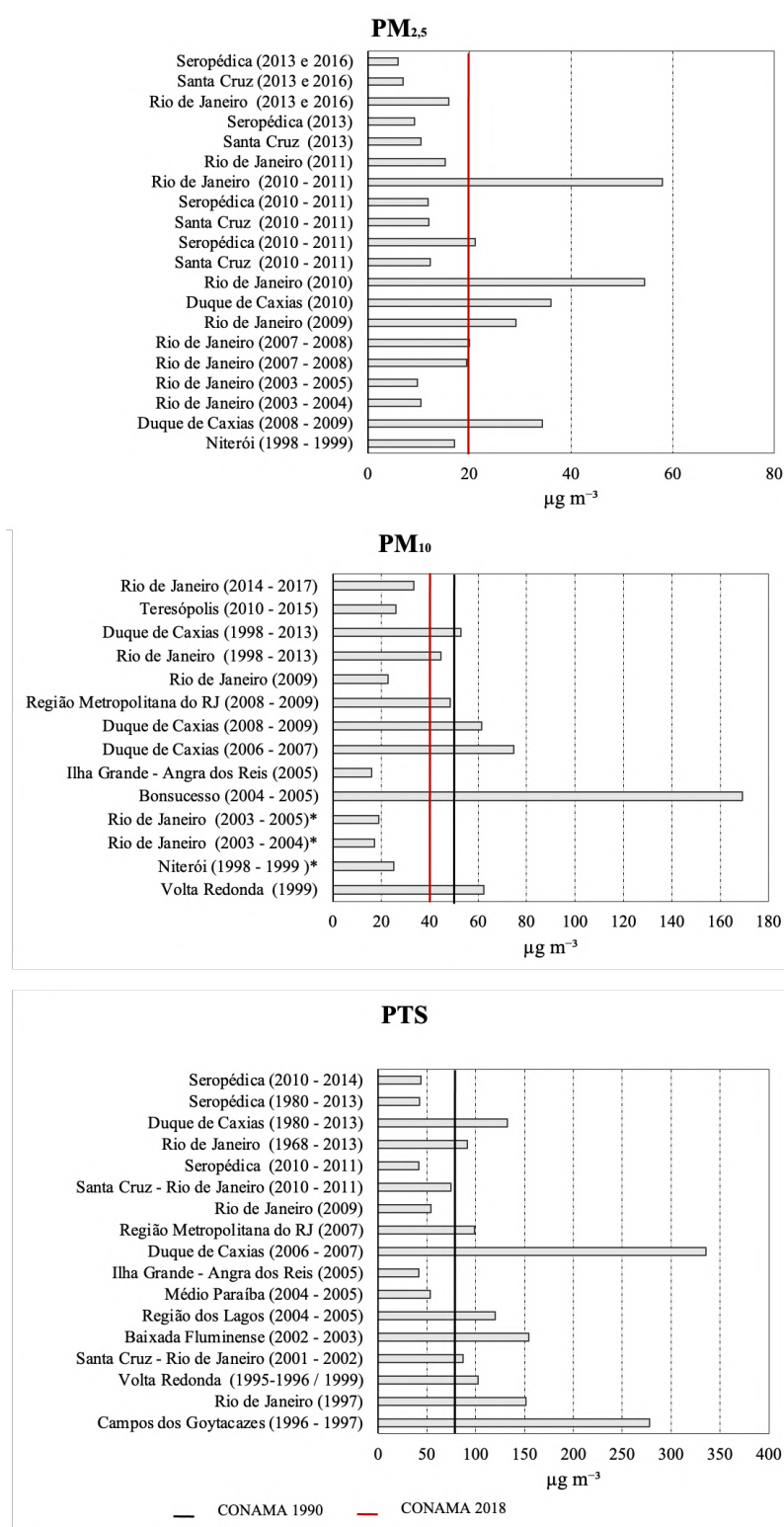


Figure 4.2 Average concentration of PM found in the studies conducted in the state of Rio de Janeiro and the limit established by CONAMA in the resolutions of 1990 and 2018. *Corresponds to the concentration of PM_{2,5-10}

The evaluation of PM_{10} concentration included 14 observations in Rio de Janeiro. Among them, five presented PM_{10} concentrations higher than the annual limit established by CONAMA in Resolution 003/1990, which was in force during the study period. However, according to the limits of the new Resolution (491/2018), the average concentrations are higher than the annual limit in six of these observations. The highest PM_{10} concentration was observed by Toledo et al. (2008) in Bonsucesso in the period between 2004 and 2005. This region, in addition to intense vehicular traffic, is influenced by petrochemical, metallurgical, power generation, ceramic, and industrial fuel industries. The authors attributed the high concentrations of PM_{10} to emissions from stationary sources. The lowest concentrations of TSP and PM_{10} were observed by Quiterio et al. (2006) in Ilha Grande.

When comparing different studies conducted in the same region, it is observed that in Duque de Caxias there was a decrease in the concentration of PM_{10} , although in all of them the average concentration was higher than the limit established by CONAMA in 2018. The city of Rio de Janeiro did not show a trend of reduction in the concentration of PM_{10} , but the different studies revealed variation in the average concentration of PM_{10} for the city. The studies by Soluri et al. (2007) and Godoy, et al. (2009) carried out in neighborhoods in all areas of the city, recorded similar concentrations for the PM fraction with diameters between 2.5 and 10 μm in the period between 2003 and 2005. The study by Loyola et al. (2012) in the Jardim Botânico neighborhood shows slightly higher concentrations than those reported by Godoy, et al. (2009). This may derive from the fact that the sampling also included particles smaller than 2.5 μm in diameter. Although the monitoring site of this study presents intense flow of cars, it is also close to parks and green areas, besides suffering influence from the ocean breeze, so the authors concluded that natural sources, such as soil resuspension was the main contributor to the concentration of PM_{10} . In a more recent study, conducted by Justo et al. (2020), between 2014 and 2017 in the southern and western neighborhoods of the city, PM_{10} concentrations were higher than those found by Godoy, et al. (2009), which may be associated with emissions generated by the construction works carried out during the city's preparation for the 2016 Olympic Games.

For $PM_{2.5}$, 20 assessments of samples obtained in the state of Rio de Janeiro were considered. Although during the period in which these studies were conducted there was no current legislation establishing a limit for $PM_{2.5}$ concentration, the annual

averages were higher than the limit established by CONAMA in 2018. The highest concentration was found by Rainho et al. (2014) in a study conducted in the city of Rio de Janeiro between 2010 and 2011. Similar concentrations were observed by Maia et al. (2014) in Duque de Caxias in 2010. In Rio de Janeiro, particulate matter was sampled near the Tunnel André Rebouças, which connects the northern and southern zones of the city and near Avenida Brasil and Linha Vermelha, two roads of intense vehicular traffic, which connect the city center to the west zone and Baixada Fluminense, respectively. In Duque de Caxias, particles were sampled at a site located on the margins of the BR-040 Federal Highway, through which part of the goods sold in the state enter. In addition, the sampling site may be influenced by the Duque de Caxias petrochemical complex, located 5 km away. The concentration of $PM_{2.5}$ observed in Duque de Caxias was about 1.2 times higher than that found by Paulino et al. (2014) in 2009 in the same region and three times higher than most concentrations found in studies conducted in other regions of Rio de Janeiro. In addition, it was four times higher than the average concentration found in Niterói by Mariani e De Mello (2007) in the dry period during thermal inversion episodes in 1999. The lowest $PM_{2.5}$ concentrations were observed by (Quijano et al., 2019) in Santa Cruz, an industrial region of the city of Rio de Janeiro, and in Seropédica, a municipality with rural characteristics.

In the state of Rio de Janeiro, especially in the metropolitan region, the main source of particulate matter emission is the vehicular fleet. This literature review includes studies conducted over a long period of time, in which changes occurred both in the number of vehicles and in the PM emission factor with the modernization of the fleet. According to the National Inventory of Atmospheric Emissions by Road Motor Vehicles (2013), between 1983 and 2012 there was a 54 - 98 % reduction in PM emissions due to fuel combustion. This percentage includes new ethanol, gasoline or diesel- powered light vehicles, motorcycles and diesel-powered heavy-duty vehicles (MMA, 2014). Although modernization has contributed to the reduction in vehicle PM emission factors, the vehicle fleet has increased substantially. According to the Rio de Janeiro State Traffic Department (Detran), between 2001 and 2010 the fleet increase was 41 % and between 2010 and 2017 the increase was 28 %, which corresponds to the increase of 58 % in 17 years (Detran, 2020).

Another factor to be highlighted is the contribution of the municipalities to the emission of air pollutants. The metropolitan region of the state of Rio e Janeiro (MRRJ)

is of greater interest due to the higher population concentration and, consequently, a greater number of emitting sources. According to the Inventory of Emissions from Vehicle Sources conducted by INEA in 2013 in the MRRJ, the municipality of Rio de Janeiro contributed almost 50 % of PM emissions. Within this municipality, the northern and western zones contributed almost 80% of vehicular emissions.

4.6. Influence of meteorological parameters on the concentration of particulate matter

The meteorological parameters (wind speed and direction, solar radiation, temperature, relative humidity and rainfall) are important in the evaluation of air quality, because they directly influence the dispersion of pollutants (Jaconis et al., 2017). These parameters can be affected by local characteristics, such as topography, land cover, presence of buildings, among others, and consequently influence the dispersion of pollutants (Santos et al., 2016). The identification of air masses origin is also important, because it helps to identify the emission sources that contribute to the concentration and composition of PM in a given region.

Most studies carried out in Rio de Janeiro do not present monthly averages of particulate matter, or separate the data by rainy or dry period; however, some of them present an evaluation of the influence of rainfall and wind speed and direction on PM concentration.

Studies carried out in municipalities of the Baixada Fluminense, in the city of Rio de Janeiro and in the Fonseca neighborhood, in the city of Niterói, showed that the highest concentrations of PM were found during the dry period, which corresponds, mainly, to the winter months (June to September) (Gioda et al., 2016; Justo et al., 2020; Miranda et al., 2012; Quiterio et al., 2004; Rainho et al., 2014; Toledo et al., 2008). In these months, the frequency of rainfall is lower, which increases the residence time of particles in the atmosphere. It was observed that in the state of Rio de Janeiro, lower temperatures favored thermal inversion, which contributes to the stagnation of pollutants in the atmosphere, making their dispersion difficult (Godoy et al., 2009; Mariani and Mello, 2007; Ventura et al., 2019). The study carried out by Mariani e Mello (2007) in Niterói reports results referring to the dry and wet periods, demonstrating that during the dry period PM_{10} and $PM_{2.5}$ concentrations were found up to 1.8 times higher than those found during the wet period. Although the concentrations were higher during the dry period, the ratio between the two particle

sizes was not affected. The maintenance of this ratio may indicate that the emission sources remained the same in both periods, and that the decrease in PM concentrations in the wet period may be attributed to the higher volume of rainfall in this period.

Although the study carried out in Niterói showed maintenance in the particle size ratio, the meteorological conditions observed in different seasons of the year may favor the formation of one particle size in detriment of the other, thus changing the ratio between different PM fractions. Particle formation by nucleation is favored in the humid period due to its hygroscopic characteristics, which may include the homogeneous nucleation process. Particle formation by Aitken mode occurs preferentially in the dry period, because the formation process involves heterogeneous reactions. The variation in the particle size ratio can be better observed when the separation of the fine PM fraction is done, because particles formed by nucleation and by the Aitken mode have sizes ranging from 2.5 to 100 nm. Mariani e Mello (2007) report that the particles formed by these processes are included in the PM_{2.5} which justifies the maintenance of the ratio compared to the coarse fraction in the dry and wet periods (Souza et al., 2017).

Mateus et al., (2020) reported concentrations for TSP and PM₁₀ for the dry and wet periods from 2010 to 2015 in Seropédica and Teresópolis. TSP concentrations in Seropédica showed no seasonal variation, although in 2011 concentrations were 1.5 times higher in the dry period and in 2014 concentrations were 1.6 times higher in the wet period. For PM₁₀, 1.7 - 3 times higher concentrations were found in the dry period in 2010 and 2011, while between 2012 and 2015 similar concentrations were observed during dry and wet periods.

Wind speed and direction can contribute to the dispersion or stagnation of pollutants. Some of the studies carried out in Rio de Janeiro considered the influence of these meteorological parameters on PM concentration, since they can contribute to the assignment of sources (Gioda et al., 2004; Paulino et al., 2014; Quiterio et al., 2005; Sella et al., 2006; Toledo et al., 2008). In the study developed by Sella et al. (2006) in Cabo Frio, an anomaly in PM concentrations was observed in the month of March, attributed to the winds of continental origin with low speed that occurred during that month. In the other months, the predominant winds were of marine origin. Paulino et al. (2014) observed that in Duque de Caxias the marine wind contributed to the transport of pollutants emitted in this industrial region to the continent, besides

promoting the mixing of pollutants in the atmosphere. This resulted in small differences in concentrations between the sampling sites. Justo et al. (2020) report that in some neighborhoods of Rio de Janeiro, the weak winds, low air humidity, and little precipitation during the winter months contribute to the occurrence of higher PM₁₀ concentrations.

In general, evaluations of the influence of meteorological variables on PM concentration show that lower concentrations are found in rainy periods. Increased rainfall and relative humidity help in removing pollutants from the atmosphere via wet deposition. Seasonality had a similar effect on the monitoring sites, since each season presents a different precipitation profile. Thus, lower PM concentrations were observed in the wettest seasons.

4.7. Particulate matter chemical characterization

The USEPA establishes reference methods for the chemical characterization of PM. According to method IO - 3.1, the determination of the elemental composition of PM can be performed by XRF, directly on filters containing particles, or through extraction using acid solution or microwave for quantification by ICP-MS, while the quantification of ions can be performed by ion chromatography (IC) after aqueous extraction (USEPA, 1999).

Sample preparation is done using an aliquot of the filters containing particulate matter. For the filters used in Hi-Vol, the aliquot suggested by the USEPA is cm 2,54 x 20,32 cm to obtain the area of 51,6 cm², which covers the entire length of the filter. However, in the studies conducted in Rio de Janeiro the filter area used for extraction varied from 9 - 129 cm² (Gioda and Reyes-Rodríguez and et al., 2011; Gioda et al., 2004; Justo et al., 2020; Loyola et al., 2006, 2009, 2012; Maia et al., 2014; Mateus et al., 2020; Mateus et al., 2013; Mateus and Gioda, 2017; Paulino et al., 2010, 2014; Quijano et al., 2019; Quiterio et al., 2004, 2005; Sella et al., 2006; Toledo et al., 2008). For the filters used in the SFU, each aliquot can be formed by fractions corresponding to 25 to 75 % of the filters (Godoy et al., 2009; Soluri et al., 2007). According to Marrero et al. (2005) there is no preferential region on the filter for the deposition of metals, and in addition most of the elements show satisfactory homogeneity, with differences of less than 15 % between the filter regions. After cutting the aliquot from the filter it should be transferred to a plastic tube for gravimetric determination of its mass.

4.7.1. Ionic characterization

The extraction of water-soluble species is done by adding ultrapure water with adjusted conductivity in the purifier. Two procedures can be adopted for this extraction: ultrasonic sonication (Gioda et al., 2011; Godoy et al., 2009; Mariani and Mello, 2007; Mateus et al., 2013; Rodríguez-Cottoa et al., 2014; Soluri et al., 2007; Ventura et al. 2014) or vortexing for 1 - 2 min (Justo et al., 2020; Mateus and Gioda, 2017; Mateus et al., 2020; Quijano et al., 2019). Subsequently, the extract is centrifuged and the supernatant is filtered with a 0.22 - 0.45 μm pore size membrane to remove insoluble particles. The extract obtained after filtration should be analyzed immediately or frozen until quantification by ion chromatography. Although in the USEPA Method 300.1 the recommendation is to use membranes with a porosity of 0.45 μm for ion determination, the filter with a porosity of 0.22 μm is also used as this ensures the removal of even smaller particles and also removes microbiological material (USEPA, 1997).

4.7.2. Elementary characterization

In the studies carried out in Rio de Janeiro, the elemental characterization of the particles followed some adaptations of the USEPA recommendations for acid extraction. However, quantification was also performed by ICP OES and FAAS, in addition to ICP-MS, a technique suggested by the environmental agency (Gioda et al., 2004; Mateus et al., 2013; Ventura et al., 2014).

The USEPA recommendation is to use a new aliquot of the filter. However, some ionic and elemental characterization studies have used the same aliquot used in the aqueous extraction to perform the acid extraction (Gioda et al., 2011). To use a new aliquot it is necessary to determine the mass of the strip and subsequently add the extraction acid. In the case of reusing the aliquot, the acid is added to the aqueous extract. In both cases, the extraction is performed under heating at 100 °C for 2 to 4 h. After cooling of the extract containing only acid, water is added to subsequently perform elemental quantification by spectrometric techniques.

According to USEPA method IO - 3.1 method, the HCl/HNO₃ mixture should be used for the extraction of the metallic elements, so some authors use these acids for the extraction (Loyola et al., 2012; Maia et al., 2014; Paulino et al., 2010, 2014; Quiterio et al., 2004, 2005; Toledo et al., 2008). However, some studies on the elemental characterization of particulate matter adopt alternative methodologies for

the extraction or leaching of elements. These procedures include microwave extraction or use of other acidic solutions such as HNO₃-HF mixtures or addition of oxidizing reagents such as HClO₄ or H₂O₂. (Salcedo et al., 2014) compared such methods and found that the use of the HNO₃-HF mixture showed satisfactory results for most elements. However, the use of the oxidants did not increase the extraction efficiency.

It is important to point out that for the use of HF some preventive measures are necessary. This acid causes pain and tissue necrosis immediately upon contact, because fluoride ions penetrate lipid membranes quickly (Steverlynck et al., 2017). Because of its corrosive potential and toxicity, HF must be used by trained professionals in appropriate locations. Some protective equipment required are: face shields, gloves and goggles, acid resistant aprons, and a respiratory filter (Bajraktarova-Valjakova et al., 2018). In addition, the purchase of this reagent is controlled by the Brazilian Army and the Civil Police, because it is considered a chemical warfare precursor agent.

Mateus et al. (2013) report that compared to the USEPA method, the use of HNO₃ alone leads to the highest extraction efficiency (EE) from NIST-SRM 1648a - Urban dust certified reference material. The high values indicate that the method using only HNO₃ is suitable for leaching metals present in particles. Low recovery was observed for some refractory metals that are, however, in a non-bioavailable form. Therefore, the procedure does not compromise the results of the studies, since the focus is on the health or ecosystem impact. Due to the improved EE, some authors have opted for extraction using only HNO₃ (Gioda and Amaral et al., 2011; Mateus and Gioda, 2017; Quijano et al., 2019; Ventura. et al., 2014; Ventura et al., 2017, 2019).

4.7.3. Quality Control

To obtain reliable data on the chemical composition of PM, the acids and ultrapure water used for elemental extraction and solubilization should be analyzed by spectrometric techniques and by ion chromatography, respectively. To check the efficiency of the acid extraction certified reference materials (CRM) 1648a (SRM 1648a, *urban dust*, NIST, USA) and CRM 2783 (SRM 2783, *air particulate matter*, NIST, USA) are used, applying the same extraction procedures used for the filters

containing PM. To ensure the homogeneity of the PM-containing filter, some samples are extracted in replicates. The precision and accuracy of the analytical equipment is ensured by the systematic use of a check standard and duplicate samples.

Some analytes of interest are present in the composition of the white filters, so it is necessary to determine their concentrations to be discounted from the final concentration. To evaluate the composition of the white filters, the sample matrix, the same procedure for acid and aqueous extraction should be applied to some aliquots of these filters (strips in the dimensions 1.7 x 21 cm). The concentrations of the analytes of interest found on the white filters should be discounted in the final concentration of the samples. Thus, so that the concentrations of the analytes in the particulate material are not underestimated or overestimated, the values obtained for the white filters can be submitted to Grubbs' test aiming to remove *outliers* before being discounted from the concentrations obtained for the samples (Mateus and Gioda, 2017; Ventura et al., 2018).

The instrumental limits of detection (LOD) and limits of quantification (LOQ) for the elemental analyses are obtained from the standard deviation of 10 measurements of the acid s_{HNO_3} used for extraction, according to equations 4.1 and 4.2.

$$LOD_{ICP-MS} = 3 \times s_{HNO_3}$$

Equation 4.1 Expression for ICP-MS Limit of Detection calculation

$$LOQ_{ICP-MS} = 10 \times s_{HNO_3}$$

Equation 4.2 Expression for ICP-MS Limit of Quantification calculation

The instrumental detection and quantification limits for ion chromatography are calculated considering the lowest concentration standard used to construct the analytical curve, according to equation 3.3 proposed by Soluri (2005) where S_{y_1} is the standard deviation of the concentrations obtained in the analyses of the lowest concentration standard solution, x_1 is the theoretical concentration for the lower concentration standard solution, and y_m is the mean of the concentrations obtained in the analyses of the lowest concentration standard solution. The LOQ can be calculated from the LOD according to equation 4.4 .

$$LD_{CI} = \frac{3,3 (S_{y1} \times x_1)}{y_m}$$

Equation 4.3 Expression for Ionic Chromatograph Limit of Detection calculation

$$LQ_{CI} = 3 \times LD_{CI}$$

Equation 4.4 Expression for Ionic Chromatograph Limit of Quantification calculation

Due to the presence of analytes of interest in the composition of the glass fiber filter, the sample matrix, LOD and LOQ must be calculated for the method. The method limits are obtained by considering the average concentration of each ion or element on the white filters ($x_{analito}$) and the standard deviation of the element and ion concentrations found on the white filters ($s_{analito}$), according to equations 4.5 and 4.6.

$$LD_{método} = x_{analito} + (3 \times s_{analito})$$

Equation 4.5 Expression for Limit of Detection of method calculation

$$LQ_{método} = 3 \times LD_{analito}$$

Equation 4.6 Expression for Limit of Quantification of method calculation

4.8. Interpretation of the PM chemical composition data

4.8.1. Enrichment Factor

The enrichment factor (EF) is a value used to predict the contribution of anthropogenic sources to the elemental composition of PM. Its calculation consists of normalizing the values by the concentration of an abundant element in the soil, such as Al and Fe, according to equation 4.7, proposed by Olmez et al. (1985) where C_x is the concentration of the analyte of interest and C_{ref} is the concentration of a reference element found in the soil. The value of the EF is given by the ratio between the proportions of the analyte and reference element in the sample and in the soil (Çevik et al., 2009; Olmez et al., 1985).

$$FE = \frac{\left(\frac{C_x}{C_{ref}}\right)_{amostra}}{\left(\frac{C_x}{C_{ref}}\right)_{solo}} \quad (7)$$

Equation 4.7 Enrichment formula calculation

For the elements present in PM, EF = 1 indicate a soil-only source, so the closer to unity, the greater the natural contribution to the composition. EF > 5 represent enrichment caused by anthropogenic sources (Elhadi et al., 2018). It is considered that 5 < EF < 10 indicates contribution from sources close to the particle collection site (Hien et al., 2001).

4.8.2. Marine contribution to the PM composition

The city of Rio de Janeiro and some neighboring municipalities are subjected to the influence of Atlantic air masses. They can carry aerosols emitted by the oceans, also called sea spray, which is an important source of ions. In seawater the ions are found in constant and well-defined ratios, which allows the evaluation of the marine contribution to the concentration of ionic species in the PM. One approach used to evaluate the contribution of non- sea salt (nss) is to consider that all Na⁺ concentration found in the samples comes from the sea (sea salt - ss). Through the known ratios between the sodium (or magnesium) cation and the other ions it is possible to calculate the concentration of the ions that would be of marine origin, which if subtracted from the total concentration obtained for each ion will provide the nss concentration. Based on the ratios of the concentrations of the ions present in seawater and the Na⁺ concentration, Morales et al. (1998) proposed equations (4.8 - 4.12) for the calculation of nss, which were applied in studies conducted in Rio de Janeiro (Godoy et al., 2009; Mateus and Gioda, 2017; Soluri et al., 2007).

$$nss - Ca^{2+} = C_{Ca^{2+}} - 0,038 \times C_{Na^+}$$

Equation 4.8 Ca²⁺ Non sea salt contribution estimation

$$nss - Mg^{2+} = C_{Mg^{2+}} - 0,12 \times C_{Na^+}$$

Equation 4.9 Mg²⁺ Non sea salt contribution estimation

$$nss - K^+ = C_{K^+} - 0,035 \times C_{Na^+}$$

Equation 4.10 K⁺ Non sea salt contribution estimation

$$nss - SO_4^{2-} = C_{SO_4^{2-}} - 0,25 \times C_{Na^+}$$

Equation 4.11 SO₄²⁻ Non sea salt contribution estimation

$$nss - Cl^- = C_{Cl^-} - 1,727 \times C_{Na^+}$$

Equation 4.12 Cl⁻ Non sea salt contribution estimation

4.9. Particulate matter acidity

The components of particulate matter determine its acidity or basicity. The acidity of PM can affect its chemical properties, because it can induce reactions between gaseous substances and particulate components. In addition, particles with high acidity contribute to the formation of acid rain, since they act as condensation nuclei for rainfall (Wu et al., 2017). Due to the formation processes, the fine fraction tends to have higher acidity, as it has a greater contribution of strong acid anions. In contrast, the coarse fraction presents higher neutralization capacity due to the presence of strong base cations in particles emitted by natural sources or construction (Masiol et al., 2015; Pernigotti et al., 2016; Ren et al., 2011; Wu and Zhang, 2018).

Ions present in PM can have acidic or basic characteristics, so depending on their concentrations, neutralization of the acidity or basicity of the particles can occur. The degree of neutralization can then be used as an indicator of the acidity of the PM. Neutralization is calculated through the ratio between the sum of the molar concentrations of cations (with basic characteristics) and anions (with acidic characteristics), considering the charge of each ion. Values less than 1 indicate that the neutralization was not complete, so that the particles can be considered acidic (Wu et al., 2017).

4.10. Elemental composition of particulate matter

4.10.1. Average concentration of elements in PM

The size of the particles can influence the concentration of their constituents due to the formation processes or the difference in the masses of the particles. Tables 4.2 – 4.5 present the concentration ranges of the metal elements and ionic species found in PM collected in Rio de Janeiro between 1995 and 2017.

The main elements found in the particles, considering the three sizes evaluated, were Fe and Al. The highest concentrations for these elements were observed by Quitério et al. (2004) in Santa Cruz, a neighborhood in Rio de Janeiro that is home to a steel mill complex. Emissions from industries near the sampling sites may have contributed to very high concentrations of these elements in the TSP, as well as the resuspension of soil dust caused by truck traffic used by the industrial companies. In other studies conducted in non-industrial areas such elements also appeared as main components of PM, together with Zn. These elements are part of the soil composition, which explains their high concentrations in TSP, since particles from soil resuspension tend to have larger diameters (Alves, 2005; Seinfeld and Pandis, 2006). Some studies reveal the importance of Zn in the composition of PM in Rio de Janeiro because, besides being present in the soil composition, this element can also be associated with vehicle emissions, burning of fossil fuels and emissions generated by industrial activities (Mateus and Gioda, 2017; Rodríguez-Cottoa et al., 2014).

Among the minority elements are Cr, Cu, Pb, and Cd. The highest concentrations of Cr and Pb were observed by Quitério et al. (2004) in the TSP collected in Santa Cruz and those of Cd by Quitério et al. (2005) in Nova Iguaçu. The authors attributed the source of these elements to the industrial activities existing in the sampling regions, such as steel and metallurgy. To corroborate the anthropogenic origin of such elements, the enrichment factor was calculated in relation to the composition of the soil, finding values of up to 1200, indicating that these elements are mostly of anthropogenic origin. The highest concentration of Cu was observed by (Gioda et al., 2011) in PM₁₀ sampled in Duque de Caxias, however, similar values were also observed in downtown Rio de Janeiro, which showed the highest annual average for this element among the monitoring sites of this study. The authors attribute the origin of Cu in downtown Rio de Janeiro to oil and fuel burning and emissions from

vehicular traffic, since it showed good correlations with Pb and Cd, but in Duque de Caxias Cu emission can also be attributed to metallurgical processes.

Some metallic elements can be associated with damage to human health, and are classified as carcinogenic substances. Although regulation of the concentration of these chemical species in air is not very common, with the exception of Pb, the European commission and some other countries set limits for the concentration of the elements Cr, Ni, Cd, and As.

According to CONAMA Resolution 491/2018, the limit of the annual average concentration of Pb measured in TSP should be $0.5 \mu\text{g m}^{-3}$. Gioda et al. (2004) and Quitério et al. (2004) found concentrations up to 6 times higher than the limit in studies conducted in Volta Redonda (1995 - 1999) and Santa Cruz (2001 - 2002), respectively. It is important to note that, according to the legislation, Pb monitoring is indicated for regions with emission potential. Since these two sites have important steel mill complexes, the values found indicate that these industrial enterprises contributed to emissions that put the population of the region at risk. A subsequent study carried out in the Volta Redonda region (2004 - 2005) by Loyola et al. (2006) recorded Pb concentrations up to 35 times lower than the current Pb limit in TSP. Mateus et al. (2013) found in Santa Cruz (2010 - 2011) Pb concentrations up to 50 times lower than the air quality standard. The reduction in Pb concentration in these industrial regions indicates that the modernization of industries has contributed to emission control.

Table 4.2 Concentration range of TSP ($\mu\text{g m}^{-3}$), of metallic elements (ng m^{-3}) and ions ($\mu\text{g m}^{-3}$) in particles sampled in Hi-Vol in the state of Rio de Janeiro between 1995 and 2011.

	Gioda. 2004	Quitério. 2004	Nascimento. 2011 ^b	Quitério. 2005	Sella. 2006	Loyola. 2006	Quitério. 2006	Loyola. 2009	Paulino. 2010	Loyola. 2012	Mateus. 2013		Mateus. 2020
Ano	1995-1996 1999	2001 -2002	2002	2002 – 2003	2004 - 2005	2004 - 2005	2005	2006 - 2007	2007	2009	2010 - 2011		2010 - 2014
Local	Volta Redonda	Santa Cruz	Ilha Grande	Baixada Fluminense	Região dos Lagos	Médio Paraíba	Ilha Grande	Duque de Caxias	MRRJ	Rio de Janeiro	Santa Cruz	Seropédica	Seropédica
n	56	43	19	262	27	186	14	33	55	31	-	-	128
Filtro (cm ²)	86	52	-	52	48	52	52	52	129	52	9	-	52
SP	68 - 163	87	-	55 - 242	36 - 204	25 - 150	20 - 60	178 - 524	64 - 211	33 - 96	22 - 245	12 - 81	5.7 - 242
Fe ^a	2.1 – 5.2	0.08 - 290	-	0.03 - 4.3	-	0.9 – 1.7	0.1	0.006 – 5.7	0.2 – 3.7	2.5 – 6.5	1.3 – 2.9	0.9	0.001 - 2.4
Al ^a	-	0.009 – 40	-	0.004 - 3.6	-	4.0 – 5.3	0.06	1.4 – 8.3	0 – 6.1	0.5 – 1.8	3.5 – 4.2	3.5	0.2 - 22.9
Zn ^a	2.4 – 6.9	0 – 15	-	0.006 - 7.5	0.008 – 0.03	0.5 – 6.6	0.01	0 – 0.5	0 – 11	0.07 – 0.08	2.8 – 3.3	3.2	0.2 - 44.4
Ca ^a	-	0.01 – 25	-	0.007 - 5.2	0.004 – 9.3	5.0 – 7.2	0.1	4.3 – 1.9	0 – 9.2	2.9 – 7.8	1.6 - 2.5	0.7	-
Mg ^a	-	0.007 – 53	-	0.0005 - 1.4	-	0.4 – 0.6	0.2	1.2 – 8.6	0.1 – 1.4	7.4 – 1.9	0.32 – 0.35	0.2	-
Mn	100 - 300	0.4 - 12000	3 - 22	1.0 - 1656	5 - 28.8	65 - 97	2.6	-	4.2 - 66.5	30 - 90	49.8 - 112.1	29.2	3.4 - 112
Cu	70 - 242	0.9 - 3444	-	2.7 - 610	5 - 140	65 - 503	1.6	6 - 1049	23.7 - 1357	130 - 253	120 - 170	400	1.8 - 566
Ni	15 - 30	0.1 - 1.3	-	0 - 4.7	-	2	-	-	0 - 8	-	3.2 - 3.4	2.2	0.7 - 111
Cd	5 - 14	0.7 - 2.4	-	0 - 468	-	0 - 1	-	-	0 - 0.5	-	0.7	1.07	0.06 - 77
Pb	90 - 610	0 - 2887	0.3 - 8.6	0 - 33	-	2 - 14	0.7	-	0 - 72.4	-	7.65 - 8.94	6.64	1.3 - 47.8
Cr	-	0 - 8678	-	0 - 33	-	4 - 115	-	-	0 - 8.8	8 - 19	6.25 - 23.4	18.9	0.6 - 5.6
K	-	0.1 - 420	-	10.3 - 7155	276 - 9370	-	-	-	-	-	360 - 560	330	-
Na	-	3.6 - 1729	-	23.3 - 23694	-	-	-	-	-	-	2790 - 3170	2530	-
Mo	-	0 - 1.2	-	-	-	-	-	-	-	-	-	-	-
Co	-	0.8 - 1.6	-	0 - 4.7	-	4 - 5	-	-	0 - 25.3	-	-	-	-
Ti	-	-	-	-	-	-	-	-	-	-	54 - 125.8	34.8	3.2 - 222
V	-	-	-	-	0.8 - 20.9	-	-	-	-	4 - 16	6.95 - 9.37	6.21	0.2 - 24
Cl ⁻	-	-	-	-	-	-	-	-	-	-	4.9 - 5.5	2.7	0.2 - 11.0
NO ₃ ⁻	-	-	-	-	-	-	-	-	-	-	4.1 - 5.1	3.6	0.3 - 15.0
SO ₄ ²⁻	-	-	-	-	-	-	-	-	-	-	3.2 - 3.9	2.7	0.8 - 13.7
NH ₄ ⁺	-	-	-	-	-	-	-	-	-	-	-	-	5.5 - 87
Na ⁺	-	-	-	-	-	-	-	-	-	-	-	-	0.1 - 18.5
K ⁺	-	-	-	-	-	-	-	-	-	-	-	-	0.04 - 2.3
Mg ²⁺	-	-	-	-	-	-	-	-	-	-	-	-	0.030 - 1.6
Ca ²⁺	-	-	-	-	-	-	-	-	-	-	-	-	0.0 - 7.3

^avalues expressed in $\mu\text{g m}^{-3}$ / ^bAetolometer

Table 4.3 Concentration range of PM₁₀ (µg m⁻³), of metallic elements (ng m⁻³) and ions (µg m⁻³) in particles sampled in Hi-Vol in the state of Rio de Janeiro between 1995 and 2017.

	Gioda. 2004	Mariani e Melo. 2007 ^{bd}	Soluri. 2007 ^{bc}	Godoy. 2009 ^{bc}	Toledo. 2008	Quitério. 2006	Loyola. 2009	Paulino. 2014	Gioda. 2011	Loyola. 2012	Justo. 2020
Ano	1995 – 1996 1999	1998 - 1999	2003 - 2004	2003 - 2005	2004 - 2005	2005	2006 - 2007	2008 - 2009	2008 - 2009	2009	2014 - 2017
Local	Volta Redonda	Niterói	Rio de Janeiro	Rio de Janeiro	Bonsucesso	Ilha Grande	Duque de Caxias	Duque de Caxias	MRRJ	Rio de Janeiro	Rio de Janeiro
n	11	50	300	300	51	14	33	68	192	31	182
Filtro (cm ²)	86	-	4.3	4.3	129	52	52	129	86	52	86
PM ₁₀	44 - 78	7 - 72	11 - 27	20 - 37	71 - 312	2 - 30	39 - 121	42 - 81	34 - 71	13 - 47	1 - 99
Fe ^a	1.4 - 3.7	-	0.3 - 0.9	0.3 - 0.9	0.2 - 2.4	0.05	0.2 - 5.3	0.05 - 2.0	0.3 - 3.1	0.4 - 1.8	0.1 - 0.7
Al ^a	-	-	0.3 - 1.2	0.3 - 1.2	0.03 - 4.5	0.004	1.4 - 7.1	0.02 - 1.0	1.1 - 1.3	0.1 - 0.7	-
Zn ^a	0.006 - 4.3	-	-	0.005 - 0.04	0.01 - 7.6	0.0008	0 - 0.3	0.002 - 0.6	0.6 - 22.3	0.02 - 0.09	-
Ca ^a	-	-	0.3 - 1.2	-	0.02 - 3.7	0.02	4.3 - 15.5	0.045 - 1.2	0.1 - 3.7	0.8 - 4.9	-
Mg ^a	-	-	0.1 - 0.2	0.15 - 0.25	0.003 - 0.9	0.03	1.9 - 7.9	0.02 - 0.3	0.04 - 0.4	0.2 - 1.3	-
Mn	100 - 200	-	-	5.2 - 20	30 - 51.6	0.6	-	1 - 36	1.02 - 60.1	5 - 24	2.2 - 13.3
Cu	50 - 580	-	-	2.7 - 17.3	4.7 - 88	0.3	0 - 51	10 - 94	40 - 11200	58 - 167	15.6 - 122
Ni	20	-	-	0.5 - 1.2	0 - 7.6	-	-	-	0.1 - 10.5	-	0.5 - 1.8
Cd	4 - 8	-	-	0.04 - 0.4	0 - 1.6	-	-	-	0.2 - 4.2	-	0.1 - 0.6
Pb	110 - 180	-	-	2.0 - 21	0 - 68.8	-	-	-	5.20 - 80.3	-	1.3 - 5.8
Cr	-	-	-	-	0 - 7.9	-	-	-	0.1 - 10.1	-	0.94 - 3.80
K	-	-	158 - 492	162 - 495	-	-	-	-	130 - 1150	-	-
Na	-	-	1020 - 1530	1068 - 1605	-	-	-	-	900 - 4630	-	-
Mo	-	-	-	0.1 - 0.5	0.2 - 2.22	-	-	-	-	-	-
Co	-	-	-	0.08 - 0.2	0 - 4.9	-	-	-	-	-	0.03 - 0.25
Ti	-	-	40 - 100	25.5 - 87.3	13.6 - 394	-	-	-	9.8 - 140	-	3.1 - 15.4
V	-	-	-	-	-	-	-	-	-	1 - 10	1.18 - 4.36
Cl ⁻	-	0.7 - 7.1	0.8 - 1.3	1.0 - 1.4	-	-	-	-	0.3 - 5.5	-	1.8 - 3.2
NO ₃ ⁻	-	0.2 - 3.8	0.9 - 1.4	1.0 - 1.8	-	-	-	-	0.7 - 12.1	-	1.9 - 3.1
SO ₄ ²⁻	-	0.3 - 9.2	0.5 - 1.1	0.4 - 0.90	-	-	-	-	0.5 - 13.2	-	1.7 - 2.9
NH ₄ ⁺	-	0.04 - 1.7	-	-	-	-	-	-	0.007 - 0.2	-	0.03 - 0.2
Na ⁺	-	0.5 - 7.8	0.7 - 1.2	1.0 - 1.3	-	-	-	-	-	-	2.3 - 3.2
K ⁺	-	0.050 - 1.8	0.09 - 0.2	-	-	-	-	-	-	-	0.2 - 0.4
Mg ²⁺	-	0.050 - 1.5	0.14 - 0.18	0.18 - 0.20	-	-	-	-	-	-	0.2 - 0.5
Ca ²⁺	-	0.010 - 1.4	-	-	-	-	-	-	-	-	0.3 - 0.6

^avalues expressed in µg m⁻³ / ^bConcentration measured in PM_{2.5-10} / ^ccollection in SFU / ^dDichotomous sampler

Table 4.4 Concentration range of PM_{2.5} (µg m⁻³), metallic elements (ng m⁻³) and ions (µg m⁻³) in particles collected in Hi-Vol in Rio de Janeiro state between 1998 and 2009.

	Mariani e Melo. 2007^c	Soluri. 2007^b	Godoy. 2009^b	Paulino. 2014	Miranda. 2012	Andrade. 2012^d	Loyola 2012
Ano	1998 - 1999	2003 - 2004	2003 - 2005	2008 - 2009	2007 - 2008	2007 - 2008	2009
Local	Niterói	Rio de Janeiro	Rio de Janeiro	Duque de Caxias	Rio de Janeiro	Rio de Janeiro	Rio de Janeiro
n	50	300	300	110	150	150	50
Filtro (cm ²)	-	4.3	4.3	129	2.7	-	52
PM _{2.5}	3 - 63	7 - 13	7 - 11	21 - 45	2 - 62	-	8 - 117
Fe ^a	-	0.07 - 0.1	0.09 - 1.5	0.008 - 1.2	0.07	0.08	0.183 - 0.570
Al ^a	-	0.07 - 0.2	0.06 - 0.2	0.02 - 0.4	0.05	0.05	0
Zn ^a	-	-	0.007 - 0.02	0.008 - 0.4	0.02	0.03	0.006 - 0.042
Ca ^a	-	0.05 - 0.1	-	0.004 - 0.6	0.04	0.004	0.028 - 0.143
Mg ^a	-	0.02 - 0.03	0.02 - 0.03	0.006 - 0.2	-	0.008	0.009 - 0.051
Mn	-	-	2.4 - 6.3	1 - 18	4.4	41	0 - 11
Cu	-	-	4.2 - 12.9	4 - 97	8.8	-	16 - 135
Ni	-	-	0.9 - 1.6	-	2.2	3	-
Cd	-	-	0.1 - 2.1	-	-	-	-
Pb	-	-	1.6 - 2.1	-	11.8	12	-
Cr	-	-	-	-	1.8	2	0
K	-	91 - 169	97.8 - 194	-	183	178	-
Na	-	160 - 280	214 - 286	-	-	-	-
Mo	-	-	0.08 - 0.3	-	-	-	-
Co	-	-	0.03 - 0.07	-	-	-	-
Ti	-	17 - 25	9.4 - 15.5	-	5.5	6	-
V	-	-	-	-	4.5	4	0 - 4
Cl ⁻	0.050 - 1.2	0.1 - 0.3	0.1 - 1.4	-	0.1	0.1	-
NO ₃ ⁻	0.03 - 2.3	0.3 - 0.5	0.2 - 1.6	-	0.6	0.6	-
SO ₄ ²⁻	0.3 - 5.0	1.4 - 2.2	0.5 - 1.4	-	1.9	1.9	-
NH ₄ ⁺	0.06 - 2.8	0.4 - 0.7	-	-	0.8	0.8	-
Na ⁺	0.1 - 0.8	0.2 - 0.3	0.2 - 0.4	-	0.2	0.2	-
K ⁺	0.05 - 2.3	0.1 - 0.2	-	-	-	-	-
Mg ²⁺	0.03 - 0.1	-	0.05 - 0.071	-	-	-	-
Ca ²⁺	0.01 - 0.03	-	-	-	-	-	-

^avalues expressed in µg m⁻³ / ^bSFU collection/ ^cDichotomous sampler / ^dHarvard mpactor

Table 4.5 MP_{2.5} concentration range ($\mu\text{g m}^{-3}$), metal elements (ng m^{-3}), and ions ($\mu\text{g m}^{-3}$) in particles sampled in Hi-Vol in Rio de Janeiro state between 2010 and 2016

	Maia. 2014	Mateus. 2013		Mateus. 2017		Ventura. 2017	Mateus. 2017		Quijano. 2019		
Ano	2010	2010 – 2011		2010 - 2011		2011	2013		2013 e 2016		
Local	Duque de Caxias	Santa Cruz	Seropédica	Santa Cruz	Seropédica	Rio de Janeiro	Santa Cruz	Seropédica	Rio de Janeiro	Santa Cruz	Seropédica
n	17	181		-		206	-		-		
Filtro (cm ²)	129	9		9		-	51		62		
PM _{2.5}	12 - 74	-	-	1 - 43	1 - 35	1 - 67	2 - 37	3 - 26	7 - 19	7	6
Fe ^a	0.002 - 0.2	0.12 - 0.15	0.14	-	-	0.1 - 0.7	-	-	-	1.0	0.7
Al ^a		5.5 - 5.6	5.4	-	-	1.6 - 6.7	-	-	-	2.1	1.2
Zn ^a	0.07 - 0.6	5.4 - 5.6	5.1	-	-	1.9 - 6.6	-	-	-	2.9	1.8
Ca ^a	0.02 - 0.1	0.2 - 0.3	0.2	-	-	1.2 - 7.6	-	-	-	-	-
Mg ^a	0.006 - 0.03	0.050	0.07	-	-	0.1 - 1.2	-	-	-	0.6	0.4
Mn		5.9 - 7.3	7.2	20.5		4.1 - 17	-	-	1.6	10.7	14.6
Cu	1.1 - 121.3	10 - 60	50	37.7	51	17 - 71	15.6	18.4	6.7 - 47	19.7	123
Ni	0 - 7.7	1.8 - 2.1	1.7	1.6	1.8	1.7 - 5.2	1.1	0.90	0.8 - 3	1.5	2.3
Cd	0 - 2.2	0.68 - 0.72	1.1	-	-	0.4 - 1.5	-	-	0.2 - 0.5	2.2	2.8
Pb	0 - 9.9	6.2 - 7.9	6.2	-	-	5.2 - 36	-	-	0.3 - 7.6	12.5	13.8
Cr	0 - 1.7	4.6 - 5.0	2.2	-	-	1.2 - 2.7	-	-	-	4.1	6.8
K	-	0.2 - 0.3	230	-	-	1000 - 5100	-	-	-	1.2	0.8
Na	-	1.3 - 1.6	1590	-	-	5800 - 13000	-	-	-	4.4	6.4
Mo	-	-	-	-	-	-	-	-	0.09 - 0.1	0.3	0.4
Co	-	-	-	-	-	-	-	-	-	-	-
Ti	-	7.9 - 8.1	7.69	8.2	7.7	7300 - 66000	7.3	6.9	-	9.6	15.4
V	-	3.9 - 4.4	3.03	5.1	4.8	-	-	-	1.0 - 8.1	2.5	3.0
Cl ⁻	-	0.9 - 1.0	1.1	1.0	1.2	-	0.5	0.4	-	-	-
NO ₃ ⁻	-	1.3 - 1.6	1.7	1.5	1.7	-	1.0	0.8	0.55 - 5.0	0.8	0.7
SO ₄ ²⁻	-	2.9 - 3.8	3.3	3.7	3.7	-	2.7	2.7	1.7 - 3.9	2.8	2.7
NH ₄ ⁺	-	-	-	-	-	-	-	-	0.01 - 0.02	-	-
Na ⁺	-	-	-	-	-	-	-	-	1.9 - 2.2	1.4	1.4
K ⁺	-	-	-	0.09	0.1	-	0.2	0.2	0.06 - 0.2	-	-
Mg ²⁺	-	-	-	0.3	0.2	-	0.070	0.060	0.03 - 0.04	0.03	-
Ca ²⁺	-	-	-	0.2	0.2	-	0.3	0.23	0.2 - 0.4	0.11	0.06

^avalues expressed in $\mu\text{g m}^{-3}$

The European commission sets limit values for the concentration of Ni (20 ng m^{-3}) and Cd (5 ng m^{-3}). The study developed by Gioda et al. (2004) in Volta Redonda reveals Ni and Cd concentrations of 1.5 -2.8 times higher than the European recommendations in both TSP and PM_{10} . For Cd, also found by Quitério et al. (2005), concentrations almost 100 times higher in Nova Iguaçu.

4.10.2. Enrichment Factor of the PM collected in Rio de Janeiro

To assess the influence of natural and anthropogenic contributions on the composition of PM, some studies have made use of the enrichment factor. Paulino et al. (2014) found that the PM emitted in the city of Duque de Caxias showed percentages of Fe, Zn, Ca and Cu higher than those verified for the earth's crust, indicating that anthropogenic activities contributed to the presence of such elements in the particles, especially the traffic of cars and petrochemical industries present in this region. Maia et al. (2014) also verified enrichment of these elements in the same region, and also observed enrichment of Ni. Besides the contribution of industrial activities and fuel burning by vehicles, some of these elements can be emitted by wear of car parts, such as tires and brake linings (Maia et al., 2014; Pant and Harrison, 2013).

Quitério et al. (2005) found high EF for Zn, Cu, Cd and Pb in the study carried out near the steel mills in Santa Cruz, indicating a greater contribution of anthropogenic sources for these elements. Moderate values were also found for Mn and Ni, indicating that natural and anthropogenic sources present similar contributions.

In the study by Loyola et al. (2012) in the André Rebouças tunnel, located between the south and north zones of the city of Rio de Janeiro, very high enrichment for Zn and Cu was verified, about 10 times higher than that observed in other studies. It is known that the dispersion of pollutants in tunnels is difficult due to the continuous emission, especially in long tunnels such as Rebouças Tunnel, which is 2.8 km long (Zhao et al., 2017). Vehicles are responsible for the emission of these elements, since they can be present in gasoline or diesel. In addition, Zn is part of the composition of tires, and can be emitted in their wear, and Cu is present in brake linings, also emitted by wear (Lin et al., 2005; Pant and Harrison, 2013). In the study conducted by Loyola et al., 2009 in a bus station in Duque de Caxias, high Cu and Zn enrichments were

also observed, confirming the association of these elements with emissions from vehicular traffic. When the composition of PM emitted in different regions of the state of Rio de Janeiro is evaluated, it is observed that the highest FE are found for Zn, Cu, Cd and Pb, which shows that these elements are associated with anthropogenic emissions, especially vehicular and industrial activities. In some regions there is also an enrichment of other elements that can also be associated with anthropogenic activities, such as Ni, Fe, and Mn.

4.11. Ionic composition of particulate matter

4.11.1.1. Average ion concentration in PM

The ionic species can represent up to 70% of the particulate matter, therefore, their concentrations are usually higher than the concentrations of the metallic elements. Among the 30 studies on PM carried out in Rio de Janeiro, the ionic composition of the particles was evaluated in only 11 studies. The average concentration ranges for the ions in the particles are presented in Tables 3.2 – 3.5 (Andrade et al., 2012; Gioda and Amaral and et al., 2011; Godoy et al., 2009; Justo et al., 2020; Mariani and Mello, 2007; Mateus and Gioda, 2017; Miranda et al., 2012; Soluri et al., 2007). Among the ions studied, NO_3^- and SO_4^{2-} stand out. These ions are associated with the burning of fossil fuels, so they are found in high concentrations in urban centers, where the main source of emission are the vehicles.

Only Mateus et al. (2013) evaluated the ionic composition of TSP, determining the concentrations of Cl^- , NO_3^- and SO_4^{2-} in particles sampled in Santa Cruz and Seropédica. These ions were found in similar concentration ranges, being related to the formation characteristics of the particles. Cl^- can be directly emitted to the atmosphere, as a primary pollutant, therefore, it tends to be present in larger particles, while NO_3^- and SO_4^{2-} are formed by reactions that occur in the atmosphere, therefore their greater association with smaller particle sizes. Another factor that can also be considered to understand the lower Cl^- concentrations in fine particles is the depletion of Cl^- through reactions in the gaseous state. The NO_3^- and SO_4^{2-} form the acids HNO_3 and H_2SO_4 , when in contact with H_2O , which react with Cl^- producing gaseous NO_3^- HCl , thus removing the chloride ions from the particulate phase (Mamane and Mehler, 1987).

In studies related to the PM_{10} fraction, the highest concentrations of NO_3^- and SO_4^{2-} were found by Gioda et al. (2011) in Duque de Caxias, a municipality in Rio de Janeiro which, besides being very populated, has highways with intense flow, including freight transport, and an important industrial complex where a petrochemical pole is located. At this particle size, the Cl^- concentrations reported by Mariani and Melo (2007) in Niterói and by Gioda et al. (2011) and Justo et al. (2020) in studies carried out in Rio de Janeiro. In these two cities there is great influence of air masses of oceanic origin and, therefore, the presence of Cl^- in PM is expected, especially in the coarse fractions.

For $PM_{2.5}$ the highest NO_3^- concentrations were observed by Quijano et al. (2019) in Copacabana, a residential-commercial neighborhood in the city of Rio de Janeiro, where the main source of pollutants are vehicles. The NO_3^- / SO_4^{2-} ratio greater than 1 indicates that there was a greater contribution from mobile sources, characterized by predominant nitrate concentration relative to sulfate. The highest SO_4^{2-} concentrations were observed by Mariani and Melo (2007) in the study carried out in Niterói.

4.11.2. Evaluation of the marine contribution in the PM composition

The average ion concentrations presented in the ionic composition assessment studies were used to calculate the non-marine contribution to the PM composition. Most studies on the water soluble PM fraction showed high *nss* for Ca^{2+} , K^+ , and SO_4^{2-} , indicating that the major source of these ions is not the sea. The lowest *nss percentages* were found for Mg^{2+} , indicating that this ion is mostly from marine *spray*.

Soluri et al. (2007) conducted a study in sites with strong influences from anthropogenic activities and found that, for the fine fraction of particulate matter, there was a contribution of *nss* greater than 90 % to the concentration of K^+ and SO_4^{2-} , while for the coarse fraction the percentages decreased to the range of 50 % to 70 % of *nss*. The higher non-marine contribution to the fine fraction may be associated with the formation of PM by combustion processes, which tend to generate particles with smaller diameters, while those present in the sea spray tend to associate with the coarse fraction. Similar behavior was later found by Godoy et al. (2009) in a study carried out at the same sampling sites.

In a study carried out in Niterói by Mariani and Mello (2007), high *nss* contribution was also observed for K^+ and SO_4^{2-} , mainly in the fine fraction. The *nss* contribution for Ca^{2+} was similar in both particle sizes and for Mg^{2+} it was higher for the coarser fraction, thus showed opposite variation to that reported by Soluri et al. (2007) and Godoy et al. (2009). According to the authors, the non-marine contribution for Ca^{2+} may be attributed to construction, emissions from vegetation, and biomass burning in the dry period. This last emission source was also associated with the non-marine contribution of K^+ and Mg^{2+} .

Gioda et al. (2011) observed in 2008 and 2009 high *nss* contribution for K^+ , Ca^{2+} , and SO_4^{2-} ions at the four sites studied. The values were similar, even when comparing sites with urban, industrial or rural characteristics. The biggest difference was found for Mg^{2+} that showed higher non-marine contribution at the rural site, which can be attributed to the greater distance from the sea and the biomass burning that occurs in the region.

Quijano et al. (2019) observed that the non-marine contribution to the concentration of Ca^{2+} , K^+ , and SO_4^{2-} in $PM_{2.5}$ sampled in the city of Rio de Janeiro was between 51 and 88 %. Among these ions, SO_4^{2-} was the one with the highest non-marine contributions, with similar percentages between urban and rural sites. For the other ions it was not possible to make this comparison because they were not detected in the samples sampled at the rural site. Similar results were observed by Justo et al. (2019) in PM_{10} , who observed non-marine contributions for Ca^{2+} , K^+ , and SO_4^{2-} between 58 and 80 %. As in the study by Quijano et al. (2019), depletion was observed for Mg^{2+} .

Miranda et al. (2012) and Andrade et al. (2012) made the determination of few ions in $PM_{2.5}$ sampled in the city of Rio de Janeiro. In both studies, non-marine source contributions of 97 % were observed for the SO_4^{2-} concentration. In the most recent study, developed by Mateus et al. (2020) in forest regions located in the municipalities of Seropédica and Teresópolis, it was observed that the largest contribution for Ca^{2+} , K^+ , and SO_4^{2-} in TSP and $PM_{2.5}$ was of non-marine origin, as well as in other studies conducted in the state.

4.11.3. Assessment of the acidity of particulate matter

Godoy et al. (2009) report results indicating that fine particles have a more acidic character than coarse particles, however, alkali ions that could be important for the neutralization of acid anions were not determined. This fact is highlighted by the cation deficiency observed through the ion balance, a measure of the ratio between cations and anions. The lower acidity of the coarse particles may be due to lower SO_4^{2-} concentrations evidenced by the increase in the $\text{NO}_3^-/\text{SO}_4^{2-}$ ratio.

The study by Soluri *et al.* (2007), the trend observed was opposite to that reported above, although the NH_4^+ cation was determined only in the fine particles. This may have contributed to the higher degree of neutralization in the $\text{MP}_{2.5}$ particles. In the study by Mariani and Mello (2007) the degree of neutralization indicated slight basicity of the particles, possibly due to the lower NO_3^- concentrations. The low levels of nitrate may have resulted from the volatilization of this ion found in the form of NH_4NO_3 , as the Teflon[®] filters used in this study facilitate the volatilization of this substance (Keck and Wittmaack, 2005). The deficiency of ions of acidic character is confirmed by the ion balance. The studies by Gioda et al. (2011) and Justo et al. (2020) showed that the PM_{10} showed better neutralization, which may be compatible with an ion balance close to unity.

Miranda et al. (2012) also report $\text{PM}_{2.5}$ with good neutralization capacity, however in this study the determination of some cations that could contribute to the alkalinity of the particles was not done. Quijano et al. (2019) observed that $\text{PM}_{2.5}$ sampled in urban sites presented slight acidity, while in rural and industrial sites the degree of neutralization was higher. This fact can be attributed to the higher concentration of nitrate at urban sites, while low values of the $\text{NO}_3^-/\text{SO}_4^{2-}$ ratio occur at rural and industrial sites.

Mateus et al. (2020) showed the occurrence of different patterns of acidity in the PM. The TSP and $\text{PM}_{2.5}$ showed high degrees of neutralization, which indicates basicity of the particles. This result can be related to the deficit of anions in relation to cations and also to the low $\text{NO}_3^-/\text{SO}_4^{2-}$ ratio.

4.12. Conclusion

The studies on concentration and composition of PM carried out in Brazil present as one of the objectives to generate information that indicates to the Government the

need for updates in environmental legislation. After almost three decades, the Brazilian legislation related to air quality was updated aiming at meeting the WHO recommendations. However, changes in air quality standards do not guarantee that pollutants will be reduced, because atmospheric monitoring is necessary to verify that the concentrations found in the air comply with the legislation. The monitoring of air pollutants in Brazil is inefficient, since only 9 of 27 states have monitoring networks. The state of Rio de Janeiro was one of the pioneers in the installation of air quality monitoring networks, so it has presented PM concentration data since the 1960s. Although the PM samplers have a wide distribution, which makes it possible to obtain information on air quality in different regions of the state, most studies have been conducted in the metropolitan region.

The highest concentrations of PM (TSP, PM₁₀ and PM_{2.5}) were observed in places with strong influence of anthropogenic activities, such as vehicular traffic and industries, while lower concentrations are in locations far from major urban centers, where few anthropogenic sources are found. Over the years, a reduction in PM concentration was observed, especially in Santa Cruz and Volta Redonda, which can be associated with the modernization of the industrial complexes installed in these two locations. In the city of Rio de Janeiro and Duque de Caxias there are variations in the concentrations of the three particle sizes within the evaluated period and concentrations above the CONAMA limits.

The main elements in the composition of particulate matter are Fe and Al, followed by Zn. These elements are commonly associated with soil composition, but can also be emitted by some anthropogenic sources. The mixed contribution to the concentration of these elements was verified by EF. Other elements such as Ni, Pb, Cu, Cd, and Mn were found at trace concentrations and their high FE indicated that they are of anthropogenic origin. As observed for PM concentrations, Santa Cruz and Volta Redonda also presented reductions in the concentration of some elements over the years.

The water-soluble PM fraction is composed mostly of the anions NO₃⁻ and SO₄²⁻, which are tracers of vehicular emissions. The assessment of the marine contribution to the ionic composition of PM showed that in most of the studies Ca²⁺, K⁺, and SO₄²⁻ had the largest contribution from other sources, while Mg²⁺ is mostly from the sea. The estimation of the degree of neutralization in PM showed that in most studies in which soluble species were quantified, the particles had an acidic character, which can be

attributed to the high concentrations of the strong acid ions NO_3^- and SO_4^{2-} . This indicates the possibility of acid rain occurring at the monitored sites, which poses a risk to the population, ecosystems, monuments, and the environment as a whole.

The meteorological variables exert great influence on the concentration and composition of PM, therefore, in periods of higher volumes of rainfall the concentrations were lower and in less rainy periods were higher. Seasonality affected the different sampling sites in a similar way, since the meteorological conditions of the state are similar, with rainy periods during spring and summer, and dry periods during fall and winter.

The evaluation of air quality in the state of Rio de Janeiro has proven to be efficient, mainly due to the interest of researchers, however, it is necessary to expand the study area, because few studies are developed in the interior of the state, where other sources of pollutants need to be evaluated. The 1st Diagnosis of the Brazilian Air Quality Monitoring Network showed that although it is a pioneer in this monitoring, the state still needs to invest more, since it was observed discontinuity in the operation of many stations and the invalidation of a significant amount of data. In addition, future studies should consider other substances that may be part of the composition of PM, since new pollutants are released into the atmosphere over the years due to the modernization of equipment and production processes. In order to improve air quality, establishing cooperative projects between research institutions and governmental environmental agencies is still a challenge to be overcome.

5 Assessment of air quality changes during COVID-19 partial lockdown in a Brazilian metropolis: from lockdown to economic opening of Rio de Janeiro, Brazil

Karmel Beringui¹, Elizanne P. S. Justo¹, Anna De Falco¹, Eduarda Santa-Helena¹, Werickson F. C. Rocha², Adrien Deroubaix³ and Adriana Gioda^{1*}

¹Pontifical Catholic University of Rio de Janeiro, 22451-900, Rio de Janeiro, RJ, Brazil

² National Institute of Metrology, Quality and Technology (INMETRO), 25250-020, Duque de Caxias, RJ, Brazil

³Environmental Modeling Group, Max Planck Institute for Meteorology, Hamburg, Germany

Corresponding author: Adriana Gioda - agioda@puc-rio.br

Published: Air Quality, Atmosphere & Health (2021) available online since 23/11/21

Abstract

During the COVID-19 pandemic, restrictive measures are taken by several cities around the world, as well as Rio de Janeiro, reducing routine activities in large urban centers and primary pollutant emissions. This study aims to assess air quality during this partial lockdown through O₃, CO, and PM₁₀ concentrations and meteorological data collected in five air quality monitoring stations spread over the whole city, considering the substantial changes in city routine. The period evaluated starts in March 2020, when the partial lockdown was decreed and ends in September 2020, when economic opening ended. Comparing with 2019 data, CO concentration reduced significantly, as expected once the main source of these pollutants is vehicular traffic. O₃ concentration increased, most probably as a consequence of the reduction in primary pollutants. On the other hand, PM₁₀ concentration did not vary significantly. From June to September pollutant concentrations increased responding

to the economic opening. Thereby, the partial lockdown contributed to improving air quality in Rio de Janeiro city, which means that changes in work format may be an alternative to reduce atmospheric pollution in big cities, once home-office contribute to mobility reductions, consequently, to vehicular emissions.

Highlights

Lockdown contributed to CO reduction and O₃ increase.

Differences on rain profile explains low variation on PM₁₀ concentrations.

Lockdown has been like a very long weekend concerning to atmospheric pollution.

Home office and distance learning improve air quality.

5.1.Introduction

The COVID-19 pandemic spread rapidly around the world in early 2020 after the first cases in Wuhan, Hubei province (China), in December 2019 (Saadat et al., 2020). On March 11 2020, there were more than 118,000 cases in 114 countries, and 4,291 people had lost their lives. Therefore, WHO assessed that COVID-19 could be characterized as a pandemic (World Health Organization, 2020). In Brazil, the first case of COVID-19 was registered on February 26 in São Paulo, while the first case in Rio de Janeiro was registered on March 5. A year later (February 26, 2021), there were more than 10 million confirmed cases in all regions of Brazil (Ministério da Saúde, 2021), the majority of confirmed cases in the southeastern region, Rio de Janeiro – RJ, with 206,149 confirmed cases (Prefeitura do Rio de Janeiro, 2021).

The health risk posed by the novel coronavirus, added to its high transmissibility, made several cities in the world stop their activities in an attempt to contain the growing number of cases of the disease and deaths. The lockdown around the world changed the pollutant emission profile, inducing improvements in primary pollutants in several cities (Bao and Zhang, 2020; Saadat et al., 2020). One of the main consequences of partial closure was the decrease in sources of air pollutants. This change in the city's routine can cause an improvement in air quality due to a decrease in the emission of pollutants (Nakada and Urban, 2020). It is worth noting that if a region already has good air quality in a routine situation, quarantine will not have a significant impact on air quality (Zangari et al., 2020).

Cities as Milan, New York, New Delhi, and London recorded an improvement in air quality (Collivignarelli *et al.*, 2020; Girdhar *et al.*, 2020; Sarfraz *et al.*, 2020). In China, an extremely high haze event was shown by Le *et al.* (2020), while O₃ has increased in many megacities (Venter *et al.*, 2020). Even in the most populated area in China an improvement in air quality was observed, which was attributed to mobility reduction (Filonchyk and Peterson, 2020). In Barcelona, there were reductions in PM₁₀ and NO₂ concentrations during the lockdown compared to the previous months (Tobías *et al.*, 2020). Some South American countries (Colombia, Ecuador, Argentina, and Peru) were also recorded an improvement in air quality due to social isolations, however, some authors predicted that pollution levels would return to normal following the return of economic activities (Bolaño-Ortiz *et al.*, 2020; Camargo-Caicedo *et al.*, 2021; Rojas *et al.*, 2021; Zambrano-Monserrate and Ruano, 2020).

Brazil declared COVID-19 a public health emergency on March 3 (Croda *et al.*, 2020). From that, Brazilian cities began to take restrictive measures to contain the progress of the disease and decreed partial lockdown (Dantas *et al.* 2020; Nakada and Urban 2020). In Rio de Janeiro state, the governor declared a public health emergency on March 16, stating that educational institutions, cultural establishments, and restaurants were closed. Subsequently (March 21st) the access to the city of Rio de Janeiro was limited by prohibiting the entry of public transport from other cities. Besides that, industries, commercial establishments, and airports have reduced their operations (Crokidakis 2020). From July 1st, the city of Rio de Janeiro started the gradual economic activities opening, which was planned to take place in six stages, which starts on September 1st.

Some studies regarding Brazil's air quality assessments and pandemic have been published. In São Paulo there was an improvement in air quality related to the PM₁₀, PM_{2.5}, and NO₂ concentrations, with a significant drop of 45 %, 46 %, and 58 %, respectively (Debone *et al.* 2020). Nakada *et al.* (2020) evaluated the variations in pollutant concentrations during the lockdown at four sites in São Paulo city. Overall, there were drastic reductions in the concentrations of NO (77 %), NO₂ (54 %), and CO (65 %) compared to the five-year monthly average. As in other megacities (Venter, 2020), in São Paulo there was also an increase in O₃ concentrations (30 %) (Nakada, 2020). In three stations in Rio de Janeiro (Bangu, Irajá, and Tijuca), CO levels showed significant reductions (30 – 48 %), followed by NO₂, while PM₁₀ levels only decreased in the first week of lockdown. Ozone concentrations have also increased in Rio de

Janeiro city (Dantas *et al.* 2020). Pollutants directly related to the vehicle, like CO and NO₂, showed the highest reduction. According to Siciliano *et al.* (2020), in Rio de Janeiro their reduction was about 10 – 40 %. Satellite data obtained for southeastern Brazilian cities also show pollutants decrease. In May 2020 a reduction of 42 % in NO₂ was recorded in São Paulo in comparison with the monthly average obtained between 2015 and 2019. Rio de Janeiro records a decrease even higher, 49.6 % (Brandao and Foroutan 2021).

Social isolation measures adopted to contain the spread of coronavirus transformed one of the major Brazilian metropolises into a real laboratory where air pollution could be studied considering changes in political restrictions. Since the concentrations of pollutants vary between different areas of the same city, and the results may not show the same reductions. The main goal of this work is to evaluate air quality changes in five air quality monitoring stations from Rio de Janeiro city, through the concentrations of O₃, CO, and PM₁₀ between March and September 2020, making a comparison with the concentrations observed in the same period of 2019 and considering the meteorology influence. Although some studies have been conducted in Rio de Janeiro, they focused on the primary effects of the partial lockdown on air quality, considering from the first weeks to the third month of social isolation. This study evaluated pollutant concentrations considering changes in political restriction since the lockdown proclamation until economic opening. Besides that, estimate meteorological conditions and urban source emission contribution.

5.2. Material and Methods

Description in topic 3.2, page 38.

5.3. Results

5.3.1. Mobility profile

The main air pollutant source in urban centers is vehicle emission, thus, changes on mobility is an indication of emission variation. According to mobility data provided by Apple and Google (Figure 18.1 – supplementary material), mobility changes in Rio de Janeiro state, Rio de Janeiro city and Brazil presented the same profile. Both datasets indicate that mobility reduction started in mid - March reaching around 90 %

of decrease at the end of April. It indicates that social isolation measures caused a reduction on emission sources, once mobility decreased after the lockdown decree.

Although the economic opening at the city occurred only from June, since May people relaxed social isolation by themselves and started to return some activities. The return of public transportation allowed by the state government has contributed to the increase in the number of people on the streets.

5.3.2. Pollutant concentration distribution

Considering the daily average concentration in 2019 and 2020 over the same period, for the whole period of 2019, the daily average concentration and standard deviation of CO was 0.32 ± 0.27 ppm, O₃ was 31 ± 26 $\mu\text{g m}^{-3}$, and PM₁₀ was 38 ± 24 $\mu\text{g m}^{-3}$. In 2020, the average concentration and standard deviation of CO was 0.23 ± 0.20 ppm, O₃ was 38 ± 27 $\mu\text{g m}^{-3}$, and PM₁₀ was 36 ± 23 $\mu\text{g m}^{-3}$. Figure 5.1 shows the difference between daily concentration in 2020 and the averaged concentration in 2019 of three gases. This difference represents an anomaly caused by COVID-19 (*i.e.* the daily concentration in 2020 minus the averaged concentration in 2019).

As expected, daily CO concentrations were lower in 2020. CO concentrations decreased quickly on 22 March (of 0.10 to 0.15 ppm, compared to early March). During this week (the second week of the lockdown), the entrance of public transport in Rio de Janeiro city was prohibited. The reduction in the vehicles traffic in the city consequently causes a decrease in the emission of CO. The anomaly of CO concentrations compared to the average on this period in 2019 remain important until the end of May.

For O₃, the anomalies are mostly positive (ranging between -5 and +20), except for one station (Bangu) presenting a different behavior. As observed in other cities (Venter *et al.* 2020), the O₃ concentration in 2020 was higher in all monitoring stations. The tropospheric O₃ chemistry is complex, primary pollutants participate both in its formation and depletion. According to Geraldino *et al.* (2017), the topography and meteorology of Rio de Janeiro city favor O₃ formation, and its photochemistry is limited by volatile organic compounds (VOCs). In this case, low NO₂ concentration, as a result of low NO concentration, leads to high O₃ concentration. It is explained by the reaction $\text{NO} + \text{O}_3$ accountable for O₃ depletion (Geraldino *et al.* 2017, 2020). Thus, because a decrease in NO₂ concentration is a direct result of a reduction in NO concentration,

higher O_3 concentration may be attributed to lower NO_x concentration indicated by low NO_2 concentration. This same relation was verified during the lockdown in other countries around the world. Dantas *et al.* 2020 reported a reduction (32 – 54 %) in NO_2 concentration in Rio de Janeiro city for the last week of March 2020 which was attributed to the reduction in car flow by 80 %.

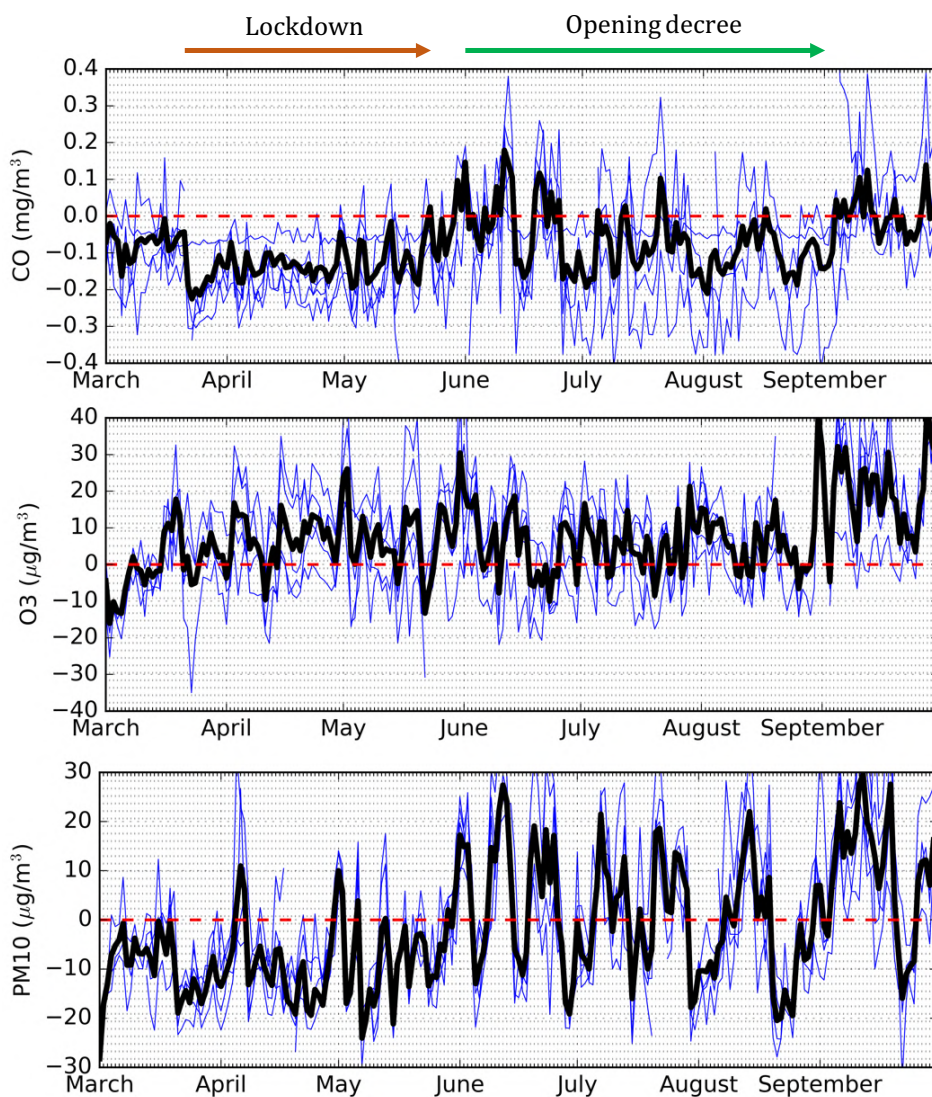


Figure 5.1 Difference between daily concentration in 2020 and the averaged concentration in 2019 of three pollutants for the same period (the black line is the mean of all stations and the blue lines are concentration at each station).

There were two high O_3 events on 1st and 31st May observed at all monitoring stations. Meteorological parameters that might enhance O_3 concentration do not

explain these events. To explain them, data for NO, NO₂, and NO_x concentration, which was provided only for the Bangu station, was evaluated. The high O₃ events coincide with days on which the lowest NO_x concentrations were recorded. As pollutants concentration profiles were similar for all stations, it is possible to infer that lower nitrogen oxides concentrations were also recorded those days. Once those gases participate in O₃ decomposition, higher O₃ concentration is observed when they are at reduced levels. As mentioned above, O₃ photochemistry is VOC limited, thus its concentration is enhanced by low NO_x levels and high temperatures.

PM₁₀ anomaly is negative during the Rio de Janeiro lockdown, mostly ranging between 0 and -15, which was expected for CO concentration. The main PM₁₀ source in urban areas is vehicle traffic (Miranda *et al.* 2012; Ali *et al.* 2019). Then, the huge traffic reduction after lockdown measures, corroborated by the mobility decrease of around 90 %, can be considered the main reason for the decrease in PM₁₀ concentration. In June, when the lockdown easing measures started, anomalies became positive, showing that PM₁₀ concentration increased, reaching values even higher than in 2019.

To assist in data interpretation, Spearman correlations (Figure 18.2 – supplementary material) were calculated to verify the relation between pollutants. It was noticed in Figure 5.1 that the two high ozone events correspond to two PM₁₀ positive anomalies (peak on the PM₁₀ time series) reaching +15. However, the Spearman correlation ($p < 0.05$) obtained between these pollutants was positive but weak ($r < 0.40$) at all monitoring stations during May 2020. On May 1st and 31st, when occurred high ozone events, the correlations between them were weekly negative. According to Nishanth *et al.* (2014), the relation between PM₁₀ and O₃ depends on particles absorption characteristics. The large particles' surface area can contribute to heterogeneous reactions involving tropospheric ozone. Particles that absorb radiation can contribute to an increase in the concentration of O₃, whereas particles that disperse light contribute to a decrease in the concentration of O₃ in the atmosphere.

In all monitoring stations, moderate positive correlations were observed between O₃ and PM₁₀. These positive correlations are related to the anthropogenic origin of these pollutants. In the Centro station, there was a correlation between O₃ and PM₁₀ in all the months of 2020, and in the Tijuca station, correlations were observed in all the evaluated months, the largest of them observed in May and June, both in 2019 and in 2020.

A descriptive statistic of meteorological variables is presented in Table 18.1 (supplementary material). Comparing both years it is possible to notice that Rio de Janeiro city was under the same meteorological conditions. However, it is possible to highlight rainfall and wind speed at Tijuca in 2020 were higher than in 2019. The rainfall was influenced by volume recorded in May, which was more than 5-times higher than other months. The wind speed about 3-times higher than the mean value of 2019, mainly from winds that come from west and northwest, where is located the Tijuca National Forest. These wind results were influenced by values record in March 2020. Although Tijuca presented these meteorological singularities in March and May, rainfall and wind speed do not explain pollutant variation. As in most months, meteorological parameters did not change, they could not be accountable for air quality variation during the period evaluated.

Positive Spearman correlations ($p < 0.05$) were observed in Bangu, Campo Grande, and Centro, from moderate to strong, between the O_3 concentrations and SR, T, and WS. It was also found to have negative correlations between O_3 and RH of the air. These correlations were already expected since the tropospheric O_3 is formed by photochemical processes, therefore, a greater solar indication favors its formation, besides it also contributes to the increase in temperature (Gioda *et al.* 2018; De La Cruz *et al.* 2019; Geraldino *et al.* 2020). The correlation with WS indicates that pollutants from other regions are participating in the O_3 formation processes. Higher RH of the air makes it harder for the sun to arrive, disfavoring O_3 formation.

In Bangu, Campo Grande, and Centro, moderate negative correlations between O_3 and CO were also observed. In Bangu, such correlations were observed only in 2019 (March and June). In Campo Grande, they were observed in May and June of both years evaluated. In Centro, they were observed, mainly in 2020. As O_3 is a secondary pollutant, explain its concentration should consider several variables, as mentioned above. Carbon monoxide concentration exerts, mainly, an indirect effect on O_3 concentrations. Negative correlations between them may indicate O_3 depletion through photochemical reaction with NO_x , once NO_x and CO may present the same source, then, O_3 decomposition is favored in polluted conditions. Another explanation is the hydrocarbon oxidation by O_3 molecules, which reduces O_3 concentration and increases CO concentration. And finally, the stratospheric O_3 intrusion in the troposphere may increase O_3 concentration while CO decreases, once this air is richer in O_3 (Voulgarakis *et al.* 2011). Since O_3 chemistry in Rio de Janeiro city is limited by

VOC, low NO_x concentrations lead to high O₃ concentrations. Considering that the main source of CO and NO_x, which includes NO₂, is fuel combustion, the reduction of mobility after the lockdown decree implies a decrease in CO and NO_x emission. Thus, the negative correlation O₃ x CO does not present a cause-and-effect relationship, nevertheless, it represents a consequence of the negative correlation between O₃ and NO₂ once CO and NO₂ come from the same source.

Except for Copacabana, all monitoring stations presented moderate to strong correlations between PM₁₀ and CO, mainly from June to September. These results show that both pollutants may present the same emission source, which could be vehicular emissions. The lack of correlation in Copacabana indicates that the main source of PM₁₀ is sea spray.

Moderate positive correlations between PM₁₀ and temperature were also observed in Bangu, Copacabana, and Tijuca these pollutants correlated in most of the evaluated months, except for June 2020 in Bangu and April 2020 in Tijuca. In general, PM₁₀ and temperature present a negative correlation, because high-temperature favor particles dispersion, which contributes to a decrease in PM₁₀ concentration (Li *et al.* 2015). The positive correlations found in this study indicate that several other variables are influencing PM₁₀ concentration that is accompanied by high temperatures (Kim 2019).

Considering that the lockdown period was between March 19th and June 19th, which coincide with the second lockdown decree and first opening decree, it was observed considerable pollutants variation, in comparison with the previous year. CO concentration reduced 21 – 62 %. O₃ increased 15 – 74 % except for Bangu where it decreased 11 %. PM₁₀ decreased 5 – 22 % except for Bangu where it increased 9 %.

5.3.3. Air pollutant time variation

Pollutant concentration averages obtained between March and September of 2019 and 2020 for all monitoring stations are presented in Figures 5.2 – 5.4 split by hour per weekday, hour, month, and weekday. Tables 18.2 – 18.4 (supplementary material) present descriptive statistic data for all monitoring stations. Table 5.1 presents the percentage of monthly variation of each pollutant at all monitoring stations in 2020 comparison with 2019. Negative values indicate lower concentration recorded in 2020.

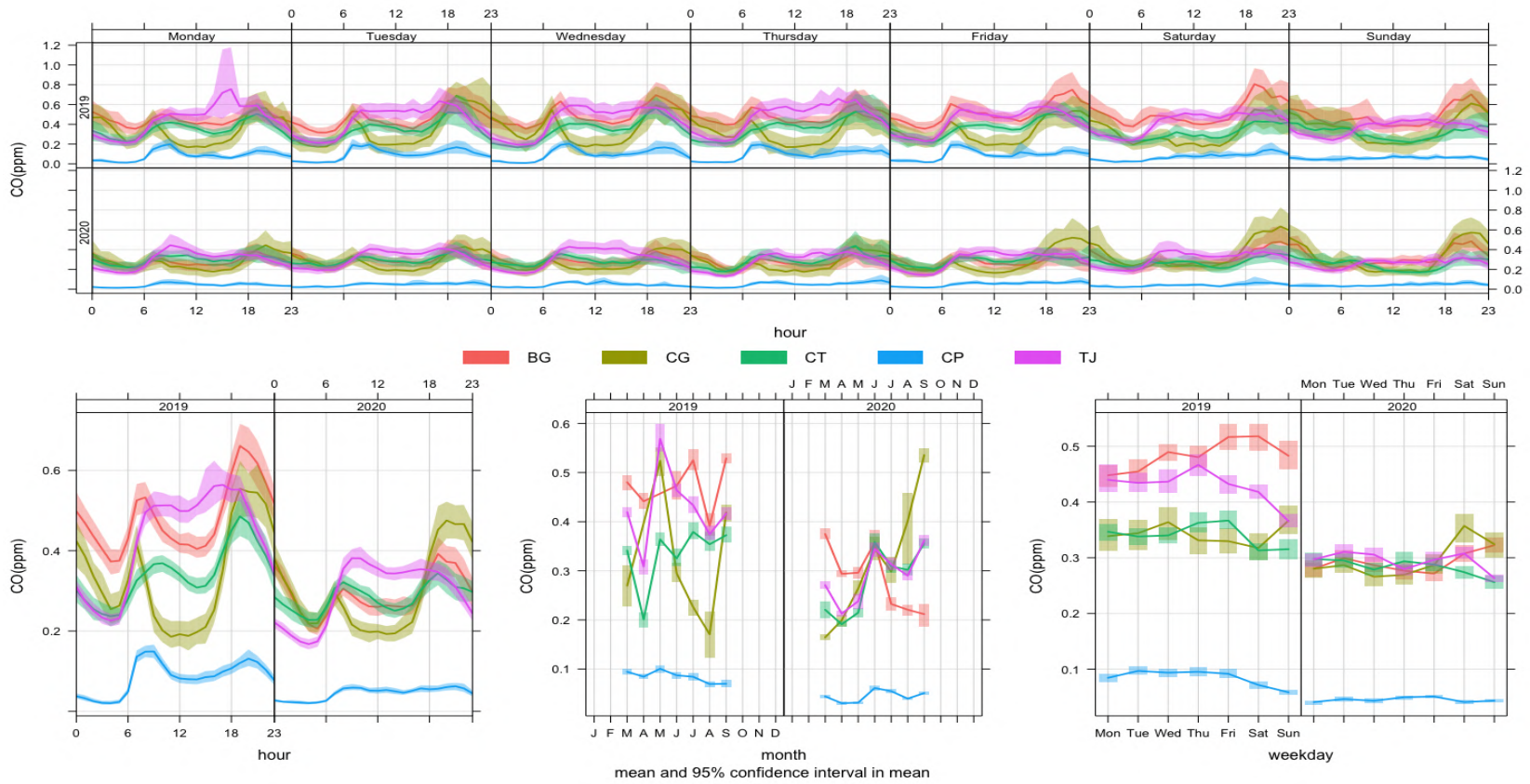


Figure 5.2 Time variation of the concentrations of CO (ppm) at Bangu (BG), Campo Grande (CG), Centro (CT), Copacabana (CP), and Tijuca (TJ) stations in 2019 and 2020.

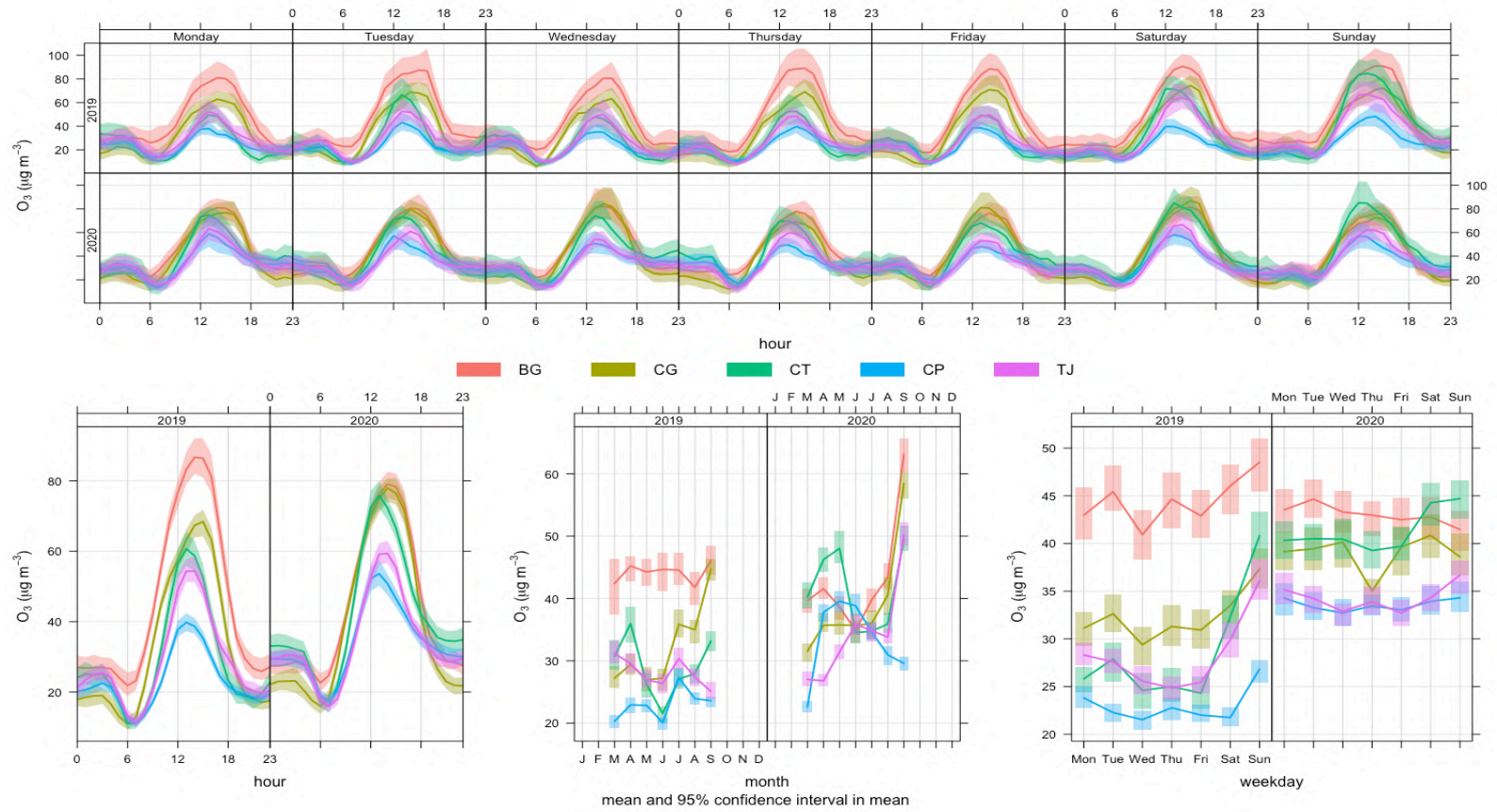


Figure 5.3 Time variation of the concentrations of O₃ (µg m⁻³) at Bangu (BG), Campo Grande (CG), Centro (CT), Copacabana (CP), and Tijuca (TJ) stations in 2019 and 2020.

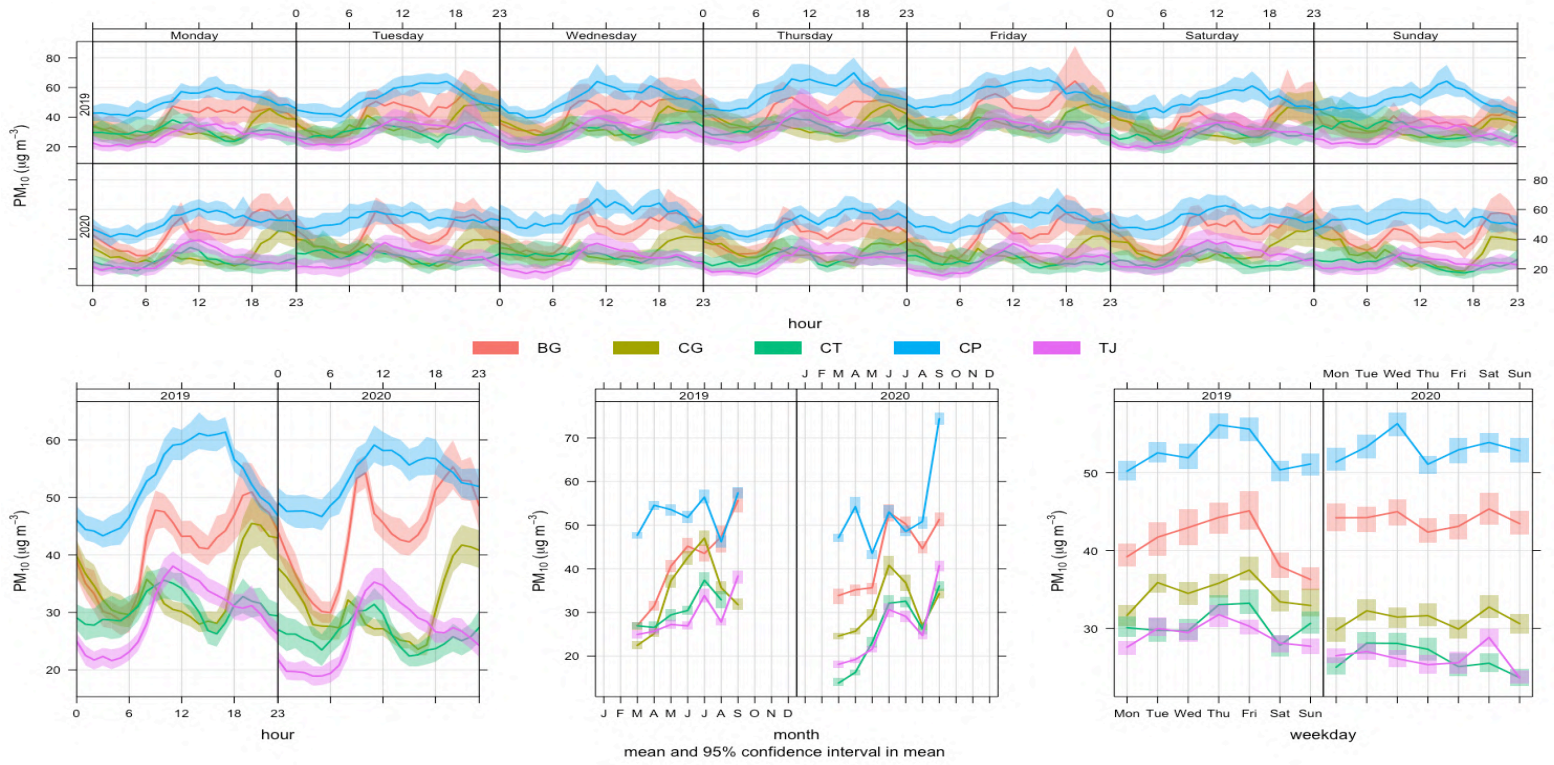


Figure 5.4 Time variation of the concentrations of PM₁₀ (µg m⁻³) at Bangu (BG), Campo Grande (CG), Centro (CT), Copacabana (CP), and Tijuca (TJ) stations in 2019 and 2020.

To evaluate pollutants concentration variation, it was investigated if there is a statistically significant difference in the concentration levels of the components CO, O₃, and PM₁₀ between the years 2019 and 2020. Due to the non-normality of the data, the Wilcoxon-Mann-Whitney nonparametric test was applied with a significance level of 5 %. In other words, we sought to verify whether there was a change in concentration from one year to another considering it as a single period from March to September (Figure 5.5). The comparison of each month from the two years is presented in Table 5.2, which shows the pairs of months that did not present statistical differences.

In general, the Copacabana station registered the lowest CO emission and the highest amount of PM₁₀ when compared to the other stations. In Bangu there was a reduction in CO emissions in 2020 when compared to 2019. An increase of O₃ is observed in Tijuca, Copacabana, and Centro in 2020 when compared to 2019.

Table 5.1 Variations in monthly concentrations of pollutants, expressed as percentage, comparing 2019 and 2020.

Station	Março	Abril	Maió	Junho	Julho	Agosto	Setembro
Ozone variation (%)							
Bangu	-7	-8	-13	-22	-11	4	37
Campo Grande	16	21	33	31	0	16	31
Centro	11	65	73	93	27	29	25
Copacabana	31	28	83	60	28	29	49
Tijuca	-13	-9	17	36	15	23	100
Carbon monoxide variation (%)							
Bangu	-22	-33	*	-24	-56	-44	-60
Campo Grande	-39	*	-50	17	32	135	28
Centro	-53	-64	-69	-30	-35	-43	-27
Copacabana	-35	-5	-41	10	-18	-15	-5
Tijuca	-35	-31	-58	-26	-28	-22	-13
Particulate matter (< 10 µm) variation (%)							
Bangu	26	12	-12	17	15	-6	-8
Campo Grande	10	2	-21	-4	-22	-25	8
Centro	-1	-1	-19	2	-14	10	30
Copacabana	-49	-39	-21	5	-13	-20	*
Tijuca	-27	-25	-21	14	-14	-11	6

*There was not data from one this month in 2019 or 2020.

Considering the whole period, it can be seen that there was no change in the concentration of O_3 in Bangu [P -value 0.9268] and PM_{10} in Copacabana [P -value 0.3532] in the period from March to September 2020 when compared to the same 2019 period.

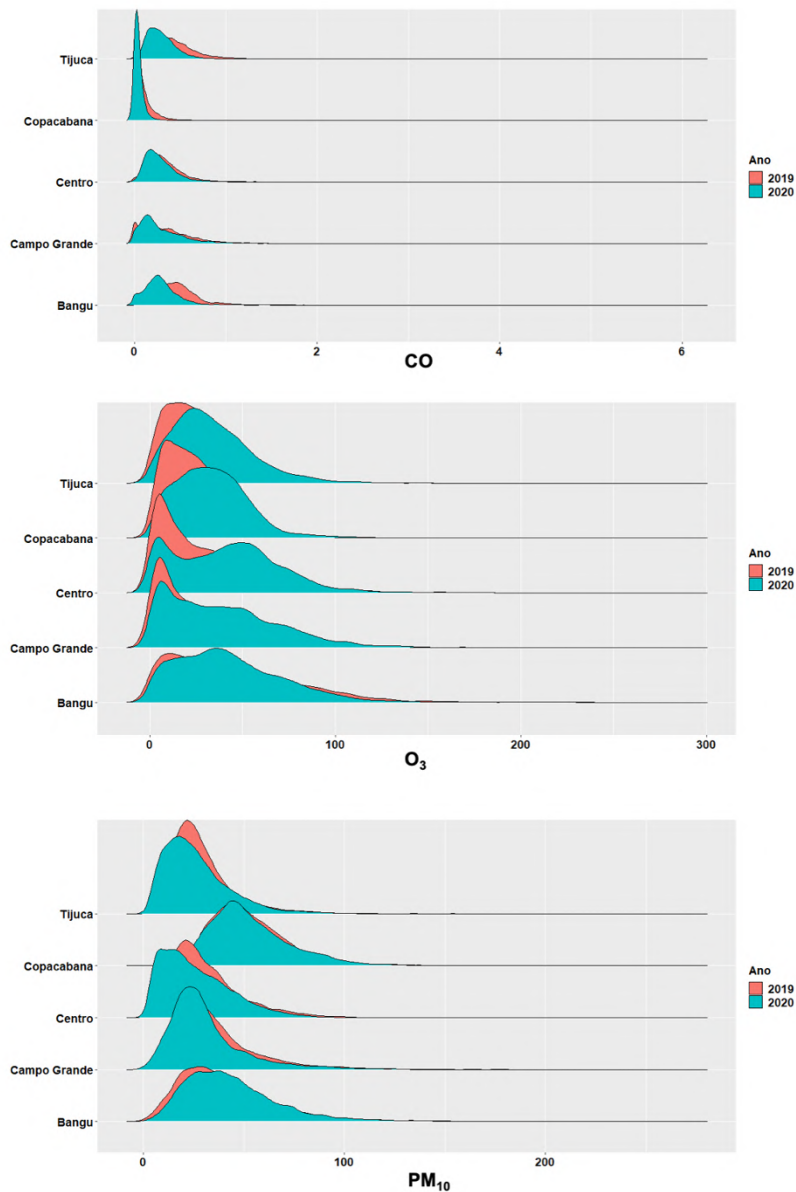


Figure 5.5 CO , O_3 and PM_{10} data distribution for the period between March and September of 2019 and 2020

Table 5.2 Results of the comparison between pairs of months (2019 vs 2020) when no statistical variations were observed in the concentration of the pollutants.

Station	CO		O ₃		PM ₁₀	
	Pairs of months (2019 vs 2020)	<i>p</i>	Pairs of months (2019 vs 2020)	<i>p</i>	Pairs of months (2019 vs 2020)	<i>p</i>
Bangu	-	-	March April August	0.31	August September	0.561 0.766
				2		
				0.62		
Campo Grande	-	-	July August	0.08	April	0.927
				2		
				0.92		
Centro	April	0.317	-	-	June	0.688
	September	0.609				
Copacabana	June	0.133	-	-	March	0.806
					April	0.072
					June	0.133
Tijuca	-	-	March April	0.16	-	-
				9		
				0.40		
				7		

5.3.4. Carbon Monoxide monthly concentration

All stations are located close to high traffic routes, therefore the concentrations of the three pollutants studied were affected. The average monthly concentration and standard deviation of CO ranged from 0.04 ± 0.04 ppm in Copacabana to 0.5 ± 0.2 ppm in Campo Grande in 2020; while in 2019 the concentrations and standard deviation ranged from 0.07 ± 0.1 ppm in Copacabana to 0.6 ± 0.4 ppm in Tijuca. However, no station exceeded the air quality standard established for CO by Brazilian legislation (9 ppm, 8-hour mobile mean) (CONAMA 2018). The average concentration in 2020 is 97 % below Brazilian standard, while in 2019 it was 96 % lower.

For most monitoring sites, monthly CO concentration obtained during 2019 presented higher values, with the exception of Campo Grande, in other words, it was verified CO reduction during lockdown. This neighborhood is characterized by a strong

presence of commercial enterprises. Beside of that, in the surroundings of this region are installed some industrial enterprises. It is observed that the first peak of concentration in 2020 occurs in June, when the restrictions measures began to be reduced and the second peak in September, when the last phase of the economic opening began. This neighborhood has one of the highest population densities, so the return of economic activities represents a greater number of people back on the streets compared to other neighborhoods in the city.

Statistically, CO concentration obtained in 2020, for mostly months, at all monitoring stations presented difference in relation to the previous year. The lower concentrations obtained in 2020 is related to the reduction in vehicle flow, corroborated by mobility data, which had the contribution of the decrease up to 50 % in public transport fleet and adoption of home office services by most part of companies.

The levels of CO in Copacabana decreased 31 % in April, 2020, in relation to March, 2020. In comparison with concentration obtained in 2019, Copacabana also presented the greatest CO concentration reduction: 63 % in April and 68 % in March. Bangu, the site with the highest CO average concentrations in 2019, presented reductions between 22 % and 60 % in 2020, comparing monthly CO average concentration with the previous year.

Considering CO concentration variation between March and September, 2020, with the exception of Bangu, in all other stations it was observed increasing concentrations from June. Although CO concentrations over the period evaluated presented an increase between 27 to 225 % in relation to CO concentration registered in March, 2020, they were, in most cases, below the values registered in the same months of 2019. Only Copacabana (June) and Centro (September) presented average concentration with no statistical difference in relation to 2019 after opening decrees. The economic opening since June contributed to the increase in CO concentration, however, it remained lower than values registered in 2019 because economic activities still remained under control, in addition, schools and universities remained closed.

5.3.5. Ozone monthly concentration

The average monthly O₃ concentration and standard deviation in 2019 ranged from 20 ± 15 µg m⁻³ in Copacabana to 46 ± 34 µg m⁻³ in Bangu; in 2020 ranged from 22 ± 15 µg m⁻³ in Copacabana to 63 ± 35 µg m⁻³ in Bangu. Considering the average

concentrations obtained between March and September of 2020, with the exception of Bangu station, other monitoring presented an increase up to 93 % in O₃ concentration, compared to the same months of 2019. The average concentration in 2020 is 73 % below Brazilian standard (140 µg m⁻³), while in 2019 it was 78 % lower.

Ozone concentrations registered in Campo Grande and Copacabana since April, 2020 were up to 85 % higher than the values registered in March 2020. Tijuca, presented concentration 16 - 86 % higher since May, 2020. In Centro, O₃ concentrations registered in April and May were 15 - 20 % higher than values obtained in March, but in June and August they decreased 14 %, in relation to March and increased again in September (23 %). In Bangu this pollutant presented a random profile, increase in April, decrease until June and again increase until September.

In comparison with average concentrations obtained in 2019, statistical differences were observed in Centro and Copacabana in all months, which presented lower concentration for the entire period. Both regions have undergone drastic routine changes after lockdown decrees, even after opening measures they did not return to the same routine observed before the pandemic, mainly because most schools opted to keep distance learning and companies choose to continue with the home office or returned to face-to-face activities on a rotating basis. Those changes in routine activities contributed to the decrease in atmospheric pollutants that participate in the O₃ formation. As observed in other cities around the world, the decrease in some pollutants, as NO_x and VOC, induced the increase in O₃ concentration.

Bangu station presented a different behavior, with lower O₃ concentration during lockdown. At this station it was recorded higher NO, NO₂ and NO_x concentration in 2020, mainly during lockdown period, in comparison with the same period of 2019. As the O₃ formation at this region is favored in low NO_x levels, during lockdown the increase in NO_x concentration conducted to lower O₃ concentration. According to Dantas *et al.* 2020, since April 6th a reduction in O₃ concentrations was recorded which was also favored by less rainfall and lower SR.

5.3.6. Particulate matter monthly concentration

The average monthly PM₁₀ concentration and standard deviation in 2020 ranged from 13 ± 10 µg m⁻³ in Centro to 74 ± 23 µg m⁻³ in Copacabana; while in 2019 ranged from 22 ± 11 µg m⁻³ in Bangu to 57 ± 22 µg m⁻³ in Copacabana. PM₁₀ concentration

profiles for the two years were similar. It was the pollutants that showed the less concentration variation. The average concentration in 2020 is 70 % below Brazilian standard, while in 2019 it was 69 % lower.

Some question that should be pointed is that the absolute value of rainfall recorded in 2019 was higher than 2020. Some months of 2020 that presented PM_{10} average concentration with no statistical difference in relation to the previous years recorded less rainfall volume in 2019. Then, in 2019 the rainfall contributed to the particle removal, decreasing PM_{10} concentration. In 2020, the less rainfall volume was compensated by the decreasing in emission caused by routine changes. Thus, even with decrease in PM_{10} emission in 2020, the average concentration remained similar with the previous years. The same behavior of rainfall was also observed by Rudke *et al.* 2021 in a study conducted in Metropolitan Area of São Paulo.

Bangu and Campo Grande presented PM_{10} concentration in March and April 2 - 15 % higher than in the same months of 2019. Other three monitoring stations presented concentrations up to 48 % lower between March and May, compared to the same months of 2019. In June, when economic activities returned partially, it was registered 2 - 13 % increase in relation to the same month of the previous year which may be attributed to differences on rainfall profile of both years.

Between March and September, 2020, the PM_{10} concentration increased over the months. The main increase was observed in Centro in June and July, when it was verified concentration 130 % higher than March. As the economic open started in June, it was the month when the highest increased concentration was observed for most monitoring stations. Only Tijuca presented the highest concentration in September.

5.3.7. CO, O₃ and PM₁₀ diurnal and weekly cycle

Pollutants diurnal cycles in 2019 and 2020 was evaluated through hourly average concentration presented in Figures 5.2 – 5.4. CO and PM_{10} concentration diurnal cycles obtained in 2020 was below the values obtained in 2019. O₃ concentration diurnal cycles obtained in 2020 presented an opposite behavior, because the average concentration in 2020 was higher than 2019. However, pollutant concentrations varied from 2019 to 2020, the peak of concentration in 2020 happened at the same time as in 2019 for the three pollutants. Only Bangu presented in 2020 an

O₃ diurnal cycle below the values obtained in 2019 and PM₁₀ diurnal cycle higher than 2019.

The careful examination of each pollutant diurnal cycle shows that the hourly CO concentration profile was similar to the PM₁₀ profile, with peak concentration in the morning. After the concentration decreases during the afternoon, another peak appears in the evening. The same hourly concentrations profile was observed in 2020, but due to the lower concentrations obtained that year, the variations in concentrations between morning and night were smaller, mainly in Copacabana and Tijuca. This concentration profile is characteristic of urban regions because it varies together with the change in the vehicles flow in the monitored region. The peak of concentration occurs at different times in each of the stations, but this concentration profile is following the times of entry and exit from school, commerce, and industries. The highest concentrations are observed in the morning when there is a large flow of people moving around the city at the same time. Due to the greater variation in the time for returning home, the concentrations at the end of the day are lower than in the morning.

Higher O₃ concentrations occurs around noon due to greater SR. In the both years, the O₃ concentration peak occurred between 1:30 pm and 3:30 pm in all monitoring stations. Bangu presented higher concentrations in 2019, Tijuca presented similar concentrations in both years and Campo Grande, Centro, and Copacabana presented higher O₃ concentrations in 2020. The lower concentrations observed in 2020 may be related to variations in the concentrations of other pollutants that participate in the mechanisms of formation and degradation of the O₃ molecule.

CO weekly cycle obtained in 2020 for all monitoring stations were very similar, while in 2019 they presented different levels of concentrations. As expected, weekday average concentrations were more similar to weekend average concentration. Meanwhile, it was observed higher concentration during weekend than in week days, which reflects that some activities that is developed during weekend continued during 2020. PM₁₀ weekly cycles present lower concentration during weekend in the two years, and as expected, the variation over the week was lower in 2020 than in 2019. However, rainfall profile for 2019 and 2020 was different, which exert huge influence in PM₁₀ concentration.

O₃ week cycles were very similar for all monitoring station. The diurnal cycle in 2019 shows that weekends present higher concentrations than week days. In 2020

the difference between week days and weekends was lower than in previous year. Beside of that, weekends in 2019 and 2020 presented lower differences in concentrations.

As in 2020 occurred a decrease on pollutant emission, it was expected that diurnal cycles would present lower levels. Despite the decrease in traffic, the main pollutant source, during first months, corroborated by mobility data, some essential services demanded workers who went to work in the morning and came home at evening. Thus, peak concentration time remained, in comparison with previous year. The weekly concentration presented a random variability during week days for both years, however in 2020 this variation was lower, which implies that the behavior of source emission were similar from Monday to Tuesdays. CO and PM₁₀ presented an increase on Friday and Saturday which is justified by higher mobility on these days. On the opposite way, O₃ presented higher levels on Monday, when the lowest mobility was recorded, since, less primary pollutants emission leads to lower O₃ concentration.

5.3.8. Time average with satellite data

An important factor that influences air quality is atmospheric transport which may carry pollutants from one region to others, which could contribute to the concentrations recorded at monitoring sites. Since the Brazilian atmospheric monitoring network is reduced, satellite data helps in better understanding. Figure 5.6 shows the time average map for CO and aerosol obtained from Giovanni/NASA. In the region of Rio de Janeiro occurred a slight increase in CO concentrations but more significant for aerosol. An interesting observation is the huge increase of CO and aerosol in the Amazon Region that also extends to the Pantanal. July to September is the period when many fires are registered in the Amazon region. Especially in 2020, Pantanal burned during the same period. Is well known that fires emit CO and particulate matter, which explains a large amount of these pollutants at Amazon and Pantanal.

Time average maps for the three periods considered indicate that CO and aerosol increased over time, as surface data demonstrated. Currently, to economic opening, which contributed to increase in mobility, consequently in pollutants emission, fires recorded at Amazon and Pantanal may transport pollutants to southeast Brazil, contributing to pollutant increasing. Rudke *et al.* 2021 also

considered that fires contributed to air pollution in São Paulo in the months that followed stricter isolation measures.

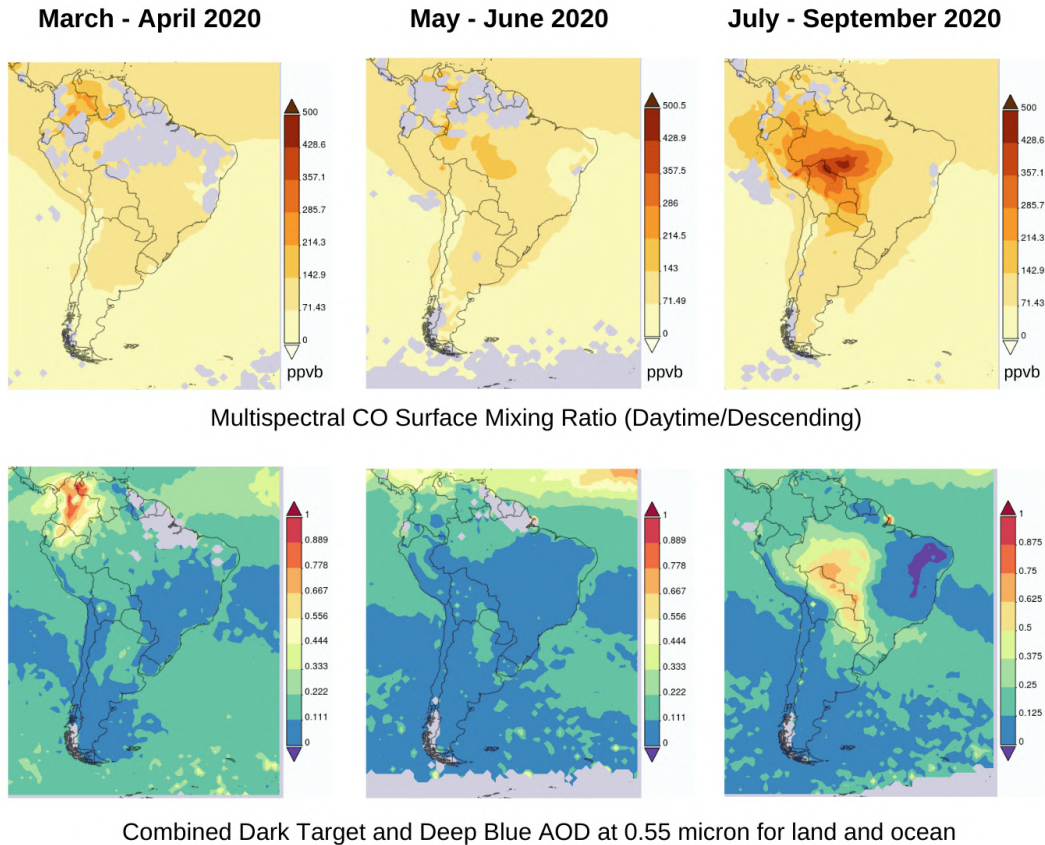


Figure 5.6 Time average map plotted with satellite data obtained by Giovanni/NASA for CO and aerosol from March to September, 2020. Source: <https://giovanni.gsfc.nasa.gov>

5.4. Conclusions

The assessment of atmospheric pollution is a complex task once depends on several factors, including pollutant emissions, meteorological conditions, and interaction of them, mainly to secondary pollutant formation. Even if it is possible to control the emission sources, the number of atmospheric processes involved and the dependency on meteorology makes the air quality highly difficult to control.

The period considered in this air quality assessment was marked by striking changes in urban routine, which represented a decrease of mobility of about 90 %, then the city presented a new emission profile. Primary pollutant concentrations (PM_{10}

and CO) were reduced as a consequence of emission sources reduction during the lockdown, however, secondary pollutants (O_3) increased as a result of several changes in atmospheric conditions. Around the world this behavior was observed after lockdown measures, highlighting the increase in O_3 concentration responding to the reduction in pollutants concentration that participates in tropospheric ozone formation.

Rio de Janeiro is one of the major Brazilian metropolises, therefore, vehicle emission is considered the main atmospheric pollutant source. Thus, the huge traffic reduction, as a consequence of mobility decrease, after lockdown decree induced a significant CO concentration reduction, once fossil combustion is its principal source. The same notable reduction was not observed for PM_{10} because of the differences in rainfall profiles between the two years. Rainfall volume recorded in Campo Grande, Centro, and Copacabana in 2019 (0.13, 0.13, and 0.20 mm) were higher than 2020 (0.08, 0.07, and 0.10 mm), thus, even with emission reduction in 2020 caused by routine changes, PM_{10} concentration varied little. As urban areas characteristic, daily concentration peak for both pollutants remained at the same time of 2019 even with lower values in 2020. As expected, and observed around the world, O_3 concentrations increased in urban areas where the O_3 production is VOC limited. The O_3 diurnal cycle presented a peak of concentrations at the same time as the previous year, which is related to the SR intensity that enhances the tropospheric O_3 formation by photochemical processes.

Once the isolation measures removed a lot of people from the street and the mobility reduced significantly during the period evaluated, pollutants concentrations recorded for weekdays became similar to the values that are usually recorded for the weekend. In other words, the lockdown period, mainly in the first months, was similar to a very long weekend period, especially during the first month. Following an increase in mobility since June 2020, pollutant concentrations also raised. At this time, people started to come back to some activities while the government scheduled an economic opening. Satellite data also show this behavior, even though they also indicate a possible contribution of fires at Amazon and Pantanal in CO e PM concentration in southeast Brazil.

Air pollution responds quickly to changes in factors that participate in the atmospheric process. While the emission sources were reduced during the isolation period it was observed a reduction in CO and PM_{10} was, but the easing measures started was followed by an increase in these pollutants. As O_3 depends on other

pollutants concentration, it presented an opposite behavior however the CONAMA standards for O₃ were not exceeding. The partial maintenance of home office and distance learning contributed to the concentrations recorded after the isolation easing remain lower than in 2019. Perhaps this could be an adequate alternative to control air pollution when the pandemic issue is resolved.

6 Time Variation of atmospheric pollutants in first weeks of COVID-19 lockdown in a Brazilian metropolis

Karmel Beringui^a, Elizanne P. S. Justo^a, Ana Carolina L. Bellot de Almeida^b,
Luciana M. Baptista Ventura^b, Michelle Branco Ramos^b, Ruan G. de Souza Gomes^a,
Pedro H. R. Valle^b, Adriana Gioda^{a*}

^a*Pontifícia Universidade Católica do Rio de Janeiro, Departamento de Química, Rio de Janeiro, Brazil*

^b*Instituto do Estadual do Ambiente (INEA), Rio de Janeiro, Brazil*

Corresponding author: Adriana Gioda - agioda@puc-rio.br

Published: Studies in Engineering and Exact Sciences, V. 3, N. 1 (2022), 95 - 106

Abstract

This study aims to assess the COVID-19 partial lockdown influence on air quality in Rio de Janeiro. Criteria pollutants (CO, SO₂, O₃, and NO₂) sampled at four sites under vehicular and industrial influences were investigated, between March 1st to April 12th, 2019 and 2020. Results showed that the partial lockdown affected pollutant levels through emission sources reduction. High decreased concentrations were observed for SO₂ (7%-89%), NO₂ (1%-65%), and CO (22%-92%); while an increase in the ozone concentration (up to 34%) was recorded. Pollutant time variation evaluations helped to understand the trend and sources in the three different periods.

Keywords: quarantine, air quality, criteria pollutants, ozone, coronavirus

6.1. Introduction

The new coronavirus has been causing the greatest pandemic of the 21st century. The impacts vary from improvements on air quality to unparalleled losses in economic systems. COVID-19 spread across the world quickly. In Brazil, the first official case was registered on February 26, 2020. Since then, many containment measures have been taken, varying from one region to another, as the virus has spread heterogeneously throughout the country (Dantas et al., 2020; Nakada and Urban, 2020).

The Rio de Janeiro city was one of the first to detect the virus in Brazil and one of the most affected by losses and overload of the health system. As a result, the government has adopted the partial lockdown to minimize the spread of the virus. The partial lockdown period started on March 16th, 2020. Until June, only essential services were allowed to work. The population was instructed to stay at home, leaving only to perform physical activities, medical services, or basic purchases. The metropolitan region of Rio de Janeiro (MRRJ) has undergone many structural changes to host the 2016 Olympic Games and the FIFA 2014 World Cup, two mega-events. The works include the construction of new streets and tunnels, closing off some avenues, new BRT, and VLT lines, among others. All of these changes have affected air quality in the region as reported in some studies (Bezerra et al., 2018; De La Cruz et al., 2019; Godoy et al., 2018; Gomes et al., 2018; Justo et al., 2020; Tsuruta et al., 2018; Ventura et al., 2019; Ventura et al., 2019).

After partial lockdown has been implemented by Rio de Janeiro government, the urban routine changed significantly, especially the traffic (Beringui et al., 2021). In this context, the present study aims to assess the Time Variation of air pollutants in the first weeks of partial lockdown, and compare with weeks before partial lockdown and with the same period in 2019.

6.2. Material and Methods

Description in topic 3.3, page 44.

6.3.Results

6.3.1. Weekly overview

Weekly pollutants variation is presented in Figure 6.1. Comparing both years, NO_2 and O_3 presented lower concentration in 2020 in all sites. Besides of that, these pollutants presented little variation during week days in 2020, which is a consequence of the mobility reduction during the lockdown weeks. In the partial lockdown, pollutants levels during the week were similar to weekend levels as a consequence of adopting remote study and home office in those critical weeks of social isolation. SO_2 levels in 2020 were higher in all sites, mainly at LB, although weekly variation was similar to the previous year. CO concentration at MG was higher in 2020 than in 2019, nevertheless the same weekly variation was observed: an increase in the middle of the week and a decrease on the weekend.

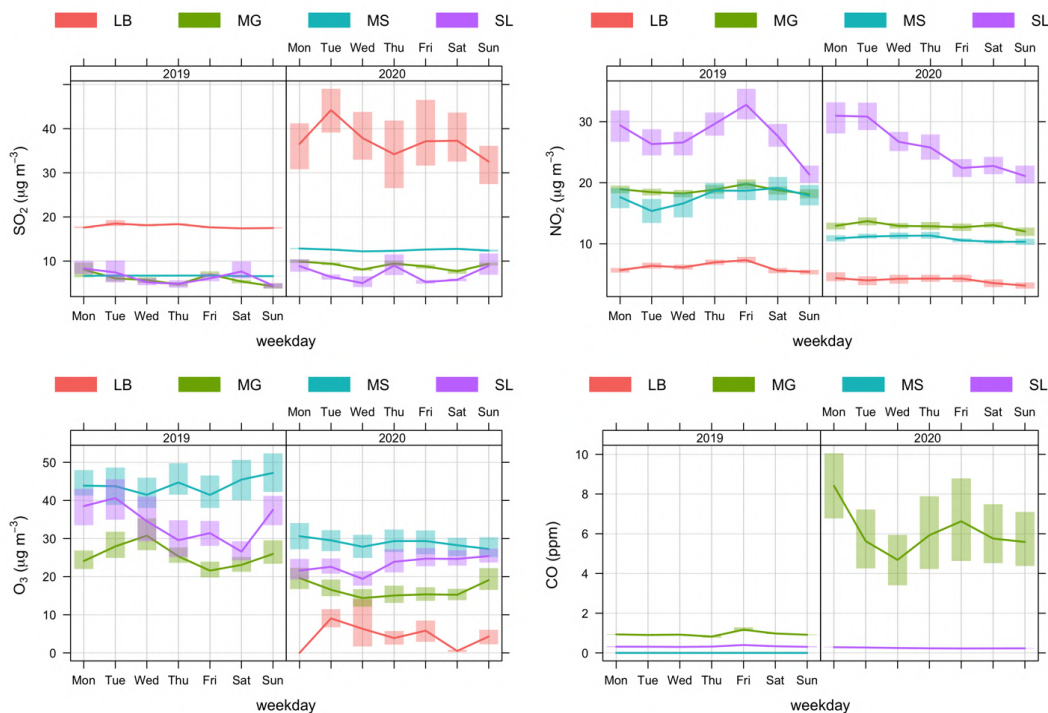


Figure 6.1 Weekly concentrations for SO_2 , NO_2 , O_3 and CO between March 1st and April 12th 2019 and 2020 in all monitoring sites (LB – Largo do Bodegão, MG – Manguinhos, MS – Monte Serrat and SL – São Luiz).

Considering difference on routine scenarios, as a consequence of lockdown decree, weekly pollutant variation for data from 2020 is presented in Figure 6.2. Evaluating 2020 as a whole dataframe, lower concentrations are observed compared

to 2019, however, when the lockdown decree (March 16th) is considered, a clear change can be associated with this new urban routine. Particularly, O₃ concentration shows a different behavior. While SO₂, NO₂ and CO decreased during lockdown, O₃ increased, which was also observed in different cities around the world and attributed to the decrease in primary pollutants, that are related with ozone formation. According to Geraldino et al. (2017), in Rio de Janeiro low NO₂ concentration leads to high O₃ concentration, once NO participates on O₃ depletion. The traffic reduction contributed to NO₂ decrease, and therefore, to O₃ increase.

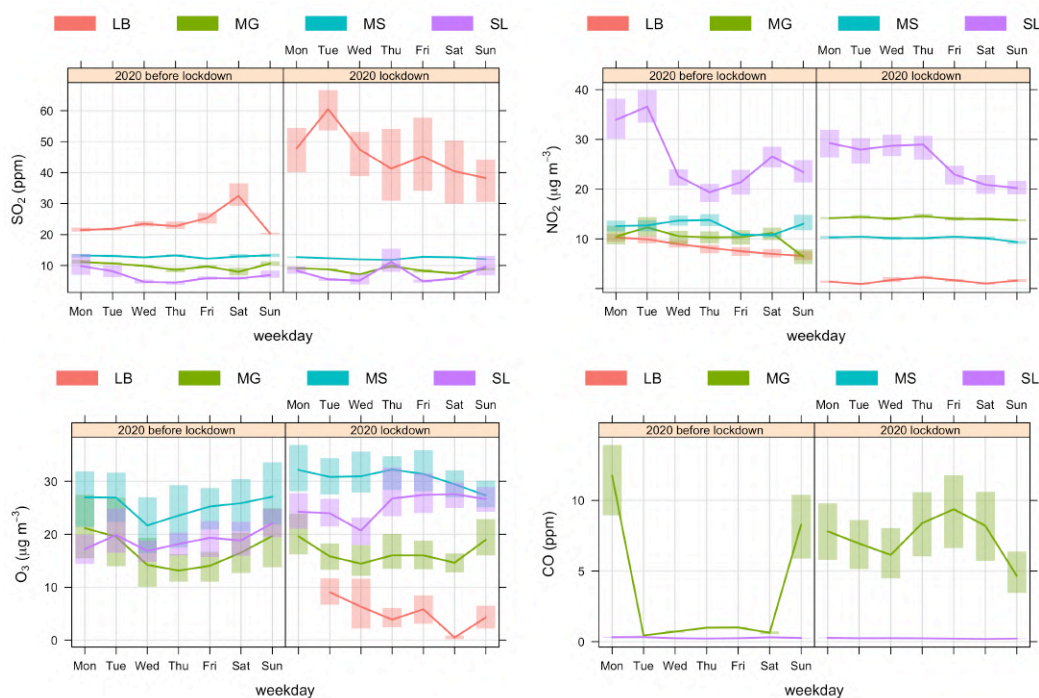


Figure 6.2 Weekly concentrations for SO₂, NO, O₃ and CO between March 1st and April 12th 2020 splitted according to lockdown decree. (LB – Largo do Bodegão, MG – Manguinhos, MS – Monte Serrat and SL – São Luiz).

Considering difference on routine scenarios, as a consequence of lockdown decree, weekly pollutant variation for data from 2020 is presented in Figure 5.3. Evaluating 2020 as a whole dataframe, lower concentrations are observed compared to 2019, however, when the lockdown decree (March 16th) is considered, a clear change can be associated with this new urban routine. Particularly, O₃ concentration shows a different behavior. While SO₂, NO₂ and CO decreased during lockdown, O₃ increased, which was also observed in different cities around the world and attributed to the decrease in primary pollutants, that are related with ozone formation. According

to Geraldino et al. (Geraldino et al., 2017), in Rio de Janeiro low NO_2 concentration leads to high O_3 concentration, once NO participates on O_3 depletion. The traffic reduction contributed to NO_2 decrease, and therefore, to O_3 increase.

6.3.2. Hourly overview

Pollutant hourly variations for all sites is presented in Figure 5.3. SO_2 hourly profile in LB and CO hourly profile in MG did not present peak concentrations, which is characteristic of industrial emission, corroborating the hypothesis that industries from Santa Cruz and Manguinhos are accountable for SO_2 and CO emission, respectively.

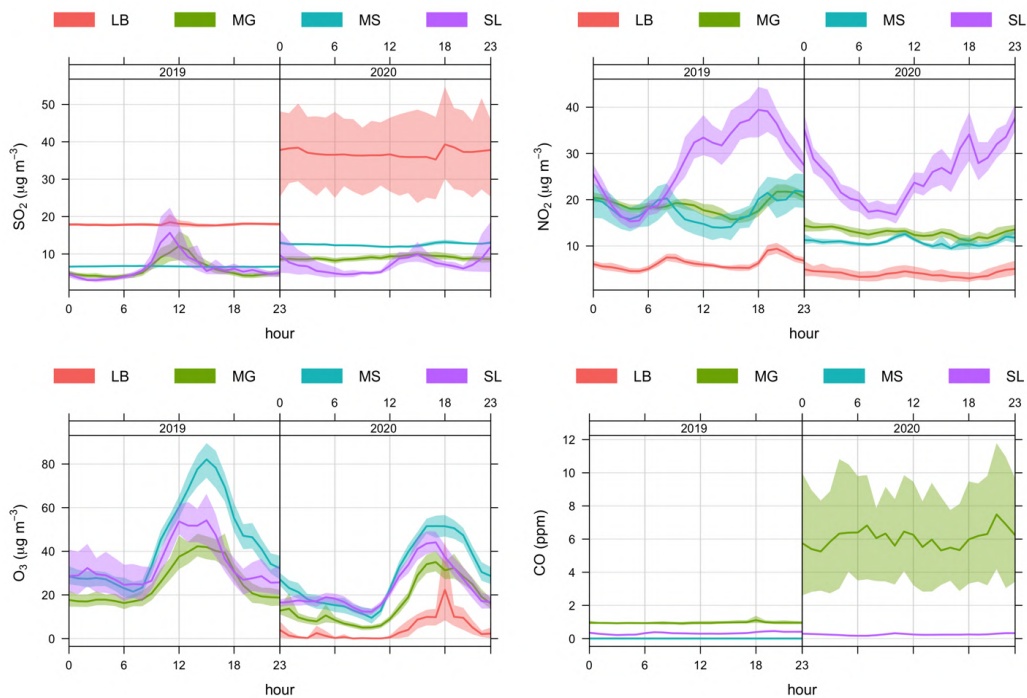


Figure 6.3 Hourly concentrations for SO_2 , NO_2 , O_3 and CO between March 1st and April 12th 2019 and 2020 in all monitoring sites. (LB – Largo do Bodegão, MG – Manguinhos, MS – Monte Serrat and SL – São Luiz).

The main source of NO_2 and SO_2 in the urban centers are vehicles, because of that, they generally present two peaks of concentration, which correspond to intense traffic times. This behavior may be observed for NO_2 in 2019, but in 2020 no peak of concentration is observed, which reflect the decrease in traffic during the partial lockdown. For SO_2 in 2019 a huge peak may be observed in the final morning, followed

by random variation in the afternoon. However, in 2020, this pollutant presented little variation, once traffic decreased.

An interesting change in diurnal pollutants cycles may be observed for O₃. Comparing both years, all sites presented peak of concentrations at different times. In 2019, the O₃ peak concentration occurs about noon, when solar radiation is more intense, favoring photochemical processes. In 2020, O₃ peak of concentration occurred in the late afternoon. While in 2019, NO₂ emission contributed to O₃ depletion throughout the afternoon, the decrease in NO₂ concentration recorded in 2020 contributed to O₃ accumulation, leading to higher concentration in the evening. After that, the absence of solar radiation implies that O₃ formation stops, thus, the concentration decrease.

Sulfur dioxide (SO₂) and nitrogen dioxide (NO₂) is generated from the combustion processes in vehicle and industries. This compound is a precursor for O₃, which is a secondary atmospheric pollutant that is formed in the troposphere by different mechanisms that depend mainly on volatile organic compounds (VOCs) and nitrogen oxides (NO_x). Carbon monoxide (CO) is derived from incomplete combustion. (Faustini et al., 2014; XuKaijie et al., 2020) All of them are directly or indirectly related to vehicle emissions. Thus, the reduction in mobility caused by social isolation has led to considerable variations in their concentrations.

According to State Environmental Institute (form Portuguese, INEA), reductions of up to 80 % NO₂ and 75 % CO were recorded in the first two weeks of partial lockdown (GEAR-INEA, 2020). In addition, reductions of up to 65 % SO₂ and increases of up to 25 % O₃. Rio de Janeiro recorded a higher SO₂, NO₂ and CO reduction comparing to Spain and some regions of Chine (Bao and Zhang, 2020; Tobías et al., 2020; Xu et al., 2020).

Studies carried out in São Paulo and Rio de Janeiro also recorded lower SO₂ and NO₂ reductions than this study(Dantas et al., 2020; Nakada and Urban, 2020). Although the percentages of reduction obtained for the monitoring stations in this study are higher, the variation profile is similar to that observed by other studies already conducted in Rio de Janeiro and São Paulo (Beringui et al., 2021; Dantas et al., 2020; Nakada and Urban, 2020). Satellite data also show significant reduction of pollutants such as CO and NO₂ around the world (Gaubert et al., 2021; Gautam, 2020). Despite recording high reductions in primary pollutants, the increase in O₃ was not as large as in other cities around the world and some other neighborhoods in Rio de Janeiro. This

behavior is related to the complex formation of ozone which in the state of Rio de Janeiro varies according to the topography of the region.

6.3.3. Conclusion

In summary, our findings indicated that control actions to prevent the spread of the pandemic had impact on the air quality levels for the four sites studied. The reduction in pollutant concentrations was related to the decrease in vehicle traffic caused by the closure of schools, industries, and commercial establishments, as well as the interruption of the activity of some transport lines. The increase in the concentration of O₃ was related to the decrease in NO₂ concentration, since the negative correlations between these pollutants indicate that NO₂ is involved in the consumption mechanism of tropospheric ozone. The importance of social isolation measures on air quality changes was certified by the comparison of the beginning of March with the period after the lockdown decree.

Acknowledgments

This study was financed in part by the Coordenação de Aperfeiçoamento de Pessoal de Nível Superior (CAPES) – Brazil (finance code 001). The authors thanks to CNPq (A.G. and K.B.), to FAPERJ (A.G.), and to CAPES (E.P.S.J.) for the scholarships.

7 Effects of the first weeks of the COVID-19 partial lockdown on air quality in Rio de Janeiro, Brazil

Karmel Beringui^a, Elizanne P. S. Justo^a, Alex Huaman De La Cruz^{abc}, Ana Carolina L. Bellot de Almeida^d, Luciana M. Baptista Ventura^d, Michelle Branco Ramos^d, Ruan G. de Souza Gomes^a, Vinícius Lionel-Mateus, Pedro H. R. Valle^d, Adriana Gioda^{a}*

^aPontifícia Universidade Católica do Rio de Janeiro (PUC-Rio), Departamento de Química, Rua Marquês de São Vicente, 225, 22451-900 Gávea-RJ, Brazil

^bUniversidad Nacional Intercultural de la Selva Central Juan Santos Atahualpa, Vicerrectorado de Investigación, Jr. Los Cedros 341, La Merced, Peru

^c Universidad Peruana Unión, Escuela de Ingeniería Ambiental, Km 19 Carretera Central, Ñaña, Lurigancho, Lima. Peru

^dInstituto do Estadual do Ambiente (INEA), Av. Venezuela, 110, 20081-312, Saúde, Rio de Janeiro, Brazil

^eUniversidade Federal do Espírito Santo (UFES), Departamento de Engenharia Ambiental, Av. Fernando Ferrari, 514, 29075-910, Goiabeiras, Vitória-ES, Brazil

Corresponding author: Adriana Gioda - agioda@puc-rio.br

Paper submitted with major review: *Journal of the Brazilian Chemical Society*

Abstract

This study evaluated the pollutant levels (NO₂, SO₂, CO, and O₃), Air Quality Index (AQI) and the influence of meteorological variables and COVID-19 pandemic on the air quality in Rio de Janeiro. The data set used comprises periods before (March-

April, 2019) and during (March-April, 2020) the pandemic. According to the AQI results, on most days, the air quality was ranked as "Good". Brazilian air quality standards for SO₂, O₃, and NO₂ were not exceeded in any of the monitoring stations during partial lockdown, while CO exceeded in all periods in one site due to industrial emission. Comparing both periods, descriptive statistics for the meteorological parameters presented no differences, which suggests similar conditions. However, when evaluated week by week in 2020, weather conditions presented some differences that probably affected pollutant concentrations. The correlations between O₃ and NO₂ and some meteorological parameters indicate that variations in both favored ozone formation, since it is a photochemical process favored by temperature and solar radiation and that, in Rio de Janeiro, low NO₂ concentrations lead to increased O₃. The improvements on air quality during the partial lockdown may be attributed mainly to a reduction on emission sources rather than weather conditions.

Keywords: Air quality, AQI, meteorological variables, COVID-19

7.1. Introduction

COVID-19 is a disease caused by coronavirus pathogen that quickly spread around the world at the beginning of 2020. In an attempt to contain the spread of the disease, governments decreed lockdown in many cities. In Brazil the first decree (March, 16th) was in Rio de Janeiro, establishing a partial lockdown, which included the closure of schools, universities, cinemas and theaters, suspension of shows, parties, sport events and reduction of public transportation by 50%. After that (March 19th), restrictions increased and beaches, bars, restaurants and shopping malls were closed, in addition, the circulation of public transport between the metropolitan region and the capital was stopped (DOERJ, 2020).

As in other cities on the world, the people circulation on the Rio de Janeiro streets had decreased. Social isolation reached 85 % in the first two weeks of the partial lockdown (March 16th-27th), according to the Rio Operations Center (Beringui and Justo and et al., 2021; Rio de Janeiro City Hall, 2020). Besides, satellite images and air quality monitoring networks recorded a reduction in the concentration of atmospheric pollutants around the world during this period (Bao and Zhang, 2020; Chen et al., 2020; Tobías et al., 2020; Zambrano-Monserrate et al., 2020).

Air pollutant levels are highly dependent of the emission sources and meteorological conditions (Tie et al., 2017; Xu et al., 2016). If the regional atmospheric emissions are roughly stable in a particular period, meteorological conditions may be the determining factor for the occurrence of air pollution (Kan et al., 2012). In Brazil, a study conducted in São Paulo compared 90 days of partial lockdown with a period of 2019 that had the same meteorological characteristics and concluded that social isolation contributed to air quality improvements. (Debone et al., 2020). Once meteorological factors play significant roles in air pollution formation, transport, and dispersion, researchers should be cautious when directly attributing air quality improvement to control measures if the effects of meteorological variations are not accounted for (Hou et al., 2019; Liu et al., 2017; Sun et al., 2019; Xu et al., 2020; Zou et al., 2017).

Studies conducted in Rio de Janeiro highlight that the main source of air pollutant emissions are the vehicles, whose fleet grows every year (Andrade et al., 2012; Dantas et al., 2020; De La Cruz et al., 2019; Pacheco et al., 2017; Quijano et al., 2019; Ventura et al., 2017). However, the metropolitan region of Rio de Janeiro also has some industrial complexes located in different cities that have varied emission profiles, but which contribute mainly to the concentration of criteria pollutant and Gioda, 2017; Mendes et al., 2020). Construction works can be considered an important source of air pollutant emissions, since the metropolis has undergone several structural changes in recent years (De La Cruz et al., 2019; Justo et al., 2020; Ventura et al., 2019; Ventura et al., 2019).

Rio de Janeiro City has a subtropical climate, characterized by intense solar radiation, consequently, high temperatures, favoring pollutants formation by photochemical processes. (Gioda et al., 2018; Soluri et al., 2007; Ventura et al., 2018) Due to the geographic differences in the city terrain, the weather can vary according to the proximity to the sea or massifs. (Neiva et al., 2017) The proximity to the sea allows for ocean-continent exchanges that favor ventilation, contributing to the dispersion of pollutants. However, the mountainous topography makes it difficult for pollutants to spread towards the continent, causing an increase in pollutant concentrations.

Considering the complex meteorological characteristics of Rio de Janeiro and changes caused by social isolation, this study aims to assess the influence of meteorological parameters and the partial lockdown on air quality. Meteorological

variables such as wind speed (WS) and direction (WD), temperature (T), relative humidity (RH), rainfall (RF), solar radiation (SR) and atmospheric pressure (P) will be considered, as well as pollutant concentrations obtained from monitoring stations located in the metropolitan region of Rio de Janeiro from March 1st to April 12, 2020. A comparison with the same period of 2019 was also made.

7.2. Material and Methods

Description in topic 3.3 , page 44.

7.3. Results

7.3.1. Pollutant concentrations and Brazilian air quality standards

During 2019, urban centers were on a routine scenario, thus, the period between March and April, 2019 will be compared with the same period of 2020, considering the partial lockdown measures. Boxplots with pollutants concentration in three periods considered are presented in Figure 7.1.

The daily SO₂ concentrations in MRRJ ranged from 0.87 µg m⁻³ to 26.60 µg m⁻³ from March 1st to April 12, 2019. During 2020, the concentrations ranged from 3.26 µg m⁻³ to 52.46 µg m⁻³, before the partial lockdown; while during the partial lockdown were 2.63 µg m⁻³ to 115.99 µg m⁻³. The daily air quality standard established for SO₂ by CONAMA (125 µg m⁻³) was not exceeded in any locations before and during the partial lockdown. Overall, SO₂ concentration was found in similar values for both years in sites, except for Largo do Bodegão. A significant increase in SO₂ concentrations in Largo do Bodegão on the first partial lockdown week may be attributed to industrial emission. During this week, SO₂ average concentration increased by 250 % in relation to the previous period at this site. In Largo do Bodegão, an average reduction of 89 % in SO₂ concentrations were observed in April, compared to the first partial lockdown weeks; and 65 % in relation to the beginning of March. At the other monitored sites, reductions of 14% at Manguinhos, 26% at São Luiz, and 7% at Monte Serrat were observed in the first weeks of partial lockdown compared to the beginning of March.

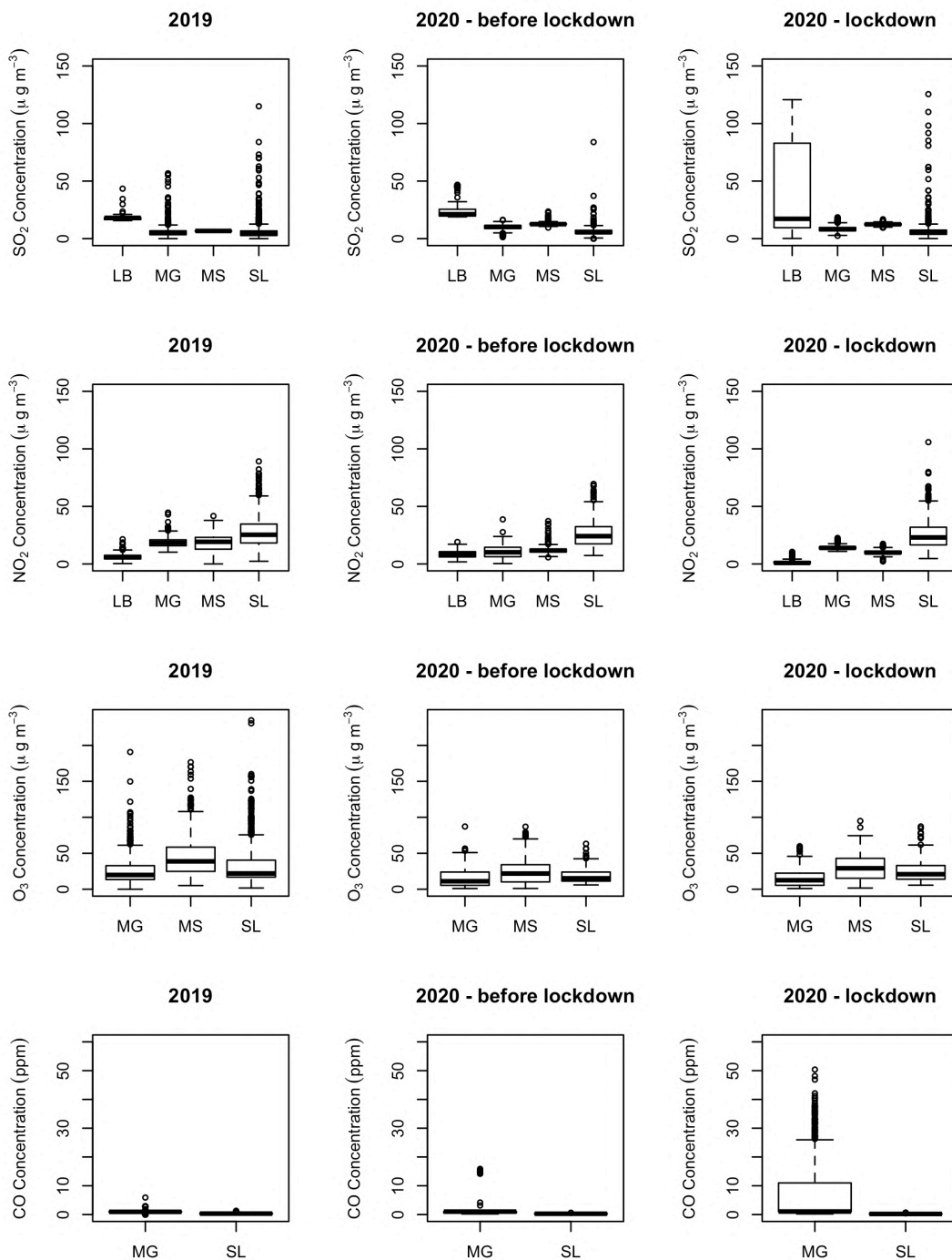


Figure 7.1 Boxplot with the distribution of the concentrations of SO₂, NO₂, and O₃ ($\mu\text{g m}^{-3}$) and CO (ppm) for Largo do Bodegão (LB, Rio de Janeiro), Manguinhos (MG, Rio de Janeiro), São Luiz (SL, Duque de Caxias) and Monte Serrat (MS, Itaguaí) stations in the three periods: 1) March 1st to April 12nd, 2019, 2) March 1st to 15th, 2020 classified as “before lockdown” and 3) March 16th to April 12nd, 2020 classified as

“lockdown”. The boxes cover the 1st quartile to the 3rd quartile. The lines in the boxes represent the median values.

The daily NO₂ concentrations during 2019 ranged from 3.14 µg m⁻³ to 41.59 µg m⁻³; before partial lockdown ranged from 3.71 µg m⁻³ to 40.58 µg m⁻³ and from 0.28 µg m⁻³ to 39.60 µg m⁻³ after the partial lockdown decree. The Brazilian air quality standard for NO₂ (260 µg m⁻³, 1-hour) was not exceeded in any monitoring site. NO₂ was found in lower concentration in 2020, mainly in Largo do Bodegão and Monte Serrat, where NO₂ concentration decreased significantly after the lockdown decree, and remained low during all the evaluated period. Once NO₂ is generally associated with traffic emission, lower NO₂ concentrations were expected due to the severe traffic reduction. In the first partial lockdown weeks, NO₂ concentration reduced about 20 % and 14 % at Largo do Bodegão and Monte Serrat, respectively. In April, the NO₂ concentration decreased 65 % at Largo do Bodegão. Alternatively, Manguinhos and São Luiz presented an increase of 31 % and 4 % in the first partial lockdown weeks; however, reductions were recorded in April (3 % and 14 %, respectively). Those last two sites are close to oil refineries and important roads that connect Rio de Janeiro City and neighboring cities, where vehicle traffic is intense. The prohibition of intercity public transport circulation on March 21st may be the explanation for the decrease in the NO₂ levels in last week of March.

The daily O₃ concentration ranged from 11.75 µg m⁻³ to 115.74 µg m⁻³ from March 1st to April 12nd, 2019; In 2020, ranged from 8.98 µg m⁻³ to 32.38 µg m⁻³ before partial lockdown and from 0.60 µg m⁻³ to 48.63 µg m⁻³ during the partial lockdown. The O₃ Brazilian air quality standard (140 µg m⁻³, 8-hours rolling mean) was not exceeded at any time. A similar trend on O₃ concentration was observed for Manguinhos, Monte Serrat and São Luiz, which indicates that O₃ is under the same formation conditions. Peaks of concentration were observed at the beginning of partial lockdown (March, 16th) and on the second week of April. The decrease in primary pollutants in the first partial lockdown week may have contributed to increasing the O₃ concentration, once NO₂ may participate on O₃ depletion. Monte Serrat presented the highest O₃ concentration on the first partial lockdown week, 25 % higher than previous weeks. Although, O₃ concentration decreased as days goes by, it remained 18 % higher than at the beginning of March. Manguinhos and São Luiz presented similar O₃ concentrations that increased about 30 % in the first partial lockdown weeks. In April, while Manguinhos recorded decreasing on O₃ concentration, 12 % lower than before

partial lockdown, in São Luiz NO₂ continues to increase, reaching values 34 % higher than before partial lockdown.

The data obtained in this study showed a certain similarity with other studies that evaluated air pollutants during the lockdown adopted due to the new Coronavirus. The highest concentration was observed in the first weeks of lockdown, followed by a slight decrease in the following weeks, but the values remained higher than in the weeks before the lockdown. In Rio de Janeiro city, high concentrations of O₃ can be attributed to the transport of pollutants and low concentrations of NO₂, which can be triggered by high temperatures and solar radiation (De La Cruz et al., 2019; Hou et al., 2019). In Monte Serrat, where the highest concentrations of ozone were observed, negative correlations were found between NO₂ and O₃, both before and during partial lockdown (-0.50 and -0.66). These negative correlations indicate that NO₂ is participating in the consumption of tropospheric O₃, which explains the increase in O₃ during the partial lockdown when the NO₂ concentration decreased. In Manguinhos, the correlation between NO₂ and O₃ was also negative during the partial lockdown (-0.53). The 30 % increase in NO₂ concentration at this station may have contributed to a smaller increase in the concentration of O₃ at that station (3 %), compared to the other stations.

The daily CO concentrations ranged from 0.09 ppm to 2.25 ppm in 2019; in 2020 ranged from 0.19 ppm to 15.10 ppm before partial lockdown and from 0.11 ppm to 35.37 ppm during lockdown. CO presented similar values for both years in São Luiz, but in Manguinhos increased significantly. The air quality standard established for CO by Brazilian legislation (9 ppm – 10,000 µg m⁻³, 8-hours rolling mean) was exceeded in Manguinhos in 2020, both before and during the lockdown. In São Luiz, a decrease trend can be observed on the first lockdown week, which may be related to the prohibition of intercity public transport circulation. As CO is formed by incomplete combustion, vehicle emission is one of the main sources of this pollutant. The decrease in vehicle traffic near São Luiz, through which a major highway passes, may have led to a decrease in the concentration of CO. On this site, a reduction of 13 % was recorded on the first lockdown week and 22 % in April. The increase in CO concentration recorded at Manguinhos (7 %) in first weeks of partial lockdown may be attributed to industrial emissions. In April CO concentration reduced 92 % in relation to beginning of March. Vehicle emissions are considered the main source of this pollutant in the MRRJ, with the largest contribution (75 %) attributed to light vehicles and motorcycles (INEA, 2016). However, it was found that in regions close to oil

refineries, events in which concentrations can reach peaks that correspond to up to 50 times higher than routine concentrations (McCoy et al., 2010).

7.3.2. Air Quality Index (AQI)

The AQI was calculated for SO₂, CO, O₃, and NO₂. For both years and for all stations, NO₂ presented AQI values lower than 40, which is classified as “Good” 100 % of the time in all sites (Figure 19.1, Supplementary Material). NO₂ concentrations were at least 7 times lower than the limit established by the Brazilian legislation. The AQI for O₃ was also ranked as “Good” in most days of the evaluated period. In a few random days in both years, the air quality was classified as “Moderate” to “Poor” (Figure 19.2, Supplementary Material). Concentrations obtained in 2020 were slightly lower than in 2019, indicating a better air quality. Some days during the partial lockdown presented higher O₃ concentrations than early March, which is related to the increase in O₃ concentration induced by the decrease in primary pollutant that participate in tropospheric ozone formation, as discussed above.

Overall, the Air Quality Index ranged from “Moderate” to “Good” for all stations. Some exceptions were observed for SO₂ (Figure 19.3) and CO (Figure 19.4). São Luiz station presented “Good” air quality for almost all days, in both years and for both pollutants. The exceptions were in some days during the partial lockdown for SO₂. In Largo do Bodegão SO₂ index was “Good” for April-2019, April-2020 and for many days in March-2020. However, during the partial lockdown days (March-2020) the index ranged from “Moderate” to “Poor”. This station is located in a populated area, near a huge industrial complex and highways with intense traffic. Therefore, the industrial activities, which were not paralyzed during the partial lockdown, could be the reason of the poor air quality. Added to that, in the region the traffic was reduced only 25% during the partial lockdown.(Companhia de Engenharia de Tráfego - CET-Rio, 2020)

Regarding CO, São Luiz station presented “Good” air quality for both years. In contrast, Manginhos presented the worst air quality because of the increase (20-30 %) in CO concentrations during the partial lockdown. On some days the air quality was ranked as “Terrible”, since the concentrations were 1.5-4.3 times greater than the CONAMA limit. During this period, CO concentration did not present daily peak values, which indicates that the industrial emission contributed to those high concentrations. The AQI obtained for Manginhos and Monte Serrat regardless of SO₂ (Figure 19.3,

Supplementary Material) indicated good air quality all days from both periods evaluated.

In some days of the evaluated period, data collection failed or they were invalidated due to the monitoring station maintenance, therefore the AQI was not performed and the days are not filled in Figure 7.2. In general, the days in which the air quality were not considered “Good” occurred in the period before the partial lockdown, except Manguinhos, which presented days with “Terrible” air quality in the second week of the partial lockdown. A previous study about Time Variation of pollutants showed that in the weeks immediately following the lockdown decrease the concentration of pollutants reduced, contributing to improved air quality (Beringui et al., 2022).

These AQI results are in agreement with studies carried out in other cities in the world. In India, the air pollution decreased after the second week of lockdown and the AQI for a total of 91 cities was rated as “Good” and “Satisfactory”, and no city was classified as “Poor”. (Anjum, 2020) The AQI for three cities in China (Wuhan, Jingmen, and Enshi) showed that 88 % of the days were classified as “Moderate” or “Good” during the lockdown, while before the lockdown the percentage of the days was 66 %. (Xu et al., 2020)

7.3.3. Statistical analysis of meteorological parameters

Table 7.1 presents the descriptive statistics for meteorological parameters before and during the partial lockdown for all monitoring stations in 2019 and 2020. In order to verify changes in meteorological conditions between the years, the Mann Withney test ($p < 0.05$) was applied. No statistical difference was observed between the periods. This observation indicates that in 2020 Rio de Janeiro was under a similar meteorological condition as in 2019, suggesting that pollutant concentrations variations were probably due to changes in emission sources. All monitoring sites presented similar meteorological conditions, but São Luiz recorded WS at least 2 times ($1.6\text{-}2.3 \text{ m s}^{-1}$) greater than the others ($0.1\text{-}1.0 \text{ m s}^{-1}$). According to the National Institute for Meteorology (INMET), WS less than 2.0 m s^{-1} does not favor atmospheric dispersions. Because of higher WS values in São Luiz, air circulation at this site affected air masses circulation, which promotes stronger pollutants dispersion.

Table 5.1. Descriptive statistics of meteorological variables before and during the partial lockdown in 2020 and in the same period in 2019.

Variables	WS (m s ⁻¹)	RF (mm)	T (° C)	SR (W m ⁻²)	RH (%)	AP (mbar)
March – April 2019						
Max	6.5	46.2	45.8	1050	99.0	1023
Min	0.0	0.0	16.9	0.0	32.0	1000
Mean	0.9	0.4	26.6	214.6	79.6	1011
Median	0.6	0.0	25.8	8.5	83.0	1010
2020 – Before the COVID-19 lockdown						
Max	5.1	80.2	43.6	1027	99.0	1018
Min	0.0	0.0	15.7	0.0	37.0	996.0
Mean	0.9	8.9	27.5	229.7	80.3	1007
Median	0.7	0.0	25.3	7.2	85.0	1007
2020 – After the COVID-19 lockdown						
Max	6.3	37.8	43.3	1042	98.0	1021
Min	0.0	0.0	10.1	0.0	31.0	991.0
Mean	0.9	2.8	27.2	216.8	78.2	1007
Median	0.6	0.0	25.1	7.8	82.3	1008

Considering that the weather conditions change frequently, the Mann Withney test test was applied to evaluate how meteorological parameters (WS, T, SR, RH, and AP) varied over the weeks in the four MRRJ monitoring stations in 2020 (Table 16.1, Supplementary Material). In the first week of March, 2020 (W1), two weeks before the partial lockdown, a cold front arrived at Rio de Janeiro, increasing air humidity (up to 93 %) and cloud cover, reducing solar radiation (167 W m^{-2}) and average temperature ($26 \text{ }^\circ\text{C}$). Heavy rain (117 mm/week) also occurred during this week, which improved the air quality as a result of the wash-out effect. However, in the middle of the second week of March (W2), a high-pressure system reached the MRRJ, which made the atmosphere more stable, with higher T ($26\text{-}34 \text{ }^\circ\text{C}$) and lower RH ($67\text{-}87 \text{ }%$) averages, and without rain. The high-pressure system produced a wind barrier, which favors the increase in pollutant concentrations. These conditions probably contributed to rise SO_2 average concentrations from $12 \text{ } \mu\text{g m}^{-3}$ (W1) to $17 \text{ } \mu\text{g m}^{-3}$ (W2).

Changes in some meteorological conditions were also observed in the third week (W3), first partial lockdown week, compared to the W2 (Table S1). In the W3 was sunny days, with temperatures around $40 \text{ }^\circ\text{C}$ and low RH ($31 \text{ }%$). Due to high

temperatures, ozone hourly concentration reached $139 \mu\text{g m}^{-3}$. At the end of W3, another cold front arrived at MRRJ, decreasing temperatures ($19 \text{ }^\circ\text{C}$), and bringing humid winds from the ocean to the continent. This system produced atmospheric instability resulting in the rain (69 mm/week), which decreased pollutant levels. SO_2 average concentration ($9.5 \mu\text{g m}^{-3}$) in this week was lower than the previous one.

In the week fourth (W4), during the partial lockdown, a high-pressure system was predominant. In this week, drops of rain (3.2 mm/day), high T ($32 \text{ }^\circ\text{C}$) and the highest levels of SR (1042 W m^{-2}) were registered. Due to these conditions, a high hourly O_3 concentration reached (up to $70 \mu\text{g m}^{-3}$). In the fifth week (W5) the weather conditions were quite similar to W1, under high atmospheric pressure system followed by a cold front.

Due to the instability in the weather conditions, the hypothesis test was applied to identify similarities and differences among weeks. In Largo do Bodegão and Monte Serrat stations meteorological parameters were different between W3 and W4, as well as between W4 and W5. In the other monitoring stations, some meteorological variables were similar (WS, SR, RH) while others were different (T, AP). The W3 and W5 presented the lowest AP average (997 and 998 mbar), while W4 presented the highest AP average (1021 mbar).

In the sixth week (W6) the meteorological parameters were different from the W5, both during the partial lockdown, for all sites, except for WS in Largo do Bodegão station. W6 was characterized by low T ($25 \text{ }^\circ\text{C}$) and SR (121.3 W m^{-2}) averages, while W5 was predominantly influenced by a high-pressure system, with higher T ($28 \text{ }^\circ\text{C}$) and SR (204 W m^{-2}), which favored O_3 maximum concentrations ($73.2 \mu\text{g m}^{-3}$) in W5. However, in both weeks, the accumulated rainfall volumes did not exceed 5 mm per day, nor 14 mm in the week.

7.3.4. Correlation between pollutants and meteorological parameters

Pearson correlations (r) and grouping by HCA were carried for the evaluation of meteorological variables and pollutant concentrations (Figure 19.4, Supplementary Material). In 2020, a moderate to strong positive correlation between O_3 and T was obtained for all monitoring stations, which is expected once this pollutant formation occurs throughout the photochemical process. O_3 was also positively correlated with

WS at all monitoring stations, which indicates that pollutants from other regions contributed to its formation. These correlations have also been observed in Rio de Janeiro City by Gioda et al., (2018) and Geraldino et al., (2020). A moderate negative correlation between O_3 and RH was verified in Manguinhos which may be explained by the limited availability SR and low photochemical activity, as a result of high cloud coverage. (De La Cruz et al., 2019)

A negative correlation between NO_2 and O_3 indicates that NO_2 participates in O_3 formation, as mentioned above. A negative correlation between NO_2 and WS suggests that wind participates in its dispersion. Considering correlations between WS with NO_2 and O_3 , it is possible to conclude that wind act on NO_2 dispersion, transporting this pollutant to the region where it participates in ozone formation. A wide group including T, WS, O_3 and NO_2 , mainly at Largo do Bodegão, corroborates the idea that NO_2 from other regions participate in complex processes of O_3 formation and depletion.

For SO_2 only weak correlations with meteorological variables were found, highlighting the correlation observed in 2020 with WS in Largo do Bodegão at ($r = -32$), with WD in Monte Serrat ($r = -24$), São Luiz ($r = -18$) and Manguinhos ($r = -11$). At most of these sites the cluster grouped SO_2 and the wind-related variables. The negative correlations are an indication that wind action is one of the factors contributing to the dispersion of pollutants.

At São Luiz, moderate correlation between CO and NO_2 ($r = 0.56$) and the grouping of NO_2 , CO, and SO_2 were verified. Those observations indicate that industrial complexes are the main factor for the concentration of pollutants. It may be corroborated by the fact of the same behavior has been observed both before and during the partial lockdown. In other words, the traffic affect pollutant emission less than industrial activities in this site.

Following Bryman and Cramer criteria, que found, in general, weak to moderate correlations ($0.1 > r < 0.7$) were found between meteorological variables and NO_2 , SO_2 and CO. Thus, these pollutants were less influenced by the meteorological conditions of the monitoring sites. However, O_3 showed moderate to strong correlations ($r > 0.6$) with meteorological variables ($r > 0.6$).

Pearson correlations obtained for data collected between March 1st and April 12th, 2019 were similar to those observed for 2020. Largo do Bodegão did not presented any important correlation, however, some parameters were not monitored

in this year. Manguinhos presented a correlation between O_3 and meteorological. Monte Serrat presented a negative correlation between O_3 and SO_2 ($r = -0.40$). São Luiz presented a moderate correlation between NO_2 and CO ($r = 0.57$) also observed in 2020.

An extrapolation of the correlation between pollutants and meteorological variables data obtained in 2020 was made considering the territory of Rio de Janeiro state. Only O_3 correlated with meteorological conditions. Positive correlations were observed between T and WS and negative between T and RH, which was already expected due to ozone photochemical formation.

Backward trajectories calculated by Hysplit Model for the period between March 1st and April 12nd 2020 (Figure 19.5 Supplementary Material) indicate that air masses that reach Rio de Janeiro state during the partial lockdown period were from the Atlantic Ocean. The maritime origin may contribute to lower temperatures in the coastal regions than the interior. Besides of that, sea breeze may contribute to transport pollutants on the coast.

7.3.5. Pollution roses

Pollution rose plots (Figure 7.2- 7.5) show the relationship between WD and WS, and pollutants concentration at monitoring stations. The left panel shows pollutant concentrations before the lockdown, while the right panel pollutant concentrations during the partial lockdown.

7.3.5.1. Largo do Bodegão

Figure 7.2 shows the pollution roses for SO_2 and NO_2 . The SO_2 increase may be related to those facilities located to east and northeast of this monitoring station that continued to work, which includes metallurgical industry, concrete factory. In addition, the Santa Cruz train station is also located in this direction. In the southwest, from where a considerable contribution to the SO_2 concentration was also observed, is located the Santa Cruz area base, the largest in the country and which was a strategic point for the logistics of material distribution during the pandemic. The NO_2 concentration was influenced by industrial facilities located to the southeast and northeast of this monitoring station. Likewise, decreasing in NO_2 concentration may be related to movement restrictions and greater average WS.

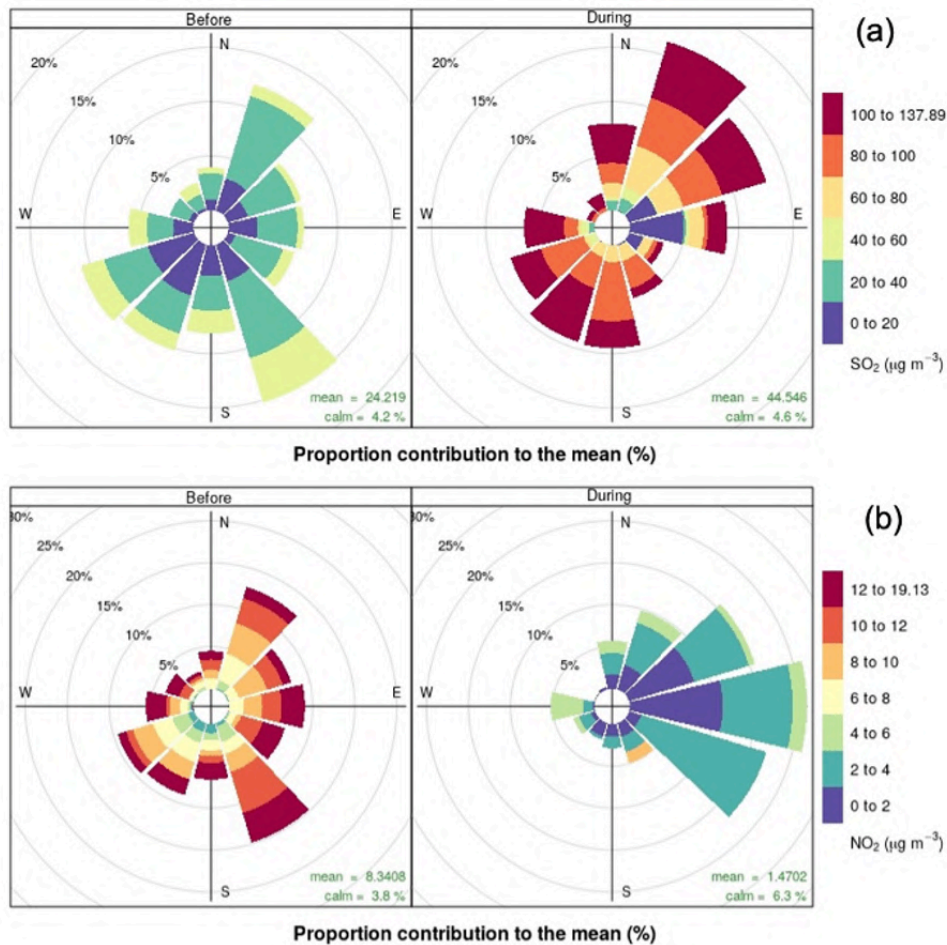


Figure 7.2 Pollution rose plot to show the relation between wind direction and pollutant concentrations at Largo do Bodegão monitoring station: (a) SO₂ and (b) NO₂. Before: March 1st to 15th, 2020 and during: March 16th to April 12nd, 2020.

7.3.5.2. Manguinhos

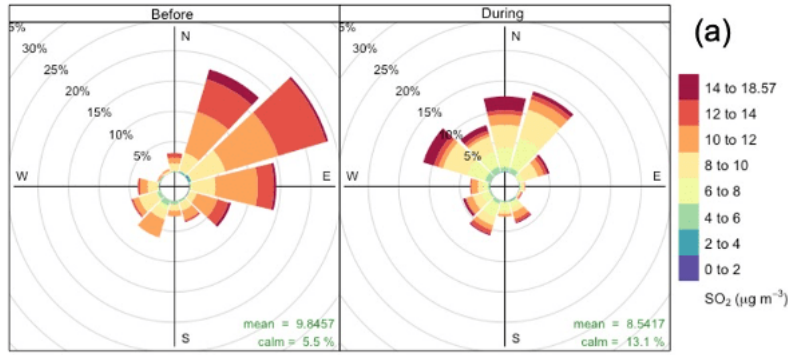
The SO₂, NO₂, O₃, and CO pollution roses for Manguinhos is presented in Figure 7.3. SO₂ decreasing may be ascribed to greater average wind speed. NO₂ concentrations were influenced by industrial facilities and traffic pollution located to the northeast of this monitoring station. Likewise, the decreasing NO₂ concentration during the partial lockdown may be attributed to movement restrictions put in place by the government and more intense average wind speed. Before partial lockdown, O₃ concentrations were mainly from east and northeast, while during the partial lockdown came from north and northeast. O₃ concentration was influenced by industrial facilities located to the north and northeast of the monitoring station. The low CO concentration

before the partial lockdown, came mainly from northeast and east, while for during the partial lockdown, high CO concentration came from the northwest and northeast. CO increasing may be related to heavy traffic in the regions located between northwest and northeast.

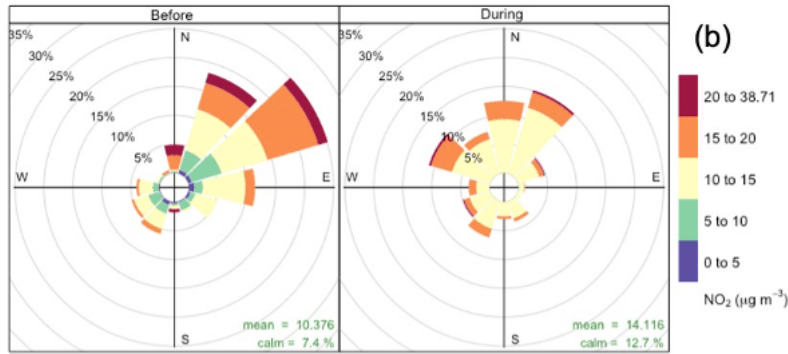
7.3.5.3.Monte Serrat

The pollution roses for Monte Serrat are presented in Figure 7.6. Calm was representative in both periods, indicating local sources of this pollutant. As well as SO₂ concentration, the NO₂ concentration before and during the partial lockdown came mainly from the southeast with calm winds. Therefore, NO₂ is source-specific and generated near the station, which is surrounded by the highway and heavy traffic.

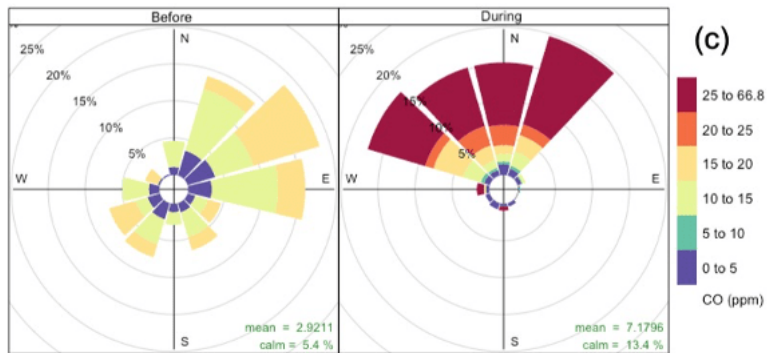
Southeast and east directions were predominant in the O₃ concentration in both periods. The calm wind was representative for both periods. O₃ is source-specific and generated, probably, from Itaguaí city. The Federal Highway (2 km), the industrial complex of Santa Cruz (3 km), and Itaguaí port (7 km) surround this city.



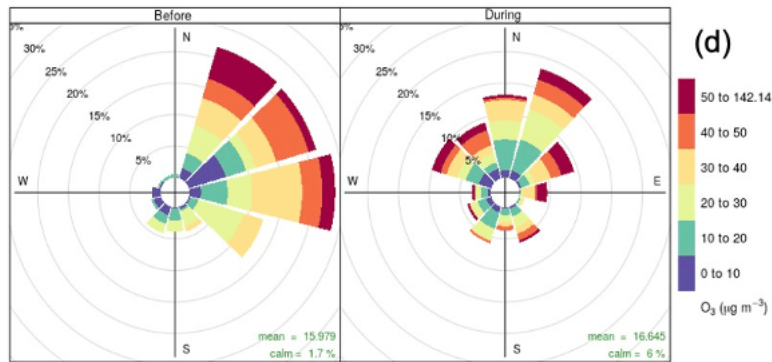
Proportion contribution to the mean (%)



Proportion contribution to the mean (%)



Proportion contribution to the mean (%)



Proportion contribution to the mean (%)

Figure 7.3 Pollution roses plot to show the relation between wind direction and pollutant concentrations at Manguinhos monitoring station: (a) SO₂, (b) NO₂, (c) CO and (d) O₃. Before: March 1st to 15th, 2020 and during: March 16th to April 12nd, 2020.

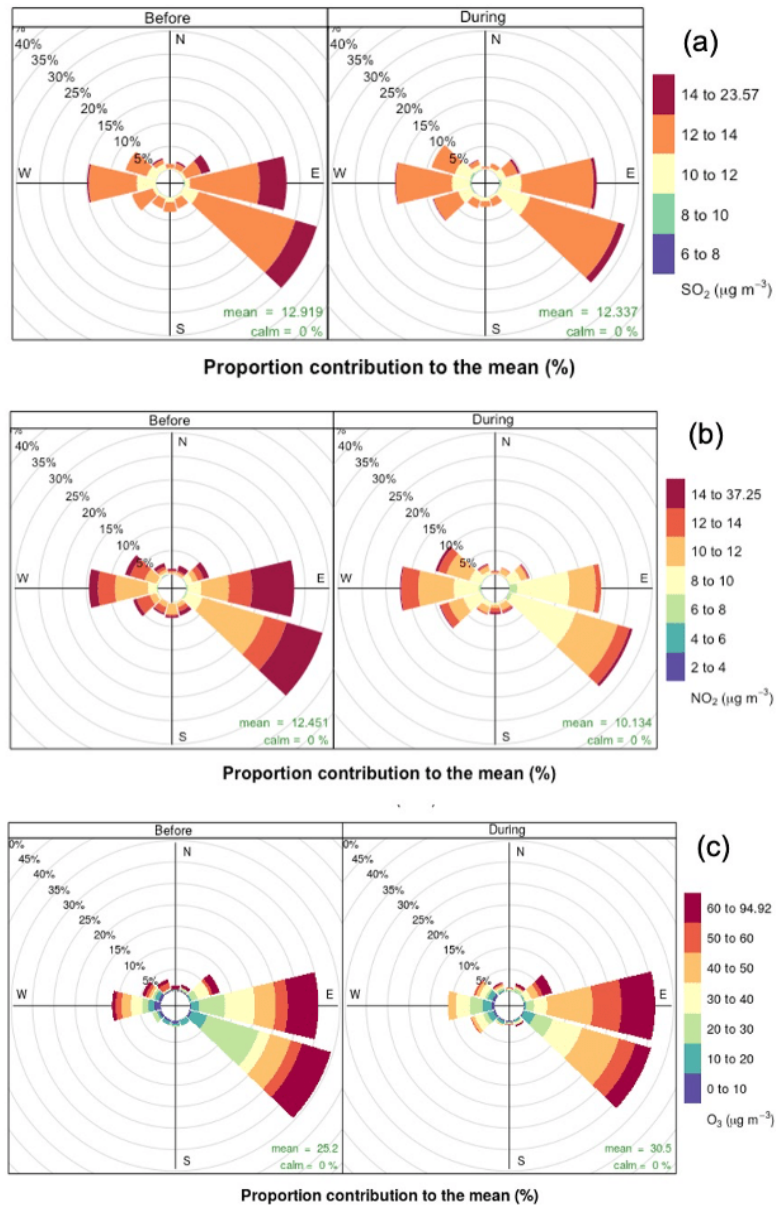


Figure 7.4 Pollution roses plot to show the relation between wind direction and pollutant concentrations at Monte Serrat monitoring station: (a) SO₂, (b) NO₂ and (c) O₃. Before: March 1st to 15th, 2020 and during: March 16th to April 12nd, 2020.

7.3.5.4.São Luiz

Pollution roses for pollutants in São Luiz are presented in Figure 7.7. Calm winds were observed in both periods, which indicates the influence of local pollution sources. In both periods O_3 is mainly coming from the east, while during the partial lockdown wind also comes from the northeast. The calm average wind was representative for both periods. Hence, it concluded that O_3 is source-specific and generated in Duque de Caxias City. The CO concentration came mainly from the east, both before and during the partial lockdown. Therefore, SO_2 , NO_2 and O_3 decreasing during the partial lockdown may be related to the restriction of main industrial facilities and traffic intensity characteristic of the Duque de Caxias City. Highways, industrial facilities, and intense traffic activity surround this city. The CO decreasing during the partial lockdown may be related to the restriction of buses, vehicles, and subways movement around the city.

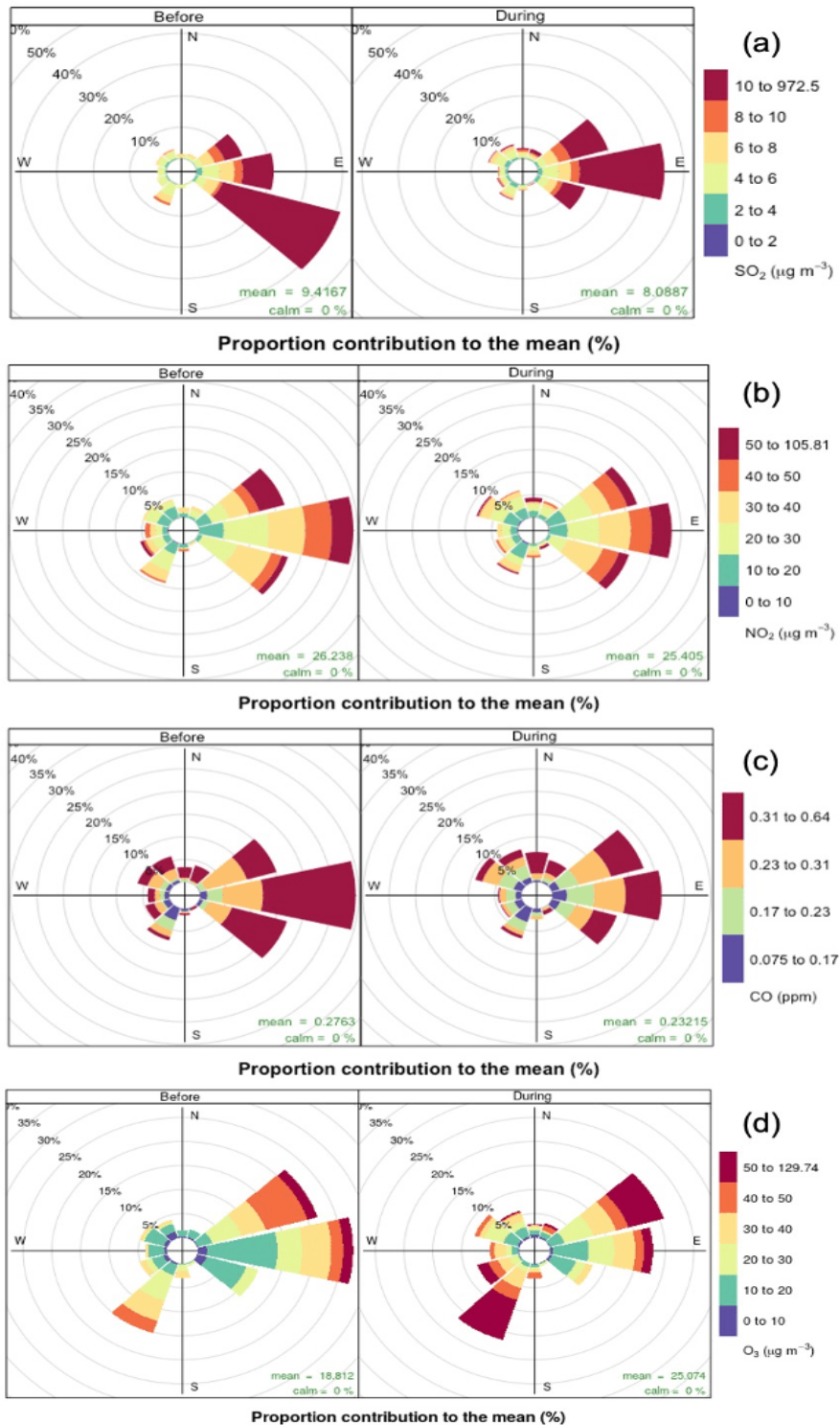


Figure 7.5 Pollution roses plot to show the relation between wind direction and pollutant concentrations at São Luiz monitoring station: (a) SO₂, (b) NO₂, (c) CO and (d) O₃. Before: March 1st to 15th, 2020 and during: March 16th to April 12nd, 2020.

7.4. Conclusions

This study evaluated the influence of meteorological variables and partial lockdown on air quality in MRRJ from March to April 2019 and 2020. As in other cities around the world, the concentrations of some air pollutants decreased during lockdown measures. However, not only emission sources but also meteorological parameters play an important role on the variability of pollutant concentrations.

The Brazilian air quality standards for SO₂, NO₂ and O₃ were not exceeded in any of the monitoring stations in the evaluated periods. However, reductions in SO₂ concentrations ranged from 7 % up to 89 % during the partial lockdown, while NO₂ reduced from 1 % to 65 %. On the other hand, O₃ concentrations increased from 2 % to 34 %, which is related to the decrease in NO₂ concentration, that participates in O₃ depletion. CO was the only pollutant that exceeded daily Brazilian air quality standard at Manguinhos in 2020, mainly during the partial lockdown, although industrial emission may be accountable for that increase, once diurnal cycle does not indicate peak concentration.

The classification of sites according to the AQI was expressed in relation to the worst result among the monitored pollutants. In 2020, Monte Serrat presented air quality classified as “Good” 100 % of the days while São Luiz presented only 7 % of days with “Moderate” to “Poor”. SO₂ was the pollutant responsible for the reduction of air quality on this monitoring station. In Manguinhos, 25 % of the period evaluated in 2020 was ranked with “Very Poor” or “Terrible” air quality due to high concentrations of CO. In Largo do Bodegão, the air quality was classified as “Moderate” to “Poor” in 47 % of the period evaluated in 2020. SO₂ was the pollutant that contributed to the low air quality.

Few strong correlations between pollutants and meteorological variables were found during the evaluated period. The main correlations were verified between O₃ and T and WS, once ozone formation occurs throughout photochemical processes and pollutants from other regions participates in this process. Correlations between O₃ and NO₂ indicates that NO₂ participates in ozone formation, which may be corroborated by the decrease in NO₂ concentration and increase in O₃ concentration.

Although meteorological parameters may influence the pollutants concentration, the air pollution reduction during the partial lockdown was mainly a consequence of

changes on emission sources. The comparison with the previous year indicated that between March 1st and April 12th Rio de Janeiro was under the same meteorological condition. Differences in weather conditions were observed between the weeks of 2020, which influenced the levels of some pollutants. Furthermore, pollution roses indicated that pollutants predominantly come from the east sector, which implies that sea breeze carries pollutants emitted by industries and vehicles on the main roads from the coastline to the continent.

Acknowledgments

This study was financed in part by the Coordenação de Aperfeiçoamento de Pessoal de Nível Superior (CAPES) – Brazil (finance code 001). The authors thanks to CNPq (A.G. and K.B.), to FAPERJ (A.G.), and to CAPES (E.P.S.J.) for the scholarships and CET-Rio for providing traffic monitoring data.

Author Contributions

Karmel Beringui: conceptualization, data curation, software, investigation, visualization, writing original draft and writing-review & editing; Elizanne P. S. Justo: investigation and writing-review & editing; Alex Huaman De La Cruz: investigation, software, writing-review & editing; Ana Carolina L. Bellot de Almeida: data curation and writing-review & editing; Luciana M. Baptista Ventura: data curation, and writing-review & editing; Michelle Branco Ramos: data curation and writing-review & editing; Ruan G. de Souza Gomes: investigation, writing-review & editing; Vinícius Lionel-Mateus: software, writing-review & editing; Adriana Gioda: conceptualization, formal analysis funding acquisition, writing-review & editing

8 Pollutant source assignment through atmospheric metal biomonitoring in a tropic urban center

Karmel Beringui^a, Maria Vitória Rocha^a, Tatiana Dillenburg Saint´Pierre^a, José Marcus de Oliveira Godoy^a, Rachel Ann Hauser-Davis^b, Adriana Gioda^a

^aChemistry Department, Pontifical Catholic University of Rio de Janeiro, Rio de Janeiro, Brazil

^bEnvironmental Health Assessment and Promotion Laboratory, Oswaldo Cruz Institute, Oswaldo Cruz Foundation, Rio de Janeiro, Brazil

Working paper: Journal of Trace Elements and Minerals (Aimed Journal)

Abstract

Urban centers are characterized by high concentrations of pollutants, due to industrialization expansion and high vehicle flow. Monitoring air quality is an environmental and public health issue, however, the high associated costs limit the areas monitored. Atmospheric biomonitoring is a suitable alternative approach to fill the monitoring gap in developing countries. This study aimed to evaluate metal concentrations in the metropolitan region of Rio de Janeiro employing *Tillandsia usneoides* and *Tillandsia stricta* in active biomonitoring. Plants were removed from a site with few pollution sources and exposed to sites with different emission characteristics (vehicular, industrial, and port). Sampling occurred in three moments, so that each period of exposure presents a specific characteristic regarding climatic conditions or urban routine. The two species showed similar enrichment profiles, indicating that both can be used in biomonitoring. Elements associated with vehicular traffic exhibited enrichment in relation to soil greater than one, indicating contribution

from anthropogenic sources. Although this is a widely used approach to assess air quality, studies on metal bioavailability in plants are required to assess exposure risks.

8.1.Introduction

Vehicle emissions are the main source of pollutants in urban centers. Exhaust and non-exhaust emissions contribute to release metals and metalloids into the atmosphere (Pant et al., 2015; Piazzetta et al., 2019). Elements present in fuels can be considered markers of exhaust emissions, such as Cu, Mn, Fe, Zn, Ba, Sn, Ni, Mo and Sb. Non-exhaust emissions, on the other hand, vary according to the traffic characteristics of each location, and depend on the manufacture of the car components. They are characterized by trace concentrations of Cd, Cu, Cr, Zn, Ba, Sb, Mn, Pb, emitted mainly by brake and tire wear (de Souza et al., 2021; Pant and Harrison, 2013; Sanderson et al., 2014).

Metals and metalloids emitted into the atmosphere are associated with particulate matter (PM) (Cardoso-Gustavson et al., 2016). To characterize emission sources and account for their contributions, several standardized instruments and methods are available, although expensive, limiting monitoring to regions with pollution potential. Due to these limitations, biomonitoring has become a widely used approach in recent decades (Aničić et al., 2011; Piazzetta et al., 2019). In this context, epiphytic plants are suitable biomonitors for atmospheric monitoring, as nutrient uptake occurs by gas exchanges, which also leads to contaminant uptake (Gioda et al., 2021; Mendoza-Ramos et al., 2021). Some of the main atmospheric biomonitors are lichen, mosses and some bromeliads, such as species belonging to the *Tillandsia* genus (Ávila-Pérez et al., 2019; Mendoza-Ramos et al., 2021; Szczepaniak and Biziuk, 2003). For metal biomonitoring, biomonitor species must exhibit adequate metal accumulation capacity (Ávila-Pérez et al., 2019). The use of accumulator species for active biomonitoring has the advantage of exposure time control and the possibility of evaluating enrichment factors (Szczepaniak and Biziuk, 2003).

In recent years, several biomonitoring assessments have been conducted in Brazil employing *Tillandsia usneoides* (Alves et al., 2008; Beringui et al., 2021; Cardoso-Gustavson et al., 2016; Giampaoli et al., 2021; Santos et al., 2017; Vianna et al., 2011), *Tillandsia stricta* (Beringui et al., 2021), *Struthanthus flexicauli* (Paula et al., 2015), *Aechmea fasciata* (Giampaoli et al., 2021), *Nicotiana tabacum* cv. *Bel W3**,

Lolium multiflorum ssp. 'italicum', *Tibouchina pulchra*, *Psidium guajava*, *Croton floribundus*, *Astronium graveolens*, *Piptadenia gonoacantha* (Nakazato et al., 2018a), *Psidium guajava* and *Tibouchina pulchra Cogn* (Nakazato et al., 2016).

Only three atmospheric biomonitoring studies have been conducted to date in Rio de Janeiro, comprising active biomonitoring of metals in the industrial area of Santa Cruz using *T. usneoides* (Santos et al., 2017), and on a federal highway in the mountainous region using *T. usneoides* and *T. stricta* (Beringui et al., 2021), and a passive biomonitoring assessment of metals in urban, industrial, and rural regions using *S. flexicauli* (Paula et al., 2015).

In addition to expanding atmospheric monitoring due to low costs, the use of biomonitors allows for prediction regarding ecosystem damage caused by urban pollution. In this context, the aim of this study is to employ *T. usneoides* and *T. stricta* as biomonitors in the assessment of metal pollution in the metropolitan region of Rio de Janeiro considering areas with different characteristics.

8.2. Materials and methods

8.3. Results and discussion

Description in topic 3.4, 3.5 and 3.9, from the page 49.

8.3.1. Elemental concentrations

The boxplots of metals measured in *T. usneoides* and *T. stricta* exposed in MRRJ between July, 2019 and November, 2020 are presented in Figures 8.1, 8.2 and 8.3. For Sampling 1 and 2, elemental concentrations decreased in the following order: Ca > K > Fe > Na > Mg > Al > Mn > Zn = Ti > Cu > Pb = Cr > V > Ni = Se > Li > Mo > As > Co > Cd. For sampling 3, the order was slightly altered, as follows: Ca > K > Na > Fe > Mg > Al > Mn > Zn = Ti > Cu > Cr > V > Ni > Li > Se > Mo = As = Co > Cd > Pb. The main difference is an ample decrease in Pb concentrations, which comprised the element detected at the lowest concentration.

Another study conducted in São Paulo, Brazil, indicated that vehicular emissions remain the main source of Pb in urban centers. Although tetraethyl lead has not been used as a gasoline additive in Brazil since 1992, Pb is still found in trace levels in gasoline, ethanol, and diesel, so vehicle exhaust continues to emit Pb into the

atmosphere (Gioia et al., 2010). In addition to exhaust emissions, vehicles can also emit Pb from tire wear, where it can be found at trace levels. Another study conducted in Rio de Janeiro reported that Pb can be found in similar amounts in different fractions of PM (de Souza et al., 2021). The authors concluded that tire wear and incineration comprised the main Pb sources. Sampling 3 of the present study was performed during the COVID-19 pandemic period, in which the city's routine was altered, with a considerable decrease in vehicle traffic. These changes may have been responsible for the decreased Pb concentrations detected in the last sampling. Duque de Caxias, a site that houses an important industrial pollutant, including an oil refinery, stood out regarding Pb concentrations in samplings 1 and 2, while Santa Cruz, which houses a steel mill complex, was noteworthy in sampling 3. Industrial emissions are the second main source of Pb, especially from metal smelting, such as steel mills and metallurgical plants (Gioia et al., 2010).

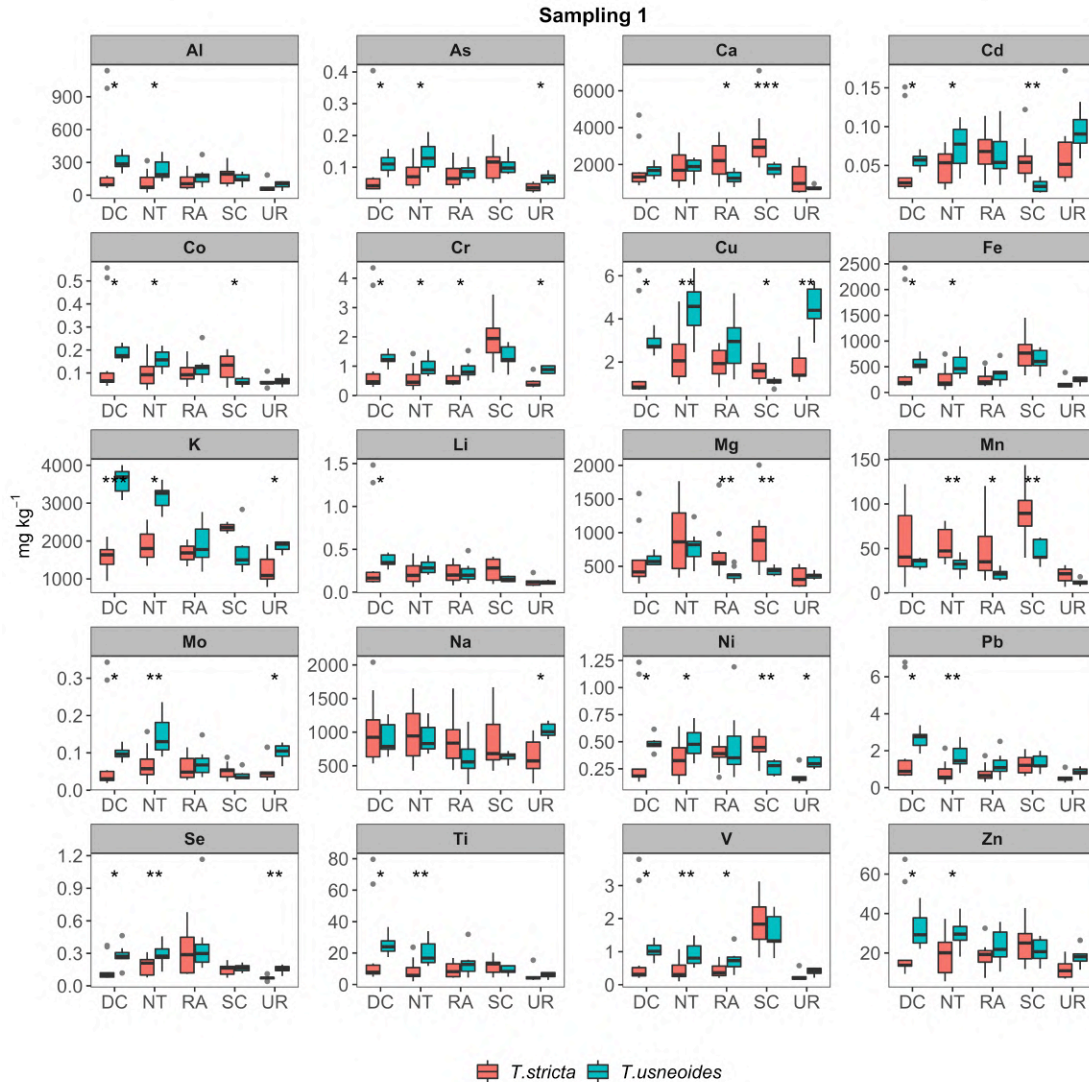


Figure 8.1 Boxplot of metals detected in *T. usneoides* and *T. stricta* sampled in October, 2019 at all monitoring sites. Differences between species exposed at the same site are indicated by * for $p < 0.05$, ** for $p < 0.01$ and *** for $p < 0.001$.

Comparisons between the concentrations detected in the two species exposed at the same monitoring site revealed that samplings 1 and 2 exhibited more statistical differences between plants than sampling 3. Two hypotheses are proposed for this: i) After a longer exposure time, the plants may adapt to the site where they are installed and absorption rate decrease, and ii) The improvement in air quality during the pandemic months contributed to lower elemental absorption.

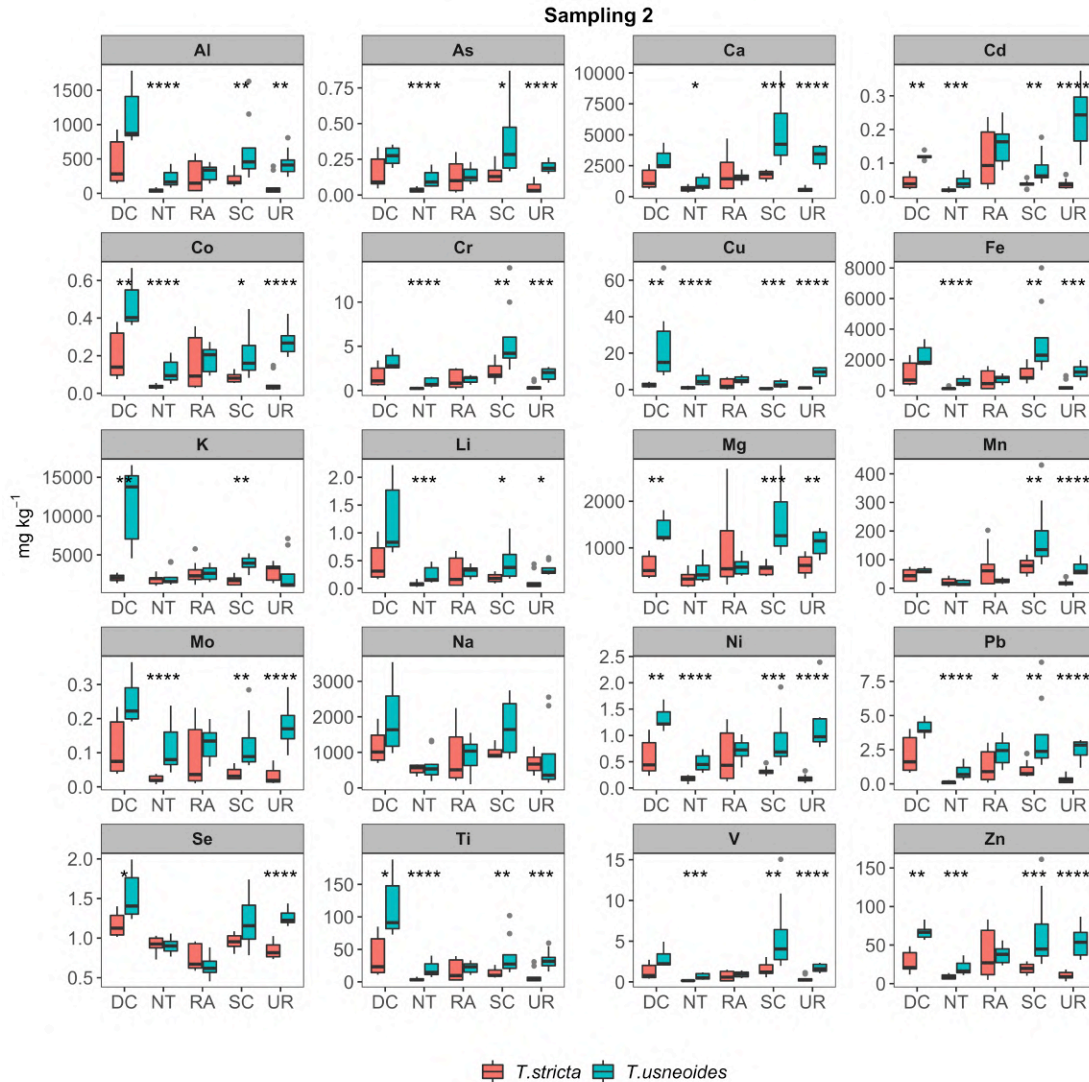


Figure 8.2 Boxplot of metals detected in *T. usneoides* and *T. stricta* sampled in January, 2020 at all monitoring sites. Differences between species exposed at the same site are indicated by * for $p < 0.05$, ** for $p < 0.01$ and *** for $p < 0.001$

Most metals were higher in *T. usneoides* compared to *T. stricta*, possibly due to plant mass differences. *T. stricta* individuals presented higher mass (15 – 20 g) than *T. usneoides*, where the samples were prepared using approximately 10 g. Another factor that may influence this is the larger surface area of *T. usneoides* that causes it to have more contact with the components of the atmosphere compared to *T. stricta*. Plant accumulation capacity varies according to species (Sevik et al., 2019). Thus, to compare the uptake capacity of both species employed herein, it is more appropriate

to evaluate their enrichment after exposure, rather than to consider only the concentrations determined directly in plant tissue.

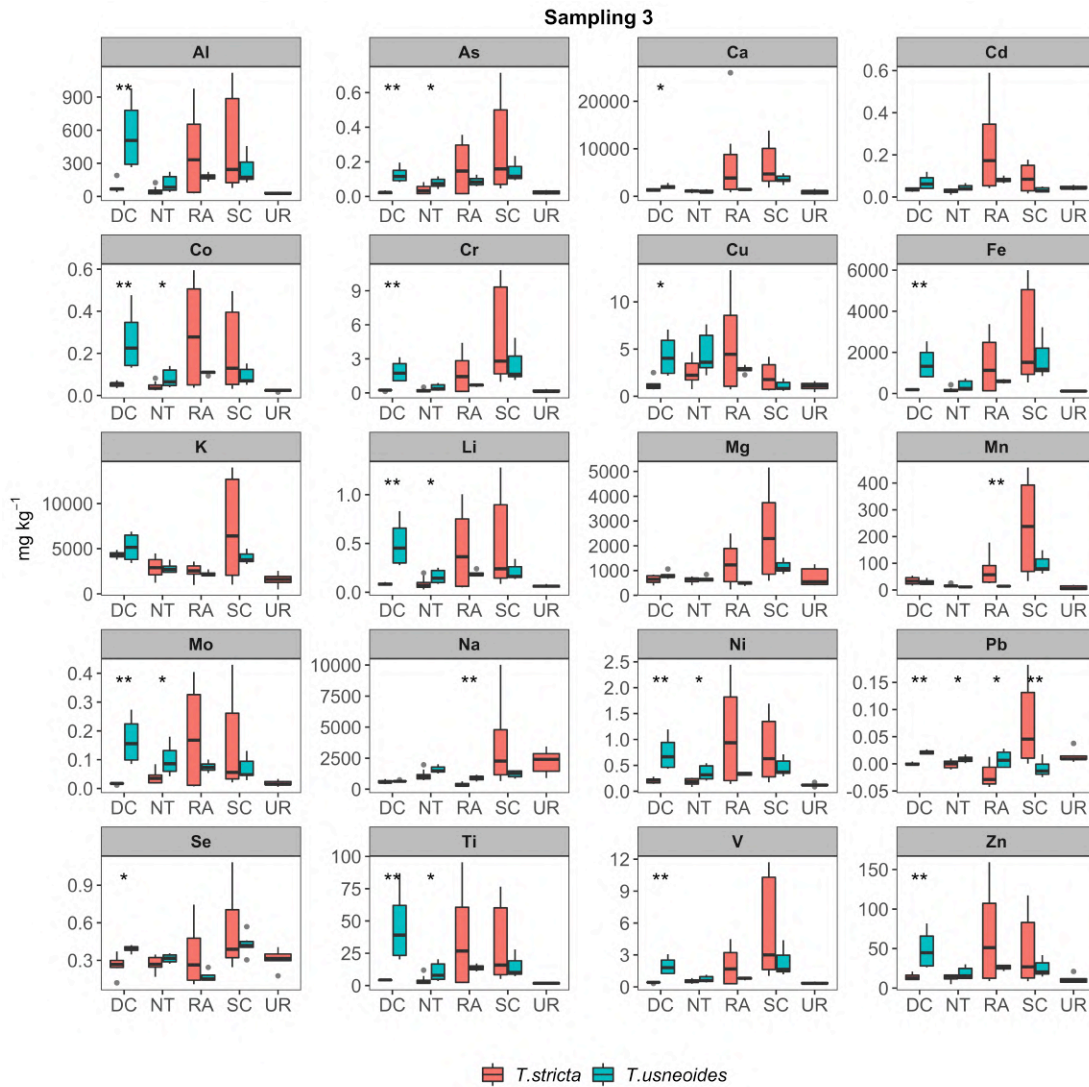


Figure 8.3 Boxplot of metals detected in *T. usneoides* and *T. stricta* sampled in November, 2020 at all monitoring sites. Differences between species exposed at the same site are indicated by * for $p < 0.05$, ** for $p < 0.01$ and *** for $p < 0.001$

8.3.2. Exposure to reference ratio (ER)

The ER calculated for *T. stricta* is presented in Table 8.1 and for *T. usneoides* in Table 8.2. According to Frati et al. (2005), $ER > 1.75$ indicates severe accumulation. Herein, both *Tillandsia* species exhibited similar enrichment behavior.

The highest enrichment compared to the reference sample were Fe and Al, followed by Ti and V. Enrichment for these metals was found in all samplings and in almost all locations in all three sampling campaigns. Some other elements such as Cr, Co, Cu, Zn, As, Se, Mo and Pb exhibited ER much higher than 1.75 at some sites in all three sampling campaigns, indicating emission sources of metallic elements into the atmosphere, which may lead local vegetation to risk due to the toxic effects of metals on plants.

According to the calculated ER values, between July 2019 and January 2020, Duque de Caxias and Santa Cruz presented the highest metal emissions, reflected in the highest metal accumulations. These sites show a strong contribution from industrial emissions, since they host large industrial complexes, but also a significant contribution from vehicle emissions, especially Duque de Caxias, due to important highways with both heavy and light vehicle traffic. A previous study evaluating the PM₁₀ composition sampled in Duque de Caxias revealed that the concentrations of elements such as Fe, Zn, Al, and Cu were almost 3-fold higher than observed in Seropédica, from where the plants were removed from before transplanting (Gioda et al., 2011). Furthermore, studies on the particulate matter composition carried out in the Santa Cruz industrial region have indicated an expressive presence of Cu, Zn, Al, and Ti (Mateus et al., 2013; Mateus and Gioda, 2017).

In November 2020, Ramos and Santa Cruz presented the highest emissions. The monitoring site where the plants were exposed in Ramos is situated on the margins of the most important highway in the city of Rio de Janeiro, Avenida Brasil. One study conducted near this site found high concentrations of Ca, Mg, Fe, Al and Zn in PM₁₀ samples (Toledo et al., 2008).

Table 8.1 Enrichment to reference ratios (ER) calculated for elements determined in *T. stricta* sampled at all three sampling sites.

Element	Sampling 1					Sampling 2					Sampling 3				
	DC	NT	RA	SC	UR	DC	NT	RA	SC	UR	DC	NT	RA	SC	UR
Li	5.3	2.9	2.9	3.5	1.6	6.3	1.0	3.8	2.5	1.6	1.1	1.2	5.6	6.6	0.82
Na	1.9	1.9	1.7	1.6	1.2	2.2	1.0	1.6	1.9	1.3	1.1	2.1	0.69	6.8	4.2
Mg	1.1	1.6	1.2	1.6	0.59	1.0	0.60	1.8	0.95	1.1	1.1	1.1	2.18	4.4	1.3
Al	29	12	13	19	7.7	45	4.4	24	21	10	8.2	4.8	39	46	2.9
Ca	1.4	1.5	1.8	2.6	0.95	1.1	0.49	1.5	1.4	0.46	1.0	0.86	5.5	5.1	0.72
Ti	20	8.6	8.9	12	5.7	38	3.3	16	13	7.9	4.0	3.8	34	30	1.6
V	16	7.5	7.5	32	4.5	22	2.7	12	28	6.5	7.1	9.3	33	92	6.1
Cr	8.7	4.4	4.2	14	3.4	12	1.7	9.1	16	3.2	1.6	1.6	12	36	1.2
Mn	1.3	1.3	1.2	2.2	0.49	1.1	0.53	1.8	1.9	0.46	0.83	0.40	1.7	5.8	0.21
Fe	17	7.7	7.4	21	4.8	30	3.2	18	30	7.6	5.1	4.7	38	76	3.2
Co	5.6	3.6	3.6	4.4	2.2	7.0	1.3	5.5	3.0	1.8	1.9	1.5	10	7.5	0.82
Ni	2.0	1.8	2.0	2.4	0.95	3.1	0.92	3.2	1.7	0.95	1.1	0.98	5.8	4.2	0.65
Cu	3.4	4.0	3.5	2.9	3.2	4.6	1.9	5.5	1.1	1.6	2.2	4.4	9.6	3.7	1.9
Zn	2.8	2.3	2.3	3.0	1.5	3.4	1.1	4.8	2.4	1.3	1.7	1.6	8.0	5.8	1.3
As	6.0	4.2	3.9	6.0	2.0	8.3	1.9	6.6	8.0	2.6	1.2	2.1	8.5	15	1.2
Se	3.0	3.8	6.2	3.1	1.5	24	19	15	20	17	5.4	5.6	6.8	11	6.4
Mo	7.1	5.6	4.8	4.1	4.2	9.2	1.8	6.9	3.1	2.5	1.4	3.2	14	13	1.5
Cd	1.3	1.2	1.8	1.5	1.8	1.1	0.51	3.0	0.99	0.99	0.91	0.72	6.1	2.4	1.2
Pb	14	5.6	5.5	8.7	3.8	15	0.79	9.0	7.2	2.4	-	-	-	0.49	0.10

ER values indicating severe accumulation (> 1.75) are displayed in bold

Table 8.2 Enrichment to reference ratios (ER) calculated for elements determined in *T. usneoides* sampled at all three sampling sites.

Element	Sampling 1					Sampling 2					Sampling 3			
	DC	NT	RA	SC	UR	DC	NT	RA	SC	UR	DC	NT	RA	SC
Li	4.8	3.9	3.0	2.0	1.5	16	3.2	4.1	6.2	4.6	6.6	2.1	2.5	2.7
Na	1.7	1.8	1.2	1.2	1.9	3.7	1.2	1.7	3.2	1.6	1.2	3.0	1.7	2.3
Mg	1.1	1.4	0.65	0.75	0.63	2.4	0.90	1.0	2.7	1.9	1.4	1.1	0.8	2.0
Al	31	23	17	15	9.5	111	21	31	64	44	56	11	18	24
Ca	1.3	1.4	0.99	1.3	0.57	2.3	0.83	1.2	4.1	2.6	1.6	0.80	1.1	2.8
Ti	25	19	13	8.9	5.8	111	19	21	38	33	45	10	13	14
V	18	16	12	27	7.0	50	11	16	99	29	34	12	14	39
Cr	9.3	7.2	6.5	9.8	6.5	24	6.6	9.6	42	14	14	3.5	5.0	18
Mn	0.83	0.72	0.51	1.1	0.29	1.5	0.44	0.62	4.4	1.7	0.72	0.28	0.36	2.3
Fe	16	14	9.6	17	6.6	61	15	21	89	34	41	10	16	46
Co	6.6	5.5	4.3	2.2	2.3	16	4.1	6.5	7.4	9.8	9.3	2.9	3.8	3.2
Ni	2.6	2.6	2.5	1.4	1.6	7.0	2.5	3.8	4.8	6.3	3.9	1.9	1.8	2.4
Cu	5.1	8.1	5.3	1.9	8.0	45	9.5	9.1	5.5	16	7.7	8.1	5.1	1.9
Zn	3.9	3.6	2.8	2.6	2.2	8.2	2.5	4.7	8.2	6.7	6.0	2.3	3.2	3.0
As	5.9	7.2	4.5	5.6	3.4	14	5.8	7.4	19.9	10	6.7	4.1	4.6	7.5
Se	5.8	6.0	7.7	3.4	3.1	31	19	13	25	26	8.0	6.5	3.5	8.8
Mo	8.0	12	5.7	3.2	8.2	20	9.0	10	10	15	13	7.9	6.0	5.5
Cd	1.4	2.0	1.6	0.62	2.4	3.1	1.1	4.0	2.2	6.1	1.8	1.2	2.1	0.88
Pb	18	11	8.3	9.4	5.9	28	5.9	16	24	17	0.15	0.06	0.06	-0.06

ER values indicating severe accumulation (> 1.75) are displayed in bold

8.3.3. Enrichment Factor

No significant difference was observed between topsoil and deep soil sample elemental concentrations. Thus, the average concentration of the two soil types was used to calculate the enrichment factor relative to soil, presented in table 8.3 for *T. stricta* and table 8.4 for *T. usneoides*.

Table 8.3 Enrichment factor in relation to soil composition calculated for *T. stricta* sampled at all sites in three sampling campaigns considering Fe concentration as standardization factor.

Element	Sampling 1					Sampling 2					Sampling 3				
	DC	NT	RA	SC	UR	DC	NT	RA	SC	UR	DC	NT	RA	SC	UR
Li	1.7	3.0	2.8	1.7	1.4	1.1	2.5	1.5	0.9	0.9	1.2	2.0	1.1	0.9	1.1
Na	167	549	384	135	287	110	703	149	109	202	326	1009	30	160	1534
Mg	3.9	31	19	8.6	7.1	2.2	28	11	3.7	8.4	14	35	6.5	6.8	23
Al	0.8	1.3	1.2	0.5	0.8	0.7	1.1	0.9	0.4	0.7	0.8	0.8	0.7	0.3	0.5
K	26	48	42	40	35	19	109	27	21	50	239	117	12	35	66
Ca	1.9	25	15	6.8	17	0.8	20	5.4	2.5	5.4	4.6	24	9.1	3.8	20
Ti	1.8	1.4	1.7	2.7	1.6	2.0	1.3	1.2	2.2	1.4	1.2	1.0	1.2	2.0	0.7
V	1.2	1.1	1.3	2.1	1.2	0.9	0.9	0.9	1.3	1.1	1.6	2.1	1.1	1.7	2.5
Cr	1.7	1.9	2.6	2.1	2.7	1.3	1.7	2.3	1.6	1.7	1.1	1.1	1.5	1.5	1.5
Mn	4.1	22	14	4.4	8.3	1.9	21	8.1	2.7	5.0	8.3	11	3.8	3.4	5.4
Co	1.6	2.5	1.9	2.0	2.2	1.2	2.1	1.2	1.0	1.2	1.8	1.7	1.0	1.0	1.3
Ni	1.3	2.0	5.4	2.6	2.4	1.1	2.5	3.5	1.3	1.6	2.3	1.8	3.0	1.3	2.5
Cu	2.1	1.4	7.8	4.3	8.8	1.7	1.6	5.1	1.1	2.8	4.7	2.5	4.2	1.6	7.9
Zn	5.1	3.5	8.5	5.6	9.1	3.5	3.9	7.3	3.2	5.0	10	3.9	5.8	3.1	13
As	3.3	1.5	4.6	3.4	2.3	2.6	1.6	3.2	3.2	2.0	2.3	1.2	2.0	2.4	2.2
Se	3.7	14	24	3.5	7.2	16	160	24	15.	53.	22	32	5.1	3.5	46
Mo	2.7	5.0	16	6.0	16	2.0	3.9	9.7	3.2	6.4	1.7	4.6	9.4	5.3	8.8
Cd	7.5	4.3	14	9.2	24	3.8	4.2	9.7	4.3	8.2	17	4.0	9.5	4.1	22
Pb	2.6	0.5	1.7	2.1	0.5	1.5	0.2	1.1	1.2	0.2	-	-	-	0.03	0.02

Table 8.4 Enrichment factor in relation to soil composition calculated for *T.usneoides* sampled at all sites in three sampling campaigns considering Fe concentration as standardization factor.

Element	Sampling 1					Sampling 2					Sampling 3			
	DC	NT	RA	SC	UR	DC	NT	RA	SC	UR	DC	NT	RA	SC
Li	1.7	2.2	2.2	1.2	1.0	1.4	1.7	1.4	0.7	0.6	0.9	1.7	1.1	0.6
Na	160	274	210	120	345	88	179	136	64	54	45	662	175	89
Mg	4.1	15	7.8	5.0	5.6	2.4	9.3	5.7	3.5	3.3	2.1	17.	5.9	5.0
Al	1.0	1.3	1.2	0.5	0.8	0.9	1.2	1.0	0.4	0.7	0.7	0.9	0.8	0.3
K	64	42	36	35	38	53	27	23	16	10	35	53	25	32
Ca	1.9	13	6.7	4.3	7.7	0.8	7.3	3.6	2.6	6.7	0.9	10	4.3	3.4
Ti	2.4	1.6	1.8	2.5	1.2	2.8	1.6	1.4	2.1	1.3	1.7	1.2	1.1	1.5
V	1.4	1.2	1.7	2.1	1.4	1.0	0.8	1.0	1.5	1.1	1.0	1.3	1.1	1.2
Cr	2.0	1.7	3.1	1.7	3.9	1.3	1.5	2.1	1.5	1.6	1.1	1.1	1.4	1.2
Mn	2.7	7.1	4.5	2.8	3.6	1.2	3.9	2.5	2.1	4.1	0.9	3.6	1.9	2.2
Co	2.1	2.0	1.7	1.2	1.7	1.3	1.5	1.2	0.8	1.4	1.1	1.5	0.9	0.7
Ni	1.7	1.6	5.1	1.8	3.1	1.2	1.5	3.6	1.3	2.3	1.0	1.6	2.2	1.2
Cu	3.5	1.5	9.2	3.5	16	7.8	1.7	7.3	1.9	6.2	2.0	2.1	5.2	1.3
Zn	7.6	2.9	8.3	5.9	10	4.1	2.0	6.2	3.6	5.9	4.5	2.6	5.4	2.6
As	3.5	1.4	4.2	3.9	3.0	2.2	1.1	3.1	2.7	1.8	1.5	1.1	2.5	2.0
Se	7.6	12	23	4.7	11	10	35	18	6.7	17	4.0	17	6.2	4.6
Mo	3.2	5.6	15	5.6	24	2.1	4.2	12	3.5	8.1	2.1	5.3	9.4	3.7
Cd	9.1	3.6	10	4.7	23	5.0	2.0	11	3.2	11.0	4.4	3.0	7.7	2.5
Pb	3.5	0.5	1.9	2.7	0.6	1.4	0.2	1.7	1.4	0.3	0.01	0.004	0.008	-

The results obtained for *T.usneoides* from *T.stricta* were similar, indicating again, that the two *Tillandsia* species exhibit similar metal uptake behavior. The elements associated with vehicular traffic showed $1 < EF < 5$, which is an indication of both anthropogenic contributions and soil resuspension. The similarity in the composition of topsoil and deep soil is an indication that the elements emitted over time at the monitoring sites are already part of the composition of an extensive soil bed. Thus, resuspension may contribute to the return of particles emitted by anthropogenic sources to the atmosphere.

The elements Zn, Cu, Cd, and Mo presented $EF > 5$, an indication of mostly anthropogenic contribution, mainly from local sources, as several locations presented $EF < 10$ (Elhadi et al., 2018; Hien et al., 2001). These elements are related to both exhaustion and non-exhaustion emissions, and all can be found in gasoline or diesel

and are emitted into the atmosphere due to fuels burning. Zn and Cd are also found in lubricating oils and Mo, in automobile catalyts. Non-exhaust emissions can contribute to the concentration of these elements by brake and tire wear (Souza et al., 2021; Pant and Harrison, 2013).

Niterói and Ramos presented the highest EF in all three samplings. Both are located near two important roads in the metropolitan region. At Niterói, the biomonitoring site is located near one of the accesses to the Rio-Niterói bridge, which is the only road connection to the city of Rio de Janeiro. In Ramos, the biomonitoring site is next to Av. Brasil, which crosses the entire city of Rio de Janeiro and undergoes one of the largest flows of light and heavy cars in the state.

8.3.4. Source assignment by metal correlation

Correlations between elements can indicate whether they are emitted by the same emission source (Elhadi et al., 2018; Wei et al., 2010). Spearman's correlations between metals are presented in Figures 8.4 and 8.5. For most elements, mainly traffic-related elements, strong Spearman correlations ($\rho > 0.7$) were observed for both *Tillandsia* species.

Ramos and Urca, which present vehicular traffic as their main emission sources, presented the most inter-elemental correlations. At Santa Cruz, almost all elements correlated in *T. usneoides*, while *T. stricta* showed less correlations and lower correlation coefficients. Duque de Caxias exhibited the greatest variation in correlation coefficients. Due to several industries in this location, emission sources with different characteristics may be present.

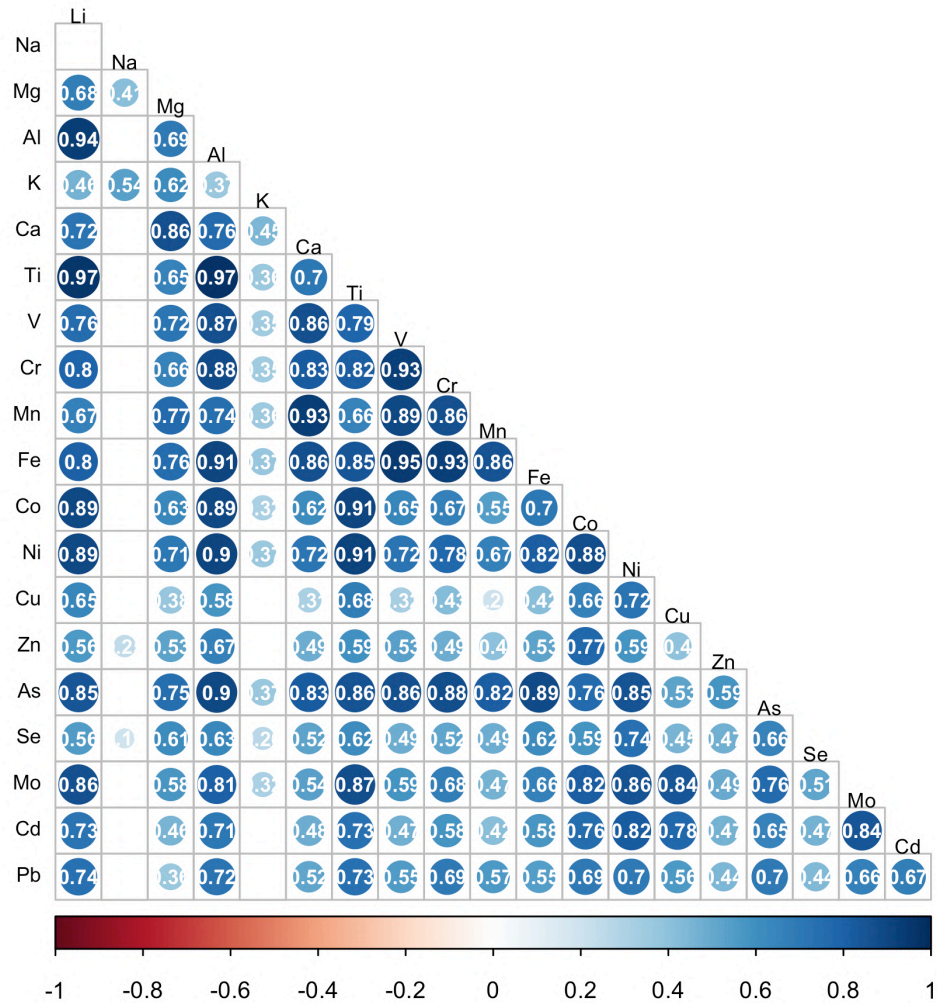


Figure 8.4 Spearman's correlations obtained between metals determined in *T. usneoides* from all sampling sites

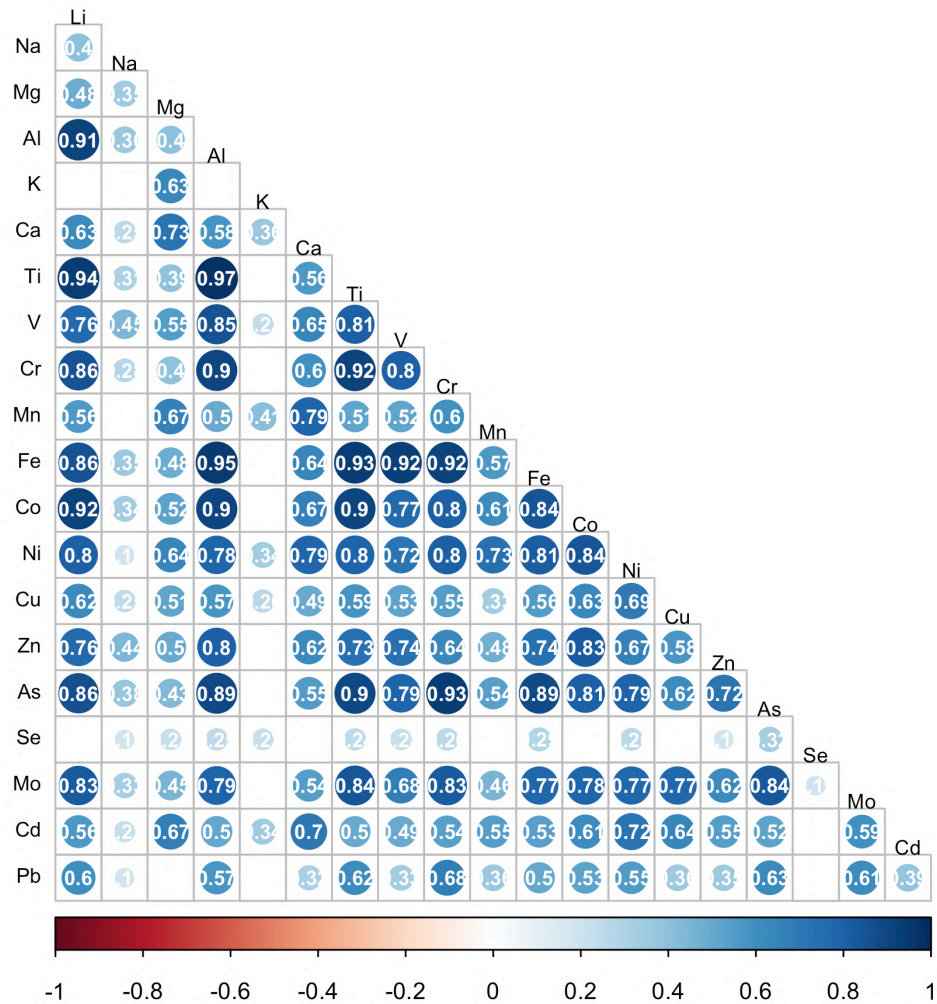


Figure 8.5 Spearman's correlations obtained between metals determined in *T. stricta* from all sampling sites

8.4. Conclusion

Elemental tissue composition of the employed plant biomonitors was similar throughout the exposure period, with the exception of Pb, which exhibited a significant decrease following over one year of exposure. This may have been due to urban mobility changes the last eight months of exposure due to the COVID-19, as the main Pb source is exhaust and non-exhaust vehicle emissions.

T. usneoides showed statistically higher elemental concentrations than *T. stricta*, although plant mass differences may be responsible. Similar enrichment to reference ratio for both species validate this hypothesis, since this factor indicates both species

display similar absorption capacity. In the last sampling campaign, few differences were observed between the species, which may be linked to plant adaptation or to air quality improvement during the COVID-19 pandemic lockdown period.

The calculated enrichment factors indicated that anthropogenic sources are the main contributors to metal emissions, mainly traffic-related metals. The similarity of the emission sources is corroborated by the strong statistical correlations obtained between metals. Finally, although biomonitoring is an appropriate approach to assess metal pollution, only the bioavailable metal fraction may actually pose a risk to human health or ecosystems. Thus, further studies are required to investigate which metals pose toxicological risks.

9 Subcellular metal distribution and detoxification in atmospheric biomonitors in a Brazilian metropolis

Karmel Beringui^a, Maria Vitória R. Gomes^a, Felipe Dias Melo^a, José Marcus Godoy^a, Tatiana D. Saint’Pierre^a, Rachel Ann Hauser-Davis^b, Adriana Gioda^{a*}

^aChemistry Department, Pontifical Catholic University of Rio de Janeiro, Marquês de São Vicente, 225, Gávea - Rio de Janeiro, Brazil

^bEnvironmental Health Assessment and Promotion Laboratory, Oswaldo Cruz Institute, Oswaldo Cruz Foundation, Av. Brasil, 4.365 – Manguinhos, Rio de Janeiro, Brazil

Paper submitted: *Science of The Total Environment*

Highlights

Tillandsias are more susceptible to oxidative stress during humid periods

Metallothionein acts in the detoxification of traffic-related metals

T. stricta was proven more resistant to metal pollution

Fe and Se exert a protective effect against toxic Pb effects

Abstract

Subcellular metal distribution assessments are the most adequate biomonitoring approach to evaluate metal toxicity. Thus, this study aimed to assess subcellular metal distribution and associations to the main metal exposure biomarker, Metallothionein (MT), in two bromeliad species established in industrial, urban, and port areas in the metropolitan region of Rio de Janeiro (MRRJ), Southeastern Brazil. An active biomonitoring approach was applied, exposing *Tillandsia usneoides* and *Tillandsia stricta* for one year to differential pollution at different sampling sites. Three subcellular fractions (insoluble, thermolabile and thermostable) were obtained from the MT purification process and extracted, separately, for metal quantification by inductively

coupled plasma mass spectrometry (ICP-MS). Lower MT concentrations were observed during the dry periods, associated to plant crassulacean acid metabolism (CAM). Sampling during the COVID-19 pandemic recorded the lowest MT concentrations due to reduced urban mobility, which decreased pollutant emissions. Increasing metal contents were observed in the insoluble fractions throughout the experiment for both species. The thermostable fraction evaluated herein contains purified MT, thus, metals found in this fraction are associated with this metalloprotein through the MT-metal detoxification route. In this regard, some elements are noteworthy in the thermostable fraction obtained in our study, namely Cr, Co, Cu, Cd, Mn, Ni, Se, and Zn. Most of these metals can be associated with vehicle emissions, the main source of pollutants in urban centers. Although some are essential for plants, they may cause toxic effects when present at high concentrations. Comparing the two species, the percentage of insoluble, and thus, non-bioavailable metal fraction, was higher in *T. stricta*, indicating that this species is less susceptible to damage from metal exposure. A potential protective effect of Se and Fe against Pb suggested by a strong negative correlation between these elements may be attributed to antioxidant role and similar uptake route, respectively.

Keywords: *Tillandsia*, metallothionein, trace elements, subcellular compartmentalization.

9.1. Introduction

Atmospheric pollutant emissions as a result of increased anthropogenic activities comprise one of the major air pollution contributors worldwide and are, therefore, of significant environmental concern (Beringui et al., 2021; Paralovo et al., 2019; Varela et al., 2018). Standard air quality assessment methods, however, include high-cost equipment and supplies, making air quality monitoring limited due to financial constraints (Ávila-Pérez et al., 2019; Vianna et al., 2011; Wannaz et al., 2006). Biomonitoring thus becomes an effective alternative approach for air quality monitoring, due to low deployment costs and the coverage of larger areas when compared to traditional techniques (Bargagli, 2016; Conti and Cecchetti, 2001).

In a sustainable scenario, pollutant toxicology effects require monitoring, and, in this context, plants display significant potential as air quality biomonitors (Techato et al., 2014). Moss, lichens and epiphyte plants are mostly employed for this purpose, as they obtain nutrients from the air by gaseous changes that occurs in their stomates and/or trichomes (Alves et al., 2008; Gioda et al., 2021; Zheng et al., 2017).

Tillandsia species are excellent biomonitors in this context, obtaining their nutrients from the atmosphere and exhibiting high absorptive capacity (Sun et al., 2021a). Furthermore, as they are widely distributed in tropical areas, *Tillandsia* species are often chosen for atmospheric biomonitoring efforts in South America (Beringui et al., 2021; De La Cruz et al., 2021; Gioda et al., 2021; Piazzetta et al., 2019). The *Tillandsia* genus is also resistant to humidity changes and metal accumulation in these plants is directly correlated to anthropogenic emissions (Piazzetta et al., 2019; Zheng et al., 2016).

Found in tropical regions, *Tillandsia usneoides* and *Tillandsia stricta* exhibit the crassulaceous acid metabolism (CAM), which results in resistance to high temperatures and humidity. Both species are frequently found in South America, and present leaves covered by trichomes for nutrient and water absorption (Nakazato et al., 2018a; Oliveira et al., 2016). *T. stricta* frequently grows associated to both biological and inert structures, and exhibits rapid metal accumulation rates (Beringui et al., 2021; Oliveira et al., 2016; Zheng et al., 2016). *T. usneoides* exhibits an extensive metal accumulation capacity and is the most employed plant in atmospheric biomonitoring assessments in the Southern Hemisphere (Figueiredo et al., 2007; Gioda et al., 2021).

Metal accumulation by *Tillandsia* has been well exploited in air pollution studies, but how these biomonitors accumulate these pollutants and their toxic physiological effects are still not clear. Furthermore, although routinely carried out, total metal determinations are not adequate to assess the actual harmful physiological effects of these contaminants (Monteiro et al., 2019), which can only be evaluated by assessing subcellular metal distributions. This is due to the fact that metals are compartmentalized upon cell entry and may interact with subcellular structures and participate in physiological processes, although some assessments in plants indicate that these compound may also remain adsorbed to the cell wall (Sun et al., 2021b; Zheng et al., 2021). This subcellular partitioning directly affects metal bioavailability and toxicity, and assessments in this regard are paramount to evaluate toxic metal

effects, including reactive oxygen species production, a significant metal toxicity pathway, consequently, inducing oxidative stress (Nakazato et al., 2018a), as well as cytotoxicity and genotoxicity endpoints.

In plants, metal detoxification usually occurs by chelation processes through amino acids, phytochelatin and metallothionein binding (TripathiPreeti et al., 2015). Metallothionein (MT), is the main metal exposure biomarker, consisting in a low-molecular-mass protein which can bind to many different metals via the sulfur atom present in the amino acid cysteine (Oaten et al., 2017; Santosa, 2016; TripathiPreeti et al., 2015). Besides participation in metal detoxification, MT also contributes to homeostasis regulation and oxidative stress prevention (Kısa et al., 2017; Oaten et al., 2017). In plants each MT type tends to predominate in one specific tissue (Kısa et al., 2017).

Few studies on the toxic effects of metals on plants are available, none concerning the effects of air pollution on plants considering an urban reality scenario. This study aimed to assess subcellular metal distribution and metal associations to the main metal exposure biomarker, MT, in two *Tillandsia* species established in industrial, urban, and port areas in the metropolitan region of Rio de Janeiro, Southeastern Brazil.

9.2. Material and Methods

Described in topics 3.6 and 3.9, from the page 49.

9.3. Results

9.3.1. MT content in *Tillandsia usneoides* and *Tillandsia stricta*

The MT concentrations detected in both *Tillandsia* species per sampling location are presented in Figure 9.1. No statistical differences ($p < 0.05$) between species exposed at the same site were observed. Data are expressed as $\mu\text{mol g}^{-1}$ wet weight (w.w.).

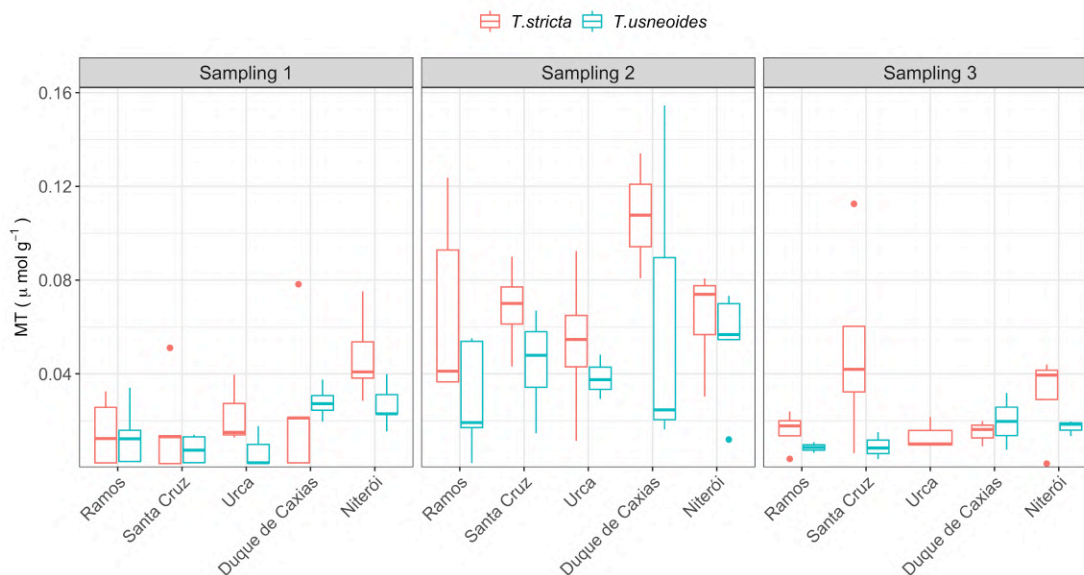


Figure 9.1 *Tillandsia stricta* and *Tillandsia usneoides* metallothionein (MT) concentrations ($\mu\text{mol g}^{-1}$ f.w.) per sampling date (1: October 2019, 2: January 2020, and 3: November 2020). The horizontal lines within the box plots display the medians, the upper line indicates the 75th quartile and the lower line, the 25th quartile. The whiskers indicate the maximum and minimum ranges, with vertical lines extending from the 10th to the 90th percentile, and the dots represents outlier values.

Samplings 1 and 3 took place following the dry period in Rio de Janeiro (from June to September). Plants with CAM metabolisms are highly adaptable to dry seasons and capture CO_2 at night (Giampaoli et al. 2021), when traffic, the main pollutant source in urban centers, decreases significantly. Gaseous changes and, thus, metal incorporation, usually occur during lower pollutant background level scenarios. Statistically higher MT values, however, were observed during the second sampling carried out in January 2020 compared to the first and third, which may be due to metabolic differences regarding seasonality and pollutant uptake. Field assessments regarding MT and metal associations in plants during different seasons are significantly lacking in the literature, preventing further discussion. However, this knowledge gap indicates that this topic should be further investigated.

Although no statistical differences were observed between Samplings 1 and 3, the boxplots indicate a lower data distribution for Sampling 3, possibly due to mobility pattern alterations, as this sampling was performed during the COVID-19 pandemic, when a global trend concerning lower atmospheric pollutant concentrations during

social isolation due to mobility reduction was observed, including in Brazilian metropolises such as Rio de Janeiro and São Paulo (Beringui et al., 2021; Brandao and Foroutan, 2021; Dantas et al., 2020; Debone et al., 2020; Rudke et al., 2021; Siciliano et al., 2020).

The similarities in MT concentrations for sampling 1 and 3 may also be related to plant metabolism, which in dry periods causes the organelles responsible for gas exchange to remain closed for a longer time to avoid loss of oxygen. Thus, because the contact with the components of the atmosphere, among them, the pollutants, occurs for reduced periods, the toxic effects are reduced, inducing lower concentrations of MT when compared to sampling 2, which occurred during the rainy season.

The MT contents suggest more active detoxification at Niterói in Sampling 1, Duque de Caxias in Sampling 2 and Santa Cruz in Sampling 3, possibly related to more pollution sources during these sampling periods. It is important to highlight that, in addition to traffic contribution, these sites present other important pollutant sources, such as port activities, near Niterói, and the industrial complexes located in Santa Cruz and Duque de Caxias. However, even with other pollutant sources, it is clear that MT is more induced in high urbanization areas, probably due to higher atmospheric metal emissions, which have been reported previously for these same areas and biomonitor species (Beringui et al., 2021; Monna et al., 2017; Paula et al., 2015; Santos et al., 2017; Vianna et al., 2011).

9.3.2. Metal and metalloid determinations

The LOQ for Li and Co were below 1 ng kg^{-1} , for Ti, V, Cr, Mn, Ni, Cu, As, Mo, Cd, and Pb were below 10 ng kg^{-1} , and for Na, Mg, Al, K, Ca, Fe, Zn and Se were below $1 \text{ } \mu\text{g kg}^{-1}$. The percentual recovery of standard reference materials determined by ICP-MS are expressed in $\text{mg kg}^{-1} \text{ w.w.}$ and presented in Table 9.1. The Cd recovery higher than 100 % was attributed to its low content and the uncertainty related to the obtained value.

Table 9.1 Measured and certified concentrations and recovery of standard reference material (SRM 1515 and SRM 1547) determined by ICP-MS.

Element	SRM 1515 – Apple leaves			SRM 1547 – Peach Leaves		
	Determined (mg kg ⁻¹)	Certified (mg kg ⁻¹)	Recovery (%)	Determined (mg kg ⁻¹)	Certified (mg kg ⁻¹)	Recovery (%)
B	17.5 ± 9.8	27.6 ± 2.8	63	23.20 ± 2.309	28.73 ± 0.081	81
Mg	2687 ± 228	2710 ± 120	99	3444.32 ± 1	4320 ± 150	80
Al	94.5 ± 3.5	284.5 ± 5.8	33	74.58 ± 40.47	248.9 ± 6.5	30
K	16078 ± 405	16080 ± 210	100	-	-	-
Ca	15173 ± 1119	15250 ± 100	99	15739 ± 218	15590 ± 160	101
V	0.07 ± 0.0010	0.25 ± 0.0027	27	0.094 ± 0.4174	0.367 ± 0.0368	26
Mn	44.0 ± 2.7	54.1 ± 1.1	81	91.8 ± 18.6	97.8 ± 1.8	94
Ni	0.98 ± 0.030	0.94 ± 0.094	104	-	-	-
Cu	4.34 ± 0.27	5.69 ± 0.13	76	2.99 ± 0.55	3.75 ± 0.37	80
Zn	8.64 ± 0.21	12.45 ± 0.43	69	15.5 ± 6.08	17.9 ± 0.53	87
Rb	7.8 ± 0.3	10.2 ± 1.6	76	14.02 ± 0.33	19.65 ± 0.89	71
Sr	20.5 ± 1.2	25.1 ± 1.1	81	57 ± 13.2	53 ± 5.0	108
Mo	0.062 ± 0.017	0.095 ± 0.011	65	0.0154 ± 0.0060	0.0603 ± 0.0068	26
Cd	0.00987 ± 0.00815	0.0132 ± 0.0015	75	0.0464 ± 0.0190	0.0261 ± 0.0022	178
Ba	-	-	-	115.6 ± 3.1	123.7 ± 5.5	93
Pb	0.24 ± 0.0391	0.47 ± 0.024	51	0.667 ± 0.054	0.869 ± 0.018	77

The subcellular metal distributions obtained for industrial sites are presented in Figure 9.2 and for urban in Figure 9.3 and in urban and port site in Figure 9.4. Insoluble metal contents increased from sampling 1 to sampling 3 for both *T. usneoides* and *T. stricta*.

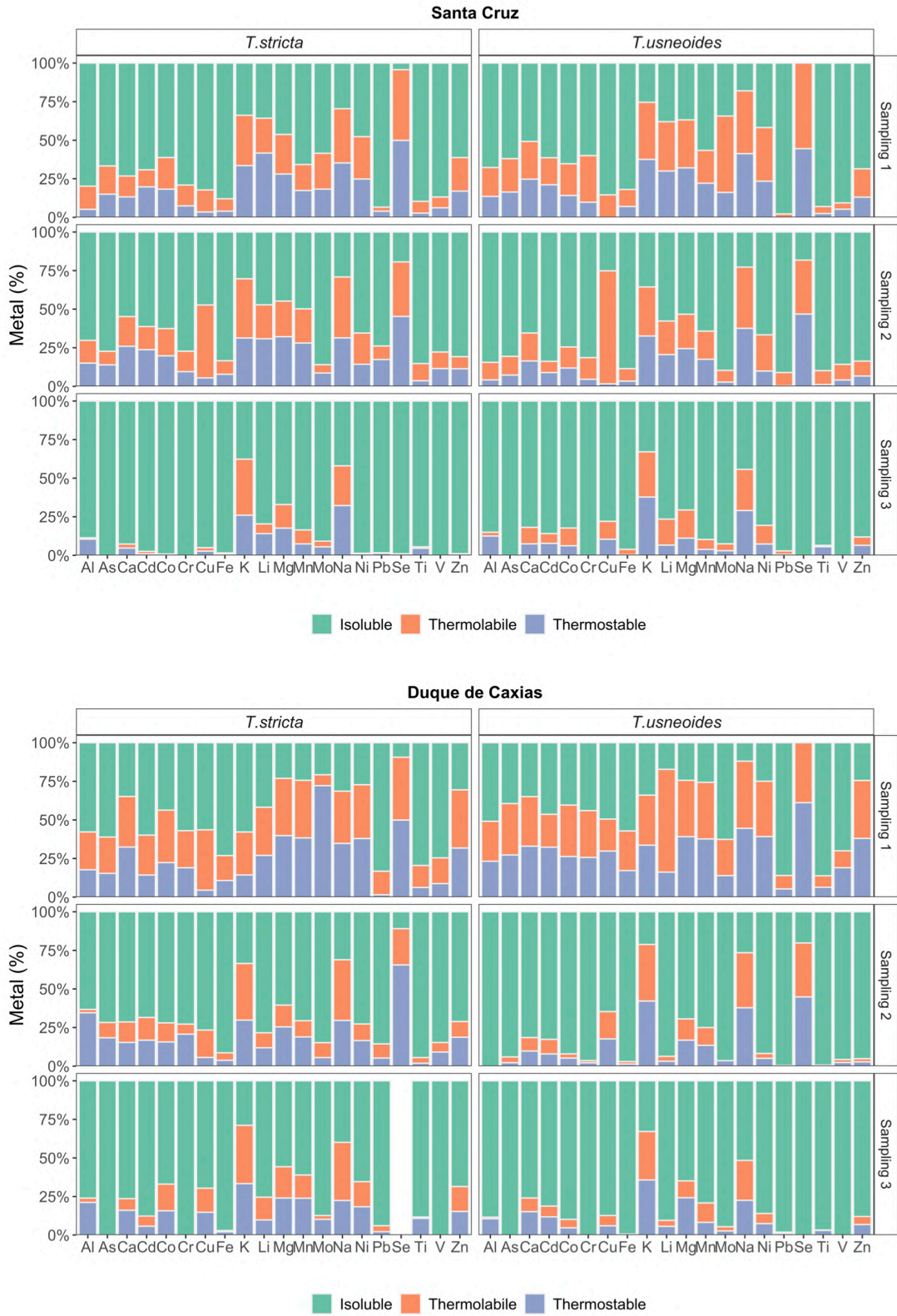


Figure 9.2 Subcellular metal distribution of metals in *T. usneoides* and *T. stricta* exposed at industrial sites.

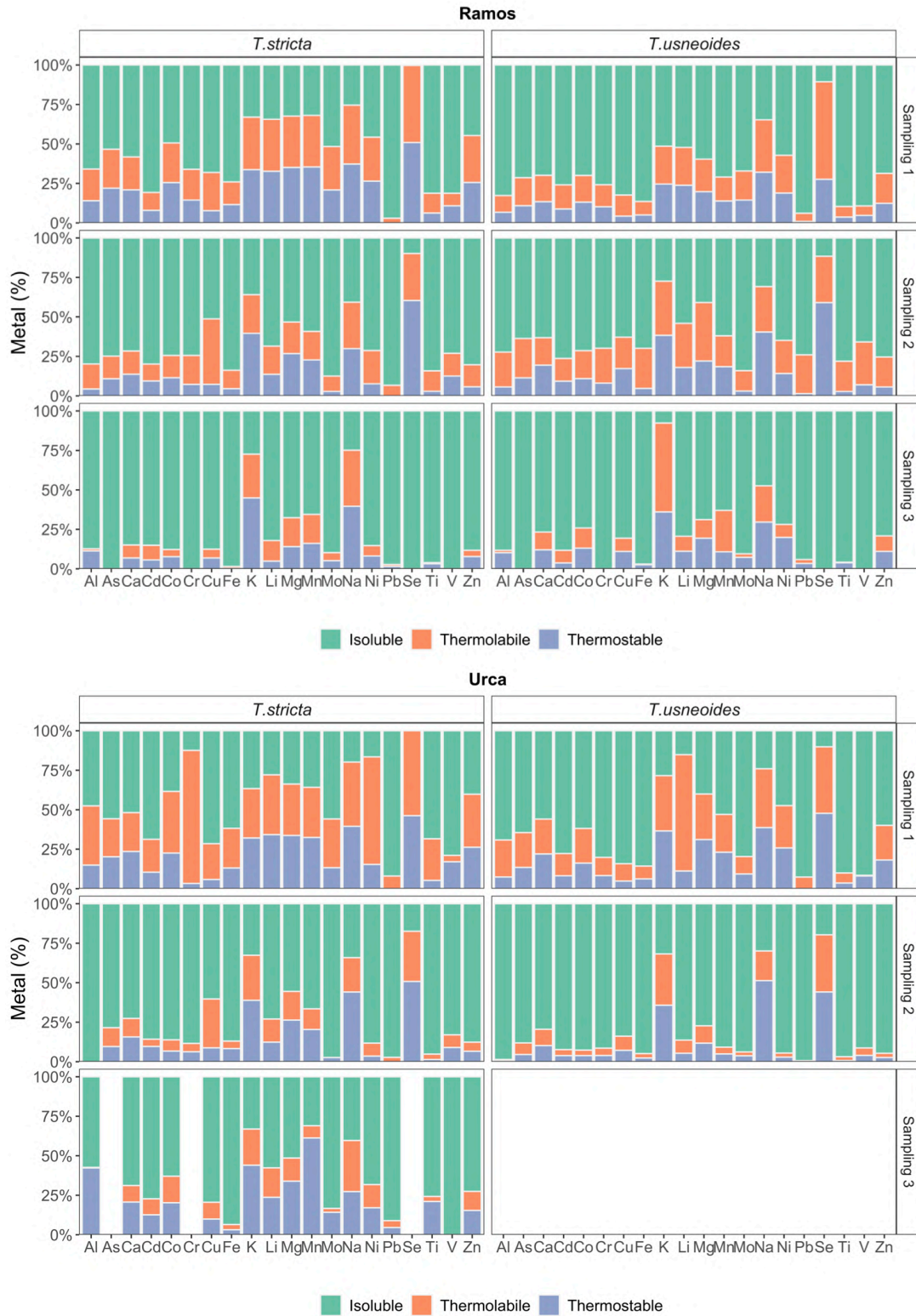


Figure 9.3 Subcellular metal distribution of metals in *T. usneoides* and *T. stricta* exposed at urban sites (Ramos and Urca)

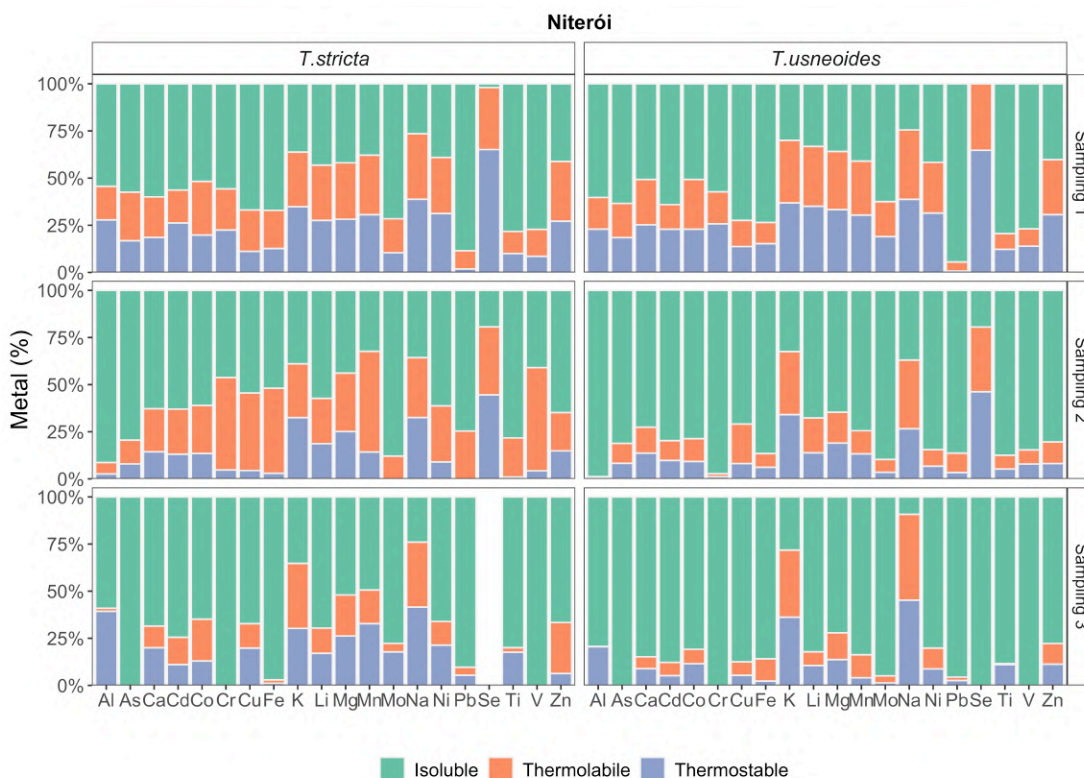


Figure 9.4 Subcellular metal distribution of metals in *T. usneoides* and *T. stricta* exposed at urban and port region (Niterói).

The wet period during sampling 2 may have contributed to remove metals from the atmosphere, resulting in decreased absorption of bioavailable metals, as metal accumulation is known to be influenced by seasonal changes (Szczepaniak and Biziuk, 2003). Previous studies have, in fact, already reported that, in tropical regions, pollutant levels tend to be lower in spring and summer (wet period) (for a review, see Beringui et al. 2021b). One study conducted in São Paulo, Brazil, reported lower atmospheric pollutants during the wet period, when a higher biomass for *T. usneoides* was noted (Giampaoli et al., 2021). Additionally, lower bioavailable content in plants from sampling 2 may be linked to a dilution effect, as both species tend to grow more during this season, requiring higher metal concentrations to cause toxic effects.

Sampling 3 took place during the aforementioned decreased mobility (25 – 80 %), seemingly resulting in reduced pollutant emissions due to the COVID-19 epidemic (Beringui et al., 2021). Both conditions are known to contribute to alterations in metal emissions in the bioavailable form. For example, Yushin et al. (2020) reported decreased Cd, Cr, Cu, and Pb concentrations in Moscow during the pandemic in a

biomonitoring assessment using the moss *Pleurozium shreberi*. In contrast, Fe concentrations increased, attributed to soil resuspension. Another biomonitoring effort using *Sphagnum* mosses in Germany and Slovenia reported decreases in Cu, Hg, Pb, Co, Ni, Sc, Ti, Ca, Ba, Cd, Pb, Sr, and Zn concentrations in 2020, in comparison with 2019 (Zupancic and Bozau, 2021). The authors attributed this variability to pollutant decreases during the COVID-19 pandemic, also citing decreased enrichment factors, indicating that anthropogenic source contributions also decreased in 2020. None of these assessments, however, verified metal bioavailability.

It is also important to note that *Tillandsias* are epiphytic plants, presenting trichomes. This feature may play an important role as a barrier against toxic metal effects, potentially explaining the expressive content of metals in the insoluble, *i.e.*, non-bioavailable form (Koul et al., 2021; Zhang et al., 2021). This was corroborated in one study concerning *Tillandsia brachycaulos*'s capacity to absorb Cs and Sr where, after 10 days of exposure following soaking in Cs and Sr solutions (0.1, 1.0, 10 and 100 mmol L⁻¹) trichome removal resulted in increased leaf metal contents (Zheng et al., 2017). Another study employing *Tillandsia brachycaulos* reported that trichome removal decreased element contents (Fe, Al, Zn, Mn, Ba, Ti, Cu, Ni, Cr, Sn, Pb, Co, As, and Se) on leaf surfaces and increased most metal concentrations inside leaf tissues. This study is one of the few that performs toxicology evaluations after exposure to natural metal deposition (Zheng et al., 2021). In another assessment regarding the importance of trichomes in metal accumulation in plants, Zhang et al. (2021) evaluated the efficiency of these organelles by breeding a genetic variety of *Nicotiana tabacum* with a high density of trichomes and observed a significant increase in Cd tolerance.

The thermostable fraction evaluated herein contains purified MT, thus, metals found in this fraction are associated with this metalloprotein through the MT-metal detoxification route. In this regard, some elements are noteworthy in the thermostable fraction obtained in our study, namely Cr, Co, Cu, Cd, Mn, Ni, Se, and Zn.

Elements like Cu, Cr, Cd, Mn, Ni, and Zn are routinely found in different samples (particulate matter and plants) from urban centers, associated, mainly, to vehicle and industrial emissions (Pant and Harrison, 2013; Sevik et al., 2019). A previous study conducted in Rio de Janeiro, for example, attributed the source of Cu and Zn found in particulate matter to light vehicles (Andrade et al., 2012). Another assessment attributed Fe, Cu, and Zn contents found in coarse particles to non-exhaust emissions,

such as brake and tire abrasion (Loyola et al., 2012). Most studies that evaluated particulate matter composition, sampled in Rio de Janeiro, reported Cu, Cr, Cd, Mn, Ni and Zn as particle components (Beringui et al., 2021; Gioda et al., 2011; Mateus and Gioda, 2017; Ventura et al., 2017).

Some of these metals, such as Zn, Cu and Fe, although required for physiological processes, becoming toxic at high levels (Nakazato et al., 2018a; Rai, 2016b; Zheng et al., 2021). For example, a study on Co and Cu effects on different barley species reported that exposure to Cu alone results in reduced growth (Wa et al., 2017).

9.3.3. Metal detoxification

Tillandsia species are widely employed to assess atmospheric metal pollution, however, few studies have evaluated the ecotoxicological effects of these pollutants in these bioindicators. In this regard, the only report found in the literature indicates that even low Hg levels induce MT detoxification in *T. usneoides* (Sun et al. 2021). Hg concentrations in the present study, however, were below the LOQ, so we could not evaluate this herein. Other bioavailable metals in the TSF were, however, correlated with MT (Table 9.2), indicating metal detoxification by this biochemical route.

Tillandsia stricta presented a higher number of correlations between metals and MT at Duque de Caxias, Ramos and Urca, while *T. usneoides* presented a higher number of correlations at Santa Cruz. Strong correlations ($\rho > 0.70$) were detected between MT and Co, V and Fe in *T. stricta*. The subcellular distribution for these metals in Duque de Caxias, Ramos and Urca indicates that most of these metals are present in insoluble form in the IF, indicating that the emission of these metals is high at those sites, and although the most part of the content accumulate as non-bioavailable form, they significantly induce MT synthesis and detoxification, in an attempt to avoid toxic effects in this species.

Iron is an essential micronutrient that participates in many processes in plants, although excessive amounts may compromise chlorophyll production, photosynthesis, and respiration. Furthermore, ionic Fe forms may contribute to the production of ROS, which can cause a range of cellular damage (Rasheed et al., 2020; Tripathi. et al., 2018). Vanadium is found in low concentration in plants, and contributes to plant growth, although also contributed to ROS production, at high concentration,

compromising main plants functions such as photosynthesis. Vanadium uptake occurs primarily through the phosphate uptake mechanism, so exposure to high V concentrations may also reduce plant biomass (Aihemaiti et al., 2020; Chen et al., 2021; Imtiaz et al., 2018). Although Co is not an essential element, it has been reported as displaying a protective effect against the adsorption of certain toxic elements, such as Cd and Pb, although, it also inhibits the uptake of some essential elements (Wa et al., 2017). Furthermore, Co has also been reported as inhibiting photosynthesis, damaging stomata, and compromising transpiration, consequently affecting the carbon cycle (Wa et al., 2017).

Table 9.2 – Associations between MT and metal and metalloids for *T. usneoides* and *T. stricta* determined by Spearman correlation coefficients (ρ).

Element	Strength of relationship (ρ)				
	Santa Cruz	Duque de Caxias	Ramos	Urca	Niterói
<i>Tillandsia usneoides</i>					
Na	0.68	0.72	0.66	-	-
Mg	0.72	-	-	-	-
K	0.64	-	-	-	-
Ca	0.66	-	-	-	-
V*	0.61	-	-	-	0.68
Mn	0.78	-	-	-	-
Co*	0.8	-	-	-	-
Ni*	-	-	-	-0.83	-
Se	0.62	-	-	1	0.79
Pb*	-	0.75	-	-	-
<i>Tillandsia stricta</i>					
Na	-	0.72	-	-	-
Al	-	-	-	-0.73	-
Ca	-	-	-	-	-0.79
V*	-	0.81	-	0.72	0.66
Mn	-	-	0.72	-	-0.53
Fe	-	0.74	0.55	0.64	-
Co*	-	0.86	-	-	-
Cu	0.75	-	-	-	-0.54
Zn	-	-	-0.58	-	-
As*	-	-	-	0.74	-
Se	-	-	0.77	0.75	0.77
Mo	-	-	-0.57	-	-0.6
Pb*	0.6	-	-	-0.63	0.61

* Toxic elements

Moderate to strong correlations between MT and metals were found in *T. usneoides* exposed at Santa Cruz. Furthermore, Co, V, Na, Mg, Ca, K, Mn and Se were also significantly correlated with MT in *T. stricta* at the other sampling sites, mostly, in the TLF and TSF. This, therefore, indicates that they are found in bioavailable forms in this species and significantly induce MT detoxification.

There is no consensus whether Se is essential or not for plants, but it is known that, at low concentrations, this element can contribute to plant development and protection against oxidative stress, while stimulating ROS production at high concentrations (Gupta and Gupta, 2017). Manganese, on the other hand, is an important micronutrient present in the composition of several proteins. It also acts in photosynthesis, respiration and in oxidative stress prevention. At excessive concentrations, Mn may compromise essential element uptake and contribute to decreased chlorophyll synthesis and photosynthesis rates, also accumulating oxidized phenolic compounds in apoplasts (Alejandro et al., 2020). High Na and K concentration in plants may be associated with high salinity conditions (Rodrigues et al., 2012). However, as for Mg and Ca, high concentrations of these elements may be associated to high CO₂ concentration conditions, common in urban centers due to anthropogenic emissions (Saraiva et al., 2018). Considering that the study region is located in the coastal area of Rio de Janeiro, sea spray may be an important source of these elements.

Plants exposed to air pollutants may suffer deleterious effects, mainly through PM exposure, which contributes to metals absorption by these organisms. Toxic effects include photosynthesis and respiration impairment, stomata blockage, oxidative stress, enzyme and protein production deregulation, senescence and, eventually, death (Rai, 2016b, a). However, concerning MT and metal associations, most assessments in this regard are carried out in laboratory settings, and deal with MT gene expression, not their actual concentrations and associations with metal levels, as reported in our study. One of the few assessments found in the literature, indicate the same behavior as observed herein, for example, in the tree species *Prosopis juliflora*, known as adapted to metal-contaminated industrial sites. In this case, three different types of MTs were shown to be induced by Cu, Zn and Cd, and one MT isoform exhibited maximum metal sequestration and was thus considered a potential candidate for use in metal phytoremediation (Usha et al., 2009)

9.3.4. Potentially protective essential metal effects

Several potentially protective effects regarding essential and toxic metal associations have been reported for a wide range of taxonomic groups in the literature. Studies concerning plants, however, are still scarce. Therefore, we assessed the significant Spearman correlations between toxic and essential elements in both *Tillandsia* species, displayed in Table 9.3. The molar ratios between the essential and toxic elements of the significant associations were then calculated to evaluate the potential protective effects (Table 9.4).

Table 9.3. Significant associations between essential and toxic metals and metalloids for *T. usneoides* and *T. stricta* and their respective Spearman correlation coefficients (ρ).

Relationship	Strength of relationship (ρ)				
	Santa Cruz	Duque de Caxias	Ramos	Urca	Niterói
<i>Tillandsia usneoides</i>					
Se x Al	-0.66	-0.82	0.61	-	-0.69
Se x Ni	-	-	-	-0.83	-
<i>Tillandsia stricta</i>					
Se x Al	-	-	-0.74	-0.96	-0.61
Se x Pb	-	-	-0.78	-0.79	-0.82
Se x Ti	-	-	-	-0.75	-
Mo x V	-	-	-0.53	-	-0.74
Fe x Pb	-	-	-0.76	-0.65	-0.59

Table 9.4. Molar ratios between essential and toxic elements in *T. usneoides* and *T. stricta*

Sites	Se x Al	Se x Pb	Se x Ti	Mo x V	Fe x Pb	Cr x Pb
<i>Tillandsia usneoides</i>						
Santa Cruz	0.01	5	1.51	0.10	301	1
Duque de Caxias	0.01	22	2.18	0.40	389	4
Ramos	0.03	84	2.61	0.17	1447	6
Urca	0.03	80	3.80	0.15	1451	4
Niterói	0.02	85	2.43	0.24	1387	7
<i>Tillandsia stricta</i>						
Santa Cruz	0.02	104	2.36	0.09	3692	11
Duque de Caxias	0.02	43	2.71	0.14	746	3
Ramos	0.05	40	2.30	0.18	1012	5
Urca	0.35	545	7.30	0.13	8817	34
Niterói	0.03	39	1.19	0.16	998	4

The main potential protective effect was observed for Pb, with the highest molar ratios observed for Se and Fe. Lead is one of the most toxic elements and can cause deleterious effects to both biochemical and physiological processes. Some studies have shown that Se has a protective effect against Pb in plants (Mroczek-Zdyrska et al., 2017; Shekari et al., 2019; Wu et al., 2016) and, although the mechanism is complex and not well explained, this effect is attributed to the antioxidant function of Se. According to Mroczek-Zdyrska et al. (2017), in *Vicia faba L. minor*, Se increased pigment assimilation, favoring the integrity of cell membranes, while Wu et al. (2016) in *Brassica napus L* reported that Se contributed to reduce uptake of Pb and performed an important role in antioxidant system reducing oxygen radicals and activating antioxidant mechanisms. In another study, Se was observed as reducing oxidative stress in *Cucumis sativus L.* and accelerate flowering as a consequence of reduced metal uptake or transfer between tissues (Shekari et al., 2019). Concerning Fe, according to Rodriguez-Hernandez et al. (2015), Pb uptake is favored in Fe deficiency conditions. One assessment on *Typha latifolia*, for example, indicated that Fe contribution to lower Pb uptake is attributed to a similar uptake mechanism for these two elements.

It is important to highlight that the main Se x Pb and Fe x Pb correlations were observed at sites with strong influence from vehicular emissions. Moreover, the subcellular distribution of metals indicated that Pb is mostly in the insoluble fraction. Thus, it is possible to infer that the effects of these protective metals may contribute to Pb immobilization. Furthermore, more correlations between elements were found for *T. stricta* than for *T. usneoides*, and previous assessments indicate that the former is more sensitive to metal uptake while *T. usneoides* is a better metal bioaccumulator (Beringui et al., 2021).

The other associations concerning protective effects against Al, Ti and V have not been described in the literature concerning plants to date, and studies are notably lacking in this regard.

9.4. Conclusions

Tillandsia samplings during dry periods (sampling 1 and 3) showed lower concentrations of MT, which is related to the biomonitors with CAM metabolism. Sampling during the pandemic recorded the lowest MT concentrations, due to reduced

urban mobility that decreased the emission of pollutants. An increasing metal contents in the insoluble fractions were noted from sampling 1 to sampling 3 for both species. The thermostable fraction evaluated herein contains purified MT, thus, metals found in this fraction are associated with this metalloprotein through the MT-metal detoxification route. In this regard, some elements are noteworthy in the thermostable fraction obtained in our study, namely Cr, Co, Cu, Cd, Mn, Ni, Se, and Zn. Most of these elements can be associated with vehicle emissions, the main source of pollutants in urban centers. Although some of them are essential for plants, in high concentrations they can cause toxic effects. Comparing the two species, the percentage of insoluble fraction of metals, and therefore not bioavailable, was higher in *T. stricta*, indicating that it is less susceptible to damage from metal exposure. Potentially protective effects against Pb were noted for Se and Fe, although studies of this type in plants are scarce.

The CAM *Tillandsia* metabolism, which performs gas exchanges at night, seemingly contributed to a lower metal absorption, especially during the dry period. In addition, decreased vehicle traffic during the pandemic was also a determining factor in pollutant absorption decreases. The observed decreases in MT content throughout the biomonitoring period corroborates the lowest metal exposure, and most of the metals detected in the thermostable fraction, probably associated with MT, are associated to vehicle emissions, the main pollutant source in urban centers. However, although MT is the main metal exposure biomarker, other oxidative stress biomarkers should be assessed for a broader evaluation of the damage that plants may be subjected to due to metal exposure.

Se and Fe seemingly exhibit a protective effect against Pb, although further studies are required to corroborate this hypothesis.

Comparing both *Tillandsia* species, *T. stricta* presented higher contribution of metals in insoluble fractions, which indicates metals are accumulated in plant tissue in order to be mobilized in the organism.

Vegetation and weather are closely interconnected, one significantly affecting the other. The increasing atmospheric pollutant emissions has become a significant risk to vegetation and biodiversity in different ecosystems worldwide. Considering that plants can rebalance themselves only within a certain limit, the current climate change scenario may contribute to even more intense environmental damage, and subcellular

compartmentalization assessments thus become a powerful approach in evaluating anthropogenic activity effects to this important environmental compartment.

Acknowledgements

This study was financed in part by the Coordenação de Aperfeiçoamento de Pessoal de Nível Superior - Brasil (CAPES) - Finance Code 001. The authors thank to CNPq and FAPERJ for research grants and financial support.

10 Oxidative stress investigation in atmospheric biomonitoring plants exposed in a large Brazilian metropolis

Karmel Beringui^a, Rachel Ann Hauser-Davis^b, Adriana Gioda^a

^aChemistry Department, Pontifical Catholic University of Rio de Janeiro, Rio de Janeiro, Brazil

^bEnvironmental Health Assessment and Promotion Laboratory, Oswaldo Cruz Institute, Oswaldo Cruz Foundation, Rio de Janeiro, Brazil

Working paper

Abstract

Plants are the main receptors of air pollutants due to their immobility. Continuous exposure to metals, constantly emitted in urban centers, can cause damage to these organisms at various levels, including the production of reactive oxygen species (ROS). Oxidative stress evaluations comprise a valuable approach to investigate the deleterious effects of metal exposure, performed through the quantification of oxidative stress biomarkers. The metropolitan region of Rio de Janeiro presents areas with different emission characteristics, although vehicular emission are one of the most noteworthy. In this context, this study aimed to investigate oxidative stress markers in two *Tillandsia* species used as air quality of through the quantification of reduced glutathione (GSH), hydrogen peroxide (H₂O₂), an important ROS, and lipid peroxidation through malondialdehyde (MDA) determinations, a lipid peroxidation subproduct. Plants exposed at different sites exhibited similar oxidative stress conditions. In *T. stricta*, oxidative stress prevention is postulated due to high GSH levels, the first line of defense against ROS damage, while *T. usneoides* exhibited high MT levels. Lipid peroxidation was noted for both species.

Keywords: reduced glutathione, lipid peroxidation, hydrogen peroxide, metals

10.1. Introduction

Urban centers are characterized by the presence of diverse anthropogenic activities that can release a variety of pollutants into the atmosphere, posing significant risks to the environment and the population (Chen et al., 2016b). A suitable approach to assessing the air quality of a given region is by monitoring the concentration of air pollutants (Gioda et al., 2016). However, this is insufficient to predict potential ecotoxicological risks caused by being continuously emitted compounds (Mansour et al., 2020).

Atmospheric biomonitoring is a cheaper approach to monitor air quality, also allowing for the assessment of ecotoxicological effects, as it employs living organisms to assess environmental changes (Ávila-Pérez et al., 2019; Bargagli, 2016; Nakazato et al., 2018b). In this regard, epiphytic plants are highly recommended for atmospheric biomonitoring, as they obtain nutrients only by gaseous exchanges (Techato et al., 2014). *Tillandsias*, a bromeliad genus, are widely employed biomonitors used for atmospheric monitoring.

Plant exposure to air pollution can induce oxidative stress, a condition in which an imbalance between the production and removal of reactive oxygen species (ROS) is observed (Rai, 2016b). This can be evaluated by means of oxidative stress biomarkers, comprising oxidative stress prevention biomarkers, such as metallothionein (MT) and reduced glutathione (GSH), and damage biomarkers, such as hydrogen peroxide (H₂O₂) and lipid peroxidation.

Metallothionein is a metalloprotein induced by high metal concentrations that plays a detoxifying role (Kısa et al., 2017). GSH is the most important non-enzymatic antioxidant that acts in the removal of reactive oxygen species (ROS). Moreover, in cases of exposure to toxic metals, GSH can also contribute to the detoxification of metals through chelation, analogous to MT function, or by inducing the production of phytochelatins in plants, which are also able to chelate metals (Hasanuzzaman et al., 2017; Liedschulte et al., 2010). Although it occurs naturally in plant tissue and participates in important biochemical processes, hydrogen peroxide (H₂O₂) is a ROS directly affected by oxidative stress situations (Cuypers et al., 2016). The antioxidant

action of GSH may contribute to the regulation of H₂O₂ levels through a direct reaction between these biomarkers (Niu and Liao, 2016). Lipid peroxidation can occur via enzymatic or non-enzymatic routes, with ROS playing a key role, as they initiate lipid peroxidation through the abstraction of a hydrogen molecule from the fatty acids that make up the cell wall. In this non-enzymatic process, the formed radicals are not deactivated and can, therefore, cause damage to cells, including cell death. One of the products of polyunsaturated fatty acid peroxidation is malondialdehyde (MDA), which has been used as a lipid peroxidation biomarker in plants, especially following metal exposure (Skórzyńska-Polit, 2007).

Particulate matter, one of the main atmospheric pollutants, can contain several metals, and some studies have indicated this in particles assessed in the city of Rio de Janeiro, Brazil. In addition, atmospheric biomonitoring studies report metal enrichment in plants exposed in urban environments. Thus, this study aims to evaluate the toxic effects of exposure to atmospheric pollutants through the evaluation of oxidative stress in atmospheric biomonitors exposed in the metropolitan region of Rio de Janeiro

10.2. Materials and Methods

Description in topic 3.7 and 3.9 from the page 49.

10.3. Results and discussion

10.3.1. GSH content in *Tillandsia* species

The GSH concentrations determined in *Tillandsia* species sampled from five sites in the city of Rio de Janeiro are presented in Figure 10.1 separated by sampling dates. Statistical differences between species were observed only in sampling 2 in Santa Cruz, where the GSH contents in *T. usneoides* were higher.

Comparing samplings, statistical differences were observed only for *T. usneoides*. At Ramos, GSH concentrations increased from sampling 1 to sampling 2 ($p = 0.032$). At Niterói, GSH concentrations in sampling 3 were statistically lower than sampling 1 ($p = 0.036$).

No statistical differences were observed comparing different sites in the same period, which implies that all regions evaluated herein lead to the same antioxidant condition in the evaluated *Tillandsia* species.

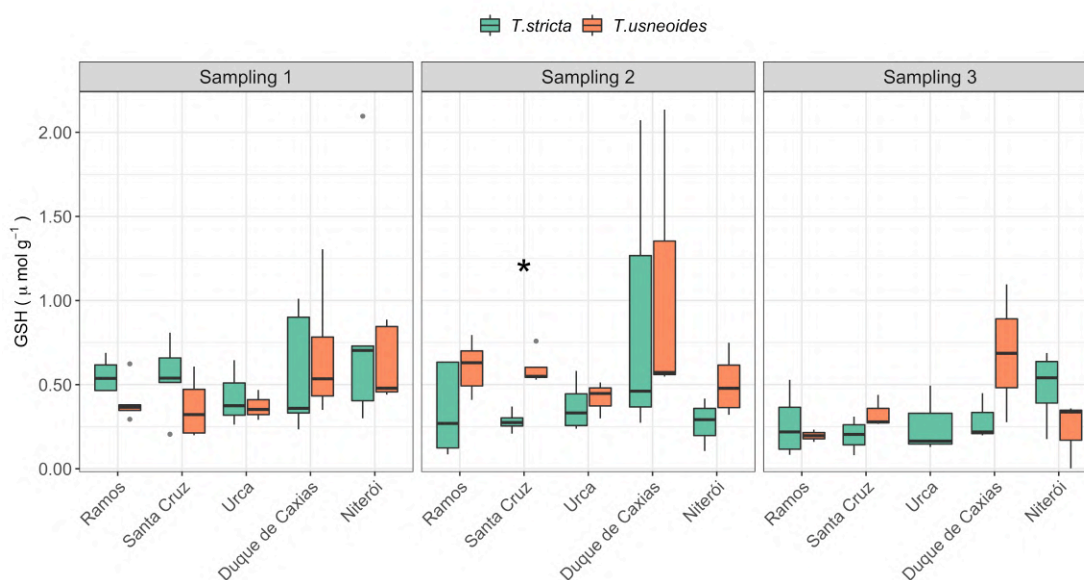


Figure 10.1 *Tillandsia stricta* and *Tillandsia usneoides* Reduced Glutathione (GSH) concentration ($\mu\text{mol g}^{-1}$) per sampling (1: October 2019, 2: January 2020, and 3: November 2020) The p-value < 0.05 obtained for comparison between species is represented by *.

A study conducted by Giampaoli et al. (2021) in the Metropolitan Region of Campinas (MRC), which exhibits similar meteorological conditions to MRRJ, found higher GSH content in two epiphytic bromeliad (*T. usneoides* and *Aechmea fasciata*). The authors reported significant correlations between GSH and NO_2 and SO_2 in *T. usneoides*, indicating that GSH plays an important antioxidant role under polluted circumstances in these biomonitors. Furthermore, wet and dry periods only influenced GSH content in *A. fasciata*. Anoted study (Kováčik et al., 2014) evaluated the tolerance of four *Tillandsia* species to Cd exposure and indicated lower GSH concentrations following exposure. The authors also indicate that each species exhibits a different response to ROS and discuss that xerophytic species, which present a higher density of trichomes, tend to present lower GSH concentrations, as trichomes would become a first defense against pollutants, whereas they accumulate the metals, preventing their mobilization.

According to Sun et al. (2021), who evaluated *T. usneoides* responses to Hg exposure, GSH production may be stimulated by Hg variations mainly at low levels, as decreases in GSH concentrations were observed after exposure to high Hg levels.. This behavior was attributed to the antioxidant action of superoxide dismutase, which performs better at high Hg levels. The same behavior regarding the increase and decrease of GSH was observed following exposure to continuously increasing Pb concentrations in a study on atmospheric exposure conducted in an airtight exposure chamber using the same *Tillandsia* specie (Li et al., 2022).

10.3.2. H₂O₂ content in *Tillandsia* species

The H₂O₂ concentrations determined in *Tillandsias* exposed at all sampling sites are presented in Figure 10.2 for the three different sampling campaigns. Statistical differences between species were observed only for sampling 2, in Santa Cruz and Niterói, where higher H₂O₂ concentrations were detected in *T. usneoides*. Santa Cruz also presented differences in GSH content, as mentioned above. Considering that H₂O₂ is a ROS produced in oxidative stress conditions, it is possible to infer that *T. usneoides* is more susceptible to damage caused by H₂O₂. Concerning Niterói, is possible to infer that the antioxidant function of GSH is not being sufficient to prevent H₂O₂ formation in *T. usneoides*.

Comparing samplings, H₂O₂ concentrations decreased from sampling 1 to sampling 2 in *T. usneoides* exposed in Ramos ($p = 0.0317$). At Santa Cruz, H₂O₂ concentrations increased in *T. usneoides* ($p = 0.0286$) and decreased in *T. stricta* ($p = 0.0317$). A statistically significant decrease was also observed at Niterói for *T. stricta* ($p = 0.0079$) in sampling 2. At Niterói, although the average H₂O₂ concentration in *T. usneoides* was lower in sampling 2 than in sampling 1, a statistical difference was observed only for sampling 3 in comparison to samplings 1 and 2 ($p = 0.0357$). However, a decreasing trend is noted from sampling 1 to sampling 3.

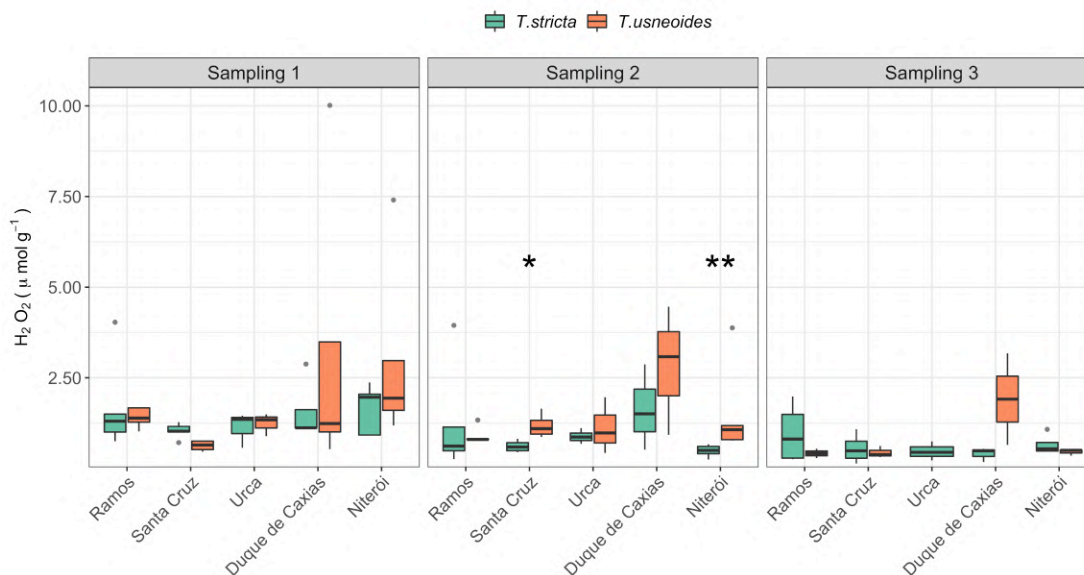


Figure 10.2 *Tillandsia stricta* and *Tillandsia usneoides* Hydrogen Peroxide (H₂O₂) concentration (µmol g⁻¹) per sampling (1: October 2019, 2: January 2020, and 3: November 2020) The p-value < 0.05 obtained for comparison between species is represented by *.

Some statistical differences were also verified comparing sites within each sampling campaign. The H₂O₂ content in *T. usneoides* sampled in Santa Cruz after the first exposure period (sampling 1) was lower than Ramos ($p = 0.016$) and Niterói ($p = 0.016$). Concerning *T. stricta*, no statistical differences were verified. After the second exposure period, the only difference noted was between H₂O₂ content in *T. stricta* sampled in Urca and Niterói. Finally, no statistical differences between sites for sampling 3 were observed, indicating similar oxidative stress condition.

Higher H₂O₂ concentrations have been reported in a study on *Sedum alfredii*, a hyperaccumulating Zn and Cd plant. However, higher concentrations were observed for plants exposed to Zn, which was directly associated to GSH function, which was lower in plants exposed to Zn (Chao et al., 2008).

10.3.3. MDA content in *Tillandsia* species

The malondialdehyde (MDA) content in both *Tillandsia* species is presented in Figure 10.3 for all monitored sites according to three exposure periods. No statistical differences ($p < 0.05$) were verified between species exposed at the same site for all periods.

Comparing the MDA content at the same site in different periods, an increase was noted for *T. usneoides* exposed in Ramos from sampling 1 to 2 ($p = 0.0079$). Some boxplots representing the MDA concentration data in sampling 3 were very compact, indicating decreased concentration, especially at Niterói, Urca, and Duque de Caxias. Statistically, a decrease was observed for *T. stricta* in Duque de Caxias ($p = 0.0357$) and Niterói ($p = 0.0159$) in comparison with sampling 1. At Niterói statistically lower concentrations were also observed for *T. usneoides* in comparison to sampling 1 and 2 ($p = 0.0357$).

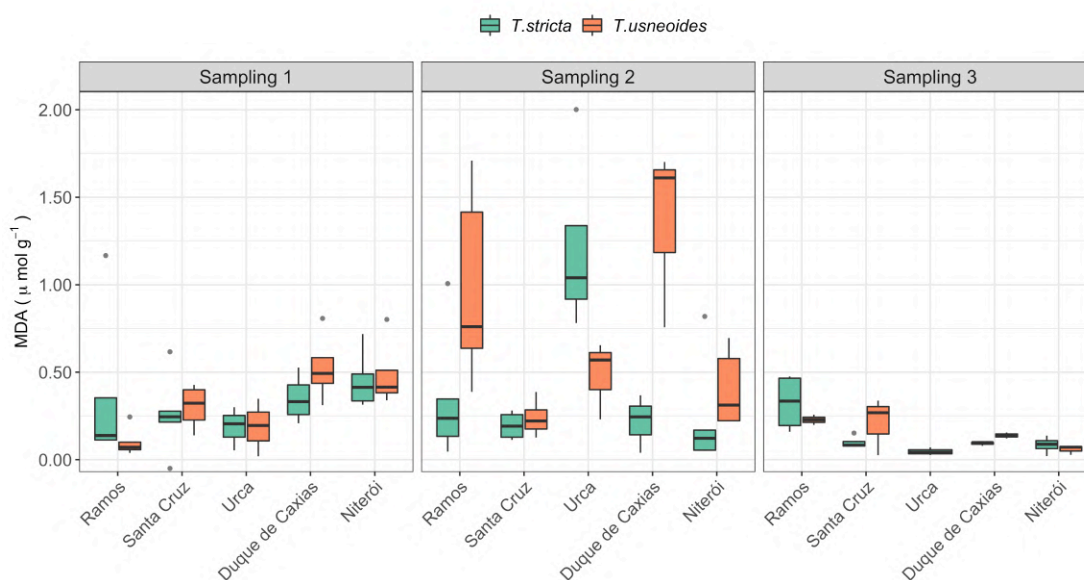


Figure 10.3 *Tillandsia stricta* and *Tillandsia usneoides* Malondialdehyde (MDA) concentration ($\mu\text{mol g}^{-1}$) per sampling (1: October 2019, 2: January 2020, and 3: November 2020)

More differences between sites were noted when comparing MDA concentrations obtained at the different sites after the exposure period than for the other biomarkers. In sampling 1, Duque de Caxias, Santa Cruz and Niterói showed statistically higher concentrations than those observed in *T. usneoides* at Ramos and Urca. Regarding *T. stricta*, values were similar, with the exception of Urca and Niterói, which presented a significant difference. In sampling 2, it is noteworthy that the MDA concentration detected in *T. usneoides* in Duque de Caxias were statistically higher than that observed in Niterói ($p = 0.0357$), as well as Ramos, statistically higher than Santa Cruz ($p = 0.0159$).

The MDA content at MRC was lower than MRRJ. In one study, *T. usneoides* was more resistant to membrane damage than *A. fasciata* (Giampaoli et al., 2021), while the aforementioned Hg exposure study revealed no significant difference in MDA concentrations with increasing Hg, indicating *T. usneoides* resistance to this metal (Sun et al., 2021a).

Bermudez and Pignata, (2011) evaluated the antioxidant response of three *Tillandsia* species exposed in areas presenting different sources of atmospheric pollutants and also pointed out that the studied species present different antioxidant system behaviors. An MDA evaluation in *Tillandsias* exposed in different regions in Córdoba, Argentina, reported similar values to those observed at MRRJ. However, MDA concentrations in *T. tricholepis* were influenced by agriculture emissions, while *T. recurvata* was affected by urban emissions and *T. capillaris* was not influenced by any exposure area.

One study evaluating the toxicity of different metals on *T. capillaris* indicated that plants exposed to Ni^{2+} , Cu^{2+} , Zn^{2+} and Pb^{2+} solutions presented up to 2.3-fold higher MDA concentrations than control plants. However, the evaluated metal concentrations did not lead to statistical differences in MDA concentrations (Wannaz et al., 2011).

Specifically concerning Pb, it has been reported that MDA variations in *T. usneoides* exposed to Pb is complex, as a dose-response relationship is noted up to a certain point, decreasing below the levels observed for the controls after this point, and increasing again, although not exceeding control concentrations (Li et al., 2022). This may indicate a certain threshold in *T. usneoides* concerning Pb toxicity effects, although further studies are required in this regard to corroborate this hypothesis.

10.3.4. Correlation between biomarkers

Since no significant difference in the concentrations found at the different sites after a given exposure period were noted when assessing the content of the main oxidative stress biomarkers in the biomonitors employed herein, no separation by site was performed to evaluate statistical correlations between the investigated biomarkers. Spearman correlations were, thus, evaluated considering the different sampling campaigns and are presented in Figures 10.4 and 10.5.

In sampling 1, the weak correlation between MT and GSH in *T.usneoides* indicates that MT plays a more important role specifically in metal detoxification, while the main GSH function is regarding the antioxidant system. In contrast, MT and GSH presented a moderate correlation in *T. stricta*, which implies that GSH may also contribute towards metal detoxification in this species. A moderate correlation detected between MT and H₂O₂ in both species indicates that ROS production probably due to metal exposure seems to induce MT synthesis. Finally, a correlation between MT and MDA was verified only for *T. usneoides*, which indicates that metals stimulated lipid peroxidation in this species.

The significant correlation between GSH and H₂O₂ reveals that the antioxidizing function of GSH contributes to decrease H₂O₂ levels. This relationship was verified in all sampling campaigns for *T. stricta*, but only in sampling campaign 2 in *T. usneoides*.

Lastly, significant correlations between MDA and H₂O₂ were observed only for *T. stricta* in sampling 3, which indicates that GSH was not sufficient to prevent H₂O₂ effect and other ROS that can participate in lipid peroxidation.

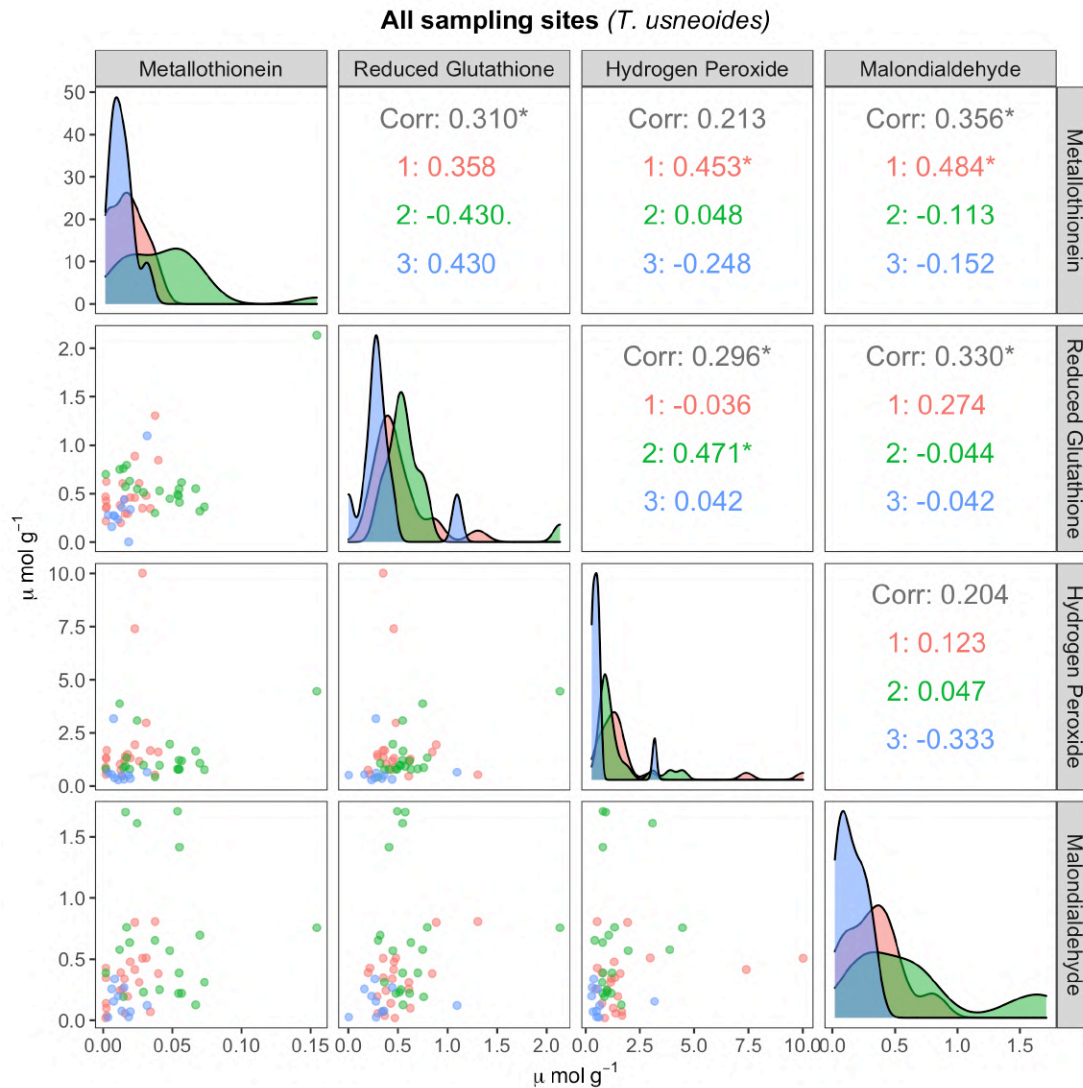


Figure 10.4 Correlation between oxidative stress biomarkers determined in *Tillandsia usneoides* exposed in MRRJ and removed in three periods (1: October 2019, 2: January 2020, and 3: November 2020) The p-value significance is represented by * for $p < 0.05$.

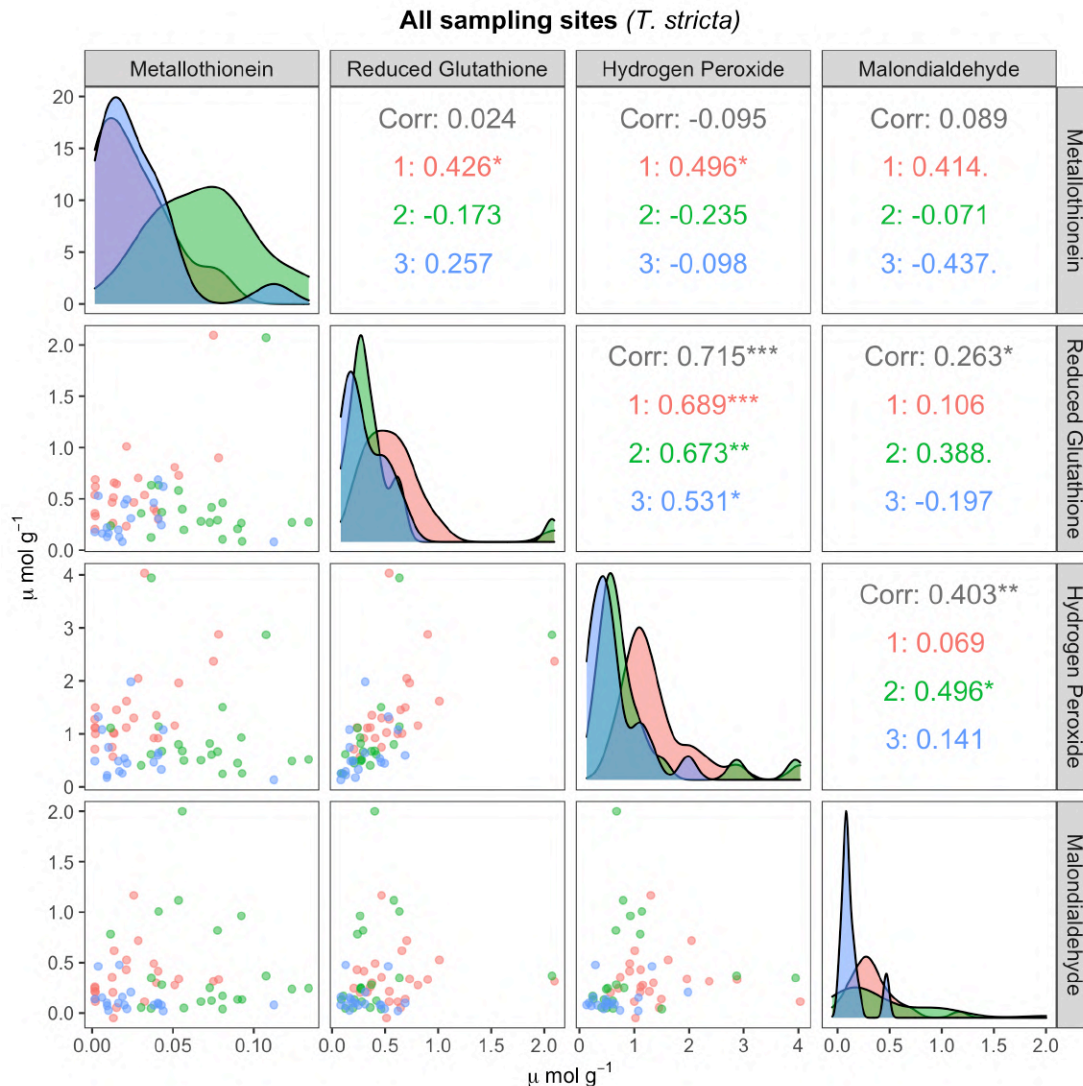


Figure 10.5 Correlation between oxidative stress biomarkers determined in *Tillandsia stricta* exposed in MRRJ and removed in three periods (1: October 2019, 2: January 2020, and 3: November 2020) The p-value significance is represented by * for $p < 0.05$.

Previous studies have also evaluated metal concentrations in plant tissue and the role of MT in metal detoxification, assessing which metals induce oxidative stress biomarkers, and significant correlations between metals and oxidative stress biomarkers indicate direct metal effects on the antioxidant system. Table 10.1 present the calculated Spearman correlations between metals and biomarkers in the present study.

Concerning *T. stricta*, a higher number of correlations was noted between metals and GSH, indicating that metal exposure is in fact directly inducing GSH in its an

antioxidant role to prevent from toxic metal effects. In *T. usneoides*, however, a higher number of correlations were observed with MT, not GSH, indicating metal dyshomeostasis and MT induction in an attempt to reestablish elemental equilibrium.

Furthermore, statistically significant correlations between metals and H₂O₂ in *T. stricta* are an indication that metal exposure directly induces ROS production, in turn requiring GSH action for ROS removal. The dyshomeostasis caused by metals in *T. usneoides*, thus, induces damage to cell membranes according to significant correlations with MDA, one of the main lipid peroxidation products.

Table 10.1 Spearman's correlation ($p < 0.05$) between total metal content of Tillandsias and oxidative stress biomarkers

Element	<i>T. usneoides</i>				<i>T. stricta</i>			
	MT	GSH	H ₂ O ₂	MDA	MT	GSH	H ₂ O ₂	MDA
Li	0.45	-	-	0.36	-	0.46	0.58	0.22
Na		-	-	-	-	-0.19		-
Mg	0.49	-	-	0.27	-	0.34	0.35	-
Al	0.46	-	0.29	0.39	-	0.32	0.45	-
K	0.26	-	-	-	-0.3	0.40	0.33	0.25
Ca	0.37	-	-	0.22	-	0.27	0.40	-
Ti	0.48	-	0.33	0.38	-	0.35	0.51	0.23
V	0.31	-	-	-	-	0.20	0.20	-
Cr	0.31	-	-	0.27	-	0.29	0.48	0.22
Mn	0.32	-	-	0.25	-	0.24	0.35	0.28
Fe	0.32	-	-	0.26	-	0.23	0.34	-
Co	0.49	0.28	0.41	0.44	-	0.45	0.56	0.20
Ni	0.47	-	0.35	0.35	-	0.35	0.52	0.25
Cu	0.33	-	0.37	0.29	-	0.44	0.53	
Zn	0.44	0.34	0.24	0.44	-	0.39	0.36	0.08
As	0.44	-	0.26	0.38	0.2	0.37	0.49	0.24
Se	0.49	-	-	0.29	0.5	-	-	-
Mo	0.41	-	0.37	0.35	-	0.50	0.65	0.26
Cd	0.31	-	0.39	0.32	-	0.33	0.48	0.29
Pb	0.50	0.27	0.44	0.52	-	0.41	0.63	0.39

10.4. Conclusion

Plants exposed at all monitoring sites exhibited similar oxidative stress conditions, although from different emission sources. As observed in a previous study for MT, *Tillandsia* presented higher oxidative stress during the humid period, in which

it exchanges gas throughout the day, thus being constantly exposed to atmospheric pollutants. The main function of GSH in both species was noted as in preventing oxidative stress, and not in metal detoxification. The presence of ROS induced GSH in both species, although not enough to prevent cell damage by lipid peroxidation.

Metal exposure in *T. stricta* induced ROS production, in turn stimulating the antioxidant system. Conversely, in *T. usneoides*, MT played the main role in preventing toxic metal effects, indicating differential physiological defense mechanisms against these pollutants.

11 Subcellular heat-stable metalloprotein assessments employing the bioanalytical SEC-HPLC-ICP-MS technique

Karmel Beringui^a, Rafael Christian Cháves Rocha^a, Tatiana D. Saint’Pierre^a,
Rachel Ann Hauser-Davis^b, Adriana Gioda^{a*}

Working paper

Abstract

Hyphenated analytical techniques are the most suitable for assessing metal-protein interactions, implicated in metal detoxification attempts by living organisms. In this regard, metallothionein, reduced glutathione, and phytochelatins comprise proteins and peptides capable of complexing metals, acting as important detoxification biomarkers. Considering that vehicular emissions are the main contributors to metal emissions in urban centers, this study aimed to investigate metal-protein associations in bromeliad *Tillandsias* employed as air pollution biomonitors in Rio de Janeiro, Brazil. Plants were exposed to differential emission sources and metal-protein associations were evaluated through size exclusion chromatography coupled to inductively coupled plasma mass spectrometry (SEC-HPLC-ICP-MS). The findings indicate that most metals eluted alongside low molecular weight proteins. The two most representative metals were Ni and Zn, two important pollutants linked to vehicular emissions, mainly associated with MT and GSH, although Mn, Fe and Ti metal-protein associations were also observed.

11.1. Introduction

It is well known that some plants are capable of accumulating metals in their tissues and can therefore be used as biomonitors (AL-Alam et al., 2019; Piazzetta et al., 2019; Szczepaniak and Biziuk, 2003). Part of the absorbed metals and metalloids remain accumulated in some tissues without representing toxicity (e.g., in trichomes)

(Zhang et al., 2021), as only the bioavailable metal fraction can actually cause deleterious effects (Varela et al., 2018).

One of the main consequences of metal exposure is oxidative stress, comprising an imbalance in the production and removal of reactive oxygen species (ROS) (Hauser-Davis et al., 2021). Some biomolecules act in prevent ROS damage, including proteins and small peptides, some of which play an important role in metal detoxification (Mansour et al., 2020). To investigate the damage caused by metals in living organisms, approaches such as determining oxidative stress biomarkers and subcellular metal distributions are increasingly being applied to understand the behavior of some plant species exposed to high metal concentrations (Bermudez and Pignata, 2011; Li et al., 2014; Sun et al., 2021a, b). However, assessments on studying the effects of plant exposure under real air pollution conditions are still lacking.

Hyphenated techniques, such as SEC-HPLC-ICP-MS, are the most appropriate for metal protein-speciation assessments and allow for investigations on metal associations with proteins that act in the antioxidant system (Baratkiewicz et al., 2009; Lavradas et al., 2016). Evaluating the association between proteins and metals is, in fact, extremely important, as several metalloproteins comprise early damage indicators (Melendez et al., 2012). Thus, chromatographic separation of proteins and peptides is an interesting approach to evaluate the metal association with biomarkers found in biomonitor tissues. These types of studies are, in fact, valuable in signalling the need for measures aimed at reducing pollutant emission that directly affect oxidative stress biomarkers.

In this context, this study aims to investigate the association of metals and metalloids to metallothionein and reduced glutathione in *Tillandsia stricta* and *T. usneoides* employed as atmospheric biomonitors in a Brazilian metropolis. For this purpose, extracts of *Tillandsia usneoides* and *Tillandsia stricta*, used as atmospheric biomarkers in the metropolitan region of Rio de Janeiro, containing purified metallothionein were submitted to SEC-HPLC-ICP-MS.

11.2. Material and Methods

Described in topic 3.8, page 49.

11.3. Results and discussion

Figure 11.1 presents the chromatographic column separation profile for MT and GSH, the biomarkers of interest evaluated herein. In an attempt to simulate a real sample, a mixture of standards (Mix) containing, MT, GSH, ferritin (450 kDa) and bovine serum albumin (66 kDa) were also analyzed. The separation of the proteins from a standard formed by mixing other proteins indicated close proximity between peaks, and the chromatogram obtained for the individual protein standards showed that a retention time for MT (7 kDa) of 20 min, and for GSH (0.3 kDa), of 25 min.

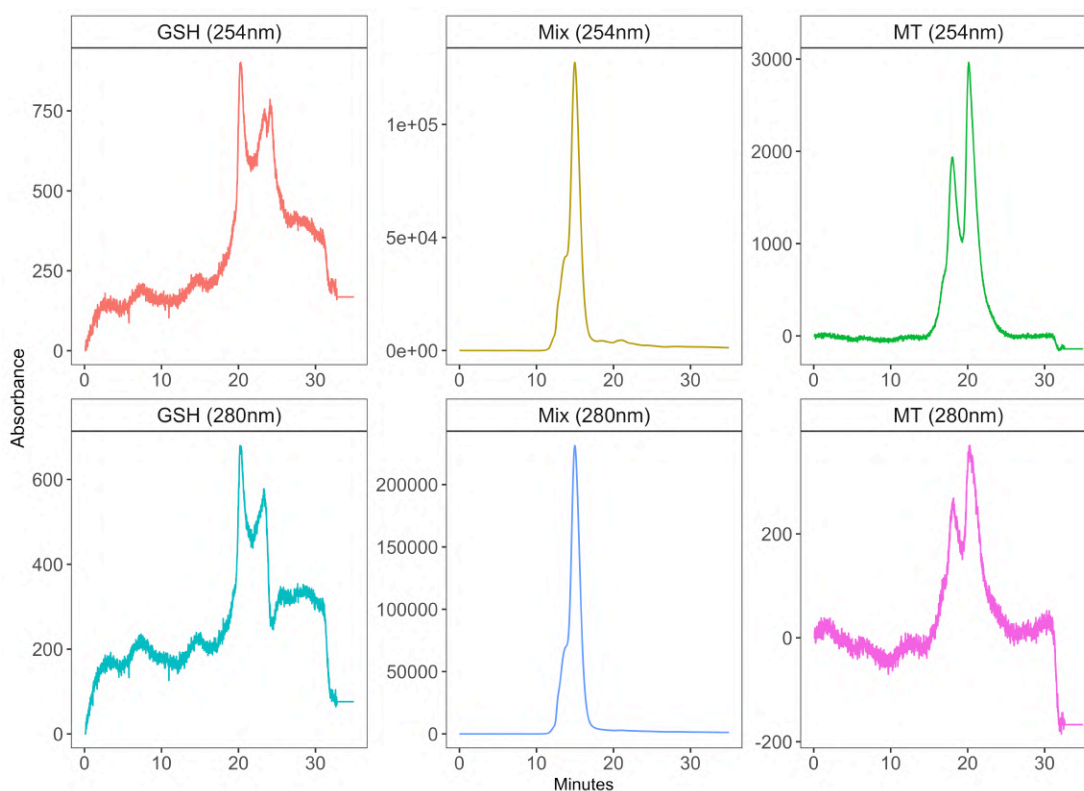


Figure 11.1 Chromatogram obtained for GSH, MT and a mixture of standards (BSA, Ferritin, GSH and MT) used to calibrate the separation column.

Online monitoring using ICP-MS coupled with HPLC allows for the observation of metal peaks that occur at the same times, such as protein and peptide peaks. Figure 11.2 shows the spectrum obtained for the standards used for separation column conditioning. MT shows an association with Zn and Cu, which are among the main elements that induce MT action, while GSH was associated with Cu and Fe. Similar

association profiles were obtained by Lavradas et al., 2016 when assessing bivalve mussels from differentially contaminated marine sites also in Rio de Janeiro.

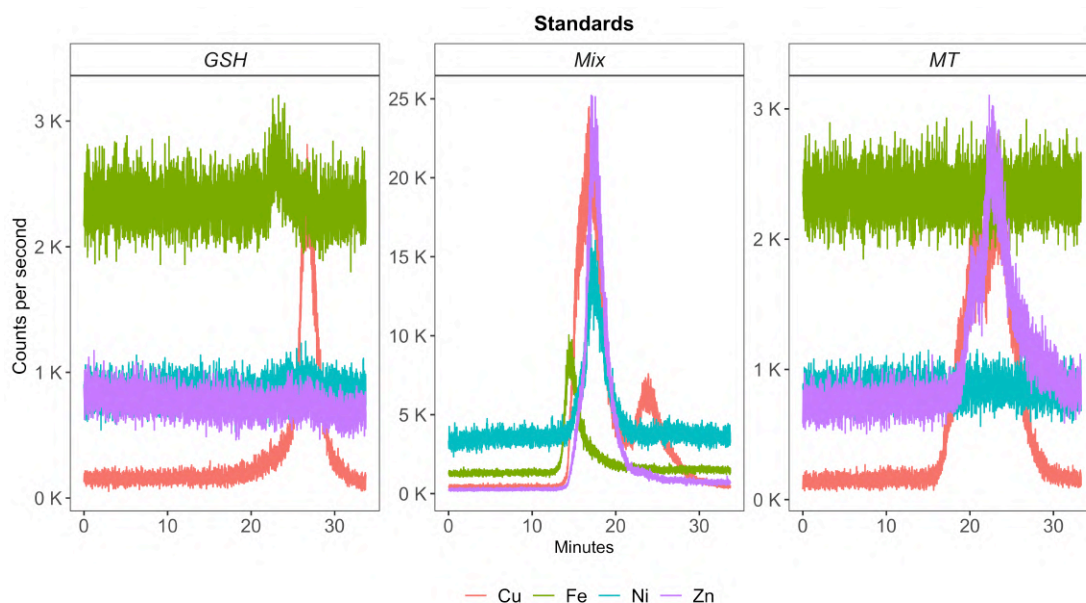


Figure 11.2 Spectra obtained by SEC-HPLC-ICP-MS for GSH, MT and a mixture of standards (BSA, Ferritin, GSH and MT) used to calibrate the separation column.

The chromatographic profile of the two *Tillandsia* species used for atmospheric monitoring was similar, eluting different elements between 15 and 50 minutes. Only Rb showed no corresponding protein peak. Most samples presented Zn and Ni peaks, while some samples also contained Mn and Ti. Figures 11.4 to 11.8 display the metal profiles for *T. stricta* and *T. usneoides* collected from all monitoring sites.

Most of the metal peaks eluted alongside low molecular weight proteins. In plants, metal detoxification is significantly affected by the contribution of phytochelatins, which are small peptides (2-11 kDa) that assist MT in chelating metals (Barakiewicz et al., 2009; Melendez et al., 2012). (Leopold and Günther, 1997) reported metal-induced elution of the phytochelatins complex at 16 minutes, although the chromatographic columns employed in each case were different. Due to the size range, it is possible that some of the peaks seen observed between 15 min and 25 min correspond to metals associated with phytochelatins. However, this hypothesis requires further studies to be confirmed.

In Duque de Caxias (Figure 11.3), both *Tillandsia* species exhibited similar metal associations in sampling campaigns 1 and 2. Ni and Zn peaks were expanded between 15 and 25 min, in some cases presenting two peaks. This is an indication that these metals may be associated with both MT and GSH. Interestingly, *T. usneoides* also displayed Ti peaks, near the retention times noted for MT, probably due to the fact that several industries use Ti compounds in their production processes at some biomonitoring sites investigated herein (Baltar et al., 2008). In sampling campaign 3, the peaks occurred near 25 min, indicating greater association with GSH. In addition to the aforementioned elements, Mn peaks were also observed in the samples exposed for a longer period of time.

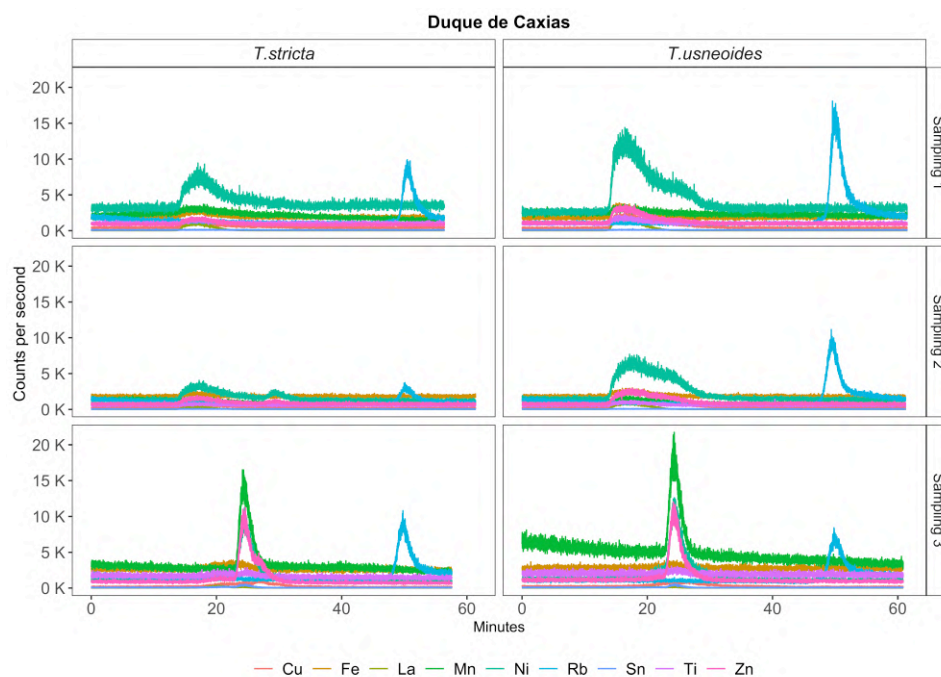


Figure 11.3 Metal bound protein observed by SEC-HPLC-ICP-MS in *T. stricta* and *T. usneoides* exposed in Duque de Caxias

At Niterói (Figure 11.4), a differential metal-protein association was observed between species and samplings. For *T. stricta*, an association of Ni and Fe with high molecular weight proteins was observed in sampling 1. In sampling 2, a more intense Ni and Zn peak was observed in the region of low molecular weight proteins. In sampling 3, although low intensity peaks of some metals were noted at 20 min, the most intense peaks were observed at 25 min for Ni, Zn and Mn, suggesting GSH binding. For *T. usneoides*, some metal peaks in sampling 1 were noted before 20 min.

However, a much wider range of metals associated with the protein was observed for this species, and differential metal-protein associations are expected as different species exhibit different tolerances to metals. Thus, *T. usneoides* seems to be less resistant to the toxic effects of metals, a hypothesis raised earlier during the subcellular evaluation of metals accumulated in both *Tillandsia* species. For the other sampling campaigns, behavior was similar in both species, suggesting a greater association of metals with GSH.

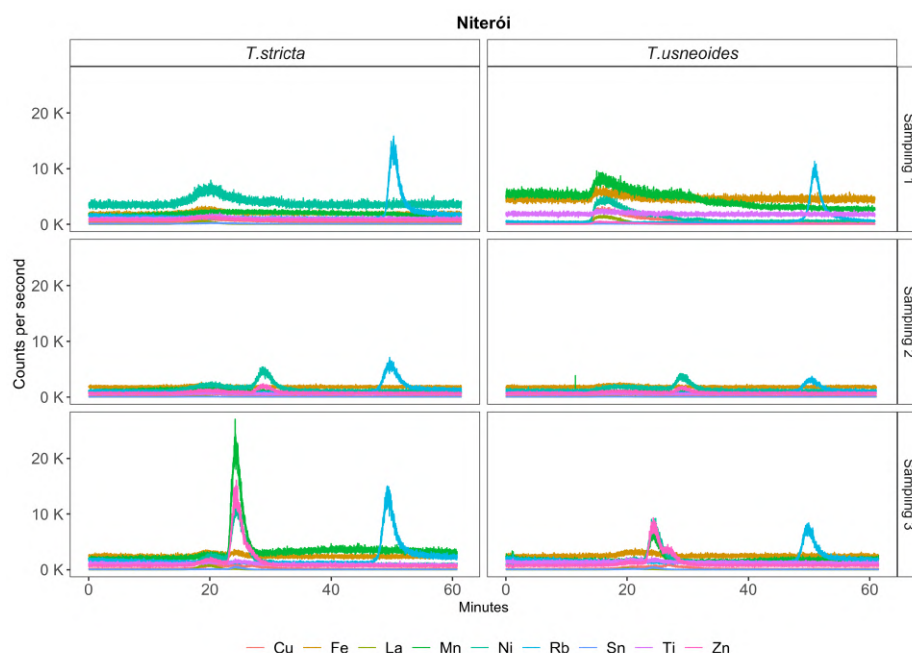


Figure 11.4 Metal bound protein observed by SEC-HPLC-ICP-MS in *T. stricta* and *T. usneoides* exposed in Niterói.

At Ramos (Figure 11.5), metal detoxification began to occur only after 6 months of exposure, after which Ni and Zn were associated with GSH in *T. stricta* and with MT in *T. usneoides*. After more than one year of exposure, an association between Fe and Mn with GSH was observed, as well as for Ni and Zn.

At Santa Cruz (Figure 11.6), low intensity Ni peaks were observed for both *Tillandsia* species in samplings 1 and 2, indicating associations with both MT and GSH. However, in sampling campaign 3, intense Mn, Ni, Zn and Fe peaks were observed in the low molecular weight protein region.

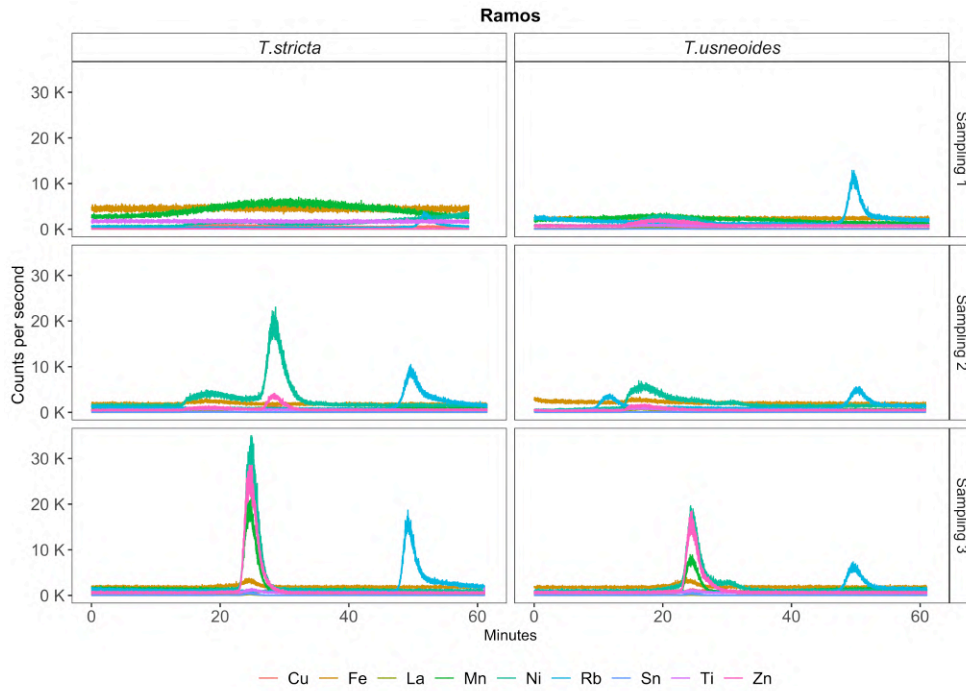


Figure 11.5 Metal bound protein observed by SEC-HPLC-ICP-MS in *T. stricta* and *T. usneoides* exposed in Ramos.

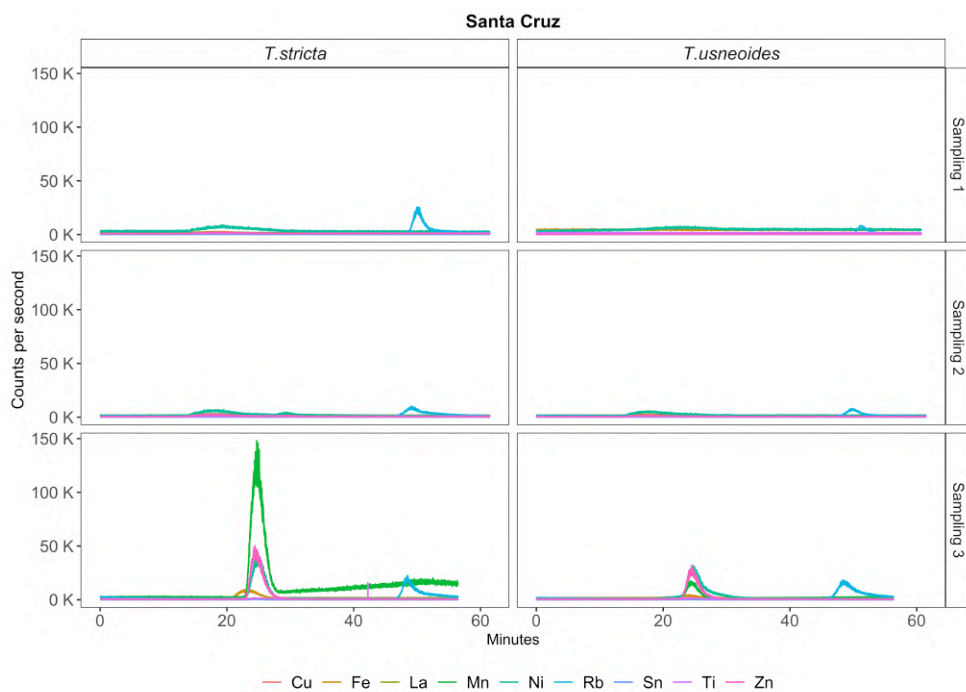


Figure 11.6 Metal bound protein observed by SEC-HPLC-ICP-MS in *T. stricta* and *T. usneoides* exposed in Santa Cruz.

At Urca (Figure 11.7), an initial association between Ni and Zn with MT was noted, altering to GSH after more than a year of exposure, also including greater intensity Ni, Zn and Mn peaks.

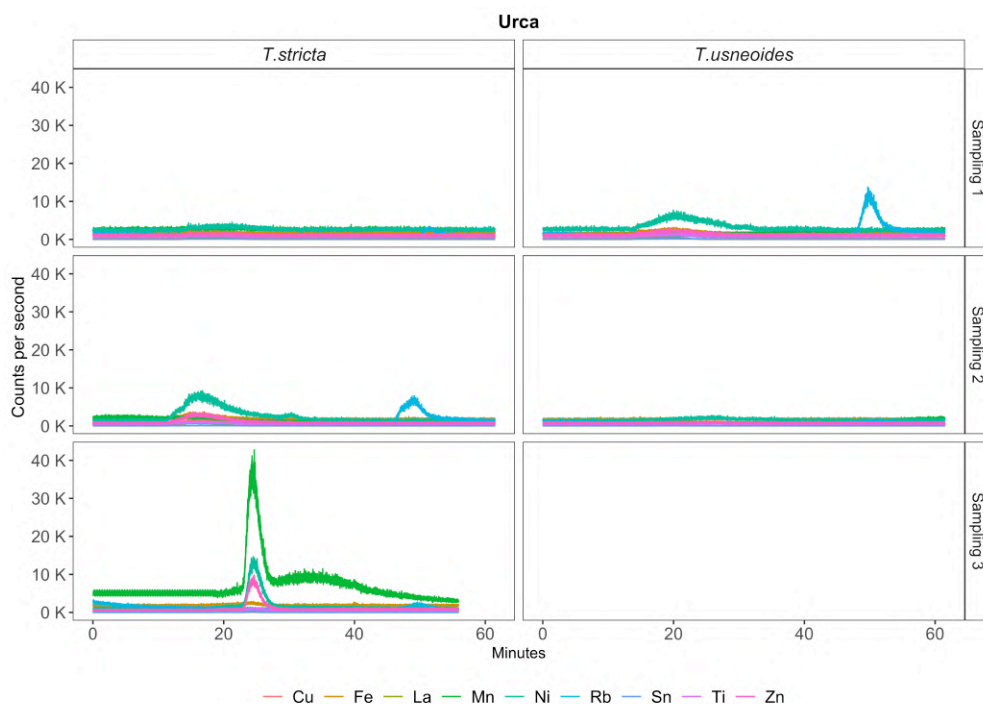


Figure 11.7 Metal bound protein observed by SEC-HPLC-ICP-MS in *T. stricta* and *T. usneoides* exposed in Urca.

11.4. Conclusion

This paper is pioneer concerning metal-protein assessments in epiphytic plants employed as biomonitors in an urban pollution setting, as these plants obtain nutrients exclusively through gas exchanges, comprising valuable atmospheric biomonitors. The findings indicate that atmospheric pollutants in the metropolitan region of Rio de Janeiro represent risks to both the population and the environment, due to the presence of toxic metals that can stimulate oxidative stress. The main metal-protein associations detected in both species were between MT and Ni and Zn, although the possibility of phytochelatin detoxification cannot be ruled out.

12 Conclusion

This work sought to comprehensively understand air pollution in the Rio de Janeiro metropolitan region and its impacts on the ecosystem. To this end, historical data of particulate matter concentration and composition were considered, as well as the effect of changes in the routine of urban centers on air quality. The environmental impacts were evaluated through biomonitoring using epiphytic plants in which oxidative stress was investigated.

The main atmospheric pollutant source in Rio de Janeiro comprises vehicular emissions. Air quality assessments during the social isolation caused by the COVID-19 pandemic revealed that the considerable urban mobility reduction observed during that period was the main cause of the decrease in the concentration of primary pollutants. This, in turn, resulted in decreased ozone concentrations, a secondary pollutant directly dependent on NO_x concentrations. This pandemic effect on air quality was also observed worldwide, attributed to the sudden change in the routine of cities. The contribution of vehicular emissions is also evident by the improved air quality observed during the 2016 Olympic games held in the city, when urban mobility underwent changes to improve the logistics of the event.

Due to the intense vehicular traffic in the metropolitan region of Rio de Janeiro, metals related to both exhaustion and non-exhaustion vehicular emissions accumulated in the tissues of the *Tillandsia* species employed as biomonitors. Although these plants are characterized by metal resistance, the oxidative stress assessments carried out herein indicated that exposure to vehicular pollutants resulted in organism dyshomeostasis. Furthermore, due to the CAM metabolism of the employed biomonitors, who carry out gas exchanges at night, climatic characteristics were proven to directly influence homeostasis. MT concentrations were lower during the dry period, due to the shorter exposure time to pollutants.

Both *T. stricta* and *T. usneoides*, displays high enrichments for traffic-related elements, although presenting differential cellular defense systems. In *T. usneoides*, MT played a metal detoxification role, but still not enough to prevent cell wall damage in the form of lipid peroxidation. In *T. stricta* however, the main defense mechanism

was observed with the increased GSH levels, stimulated by ROS production in the presence of metals, resulting in lower lipid peroxidation levels in this species.

This work is pioneering in the association of air pollution and toxic effects to ecosystems. Through this study it was possible to verify that air pollution can represent an ecological risk, thus signaling the need for measures to monitor, monitor and reduce this impact. Considering that Rio de Janeiro is the second largest metropolis in Brazil and is home to important Atlantic Forest remnants, further and continuous environmental pollution control and ecotoxicological studies are required to ensure ecosystem preservation, especially considering the devastation history of the local Atlantic Forest. The refinement of the methodology presented in this paper may lead to the development of new protocols for ecological risk assessment.

Finally, the significant contribution of vehicle emissions to the concentrations of air pollutants is an indication that government agencies need to take stronger measures to control air quality, especially when it comes to fuel quality and modernization and maintenance of the vehicle fleet, which are related to emission factors.

13 References

ABCAM. **Lipid Peroxidation (MDA) Assay Kit (Colorimetric / Fluorometric)**. [S.l: s.n.], 2019.

AIHEMAITI ET AL. Review of plant-vanadium physiological interactions, bioaccumulation, and bioremediation of vanadium-contaminated sites. **Science of the Total Environment**, v. 712, p. 135637, 2020.

AL-ALAM ET AL. The use of vegetation, bees, and snails as important tools for the biomonitoring of atmospheric pollution—a review. **Environmental Science and Pollution Research**, v. 26, n. 10, p. 9391–9408, 2019.

AL-THANI; KOÇ; ISAIFAN. A review on the direct effect of particulate atmospheric pollution on materials and its mitigation for sustainable cities and societies. **Environmental Science and Pollution Research**, v. 25, n. 28, p. 27839–27857, 2018.

ALEJANDRO ET AL. Manganese in Plants: From Acquisition to Subcellular Allocation. **Frontiers in Plant Science**, v. 11, n. March, p. 1–23, 2020.

ALEXIEVA ET AL. The effect of drought and ultraviolet radiation on growth and stress markers in pea and wheat. **Plant, Cell and Environment**, v. 24, n. 12, p. 1337–1344, 2001.

ALVES, C. A. Aerossóis atmosféricos: Perspectiva histórica, fontes, processos químicos de formação e composição orgânica. **Química Nova**, v. 28, n. 5, p. 859–870, 2005.

ALVES, E. S.; MOURA; DOMINGOS. Structural analysis of *Tillandsia usneoides* L. exposed to air pollutants in São Paulo City-Brazil. **Water, Air, and Soil Pollution**, v. 189, n. 1–4, p. 61–68, 2008.

ANDRADE ET AL. Vehicle emissions and PM 2.5 mass concentrations in six Brazilian cities. **Air Quality, Atmosphere and Health**, v. 5, n. 1, p. 79–88, 2012.

ANIČIĆ ET AL. Trace elements accumulation and temporal trends in leaves of urban deciduous trees (*Aesculus hippocastanum* and *Tilia* spp.). **Ecological Indicators**, v. 11, n. 3, p. 824–830, 2011.

ANJUM. Good in The Worst: COVID-19 Restrictions and Ease in Global Air

Pollution. **Preprints**, n. April, 2020.

ATKINSON ET AL. Urban Ambient Particle Metrics and Health: A Time-series Analysis. **Lippincott Williams & Wilkins**, v. 21, n. 4, p. 501–511, 2010.

ÁVILA-PÉREZ ET AL. Determining of risk areas due to exposure to heavy metals in the Toluca Valley using epiphytic mosses as a biomonitor. **Journal of Environmental Management**, v. 241, n. November 2018, p. 138–148, 2019.

AZEVEDO; MOREIRA. Composition of extractable organic matter in aerosols from urban areas of Rio de Janeiro city , Brazil. v. 33, 1999.

BAHINO ET AL. A pilot study of gaseous pollutants' measurement (NO₂, SO₂, NH₃, HNO₃ and O₃) in Abidjan, Côte d'Ivoire: contribution to an overview of gaseous pollution in African cities. **Atmospheric Chemistry and Physics**, v. 18, n. 7, p. 5173–5198, 2018.

BAJRAKTAROVA-VALJAKOVA ET AL. hydrofluric acid: Protective Measures, Immediate and Hospital Medical Treatment. Open Access Maced. **Access Macedonian Journal of Medical Sciences**, v. 6, n. 11, p. 2257, 2018.

BALDAUF. Roadside vegetation design characteristics that can improve local, near-road air quality. **Transportation Research Part D**, v. 52, p. 354–361, 2017.

BALTAR ET AL. Minerais de Titânio. In: ENGO, A. B. da L.; LINS, F. A. F. (Org.). **Rochas e Minerais Ind. Usos e especificações**. 2. ed. [S.l.]: CETEM, 2008. p. 841–863.

BAO; ZHANG. Does lockdown reduce air pollution? Evidence from 44 cities in northern China. **Science of the Total Environment**, v. 731, n. 1954, p. 139052, 2020.

BARAŁKIEWICZ ET AL. Determination of cadmium and lead species and phytochelatins in pea (*Pisum sativum*) by HPLC-ICP-MS and HPLC-ESI-MSn. **Talanta**, v. 79, n. 2, p. 493–498, 2009.

BARBOSA ET AL. Plant generation and enzymatic detoxification of reactive oxygen species. **Ciência Rural**, p. 453–460, mar. 2014.

BARGAGLI. Moss and lichen biomonitoring of atmospheric mercury: A review. **Science of the Total Environment**, v. 572, p. 216–231, 2016.

BELL; DAVIS; FLETCHER. A retrospective assessment of mortality from the London smog episode of 1952: The role of influenza and pollution. **Environmental Health Perspectives**, v. 112, n. 1, p. 6–8, 2004.

BERINGUI; JUSTO; ET AL. Assessment of air quality changes during COVID - 19 partial lockdown in a Brazilian metropolis : from lockdown to economic opening of Rio.

Air Quality, Atmosphere & Health, 2021.

BERINGUI; HUAMÁN DE LA CRUZ; ET AL. Atmospheric Metal Biomonitoring Along a Highway Near Atlantic Rainforest Environmental Protection Areas in Southeastern Brazil. **Bulletin of Environmental Contamination and Toxicology**, 2021.

BERINGUI; QUIJANO; ET AL. Avaliação da concentração e composição inorgânica do material particulado coletado no estado do Rio de Janeiro. **Quimica Nova**, p. 1–18, 2021.

BERINGUI ET AL. Time variation of atmospheric pollutants in first weeks of COVID-19 lockdown in the Metropolitan Region of Rio de Janeiro Variação temporal dos poluentes atmosféricos nas primeiras semanas de encerramento da COVID-19 na Região Metropolitana do Rio de Jane. **Studies in Engineering and Exact Sciences**, v. 3, n. 1, p. 95–106, 2022.

BERMUDEZ; PIGNATA. Antioxidant response of three Tillandsia species transplanted to urban, agricultural, and industrial areas. **Archives of Environmental Contamination and Toxicology**, v. 61, n. 3, p. 401–413, 2011.

BEZERRA ET AL. Air quality in the maracanã and deodoro zones during the rio 2016 olympic games. **Journal of the Brazilian Chemical Society**, v. 29, n. 11, p. 2220–2232, 2018.

BILOS ET AL. Sources, distribution and variability of airborne trace metals in La Plata City area, Argentina. **Environmental Pollution**, v. 111, n. 1, p. 149–158, 2001.

BOLAÑO-ORTIZ ET AL. Spread of covid-19, meteorological conditions and air quality in the city of buenos aires, argentina: Two facets observed during its pandemic lockdown. **Atmosphere**, v. 11, n. 10, p. 1–23, 2020.

BRANDAO; FOROUTAN. Air quality in Southeast Brazil during COVID-19 lockdown: A combined satellite and ground-based data analysis. **Atmosphere**, v. 12, n. 5, 2021.

BROOK; DANN; BURNETT. The Relationship Among TSP, PM10, PM2.5, and Inorganic Constituents of Atmospheric Participate Matter at Multiple Canadian Locations. **Journal of the Air and Waste Management Association**, v. 47, n. 1, p. 2–19, 1997.

BRYMAN; CRAMER. **Quant. Data Anal. with SPSS 12 13**. [S.l: s.n.], 2004.

CABALLERO-SEGURA ET AL. Metal content in mosses from the Metropolitan Area of the Toluca Valley: a comparative study between inductively coupled plasma optical emission spectrometry (ICP-OES) and total reflection X-ray fluorescence spectrometry (TXRF). **International Journal of Environmental Analytical**

Chemistry, v. 94, n. 13, p. 1288–1301, 2014.

CALEF; GOBLE. The allure of technology: How France and California promoted electric and hybrid vehicles to reduce urban air pollution. **Policy Sciences**, v. 40, n. 1, p. 1–34, 2007.

CAMARGO-CAICEDO; MANTILLA-ROMO; BOLAÑO-ORTIZ. Emissions reduction of greenhouse gases, ozone precursors, aerosols and acidifying gases from road transportation during the COVID-19 lockdown in Colombia. **Applied Sciences (Switzerland)**, v. 11, n. 4, p. 1–18, 2021.

CARDOSO-GUSTAVSON ET AL. Tillandsia usneoides: a successful alternative for biomonitoring changes in air quality due to a new highway in São Paulo, Brazil. **Environmental Science and Pollution Research**, v. 23, n. 2, p. 1779–1788, 2016.

CARSLAW; ROPKINS. Openair - An r package for air quality data analysis. **Environmental Modelling and Software**, v. 27–28, p. 52–61, 2012.

CAVERZAN; CASASSOLA; BRAMMER. Antioxidant responses of wheat plants under stress. **Genetics and Molecular Biology**, v. 39, n. 1, p. 1–6, 2016.

CEPEDA ET AL. Levels of ambient air pollution according to mode of transport: a systematic review. **The Lancet Public Health**, v. 2, n. 1, p. e23–e34, 2017.

ÇEVİK ET AL. An assessment of metal pollution in surface sediments of Seyhan dam by using enrichment factor, geoaccumulation index and statistical analyses. **Environmental Monitoring and Assessment**, v. 152, n. 1–4, p. 309–317, 2009.

CHALIGAVA ET AL. Characterization of Trace Elements in Atmospheric Deposition Studied by Moss Biomonitoring in Georgia. **Archives of Environmental Contamination and Toxicology**, n. 0123456789, 2020.

CHAO ET AL. Differential generation of hydrogen peroxide upon exposure to zinc and cadmium in the hyperaccumulating plant specie (Sedum alfredii Hance). **Journal of Zhejiang University: Science B**, v. 9, n. 3, p. 243–249, 2008.

CHEN, C. W. ET AL. Distribution and accumulation of heavy metals in the sediments of Kaohsiung Harbor, Taiwan. **Chemosphere**, v. 66, n. 8, p. 1431–1440, 2007.

CHEN, K. ET AL. Air pollution reduction and mortality benefit during the COVID-19 outbreak in China. **The Lancet Planetary Health**, v. 4, p. 210–212, 2020.

CHEN, LI ET AL. Vanadium in soil-plant system: Source, fate, toxicity, and bioremediation. **Journal of Hazardous Materials**, v. 405, n. July 2020, p. 124200, 2021.

CHEN, LIXIN ET AL. Experimental examination of effectiveness of vegetation as bio-filter of particulate matters in the urban environment. **Environmental Pollution**, v. 208, p. 198–208, 2016a.

_____. Experimental examination of effectiveness of vegetation as bio-filter of particulate matters in the urban environment. **Environmental Pollution**, v. 208, p. 198–208, 2016b.

COLLIVIGNARELLI ET AL. Lockdown for CoViD-2019 in Milan: What are the effects on air quality? **Science of the Total Environment**, v. 732, n. February, p. 1–9, 2020.

COMPANHIA DE ENGENHARIA DE TRÁFEGO - CET-RIO. **Dados de Fluxo**. Disponível em: <<http://riodejaneiro.rio/web/cetrio/exibeconteudo?id=9050075>>. Acesso em: 27 jan. 2020.

CONAMA. **Resolução nº 491/18 de 18 de novembro de 2018**. . Brasil: [s.n.]. Disponível em: <<http://www2.mma.gov.br/port/conama/legiabre.cfm?codlegi=740>>. , 2018

CONTI; CECCHETTI. Biological monitoring with lichens as bioindicators of air pollution assessment (A review). **Environmental Pollution**, v. 114, p. 471–492, 2001.

CRUZ ET AL. Exploratory analysis of the atmospheric levels of BTEX, criteria air pollutants and meteorological parameters in a tropical urban area in Northeastern Brazil. **Microchemical Journal**, v. 152, n. September 2019, p. 104265, 2020.

CUYPERS ET AL. Hydrogen Peroxide, Signaling in Disguise during Metal Phytotoxicity. **Frontiers in Plant Science**, v. 7, n. 470, 2016.

DANTAS ET AL. The impact of COVID-19 partial lockdown on the air quality of the city of Rio de Janeiro, Brazil. **Science of the Total Environment**, v. 729, p. 139085, 2020.

DARESTA ET AL. Atmospheric particulate matter (PM) effect on the growth of *Solanum lycopersicum* cv. Roma plants. **Chemosphere**, v. 119, p. 37–42, 2015.

DATTA ET AL. Quantification and characterization of particulate matter generated from unpaved roads in the oil development area of Western North Dakota. 2016, Orlando, EUA: [s.n.], 2016.

DE ALMEIDA AZEVEDO; DOS SANTOS; DE AQUINO NETO. Identification and seasonal variation of atmospheric organic pollutants in Campos dos Goytacazes, Brazil. **Atmospheric Environment**, v. 36, n. 14, p. 2383–2395, 2002.

DE LA CRUZ ET AL. Air quality biomonitoring of trace elements in the metropolitan area of Huancayo, Peru using transplanted *Tillandsia capillaris* as a biomonitor. **Anais**

da **Academia Brasileira de Ciências**, v. 92, n. 1, p. 1–17, 2020.

DE LA CRUZ ET AL. Evaluation of the impact of the Rio 2016 Olympic Games on air quality in the city of Rio de Janeiro, Brazil. **Atmospheric Environment**, v. 203, n. February, p. 206–215, 2019.

DE LA CRUZ ET AL. Biomonitoring of Potentially Toxic Elements in Two Polluted Areas from Lurigancho-Chosica Using the genus *Tillandsia latifolia* and *T. purpurea* as Biomonitor. **Bulletin of Environmental Contamination and Toxicology**, p. 1–8, 2021.

DE SOUZA ET AL. Determination of trace elements in the nanometer, ultrafine, fine, and coarse particulate matters in an area affected by light vehicular emissions in the city of Rio de Janeiro. **Environmental Monitoring and Assessment**, v. 193, n. 2, 2021.

DEBONE; DA COSTA; MIRAGLIA. 90 days of COVID-19 social distancing and its impacts on air quality and health in Sao Paulo, Brazil. **Sustainability (Switzerland)**, v. 12, n. 18, p. 1–16, 2020.

DETRAN. **Detran Estatísticas**. Disponível em: <http://www.detran.rj.gov.br/_estatisticas.veiculos/07.asp?menuzinho=07.asp>.

DG ENVIRONMENT STANDARDS. **Air Quality Standards**. Disponível em: <<https://ec.europa.eu/environment/air/quality/standards.htm>>. Acesso em: 27 jan. 2020.

DOERJ. **Diário Oficial do Estado do Rio de Janeiro (DOERJ) Decreto N° 47010 DE 31/03/2020**. . [S.l.: s.n.]. , 2020

DRAGULESCU; ARENDT. **Read, Write, Format Excel 2007 and Excel 97/2000/XP/2003 Files**. . [S.l.]: Files. R package version 0.6.5. , 2020

EDWARDS; DIXON; WALBOT. Plant glutathione S-transferases: enzymes with multiple functions in sickness and in health. **Trends in plant science Reviews**, v. 5, n. 5, p. 193–198, 2000.

ELHADI ET AL. Seasonal variations of atmospheric particulate matter and its content of heavy metals in Klang valley, Malaysia. **Aerosol and Air Quality Research**, v. 18, n. 5, p. 1148–1161, 2018.

ERK ET AL. Evaluation of different purification procedures for the electrochemical quantification of mussel metallothioneins. **Talanta**, v. 57, n. 6, p. 1211–1218, 2002.

ESCOBEDO; KROEGER; WAGNER. Urban forests and pollution mitigation: Analyzing ecosystem services and disservices. **Environmental Pollution**, v. 159, n.

8–9, p. 2078–2087, 2011.

FAJERSZTAJN ET AL. Short-term effects of fine particulate matter pollution on daily health events in Latin America: a systematic review and meta-analysis. **International Journal of Public Health**, v. 62, n. 7, p. 729–738, 2017.

FALLA ET AL. Biological air quality monitoring: A review. **Environmental Monitoring and Assessment**, v. 64, n. 3, p. 627–644, 2000.

FAUSTINI; RAPP; FORASTIERE. Nitrogen dioxide and mortality: Review and meta-analysis of long-term studies. **European Respiratory Journal**, v. 44, n. 3, p. 744–753, 2014.

FIGUEIREDO ET AL. Assessment of atmospheric metallic pollution in the metropolitan region of São Paulo, Brazil, employing *Tillandsia usneoides* L. as biomonitor. **Environmental Pollution**, v. 145, n. 1, p. 279–292, 2007.

FILONCHYK; PETERSON. Air Quality Changes in Shanghai, China, and the Surrounding Urban Agglomeration During the COVID-19 Lockdown. **Journal of Geovisualization and Spatial Analysis**, v. 4, n. 2, 2020.

FIOLETOV ET AL. Lifetimes and emissions of SO₂ from point sources estimated from OMI. **Geophysical Research Letters**, v. 42, p. 1969–1976, 2015.

FRATI; BRUNIALTI; LOPPI. Problems related to lichen transplants to monitor trace element deposition in repeated surveys: A case study from central Italy. **Journal of Atmospheric Chemistry**, v. 52, n. 3, p. 221–230, 2005.

FUZZI ET AL. Particulate matter , air quality and climate : lessons learned and. **Atmospheric Chemistry and Physics**, v. 15, p. 8217–8299, 2015.

GAUBERT ET AL. Global Changes in Secondary Atmospheric Pollutants during the 2020 COVID-19 Pandemic. **Journal of Geophysical Research: Atmospheres**, 2021.

GAUTAM. COVID-19: air pollution remains low as people stay at home. **Air Quality, Atmosphere and Health**, v. 13, n. 7, p. 853–857, 2020.

GEAR-INEA. **Nota Técnica 19/2020**. . [S.l: s.n.], 2020.

GERALDINO ET AL. An Analytical Investigation of Ozone Episodes in Bangu, Rio de Janeiro. **Bulletin of Environmental Contamination and Toxicology**, v. 98, n. 5, p. 632–637, 2017.

_____. Understanding high tropospheric ozone episodes in Bangu, Rio de Janeiro, Brazil. **Environmental Monitoring and Assessment**, v. 192, n. 3, 2020.

GIAMPAOLI; TAVARES; DOMINGOS. Physiological responses of two different

epiphytic bromeliads exposed in a polluted subtropical region in southeast Brazil characterized by seasonal climate. **Ecological Indicators**, v. 120, n. September 2020, p. 106945, 2021.

GILES ET AL. From good intentions to proven interventions: Effectiveness of actions to reduce the health impacts of air pollution. **Environmental Health Perspectives**, v. 119, n. 1, p. 29–36, 2011.

GILL ET AL. Glutathione and glutathione reductase: A boon in disguise for plant abiotic stress defense operations. **Plant Physiology and Biochemistry**, v. 70, p. 204–212, 2013.

GIODA ET AL. A Review on Atmospheric Analysis Focusing on Public Health, Environmental Legislation and Chemical Characterization. **Critical Reviews in Analytical Chemistry**, v. 0, n. 0, p. 1–23, 2021.

GIODA; AMARAL; ET AL. Chemical composition, sources, solubility, and transport of aerosol trace elements in a tropical region. **Journal of Environmental Monitoring**, v. 13, n. 8, p. 2134–2142, 2011.

GIODA ET AL. Chemical constituents in clouds and rainwater in the Puerto Rican rainforest: Potential sources and seasonal drivers. **Atmospheric Environment**, v. 68, n. x, p. 208–220, 2013.

_____. Evaluation of air quality in Volta Redonda, the main metallurgical industrial city in Brazil. **Journal of the Brazilian Chemical Society**, Ventos vindos do leste, variando de nordeste a sudeste., v. 15, n. 6, p. 856–864, 2004.

_____. Half Century Monitoring Air Pollution in a Megacity : a Case Study of Rio de Janeiro. **Water Air Soil Pollution**, Comentário sobre período seco e úmido, v. 227:86, p. 1–17, 2016.

GIODA; REYES-RODRÍGUEZ; ET AL. Speciation of water-soluble inorganic, organic, and total nitrogen in a background marine environment: Cloud water, rainwater, and aerosol particles. **Journal of Geophysical Research Atmospheres**, v. 116, n. 5, 2011.

GIODA ET AL. Understanding ozone formation at two islands of Rio de Janeiro, Brazil. **Atmospheric Pollution Research**, v. 9, n. 2, p. 278–288, 2018.

GIOIA ET AL. Insights into the dynamics and sources of atmospheric lead and particulate matter in São Paulo, Brazil, from high temporal resolution sampling. **Atmospheric Research**, v. 98, n. 2–4, p. 478–485, 2010.

GIRDHAR ET AL. Effect of COVID-19 outbreak on urban health and environment.

Air Quality, Atmosphere and Health, n. June 2020, p. 389–397, 2020.

GODOY, MARIA LUIZA D.P. ET AL. Coarse and fine aerosol source apportionment in Rio de Janeiro, Brazil. **Atmospheric Environment**, v. 43, n. 14, p. 2366–2374, 2009.

GODOY, MARIA LUÍZA D.P. ET AL. Fine and coarse aerosol at Rio de Janeiro prior to the olympic games: Chemical composition and source apportionment. **Journal of the Brazilian Chemical Society**, v. 29, n. 3, p. 499–508, 2018.

GOMES ET AL. Efeitos da gestão de mobilidade urbana para os Jogos Olímpicos sobre a qualidade do ar na região central da cidade do Rio de Janeiro. **urbe. Revista Brasileira de Gestão Urbana**, v. 10, n. suppl 1, p. 129–142, 2018.

GONZÁLEZ; ARISTIZÁBAL. Acid rain and particulate matter dynamics in a mid-sized Andean city: The effect of rain intensity on ion scavenging. **Atmospheric Environment**, v. 60, p. 164–171, 2012.

GRANTZ; GARNER; JOHNSON. Ecological effects of particulate matter. **Environment International**, v. 29, n. 2–3, p. 213–239, 2003.

GUAITA ET AL. Short-term impact of particulate matter (PM 2 . 5) on respiratory mortality in Madrid. **International Journal of Environmental Health Research**, v. 21, p. 260–274, 2011.

GULIA ET AL. Urban air quality management-A review. **Atmospheric Pollution Research**, v. 6, n. 2, p. 286–304, 2015.

GUO; WANG; ZHANG. Characterization of criteria air pollutants in Beijing during 2014–2015. **Environmental Research**, v. 154, n. October 2016, p. 334–344, 2017.

GUPTA; GUPTA. An overview of selenium uptake, metabolism, and toxicity in plants. **Frontiers in Plant Science**, v. 7, n. January, p. 1–14, 2017.

HAMRA ET AL. Outdoor particulate matter exposure and lung cancer: A systematic review and meta-analysis. **Environmental Health Perspectives**, v. 122, n. 9, p. 906–911, 2014.

HASANUZZAMAN ET AL. Glutathione in plants: biosynthesis and physiological role in environmental stress tolerance. **Physiology and Molecular Biology of Plants**, v. 23, n. 2, p. 249–268, 2017.

HAUSER-DAVIS ET AL. Biochemical metal accumulation effects and metalloprotein metal detoxification in environmentally exposed tropical *Perna perna* mussels. **Ecotoxicology and Environmental Safety**, v. 208, 2021.

HAYS ET AL. Particle size distributions of metal and non-metal elements in an

urban near-highway environment. **Atmospheric Environment**, v. 45, n. 4, p. 925–934, 2011.

HE ET AL. Fine particulate matter concentrations in urban Chinese cities, 2005–2016: A systematic review. **International Journal of Environmental Research and Public Health**, v. 14, n. 2, 2017.

HIEN ET AL. Comparative receptor modelling study of TSP , PM and PM in Ho Chi Minh City. **Atmospheric Environment**, v. 35, n. September 1996, p. 2669–2678, 2001.

HOPKE ET AL. Characterization of the gent stacked filter unit pm10 sampler. **Aerosol Science and Technology**, v. 27, n. 6, p. 726–735, 1997.

HOSSAIN ET AL. Hydrogen peroxide priming modulates abiotic oxidative stress tolerance: insights from ROS detoxification and scavenging. **Frontiers in Plant Science**, v. 6, p. 1–19, 2015.

HOU ET AL. Inter-annual variability in fine particulate matter pollution over China during 2013–2018: Role of meteorology. **Atmospheric Environment**, v. 214, n. July, p. 116842, 2019.

IBGE. **Cidades Brasileiras**. Disponível em: <<https://cidades.ibge.gov.br/brasil/rj/rio-de-janeiro/panorama>>.

IEMA. **Primeiro diagnóstico da rede de monitoramento da qualidade do ar no Brasil**. Instituto de Energia e Meio Ambiente. [S.l: s.n.], 2014.

_____. **Qualidade do AR**. Disponível em: <<http://qualidadedoar.org.br>>. Acesso em: 27 jan. 2020.

IMTIAZ ET AL. Vanadium toxicity in chickpea (*Cicer arietinum* L.) grown in red soil: Effects on cell death, ROS and antioxidative systems. **Ecotoxicology and Environmental Safety**, v. 158, n. December 2017, p. 139–144, 2018.

INEA. **Inventário de emissões de fontes veiculares: região metropolitana do Rio de Janeiro**. . [S.l: s.n.], 2016

INMETRO. Guidance in validation of analytical methods (in Portuguese). **Instituto Nacional de Metrologia, Qualidade e Tecnologia**, p. 31, 2016.

INSTITUTO ESTADUAL DO AMBIENTE. **Monitoramento do Ar - Emissões e Qualidade**. Disponível em: <<http://www.inea.rj.gov.br/Portal/MegaDropDown/Monitoramento/Monitoramentodoar-EmiQualidade/index.htm&lang=PT-BR>>. Acesso em: 27 jan. 2020.

IPEA. **Governança Metropolitana no Brasil**. . [S.l: s.n.], 2015. Disponível em:

<http://ipea.gov.br/agencia/images/stories/PDFs/relatoriopesquisa/book_relatorio_analise_web.pdf>.

_____. **Governança Metropolitana no Brasil**. . [S.l: s.n.], 2018. Disponível em:

<http://ipea.gov.br/agencia/images/stories/PDFs/relatoriopesquisa/book_relatorio_analise_web.pdf>.

JACONIS; CULLEY; MEIER. Does particulate matter along roadsides interfere with plant reproduction? A comparison of effects of different road types on *Cichorium intybus* pollen deposition and germination. **Environmental Pollution**, v. 222, p. 261–266, 2017.

JANHÄLL. Review on urban vegetation and particle air pollution - Deposition and dispersion. **Atmospheric Environment**, v. 105, p. 130–137, 2015.

JUSTO ET AL. Assessment of Atmospheric PM10 Pollution Levels and Chemical Composition in Urban Areas near the 2016 Olympic Game Arenas. **Journal of the Brazilian Chemical Society**, v. 31, n. 5, p. 1043–1054, 2020.

KAN; CHEN; TONG. Ambient air pollution, climate change, and population health in China. **Environment International**, v. 42, n. 1, p. 10–19, 2012.

KASSAMBARA. Ggpubr: “Ggplot2” Based Publication Ready Plots. **R Documentation**, 2020.

KECK; WITTMACK. Effect of filter type and temperature on volatilisation losses from ammonium salts in aerosol matter. **Atmospheric Environment**, v. 39, n. 22, p. 4093–4100, 2005.

KIM; KABIR; KABIR. A review on the human health impact of airborne particulate matter. **Environment International**, v. 74, p. 136–143, 2015.

KISKU ET AL. Pollution in Lucknow City and its health implication on exposed vendors, drivers and traffic policemen. **Air Quality, Atmosphere and Health**, v. 6, n. 2, p. 509–515, 2013.

KISA ET AL. Expression analysis of metallothioneins and mineral contents in tomato (*Lycopersicon esculentum*) under heavy metal stress. **Journal of the Science of Food and Agriculture**, v. 97, n. 6, p. 1916–1923, 2017.

KOUL; THOMAS; KARMAKAR. Functional aspects of solanaceae trichomes in heavy metal detoxification. **Nordic Journal of Botany**, v. 39, n. 5, p. 1–14, 2021.

KOVÁČIK ET AL. Comparison of oxidative stress in four *Tillandsia* species exposed to cadmium. **Plant Physiology and Biochemistry**, v. 80, p. 33–40, 2014.

LANDRIGAN. Air pollution and health. **The Lancet Public Health**, v. 2, n. 1, p. e4–e5, 2017.

LAVRADAS ET AL. Investigation of thermostable metalloproteins in Perna perna mussels from differentially contaminated areas in Southeastern Brazil by bioanalytical techniques. **Journal of Trace Elements in Medicine and Biology**, v. 34, p. 70–78, 2016.

LE ET AL. Unexpected air pollution with marked emission reductions during the COVID-19 outbreak in China. **Science**, v. 369, n. 6504, p. 702–706, 2020.

LENZI; FÁVERO. **Introdução à Química da Atmosfera: Ciência, Vida e Sobrevivência**. 1st. ed. Rio de Janeiro: [s.n.], 2008.

LEOPOLD; GÜNTHER. Investigation of the binding properties of heavy-metal-peptide complexes in plant cell cultures using HPLC-ICP-MS. **Fresenius' Journal of Analytical Chemistry**, v. 359, n. 4–5, p. 364–370, 1997.

LI, C. C. ET AL. Integration of metal chemical forms and subcellular partitioning to understand metal toxicity in two lettuce (*Lactuca sativa* L.) cultivars. **Plant and Soil**, v. 384, n. 1–2, p. 201–212, 2014.

LI, P. ET AL. Atmospheric Pb induced hormesis in the accumulator plant *Tillandsia usneoides*. **Science of the Total Environment**, v. 811, p. 152384, 2022.

LI, S. ET AL. Determination of Metallothionein Isoforms in Fish by Cadmium Saturation Combined with Anion Exchange HPLC-ICP-MS. **Chromatographia**, v. 81, n. 6, p. 881–889, 2018.

LIEDSCHULTE ET AL. Exploiting plants for glutathione (GSH) production: Uncoupling GSH synthesis from cellular controls results in unprecedented GSH accumulation. **Plant Biotechnology Journal**, v. 8, n. 7, p. 807–820, 2010.

LIN ET AL. Characteristics of metals in nano/ultrafine/fine/coarse particles collected beside a heavily trafficked road. **Environmental Science and Technology**, v. 39, n. 21, p. 8113–8122, 2005.

LIU ET AL. Attributions of meteorological and emission factors to the 2015 winter severe haze pollution episodes in China's Jing-Jin-Ji area. **Atmospheric Chemistry and Physics**, v. 17, n. 4, p. 2971–2980, 2017.

LÖNDAHL ET AL. A set-up for field studies of respiratory tract deposition of fine and ultrafine particles in humans. **Journal of Aerosol Science**, v. 37, p. 1152–1163, 2006.

LOYOLA ET AL. Concentration and emission sources of airborne metals in

particulate matter in the industrial district of Médio Paraíba, State of Rio de Janeiro, Brazil. **Archives of Environmental Contamination and Toxicology**, v. 51, n. 4, p. 485–493, 2006.

_____. Concentration of airborne trace metals in a bus station with a high heavy-duty diesel fraction. **Journal of the Brazilian Chemical Society**, v. 20, n. 7, p. 1343–1350, 2009.

_____. Trace metals in the urban aerosols of Rio De Janeiro city. **Journal of the Brazilian Chemical Society**, v. 23, n. 4, p. 628–638, 2012.

MAHAPATRA ET AL. Perspective of mitigating atmospheric heavy metal pollution: using mosses as biomonitoring and indicator organism. **Environmental Science and Pollution Research**, descrição da interação das plantas com substâncias tóxicas. Parece muito bom., v. 26, n. 29, p. 29620–29638, 2019.

MAIA ET AL. Characterization of trace metals present in atmospheric particulate matter inferior to 2,5µm (PM2,5) around an industrial area. **Perspectivas da Ciência e Tecnologia**, v. 6, n. 1/2, p. 2–13, 2014.

MAMANE; MEHLER. ON THE NATURE OF NITRATE PARTICLES IN A COASTAL URBAN AREA to total particle number concentration , provides information about the nature of nitrate particles (for The presence of nitrate particles in the atmosphere has example their mixture with other. **Atmospheric Environment**, v. 21, n. 9, p. 1989–1994, 1987.

MANSOUR ET AL. Oxidative Stress and Damage Biomarkers in Clam *Ruditapes decussatus* Exposed to a Polluted Site: The Reliable Biomonitoring Tools in Hot and Cold Seasons. **Archives of Environmental Contamination and Toxicology**, 2020.

MARGUT; COSTA; FAVARÃO. **Territórios em números: insumos para políticas públicas a partir da análise de IDHM e dos IVS de UDHS e regiões metropolitanas brasileiras**. Brasília: IPEA:INCT, 2017.

MARIANI; MELLO. PM2.5-10, PM2.5 and associated water-soluble inorganic species at a coastal urban site in the metropolitan region of Rio de Janeiro. **Atmospheric Environment**, Avalia período seco e período úmido. O período seco teve concentração 1,7-1,8 maior que o úmido. A relação entre pm2,5 e pm10 não muda muito de um período para outro., v. 41, n. 13, p. 2887–2892, 2007.

MARRERO ET AL. A study of uniformity of elements deposition on glass fiber filters after collection of airborne particulate matter (PM-10), using a high-volume sampler. **Talanta**, v. 68, n. 2, p. 442–447, 2005.

MASIOL ET AL. The size distribution of chemical elements of atmospheric aerosol at a semi-rural coastal site in Venice (Italy). The role of atmospheric circulation. **Chemosphere**, v. 119, p. 400–406, 2015.

MATEUS.; GIODA. A candidate framework for PM2.5 source identification in highly industrialized urban-coastal areas. **Atmospheric Environment**, v. 164, p. 147–164, 2017.

MATEUS ET AL. Assessment of ambient aerosol sources in two important Atlantic Rain Forest hotspots in the surroundings of a megacity. **Urban Forestry & Urban Greening**, v. 56, n. June 2019, p. 126858, 2020.

MATEUS ET AL. Study of the chemical composition of particulate matter from the Rio de Janeiro metropolitan region, Brazil, by inductively coupled plasma-mass spectrometry and optical emission spectrometry. **Spectrochimica Acta - Part B**, v. 86, p. 131–136, 2013.

MATEUS; GIODA. A candidate framework for PM2.5 source identification in highly industrialized urban-coastal areas. **Atmospheric Environment**, v. 164, p. 147–164, 2017.

MCCOY; FISCHBECK; GERARD. How big is big? How often is often? Characterizing Texas petroleum refining upset air emissions. **Atmospheric Environment**, v. 44, n. 34, p. 4230–4239, 2010.

MELLENDEZ ET AL. Determinação de Metalotioneínas e Fitoquelatinas utilizando a técnica de HPLC-ICP-MS. **Revista Virtual de Química**, v. 4, n. 6, p. 612–622, 2012.

MENDES ET AL. Impact of the Petrochemical Complex on the Air Quality of an Urban Area in the City of Rio de Janeiro, Brazil. **Bulletin of Environmental Contamination and Toxicology**, v. 104, n. 4, p. 438–443, 2020.

MENDOZA-RAMOS ET AL. Biomonitoring and Sourcing Toxic Elements Using Vascular Epiphytes of the Tillandsia Genus in the Mining Region of Taxco de Alarcón, Guerrero, Southern Mexico. **Water, Air, and Soil Pollution**, v. 232, n. 1, 2021.

MINISTÉRIO DA SAÚDE. **Painel Coronavírus**. Disponível em: <<https://covid.saude.gov.br>>. Acesso em: 3 maio 2021.

MIRANDA ET AL. Urban air pollution: A representative survey of PM 2.5 mass concentrations in six Brazilian cities. **Air Quality, Atmosphere and Health**, v. 5, n. 1, p. 63–77, 2012.

MISCELLANEOUS; YES. Hmisc: Harrell Miscellaneous. **Frank E Harrell Jr**, 2021.

MMA. **Guia Técnico para o Monitoramento e Avaliação da Qualidade Do Ar**.

. [S.l: s.n.]. , 2019

_____. **Inventário Nacional de Emissões Atmosféricas por Veículos Automotores Rodoviários.** . [S.l: s.n.]. Disponível em: <http://www.mma.gov.br/images/arquivo/80060/Inventario_de_Emissoes_por_Veiculos_Rodoviarios_2013.pdf>. , 2014

MÖLTER ET AL. Research | Children ' s Health Long-term Exposure to PM 10 and NO 2 in Association with Lung Volume and Airway Resistance in the MAAS Birth Cohort. **Environmental health Perspectives**, v. 121, n. 10, p. 1232–1238, 2013.

MONNA ET AL. Perturbation vectors to evaluate air quality using lichens and bromeliads: a Brazilian case study. **Environmental Monitoring and Assessment**, v. 189, n. 11, p. 1–10, 2017.

MONTEIRO ET AL. Subcellular metal distributions and metallothionein associations in rough-toothed dolphins (*Steno bredanensis*) from Southeastern Brazil. **Marine Pollution Bulletin**, v. 146, n. April, p. 263–273, 2019.

MORALES ET AL. Inorganic water soluble ions in atmospheric particles over Maracaibo Lake Basin in the western region of Venezuela. **Atmospheric Research**, v. 46, n. 3–4, p. 307–320, 1998.

MROCZEK-ZDYRSKA; STRUBIŃSKA; HANAKA. Selenium Improves Physiological Parameters and Alleviates Oxidative Stress in Shoots of Lead-Exposed *Vicia faba* L. minor Plants Grown Under Phosphorus-Deficient Conditions. **Journal of Plant Growth Regulation**, v. 36, n. 1, p. 186–199, 2017.

MUNN. Pollution wind-rose analysis. **Atmosphere**, v. 7, n. 3, p. 97–105, 1969.

NAKADA; URBAN. COVID-19 pandemic: Impacts on the air quality during the partial lockdown in São Paulo state, Brazil. **Science of the Total Environment**, v. 730, p. 139087, 2020.

NAKAZATO, RICARDO K.; RINALDI; DOMINGOS. Tropical trees: Are they good alternatives for biomonitoring the atmospheric level of potential toxic elements near to the Brazilian Atlantic Rainforest? **Ecotoxicology and Environmental Safety**, v. 134, p. 72–79, 2016.

NAKAZATO, RICARDO KEIICHI ET AL. Efficiency of biomonitoring methods applying tropical bioindicator plants for assessing the phytotoxicity of the air pollutants in SE, Brazil. **Environmental Science and Pollution Research**, v. 25, n. 20, p. 19323–19337, 2018a.

_____. Efficiency of biomonitoring methods applying tropical bioindicator plants

for assessing the phytotoxicity of the air pollutants in SE, Brazil. **Environmental Science and Pollution Research**, v. 25, n. 20, p. 19323–19337, 2018b.

NASCIMENTO ET AL. Atmospheric total suspended particulate trace element identification by XRF at Ilha Grande, State of Rio de Janeiro, Brazil. **Water, Air, and Soil Pollution**, não tem concentração de MP, v. 214, n. 1–4, p. 525–538, 2011.

NEIVA; DA SILVA; CARDOSO. Analysis of climate behavior and land use in the city of Rio de Janeiro, RJ, Brazil. **Climate**, v. 5, n. 3, p. 1–14, 2017.

NEUWIRTH. **RColorBrewer: ColorBrewer Palettes**. . [S.l: s.n.]. , 2014

NIU; LIAO. Hydrogen peroxide signaling in plant development and abiotic responses: Crosstalk with nitric oxide and calcium. **Frontiers in Plant Science**, v. 7, n. MAR2016, p. 1–14, 2016.

OATEN ET AL. Metal Accumulation and Metallothionein Response in *Fucus Spiralis*. **International Journal of Environmental Pollution and Remediation**, v. 5, 2017.

OCHOA-HUESO ET AL. Ecological impacts of atmospheric pollution and interactions with climate change in terrestrial ecosystems of the Mediterranean Basin: Current research and future directions. **Environmental Pollution**, v. 227, p. 194–206, 2017.

OLIVEIRA; DE MELO; MIGUENS. *Tillandsia stricta* Sol (Bromeliaceae) leaves as monitors of airborne particulate matter-A comparative SEM methods evaluation: Unveiling an accurate and odd HP-SEM method. **Microscopy research and technique**, v. 79, n. 9, p. 869–879, 2016.

OLMEZ; CETIN GULOVALI; GORDON. Trace element concentrations in lichens near a coal-fired power plant. **Atmospheric Environment**, v. 19, n. 10, p. 1663–1669, 1985.

OMIDVARBORNA; BAAWAI; AL-MAMUN. Ambient air quality and exposure assessment study of the Gulf Cooperation Council countries: A critical review. **Science of the Total Environment journal**, v. 636, p. 437–448, 2018.

PACHECO ET AL. A review of emissions and concentrations of particulate matter in the three major metropolitan areas of Brazil. **Journal of Transport and Health**, v. 4, n. October 2016, p. 53–72, 2017.

PANT ET AL. The PM10 fraction of road dust in the UK and India: Characterization, source profiles and oxidative potential. **Science of the Total Environment**, v. 530–531, p. 445–452, 2015.

PANT; HARRISON. Estimation of the contribution of road traffic emissions to particulate matter concentrations from field measurements: A review. **Atmospheric Environment**, v. 77, p. 78–97, 2013.

PARALOVO ET AL. Observations of particulate matter, NO₂, SO₂, O₃, H₂S and selected VOCs at a semi-urban environment in the Amazon region. **Science of the Total Environment**, v. 650, n. 2, p. 996–1006, 2019.

PAULA ET AL. Biomonitoring of metals for air pollution assessment using a hemiepiphyte herb (*Struthanthus flexicaulis*). **Chemosphere**, v. 138, p. 429–437, 2015.

PAULINO ET AL. Evolution of particulate matter and associated metal levels in the Urban Area of Rio de Janeiro, Brazil. **Bulletin of Environmental Contamination and Toxicology**, v. 84, n. 3, p. 315–318, 2010.

_____. Trace metals in PM₁₀ and PM_{2.5} samples collected in a highly industrialized chemical/petrochemical area and its urbanized surroundings. **Bulletin of Environmental Contamination and Toxicology**, v. 92, n. 5, p. 590–595, 2014.

PAULO ET AL. Association between Air Pollution and Intrauterine Mortality. v. 106, n. 6, p. 325–329, 1998.

PERNIGOTTI; BELIS; SPANÓ. SPECIEUROPE: The European data base for PM source profiles. **Atmospheric Pollution Research**, v. 7, n. 2, p. 307–314, 2016.

PETERSON. of the Protein Assay Method of Lowry et al. Which is More Generally Applicable. **Analytical Biochemistry**, v. 83, p. 346–356, 1977.

PIAZZETTA; RAMSDORF; MARANHO. Use of airplant *Tillandsia recurvata* L., Bromeliaceae, as biomonitor of urban air pollution. **Aerobiologia**, v. 35, n. 1, p. 125–137, 2019.

PIGNATA ET AL. Atmospheric quality and distribution of heavy metals in Argentina employing *Tillandsia capillaris* as a biomonitor. **Environmental Pollution**, v. 120, n. 1, p. 59–68, 2002.

POPE ET AL. Particulate Air Pollution as a Predictor of Mortality in a Prospective Study of U.S. Adults. **American Journal of Respiratory and Critical Care Medicine**, v. 151, p. 669–674, 1995.

PÖSCHL. Atmospheric aerosols: Composition, transformation, climate and health effects. **Atmospheric Chemistry**, v. 44, n. 46, p. 7520–7540, 2005.

PREFEITURA DO RIO DE JANEIRO. Painel Rio COVID-19. p. 24, 2021.

QUIJANO ET AL. Exploratory and comparative analysis of the morphology and

chemical composition of PM 2.5 from regions with different socioeconomic characteristics. **Microchemical Journal**, v. 147, n. March, p. 507–515, 2019.

QUITERIO, S. L. ET AL. Particulate matter and associated metal levels in a conservation area in the remaining tropical forest of Mata Atlântica, Brazil. **Bulletin of Environmental Contamination and Toxicology**, v. 77, n. 5, p. 651–657, 2006.

QUITERIO, SIMONE LORENA ET AL. Evaluation of levels, sources and distribution of airborne trace metals in seven districts of the Baixada Fluminense, Rio de Janeiro, Brazil. **Atmospheric Environment**, Local: Baixada (Japeri, Queimado, Nova Iguaçu, Mesquita, Belford Roxo, São João de Meriti, Magé)Boa correlação entre a precipitação e a concentração de PTS, v. 39, n. 19, p. 3503–3512, 2005.

_____. Metals in airborne particulate matter in the industrial district of Santa Cruz, Rio de Janeiro, in an annual period. **Atmospheric Environment**, Local: Santa CruzMaiores concentrações no período de abril a setembro(seco).Maiores temperaturas favoreceram ressuspensão do solo, v. 38, n. 2, p. 321–331, 2004.

R CORETEAM. **R: A Language and Environment for Statistical Computing**. Vienna, Austria: R Foundation for Statistical Computing, 2019. Disponível em: <<https://www.r-project.org/>>.

RAI. Biodiversity of roadside plants and their response to air pollution in an Indo-Burma hotspot region: Implications for urban ecosystem restoration. **Journal of Asia-Pacific Biodiversity**, v. 9, n. 1, p. 47–55, 2016a.

_____. Impacts of particulate matter pollution on plants: Implications for environmental biomonitoring. **Ecotoxicology and Environmental Safety**, v. 129, p. 120–136, 2016b.

RAINHO, C. R. ET AL. Seasonal variations in the level of mutagenicity: An assessment of respirable particulate matter in Rio de Janeiro, Brazil. **WIT Transactions on Ecology and the Environment**, v. 183, n. May 2011, p. 87–101, 2014.

RAINHO, CLAUDIA RAMOS DE ET AL. Genotoxicity of Polycyclic Aromatic Hydrocarbons and Nitro-Derived in Respirable Airborne Particulate Matter Collected from Urban Areas of Rio de Janeiro (Brazil). v. 2013, 2013.

RASHEED ET AL. Iron toxicity, tolerance and quantitative trait loci mapping in rice; a review. **Applied Ecology and Environmental Research**, v. 18, n. 6, p. 7483–7498, 2020.

REN ET AL. Comparison and trend study on acidity and acidic buffering capacity

of particulate matter in China. **Atmospheric Environment**, v. 45, n. 39, p. 7503–7519, 2011.

Resolução CONAMA N°3/90 de 28 de junho de 1990. . Brasil: [s.n.]. Disponível em: <<http://www2.mma.gov.br/port/conama/legiabre.cfm?codlegi=100>>. , 1990

RIO DE JANEIRO CITY HALL. Prefeitura vai informar a quantidade de pessoas circulando em alguns bairros Autarquias. p. 20211, 2020.

RODRIGUES ET AL. Transporte e distribuição de potássio atenuam os efeitos tóxicos do sódio em plantas jovens de pinhão-manso. **Revista Brasileira de Ciencia do Solo**, v. 36, n. 1, p. 223–232, 2012.

RODRÍGUEZ-COTTOA ET AL. Particle Pollution in Rio de Janeiro, Brazil: Increase and Decrease of Pro-inflammatory Cytokines IL-6 and IL-8 in Human Lung Cells. **Environmental Pollution**, v. 194, p. 112–120, 2014.

RODRIGUEZ-HERNANDEZ ET AL. Increased accumulation of cadmium and lead under Ca and Fe deficiency in *Typha latifolia*: A study of two pore channel (TPC1) gene responses. **Environmental and Experimental Botany**, v. 115, p. 38–48, 2015.

ROJAS ET AL. Effects of COVID-19 pandemic control measures on air pollution in Lima metropolitan area, Peru in South America. **Air Quality, Atmosphere and Health**, v. 14, n. 6, p. 925–933, 2021.

ROLPH; STEIN; STUNDER. Real-time Environmental Applications and Display sYstem: READY. **Environmental Modelling and Software**, v. 95, p. 210–228, 2017.

RUDKE ET AL. How mobility restrictions policy and atmospheric conditions impacted air quality in the State of São Paulo during the COVID-19 outbreak. **Environmental Research**, v. 198, n. April, 2021.

SAADAT; RAWTANI; HUSSAIN. Environmental perspective of COVID-19. **Science of the Total Environment**, v. 728, p. 138870, 2020.

SALCEDO ET AL. Assessment of sample preparation methods for the analysis of trace elements in airborne particulate matter. **Journal of Analytical Atomic Spectrometry**, v. 29, n. 4, p. 753–761, 2014.

SALDIVA ET AL. Air pollution and mortality in elderly people: Atime-series study in sao paulo, Brazil. **Archives of Environmental Health**, v. 50, n. 2, p. 159–163, 1995.

SANDERSON; DELGADO-SABORIT; HARRISON. A review of chemical and physical characterisation of atmospheric metallic nanoparticles. **Atmospheric Environment**, v. 94, p. 353–365, 2014.

SANTOS, L. B.; ALMEIDA; GODOY. Alternative Source Apportionment in the Surrounding Region of a Large Steel Industry Applying *Tillandsia usneoides* as Biomonitor. **Química Nova**, v. 15, p. 1–6, 2017.

SANTOS, T. C.; CARVALHO; REBOITA. Avaliação da influência das condições meteorológicas em dias com altas concentrações de material particulado na Região Metropolitana do Rio de Janeiro. **Engenharia Sanitaria e Ambiental**, v. 21, n. 2, p. 307–313, 2016.

SANTOSA. The analysis, identification, and formulation of metallothionein extract available in roots, stems, leaves, flowers, and grains of rice, corns, beans, and soybeans. **International Journal of Science and Engineering(IJSE)**, v. 10, p. 17–20, 2016.

SARAIVA ET AL. High CO₂ effects on growth and biometal contents in the pioneer species *Senna reticulata*: climate change predictions. **Journal of Trace Elements in Medicine and Biology**, v. 50, p. 130–138, 2018.

SARFRAZ; SHEHZAD; FARID. Gauging the air quality of New York: a non-linear Nexus between COVID-19 and nitrogen dioxide emission. **Air Quality, Atmosphere and Health**, v. 13, n. 9, p. 1135–1145, 2020.

SEINFELD; PANDIS. **Atmospheric Chemistry and Physics: From air pollution to climate change**. 2nd. ed. New Jersey: [s.n.], 2006.

SEINFELD; PANDIS; NOONE. Atmospheric Chemistry and Physics: From Air Pollution to Climate Change. **Physics Today**, v. 51, p. 1326–1336, 1998.

SELLA ET AL. Biogenic vanadium in total suspended particulate matter from Cabo Frio upwelling region, Southeast, Brazil. **Atmospheric Environment**, Local: Cabo Frio Tem valores mensais de PTSEstação de Cambinhas e INMETSó avalia direção do vento, v. 40, n. 32, p. 6181–6191, 2006.

SEVIK ET AL. Determination of changes in heavy metal accumulation depending on plant species, plant organism, and traffic density in some landscape plants. **Air Quality, Atmosphere and Health**, v. 12, n. 2, p. 189–195, 2019.

SHAHID ET AL. Foliar heavy metal uptake, toxicity and detoxification in plants: A comparison of foliar and root metal uptake. **Journal of Hazardous Materials**, Review, v. 325, p. 36–58, 2017.

SHEKARI ET AL. Protective role of selenium on cucumber (*Cucumis sativus* L.) exposed to cadmium and lead stress during reproductive stage role of selenium on heavy metals stress. **Journal of Plant Nutrition**, v. 42, n. 5, p. 529–542, 2019.

SHEN ET AL. Ionic composition of TSP and PM_{2.5} during dust storms and air pollution episodes at Xi'an, China. **Atmospheric Environment**, v. 43, n. 18, p. 2911–2918, 2009.

SICILIANO ET AL. The Impact of COVID-19 Partial Lockdown on Primary Pollutant Concentrations in the Atmosphere of Rio de Janeiro and São Paulo Megacities (Brazil). **Bulletin of Environmental Contamination and Toxicology**, v. 105, n. 1, p. 2–8, 2020.

SKÓRZYŃSKA-POLIT. Lipid Peroxidation in Plant Cells, Its Physiological Role and Changes Under Heavy Metal Stress. **Acta Societatis Botanicorum Poloniae**, v. 76, n. 1, p. 49–54, 2007.

SOLURI ET AL. Multi-site PM_{2.5} and PM_{2.5-10} Aerosol Source Apportionment in Rio de Janeiro, Brazil Daniela. **Journal of Brazilian Chemistry Society**, Maiores concentrações para período seco e menores para período úmido. As estações do ano tem influencia similar em diferentes pontos., v. 18, n. 4, p. 838–845, 2007.

SOLURI. **Study of the Chemical Composition of the Suspended Particulate Matter in the Air in Rio De Janeiro City**. , Tese de Doutorado. Rio de Janeiro: [s.n.], 2005. Disponível em: <http://www.maxwell.vrac.puc-rio.br/Busca_etds.php?strSecao=resultado&nrSeq=7365@2>.

SONG; GAO. Size distributions of trace elements associated with ambient particular matter in the affinity of a major highway in the New Jersey-New York metropolitan area. **Atmospheric Environment**, v. 45, n. 37, p. 6714–6723, 2011.

SOUSA; LOPES; DE ANDRADE. Fontes, formação, reatividade e determinação de quinonas na atmosfera. **Quimica Nova**, v. 39, n. 4, p. 486–495, 2016.

SOUZA, M. L.; ALLEN; CARDOSO. Understanding aerosol formation mechanisms in a subtropical atmosphere impacted by biomass burning and agroindustry. **Atmospheric Research**, v. 183, p. 94–103, 2017.

SPENCER; VAN HEYST. A review of particulate matter emissions and impacts on human health: A focus on Canadian agricultural and rural emission sources. **Canadian Biosystems Engineering / Le Genie des biosystems au Canada**, v. 60, n. 1, p. 69–621, 2019.

STEIN ET AL. Noaa's hysplit atmospheric transport and dispersion modeling system. **Bulletin of the American Meteorological Society**, v. 96, n. 12, p. 2059–2077, 2015.

STEVERLYNCK ET AL. Combined acute inhalation of hydrofluoric acid and nitric

acid: a case report and literature review. **Acta Clinica Belgica: International Journal of Clinical and Laboratory Medicine**, v. 72, n. 4, p. 278–288, 2017.

SULAYMON ET AL. COVID-19 pandemic in Wuhan: Ambient air quality and the relationships between criteria air pollutants and meteorological variables before, during, and after lockdown. **Atmospheric Research**, v. 250, p. 105362, 2021.

SUN, J. ET AL. Analysis of PM2.5 pollution episodes in Beijing from 2014 to 2017: Classification, interannual variations and associations with meteorological features. **Atmospheric Environment**, v. 213, p. 384–394, 2019.

SUN, X.; LI; ZHENG. Biomarker Responses of Spanish Moss *Tillandsia usneoides* to Atmospheric Hg and Hormesis in This Species. **Frontiers in Plant Science**, v. 12, n. January, p. 1–8, 2021a.

_____. Cellular and subcellular distribution and factors influencing the accumulation of atmospheric Hg in *Tillandsia usneoides* leaves. **Journal of Hazardous Materials**, v. 414, n. November 2020, p. 125529, 2021b.

SZCZEPANIAK; BIZIUK. Aspects of the biomonitoring studies using mosses and lichens as indicators of metal pollution. **Environmental Research**, v. 93, n. 3, p. 221–230, 2003.

TAÏBI ET AL. Effect of salt stress on growth, chlorophyll content, lipid peroxidation and antioxidant defence systems in *Phaseolus vulgaris* L. **South African Journal of Botany**, v. 105, p. 306–312, 2016.

TECHATO; SALAEH; VAN BEEM. Use of Atmospheric Epiphyte *Tillandsia usneoides* (Bromeliaceae) as Biomonitor. **APCBEE Procedia**, v. 10, p. 49–53, 2014.

TIE ET AL. Severe Pollution in China Amplified by Atmospheric Moisture. **Scientific Reports**, v. 7, n. 1, p. 1–9, 2017.

TOBIÁS ET AL. Changes in air quality during the lockdown in Barcelona (Spain) one month into the SARS-CoV-2 epidemic. **Science of the Total Environment**, v. 726, p. 138540, 2020.

TOLEDO ET AL. Evaluation of levels, sources and distribution of toxic elements in PM10 in a suburban industrial region, Rio de Janeiro, Brazil. **Environmental Monitoring and Assessment**, maiores concentrações nos meses do período seco, v. 139, n. 1–3, p. 49–59, 2008.

TRIPATHI ET AL. Acquisition and homeostasis of Iron in higher plants and their probable role in abiotic stress tolerance. **Frontiers in Environmental Science**, v. 5, n. FEB, p. 1–15, 2018.

TRIPATHI ET AL. Recent Advances in the Expression and Regulation of Plant Metallothioneins for Metal Homeostasis and Tolerance. In: CHANDRA, R. (Org.). . **Environ. Waste Manag.** 1. ed. Boca Raton: Taylor & Francis Group, 2015. p. 551–564.

TSURUTA ET AL. Air Quality Indexes in the City of Rio de Janeiro During the 2016 Olympic and Paralympic Games. **Journal of Brazilian Chemistry Society**, v. 29, n. 6, p. 1291–1303, 2018.

US EPA. METHOD 6020B INDUCTIVELY COUPLED PLASMA—MASS SPECTROMETRY SW-846. **METHOD 6020B**, n. July, p. 634, 2014.

USEPA. **Compendium Method IO-3.1: Selection, preparation and extraction of filter material.** Center for Environmental Research Information Office of Research and Development US Environmental Protection Agency. [S.l: s.n.]. , 1999

_____. **Reviewing National Ambient Air Quality Standards (NAAQS): Scientific and Technical Informatio, Table of current NAAQS Table.** Disponível em: <<https://www.epa.gov/criteria-air-pollutants/naaqs-table>>. Acesso em: 27 jan. 2020.

_____. **USEPA Method 300.1, Determination of inorganic anions in drinking water by ion chromatography.** . [S.l: s.n.]. Disponível em: <<https://www.epa.gov/sites/production/files/2015-06/documents/epa-300.1.pdf>>. , 1997

USHA; VENKATARAMAN; PARIDA. Heavy metal and abiotic stress inducible metallothionein isoforms from *Prosopis juliflora* (SW) D.C. show differences in binding to heavy metals in vitro. **Molecular Genetics and Genomics**, v. 281, n. 1, p. 99–108, 2009.

VARELA ET AL. Levels of antioxidant compound glutathione in moss from industrial areas. **Atmosphere**, v. 9, n. 7, p. 1–8, 2018.

VENTER ET AL. COVID-19 lockdowns cause global air pollution declines. **Proceedings of the National Academy of Sciences of the United States of America**, v. 117, n. 32, p. 18984–18990, 2020.

VENTURA ET AL. Air quality monitoring assessment during the 2016 Olympic Games in Rio de Janeiro, Brazil. **Environmental Monitoring and Assessment**, v. 191, n. 6, p. 369, 2019.

VENTURA, LUCIANA M.B.; RAMOS; SANTOS; ET AL. Monitoring of air quality before

the olympic games Rio 2016. **Anais da Academia Brasileira de Ciencias**, v. 91, n. 1, p. 1–14, 2019.

VENTURA ET AL. Validation method to determine metals in atmospheric particulate matter by inductively coupled plasma optical emission spectrometry. **Journal of the Brazilian Chemical Society**, v. 25, n. 9, p. 1571–1582, 2014.

VENTURA ET AL. Chemical composition of fine particles (PM_{2.5}): water-soluble organic fraction and trace metals. **Air Quality, Atmosphere and Health**, v. 10, n. 7, p. 845–852, 2017.

_____. Evaluation of air quality in a megacity using statistics tools. **Meteorology and Atmospheric Physics**, v. 130, n. 3, p. 361–370, 2018.

_____. Forecast of daily PM 2.5 concentrations applying artificial neural networks and Holt–Winters models. **Air Quality, Atmosphere and Health**, v. 12, n. 3, p. 317–325, 2019.

VIANNA ET AL. Assessment of heavy metals in the particulate matter of two Brazilian metropolitan areas by using *Tillandsia usneoides* as atmospheric biomonitor. **Environmental Science and Pollution Research**, v. 18, n. 3, p. 416–427, 2011.

VIARENGO ET AL. A simple spectrophotometric method for metallothionein evaluation in marine organisms: An application to Mediterranean and Antarctic molluscs. **Marine Environmental Research**, v. 44, n. 1, p. 69–84, 1997.

VILLANUEVA ET AL. Ambient levels of volatile organic compounds and criteria pollutants in the most industrialized area of central Iberian Peninsula: intercomparison with an urban site. **Environmental Technology (United Kingdom)**, v. 37, n. 8, p. 983–996, 2016.

WA LWALABA ET AL. The effect of cobalt stress on growth and physiological traits and its association with cobalt accumulation in barley genotypes differing in cobalt tolerance. **Journal of Plant Nutrition**, v. 40, n. 15, p. 2192–2199, 2017.

WANNAZ ET AL. Assessment of heavy metal accumulation in two species of *Tillandsia* in relation to atmospheric emission sources in Argentina. **Science of the Total Environment**, v. 361, n. 1–3, p. 267–278, 2006.

_____. Maximum values of Ni²⁺, Cu²⁺, Pb²⁺ and Zn²⁺ in the biomonitor *Tillandsia capillaris* (Bromeliaceae): Relationship with cell membrane damage. **Environmental and Experimental Botany**, v. 74, n. 1, p. 296–301, 2011.

WARE; THIBODEAU; SPEIZER. Assessment of the health effects of atmospheric sulfur oxides and particulate matter: Evidence from observational studies.

Environmental Health Perspectives, v. Vol. 41, n. October, p. 255–276, 1981.

WEI ET AL. Heavy metal induced ecological risk in the city of Urumqi, NW China. **Environmental Monitoring and Assessment**, v. 160, n. 1–4, p. 33–45, 2010.

WHO. **Air Pollution**. Disponível em: <https://www.who.int/health-topics/air-pollution#tab=tab_1>. Acesso em: 17 mar. 2020.

_____. **Air quality guidelines for particulate matter, ozone, nitrogen dioxide and sulfur dioxide**. . Genebra: [s.n.], 2005.

WICKHAM, HADDLEY. **Elegant Graphics for Data Analysis Second Edition**. Second ed. [S.l.]: Springer, 2016. Disponível em: <<http://www.springer.com/series/6991>>.

WICKHAM, HADLEY ET AL. dplyr: A Grammar of Data Manipulation. **R documentation**, v. R package, 2022.

_____. Reshaping Data with the reshape Package. **Journal of Statistical Software**, v. 21, n. 12, p. 1–20, 2007.

WICKHAM, HADLEY; GIRLICH. tidy: Tidy Messy Data. R package version 1.2.0. 2022.

WORLD HEALTH ORGANIZATION. **WHO Director-General's opening remarks at the media briefing on COVID-19 - 11 March 2020**. Disponível em: <<https://www.who.int/dg/speeches/detail/who-director-general-s-opening-remarks-at-the-media-briefing-on-covid-19---11-march-2020>>.

WU.; ZHANG. Effects of particulate matter (PM_{2.5}) and associated acidity on ecosystem functioning: response of leaf litter breakdown. **Environmental Science and Pollution Research**, v. 25, n. 30, p. 30720–30727, 2018.

WU ET AL. Characteristics of water-soluble inorganic components and acidity of PM_{2.5} in a coastal city of China. **Aerosol and Air Quality Research**, v. 17, n. 9, p. 2152–2164, 2017.

WU ET AL. Indications of selenium protection against cadmium and lead toxicity in oilseed rape (*brassica napus* L.). **Frontiers in Plant Science**, v. 7, n. DECEMBER2016, p. 1–10, 2016.

XIE ET AL. A dynamic processes study of PM retention by trees under different wind conditions. **Environmental Pollution**, v. 233, p. 315–322, 2018.

XU ET AL. Air quality index, indicator air pollutants and impact of covid-19 event on the air quality near central china. **Aerosol and Air Quality Research**, v. 20, n. 6, p. 1204–1221, 2020.

XU ET AL. Climate modulation of the Tibetan Plateau on haze in China. **Atmospheric Chemistry and Physics**, v. 16, n. 3, p. 1365–1375, 2016.

XU ET AL. Spatiotemporal variation in the impact of meteorological conditions on PM2.5 pollution in China from 2000 to 2017. **Atmospheric Environment**, v. 223, p. 117215, 2020.

YUSHIN ET AL. Mosses as bioindicators of heavy metal air pollution in the lockdown period adopted to cope with the covid-19 pandemic. **Atmosphere**, v. 11, n. 11, 2020.

ZAMBRANO-MONSERRATE; RUANO. Has air quality improved in Ecuador during the COVID-19 pandemic? A parametric analysis. **Air Quality, Atmosphere and Health**, v. 13, n. 8, p. 929–938, 2020.

ZAMBRANO-MONSERRATE; RUANO; SANCHEZ-ALCALDE. Indirect effects of COVID-19 on the environment. **Science of the Total Environment**, v. 728, 2020.

ZANGARI ET AL. Air quality changes in New York City during the COVID-19 pandemic. n. January, 2020.

ZHANG ET AL. Excretion from long glandular trichomes contributes to alleviation of cadmium toxicity in *Nicotiana tabacum*. **Environmental Pollution**, v. 285, n. February, p. 117184, 2021.

ZHAO ET AL. Numerical investigation of Pollutant Dispersion around two Adjacent Super-long Urban Road Tunnels. **Procedia Engineering**, v. 205, p. 1331–1336, 2017.

ZHENG ET AL. Foliar uptake and transport of atmospheric trace metals bounded on particulate matters in epiphytic *Tillandsia brachycaulos*. **International Journal of Phytoremediation**, v. 23, n. 4, p. 400–406, 2021.

ZHENG; PEMBERTON; LI. Assessment of Cs and Sr accumulation in two epiphytic species of *Tillandsia* (Bromeliaceae) in vitro. **Chemistry and Ecology**, v. 33, n. 1, p. 51–60, 2017.

_____. Bioindicating potential of strontium contamination with Spanish moss *Tillandsia usneoides*. **Journal of Environmental Radioactivity**, v. 152, p. 23–27, 2016.

ZOU ET AL. Arctic sea ice, Eurasia snow, and extreme winter haze in China. **Science Advances**, v. 3, n. 3, p. 1–9, 2017.

ZUPANCIC; BOZAU. Effect of Corona Virus Pandemic Lockdown to Chemical Composition of Peat Mosses. p. 1–19, 2021.

14 Appendix A – Published papers

Quím. Nova, Vol. 44, No. 6, 737-754, 2021

<http://dx.doi.org/10.21577/0100-4042.20170717>

AVALIAÇÃO DA CONCENTRAÇÃO E COMPOSIÇÃO INORGÂNICA DO MATERIAL PARTICULADO COLETADO NO ESTADO DO RIO DE JANEIRO

Karmel Beringui^a, Maria Fernanda C. Quijano^a, Elizanne P. S. Justo^a, Luciana Maria Baptista Ventura^{ab} e Adriana Gioda^{a*}

^aDepartamento de Química, Pontifícia Universidade Católica do Rio de Janeiro, 22451-900 Rio de Janeiro – RJ, Brasil

^bInstituto Estadual do Ambiente, 20081-312 Rio de Janeiro – RJ, Brasil

Recebido em 21/11/2020; aceito em 28/01/2021; publicado na web em 18/02/2021

Revisão

Figure 14.1 Beringui, Karmel et al. Avaliação da concentração e composição inorgânica do material particulado coletado no estado do Rio de Janeiro. *Química Nova*. 2021, v. 44, n. 6 described in chapter 3.



Time variation of atmospheric pollutants in first weeks of COVID-19 lockdown in the Metropolitan Region of Rio de Janeiro

Figure 14.2 Beringui, Karmel et al. *Studies in Engineering and Exact Sciences*, 2022, v 3., n 1, 95 – 106 described in chapter 5.

Air Quality, Atmosphere & Health
<https://doi.org/10.1007/s11869-021-01127-2>



Assessment of air quality changes during COVID-19 partial lockdown in a Brazilian metropolis: from lockdown to economic opening of Rio de Janeiro, Brazil

Karmel Beringui¹ · Elizanne P. S. Justo¹ · Anna De Falco¹ · Eduarda Santa-Helena¹ · Werickson F. C. Rocha² · Adrien Deroubaix³ · Adriana Gioda¹

Figure 14.3 Beringui et al. *Air quality, Atmosphere & Health*, nov 2021, described in chapter 6.

15 Appendix B - Published papers in the scope of this thesis

Bulletin of Environmental Contamination and Toxicology
<https://doi.org/10.1007/s00128-021-03185-9>



Atmospheric Metal Biomonitoring Along a Highway Near Atlantic Rainforest Environmental Protection Areas in Southeastern Brazil

Karmel Beringui¹ · Alex Rubén Huamán De La Cruz^{1,2,3} · Luiz Francisco Pires Guimarães Maia⁴ · Adriana Gioda¹

Figure 15.1 Beringui, K. et. al, Atmospheric Metal Biomonitoring Along a Highway Near Atlantic Rainforest Environmental Protection Areas in Southeastern Brazil. Bull Environ Contam Toxicol 107, 84–91 (2021)

Bulletin of Environmental Contamination and Toxicology
<https://doi.org/10.1007/s00128-021-03143-5>



Biomonitoring of Potentially Toxic Elements in Two Polluted Areas from Lurigancho-Chosica Using the genus *Tillandsia latifolia* and *T. purpurea* as Biomonitor

Alex Rubén Huamán De La Cruz¹ · Hérica Yauri Molina¹ · Xiomara Rosa Vilca Monrroy¹ · Karmel Beringui^{1,2} · Andres Camargo Caysahuana³ · Julio Angeles Suazo⁴ · Nancy Curasi Rafael¹ · Adriana Gioda² · Ide Gelmora Unchupaico Payano⁵

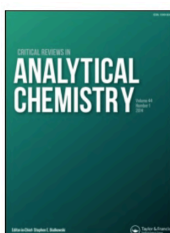
Figure 15.2 De La Cruz, A.R.H. et al. Biomonitoring of Potentially Toxic Elements in Two Polluted Areas from Lurigancho-Chosica Using the genus *Tillandsia latifolia* and *T. purpurea* as Biomonitor. Bull Environ Contam Toxicol 107, 69–76 (2021).



Assessment of Atmospheric PM₁₀ Pollution Levels and Chemical Composition in Urban Areas near the 2016 Olympic Game Arenas

Elizanne P. S. Justo,^a Maria Fernanda C. Quijano,^a Karmel Beringui,^a Tatiana D. Saint'Pierre^a and Adriana Gioda^{,a}*

Figure 15.3 Justo, Elizanne P. S. et al. Assessment of Atmospheric PM₁₀ Pollution Levels and Chemical Composition in Urban Areas near the 2016 Olympic Game Arenas. *Journal of the Brazilian Chemical Society*. 2020, v. 31, n. 5



Critical Reviews in Analytical Chemistry



ISSN: (Print) (Online) Journal homepage: <https://www.tandfonline.com/loi/batc20>

A Review on Atmospheric Analysis Focusing on Public Health, Environmental Legislation and Chemical Characterization

Adriana Gioda, Karmel Beringui, Elizanne P. S. Justo, Luciana M. B. Ventura, Carlos G. Massone, Silvano Silvério Lopes Costa, Sidimar Santos Oliveira, Rennan Geovanny Oliveira Araujo, Nivia de M. Nascimento, Hemmely Guilhermond S. Severino, Christiane B. Duyck, Jefferson Rodrigues de Souza & Tatiana D. Saint Pierre

Figure 15.4 Adriana Gioda, et. al (2021): A Review on Atmospheric Analysis Focusing on Public Health, Environmental Legislation and Chemical Characterization, *Critical Reviews in Analytical Chemistry*

16 Appendix E - Participation in Congress

Oral presentations

Beringui, Karmel; Gomes, Maria Vitória R.; Hauser-Davis, Rachel Ann; Gioda, Adriana. Subcellular metal distribution in atmospheric biomonitors from industrial áreas. Online Congress of ASTOXILATIN, 2021. (Environmental toxicology pizer winner)

Beringui, Karmel; Sousa, Lucia H.S.P; Hauser-Davis, Rachel Ann; Maia, Luiz Francisco P.G; Gioda, Adriana. Use of two *Tillandsia species* as air quality biomonitors at an important Brazilian highway. 42^a RASBQ, 2019, Joinville – SC.

Beringui, Karmel; Sousa, Lucia Helena; Saint’Pierre, Tatiana; Hauser-Davis, Rachel Ann; Gioda, Adriana. Metal exposure biomarker evaluation in exposed atmospheric biomonitors in the port region of Niterói, RJ. 43^a RASBQ, 2020, Online event.

Posters

Cáceres Quijano, M.F; Justo, E.P.S.; **Beringui, K.**; Calderon, E.R.D.; Gioda, A. Determination of the chemical composition and its distribution according to the particles sizes. 42^a RASBQ, 2019, Joinville – SC.

Beringui, Karmel; Hauser-Davis, Rachel. Ann; Gioda, Adriana. . Assessment of air quality in Rio de Janeiro by traditional monitoring and biomonitoring. SPSAS on Atmospheric Aerosol, 2019, São Paulo – SP.

Meziat, Guilherme; **Beringui Karmel;** Justo, Elizanne Porto de Souza; Calderon, Enrique D. ; Andrade, Vinícius de Paiva; Modé, Natália C.; Mello, Felipe M.M.D., Gioda, Adriana. Avaliação da qualidade do ar através da concentração de PM2.5 e PM10 na Gávea, Rio de Janeiro. XVII Encontro Regional da SBQ-Rio, 2019 (Rio de Janeiro – RJ).

Beringui, Karmel; Quijano, Maria Fernanda C.; Justo, Elizanne P.S.; Gioda, Adriana. Determinação da concentração e da composição elementar de material particulado coletado na Gávea, Rio de Janeiro. XVII Encontro Regional da SBQ-Rio, 2019 Rio de Janeiro – RJ.

17 Supplementary Material – 1

This material refers to the article described in Chapter 4.

Table 17.1 Automatic (A) and semi-automatic (S) stations of INEA's air quality monitoring system with TSP and PM₁₀ concentration data used for the 1st Diagnosis of the air quality monitoring network in Brazil

Região Metropolitana				Região do Médio Paraíba				Região Norte Fluminense			
Município	Estação	PM	Tipo	Município	Estação	PM	Tipo	Município	Estação	PM	Tipo
Belford Roxo	Secretaria de Transporte	TSP	S		Jardim Paraiba	TSP	S		Águas do Paraiba	TSP e PM ₁₀	S
S. Joao de Meriti	Vilar dos Teles	PM ₁₀	S		Volta Grande	TSP	S	Campos dos Goytacazes	Goytacazes	TSP e PM ₁₀	S
São Gonçalo	Prefeitura	TSP e PM ₁₀	S		Aeroclube	TSP e PM ₁₀	S		Centro	TSP	S
Seropédica	Embrapa	TSP e PM ₁₀	S		Conforto	TSP e PM ₁₀	S	São João da Barra	Água Pretra	TSP e PM ₁₀	A
Guapimirim	APA	TSP e PM ₁₀	S	Volta Redonda	Vila Mury	TSP e PM ₁₀	S	Macaé	Cabiunas	TSP e PM ₁₀	A
Nilópolis	Rodoviária	PM ₁₀	S		SIDERVILE	TSP e PM ₁₀	S				
Niterói	Centro	PM ₁₀	S		Santa Rita do Zarur	TSP e PM ₁₀	S				
Nova Iguaçu	Monteiro Lobato	PM ₁₀	S e A		Belmonte	TSP e PM ₁₀	A				
	Conjunto Alvorada	TSP	S		Retiro	TSP e PM ₁₀	A				
	João XXIII	TSP	S		Santa Cecília	TSP e PM ₁₀	A				
Santa Cruz	João 23 A	TSP e PM ₁₀	S		Ano Bom	TSP	S				
	João 23 B	TSP e PM ₁₀	S	Barra Mansa	Bocaininha	TSP e PM ₁₀	A				
	Largo do Bodegão	TSP e PM ₁₀	A		Roberto Silveira	TSP e PM ₁₀	A				
	Adalgisa Nery	TSP e PM ₁₀	A		Vista Alegre	TSP e PM ₁₀	A				
	Monte Serrat	TSP e PM ₁₀	A		Boa Sorte	TSP e PM ₁₀	A				
	Brisamar	PM ₁₀	S		Sesi	TSP e PM ₁₀	A				
Itaguaí	Sítio Terezinha	PM ₁₀	S		UERJ	TSP	S				
	Vila Aparecida	PM ₁₀	S	Resende	Casa da Lua	TSP e PM ₁₀	A				
	Vila Califórnia	PM ₁₀	S		Cidade Alegria	TSP e PM ₁₀	A				
	Auto do Jacú	TSP e PM ₁₀	S	Itatiaia	Campoo Alegre	TSP e PM ₁₀	A				
	Fazendo do Macuco	TSP e PM ₁₀	S	Porto real	Porto Real	PM ₁₀	A				
	Itambi	PM ₁₀	S	Quatis	Bom Retiro	PM ₁₀	A				
Itaboraí	Sambaetiba	PM ₁₀	A								
	Porto das Caixas	PM ₁₀	A								
	Ilha do Governador	PM ₁₀	A								
	Ilha de Paquetá	PM ₁₀	A								
Japeri	Engenheiro Pedreira	PM ₁₀	A								
	São Cristóvão	TSP	S								
	Castelo	TSP e PM ₁₀	S								
	Realengo	TSP	S								
	Benfica	TSP	S								
Rio de Janeiro	Santa Tereza	TSP	S								
	Sumaré	TSP e PM ₁₀	S								
	Botafogo	PM ₁₀	S								
	Bonsucesso	PM ₁₀	S								
	Maracanã	PM ₁₀	S								

	Cidade de Deus	PM ₁₀	S
	Taquara	PM ₁₀	A
	Laboratório INEA	PM ₁₀	A
	INSS	PM ₁₀	S
	CaPMos Eliseos	PM ₁₀	A
Duque de Caxias	Pilar	PM ₁₀	A
	Jardim Primavera	PM ₁₀	A
	São Bento	PM ₁₀	A
	Vila São Luiz	PM ₁₀	A

Table 17.2 TSP concentrations obtained by the monitoring network of the state of Rio de Janeiro (INEA) between 2000 and 2012. Data available in the first diagnosis of the air quality monitoring network in Brazil

Local	2000	2001	2002	2003	2004	2005	2006	2007	2008	2009	2010	2011	2012
Belford Roxo	188	-	-	-	-	164	161	-	-	-	-	208	-
São Gonçalo	-	-	185	158	-	143	-	-	-	-	-	-	138
Rio de Janeiro	61	94	87	80	55	90	95	89	-	63	-	208	77
Santa Cruz	-	-	-	-	-	-	-	-	74	45	48	63	61
Itaboraí	-	-	-	-	-	-	-	-	-	-	-	30	34
Guapimirim	-	-	-	-	-	-	-	-	-	-	35	40	32
Itaguaí	-	-	-	-	-	-	-	-	-	43	42	41	-
Volta Redonda	58	46	49	45	42	39	49	54	47	51	60	64	58
Barra Mansa	-	-	-	-	-	63	59	65	54	54	73	55	58
Resende	-	-	-	-	-	-	-	-	-	-	44	-	48
Itatiaia	-	-	-	-	-	-	-	-	-	-	39	51	-
Campos dos Goytacazes	-	-	-	-	-	-	-	-	-	-	-	83	86
São João da Barra	-	-	-	-	-	-	-	-	-	-	32	-	-
Macaé	-	-	-	-	-	-	-	-	-	-	27	35	-

Bold values correspond to only one station

Table 17.3 PM₁₀ concentrations obtained by the monitoring network of the state of Rio de Janeiro (INEA) between 2000 and 2012. Data available in the 1st Diagnosis of the air quality monitoring network in Brazil

Local	2000	2001	2002	2003	2004	2005	2006	2007	2008	2009	2010	2011	2012
São Joao de Meriti	110	-	112	9	93	78	90	-	-	-	-	-	-
São Gonçalo	-	-	79	70	41	79	-	-	-	76	-	74	85
Seropédica	34	-	-	34	30	29	-	-	-	-	34	34	31
Guapimirim	-	-	-	-	-	-	-	-	-	-	23	22	16
Nilópolis	73	72	-	64	56	53	-	-	-	-	-	60	56
Niterói	-	-	96	88	82	87	-	-	-	-	-	91	-
Nova Iguaçu	127	121	56	115	70	63	-	-	-	84	43	-	89
Santa Cruz	-	-	-	-	-	-	-	-	36	31	33	39	36
Itaguaí	-	46	45	44	-	-	42	43	30	34	35	32	30
Duque de Caxias	109	-	-	-	50	46	40	42	39	46	41	44	53
Itaboraí	-	-	-	-	-	-	-	-	-	-	46	41	39
Japeri	-	-	-	-	-	-	-	-	-	-	-	-	31
Rio de Janeiro	56	32	58	51	42	47	63	28	72	49	60	57	70
Volta Redonda	-	34	35	34	28	28	37	45	32	30	33	36	31
Barra Mansa	-	-	-	-	-	-	46	44	40	34	41	36	-
Resende	-	-	-	-	-	-	-	-	-	-	27	43	33
Itatiaia	-	-	-	-	-	-	-	-	-	-	30	38	33
Porto Real	38	40	-	-	-	-	-	-	-	24	30	33	-
Quatis	31	-	-	31	-	-	-	-	-	20	22	25	26
São Joao da Barra	-	-	-	-	-	-	-	-	-	-	22	-	-
Macaé	-	-	-	-	-	-	-	-	-	-	-	18	20

Bold values correspond to only one statio

18 Supplementary Material – 2

This material refers to paper described in Chapter 5.

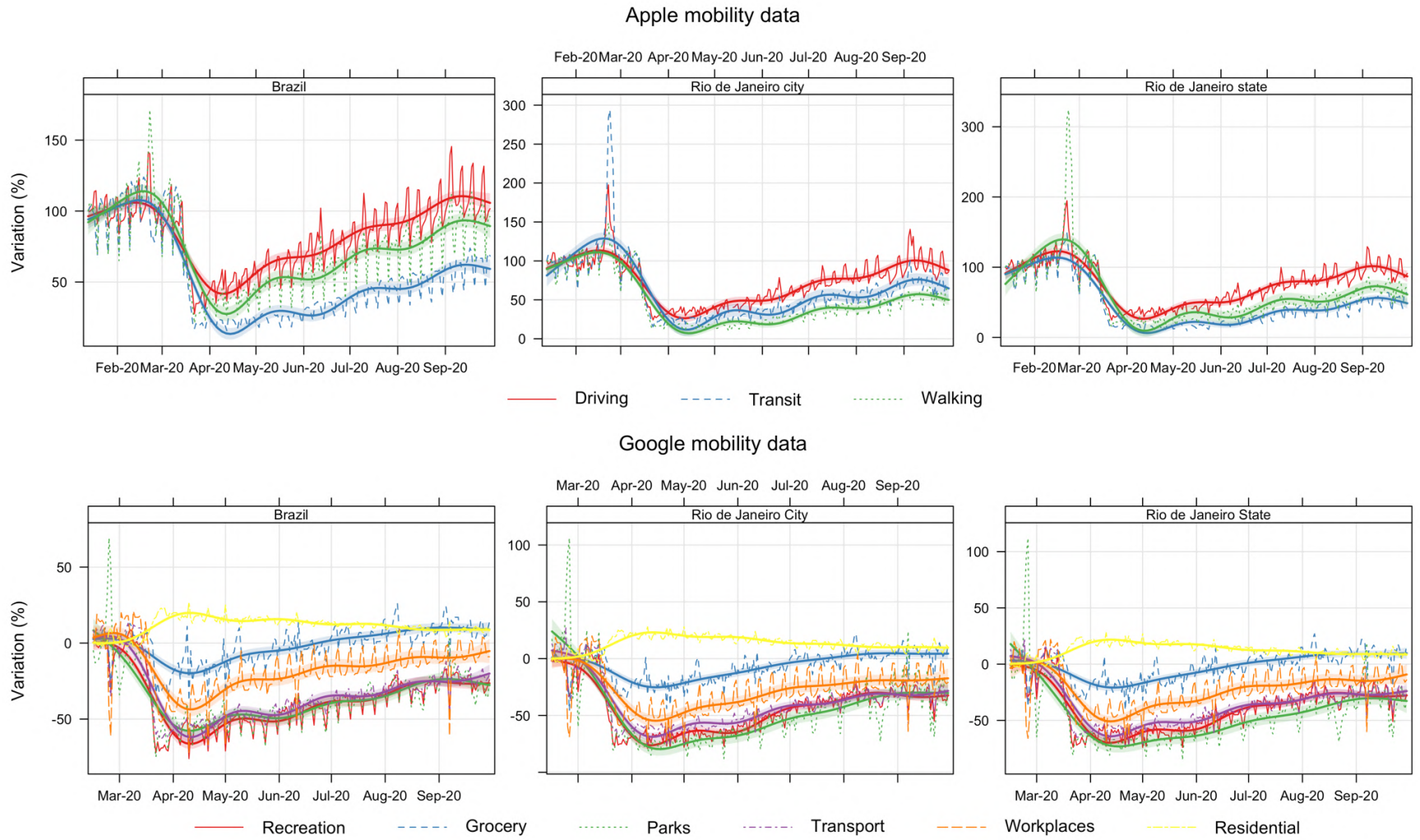


Figure 18.1 Mobility variability measured by Apple and Google from March,2020 to September,2020

Table 18.1 Descriptive statistic (Mean \pm standard deviation and largest and smallest value of meteorological data obtained for five monitoring station in 2019 and 2020.

Site	Rainfall (mm)	Pression (mbar)	Solar Radiation ($W m^{-2}$)	Temperature ($^{\circ}C$)	Relative Humidity (%)	Wind Speed ($m s^{-1}$)
2019						
Bangu	0.07 \pm 0.59 (0 – 22)	1012 \pm 5 (999 – 1027)	155 \pm 235 (0 – 931)	25.0 \pm 4.6 (15.3 – 42.8)	79.9 \pm 21.2 (18.1 – 99.8)	1.7 \pm 1.1 (0.25 – 9.02)
Campo Grande	0.13 \pm 1.03 (0 – 29)	1016 \pm 5 (1002 – 1031)	126 \pm 198 (0 – 826)	26.5 \pm 4.7 (15.8 – 43.4)	77.7 \pm 21.7 (17.2 – 99.3)	1.5 \pm 0.9 (0.2 – 6.8)
Centro	0.13 \pm 1.24 (0 – 65)	1017 \pm 5 (1004 – 1032)	91 \pm 156 (0 – 666)	25.7 \pm 4.0 (16.4 – 40.9)	75.7 \pm 15.9 (23.1 – 99.9)	0.8 \pm 0.44 (0.13 – 3.2)
Copacabana	0.20 \pm 1.69 (0 – 47)	1017 \pm 5 (1005 – 1032)	75 \pm 139 (0 – 784)	-	87.6 \pm 3.6 (82.5 – 93.9)	0.7 \pm 0.32 (0.1 – 3.3)
Tijuca	0.18 \pm 1.3 (0 – 31)	1021 \pm 5 (1008 – 1036)	112 \pm 201 (0 – 910)	22.7 \pm 5.0 (12.4 – 40.6)	65.6 \pm 19.0 (12.8 – 98.7)	0.6 \pm 0.41 (0.1 – 5.8)
2020						
Bangu	0.12 \pm 1.15 (0 – 55)	1016 \pm 4 (979 – 1028)	155 \pm 233 (0 – 1010)	25.8 \pm 4.4 (15.0 – 42.3)	73.6 \pm 23.8 (15.3 – 99.8)	1.7 \pm 1.0 (0.1 – 6.8)
Campo Grande	0.08 \pm 0.67 (0 – 19)	1015 \pm 4 (924 – 1027)	136 \pm 203 (0 – 878)	26.3 \pm 4.3 (15.9 – 42.4)	74.4 \pm 22.6 (14.7 – 98.4)	1.4 \pm 0.9 (0.2 – 5.6)
Centro	0.07 \pm 0.54 (0 – 15)	1016 \pm 5 (924 – 1028)	133 \pm 212 (0 – 840)	25.4 \pm 4.1 (16.5 – 41.0)	73.0 \pm 20.6 (14.7 \pm 99.8)	0.65 \pm 0.4 (0 – 3.5)
Copacabana	0.10 \pm 0.77 (0 – 23.2)	1018 \pm 4 (1005 – 1029)	42.2 \pm 81 (0 – 659)	23.7 \pm 3.5 (14.0 – 40.9)	80.55 \pm 15.3 (25.4 – 99.6)	0.7 \pm 0.4 (0.2 – 4.5)
Tijuca	0.99 \pm 15 (0 – 426)	1020 \pm 5 (1005 \pm 1032)	76.8 \pm 151 (0 – 776)	22.4 \pm 4.9 (12.3 – 41.7)	69.7 \pm 19.1 (18.3 – 99.6)	2.8 \pm 6.4 (0.1 – 25)

Table 18.2 CO monthly average concentration \pm standard deviation (ppm) and data range obtained for all monitoring station between March and September of 2019 and 2020.

Monitoring station	2019							
	March	April	May	June	July	August	September	Mar - Sept
Bangu	0.48 \pm 0.17 (0.01 - 0.95)	0.44 \pm 0.15 (0.09 - 1.85)	(0.14 - 1.87)	0.47 \pm 0.29 (0.05 - 1.59)	0.52 \pm 0.29 (- - -)	0.39 \pm 0.25 (0.14 - 1.41)	0.53 \pm 0.17 (0.22 - 1.43)	0.47 \pm 0.22 (0.01 - 1.87)
Campo Grande	0.27 \pm 0.12 (0.00 - 0.00)	(0.02 - 0.61)	0.52 \pm 0.28 (0.01 - 1.55)	0.29 \pm 0.29 (0.01 - 1.44)	0.23 \pm 0.26 (0.03 - 1.46)	0.17 \pm 0.17 (0.08 - 0.51)	0.42 \pm 0.23 (0.07 - 1.99)	0.32 \pm 0.22 (0.01 - 1.99)
Centro	0.34 \pm 0.16 (0.01 - 1.20)	0.20 \pm 0.16 (0.03 - 2.17)	0.36 \pm 0.20 (0.01 - 1.71)	0.33 \pm 0.21 (0.01 - 1.92)	0.38 \pm 0.26 (0.05 - 1.51)	0.35 \pm 0.26 (0.03 - 1.09)	0.37 \pm 0.25 (0.06 - 2.41)	0.33 \pm 0.22 (0.01 - 2.41)
Copacabana	0.09 \pm 0.10 (0.01 - 0.62)	0.08 \pm 0.09 (0.01 - 1.33)	0.10 \pm 0.11 (0.01 - 0.93)	0.09 \pm 0.09 (0.01 - 0.70)	0.08 \pm 0.12 (0.01 - 0.67)	0.07 \pm 0.10 (0.01 - 0.72)	0.07 \pm 0.11 (0.01 - 0.86)	0.08 \pm 0.10 (0.01 - 1.33)
Tijuca	0.42 \pm 0.15 (0.01 - 1.54)	0.31 \pm 0.22 (0.01 - 1.20)	0.57 \pm 0.41 (0.03 - 1.58)	0.46 \pm 0.20 (0.09 - 1.23)	0.43 \pm 0.24 (0.01 - 6.19)	0.37 \pm 0.19 (0.08 - 1.00)	0.42 \pm 0.21 (0.07 - 1.28)	0.43 \pm 0.23 (0.01 - 6.19)
	2020							
	March	April	May	June	July	August	September	Mar - Sept
Bangu	0.37 \pm 0.15 (0.07 - 0.94)	0.29 \pm 0.10 (0.01 - 0.97)	0.30 \pm 0.14 (0.01 - 1.66)	0.36 \pm 0.26 (0.01 - 1.53)	0.23 \pm 0.22 (0.01 - 1.11)	0.22 \pm 0.18 (0.05 - 1.06)	0.21 \pm 0.17 (0.01 - 0.77)	0.28 \pm 0.17 (0.01 - 1.66)
Campo Grande	0.16 \pm 0.10 (0.01 - 0.83)	0.20 \pm 0.14 (0.02 - 0.98)	0.26 \pm 0.24 (0.01 - 1.58)	0.35 \pm 0.31 (0.01 - 1.67)	0.30 \pm 0.31 (0.01 - 1.69)	0.40 \pm 0.28 (0.01 - 0.56)	0.54 \pm 0.19 (0.24 - 1.47)	0.32 \pm 0.22 (0.01 - 1.69)
Centro	0.22 \pm 0.15 (0.03 - 0.67)	0.19 \pm 0.09 (0.02 - 1.01)	0.21 \pm 0.14 (0.04 - 1.11)	0.36 \pm 0.25 (0.01 - 1.56)	0.31 \pm 0.17 (0.01 - 0.99)	0.30 \pm 0.16 (0.01 - 0.65)	0.36 \pm 0.16 (0.14 - 1.46)	0.28 \pm 0.16 (0.01 - 1.56)
Copacabana	0.04 \pm 0.06 (0.01 - 0.29)	0.03 \pm 0.04 (0.01 - 0.34)	0.03 \pm 0.04 (0.01 - 0.66)	0.06 \pm 0.07 (0.01 - 0.66)	0.05 \pm 0.06 (0.01 - 0.41)	0.04 \pm 0.03 (0.01 - 0.55)	0.05 \pm 0.05 (0.01 - 0.50)	0.04 \pm 0.05 (0.01 - 0.66)
Tijuca	0.27 \pm 0.13 (0.07 - 0.49)	0.21 \pm 0.08 (0.01 - 0.90)	0.24 \pm 0.13 (0.01 - 1.37)	0.34 \pm 0.19 (0.01 - 1.51)	0.31 \pm 0.17 (0.01 - 0.82)	0.29 \pm 0.14 (0.05 - 0.77)	0.36 \pm 0.16 (0.02 - 1.06)	0.29 \pm 0.14 (0.01 - 1.51)

Table 18.3. O₃ monthly average concentration \pm standard deviation ($\mu\text{g m}^{-3}$) and data range obtained for all monitoring station between March and September of 2019 and 2020.

Monitoring station	2019							
	March	April	May	June	July	August	September	Mar - Sept
Bangu	42 \pm 29	45 \pm 36	44 \pm 32	45 \pm 31	45 \pm 32	42 \pm 32	46 \pm 34	44 \pm 32
	(1 - 231)	(0 - 131)	(0 - 159)	(4 - 129)	(3 - 159)	(3 - 117)	(0 - 198)	(0 - 231)
Campo Grande	27 \pm 26	29 \pm 27	27 \pm 25	27 \pm 25	36 \pm 30	35 \pm 27	45 \pm 29	32 \pm 27
	(0 - 129)	(3 - 152)	(3 - 157)	(3 - 125)	(0 - 129)	(0 - 142)	(3 - 147)	(0 - 157)
Centro	31 \pm 31	36 \pm 34	26 \pm 25	22 \pm 21	27 \pm 27	28 \pm 25	33 \pm 25	29 \pm 27
	(1 - 172)	(0 - 167)	(2 - 185)	(0 - 111)	(1 - 175)	(1 - 201)	(0 - 156)	(0 - 201)
Copacabana	20 \pm 15	23 \pm 16	23 \pm 17	20 \pm 14	27 \pm 19	24 \pm 14	24 \pm 13	23 \pm 16
	(3 - 113)	(3 - 88)	(3 - 125)	(3 - 89)	(3 - 134)	(3 - 120)	(3 - 73)	(3 - 134)
Tijuca	31 \pm 25	30 \pm 23	27 \pm 21	26 \pm 21	30 \pm 21	27 \pm 21	25 \pm 17	28 \pm 21
	(1 - 164)	(0 - 150)	(1 - 139)	(1 - 174)	(1 - 153)	(2 - 188)	(1 - 92)	(0 - 188)
2020								
	March	April	May	June	July	August	September	Mar - Sept
Bangu	40 \pm 26	42 \pm 25	39 \pm 25	35 \pm 24	40 \pm 27	43 \pm 29	63 \pm 35	43 \pm 27
	(3 - 129)	(1 - 134)	(0 - 138)	(0 - 133)	(2 - 119)	(0 - 133)	(2 - 221)	(0 - 221)
Campo Grande	32 \pm 25	36 \pm 25	36 \pm 27	36 \pm 29	36 \pm 27	41 \pm 33	58 \pm 36	39 \pm 29
	(3 - 131)	(0 - 145)	(1 - 150)	(2 - 138)	(2 - 146)	(3 - 122)	(1 - 241)	(0 - 241)
Centro	40 \pm 26	46 \pm 27	48 \pm 39	35 \pm 28	35 \pm 24	36 \pm 23	49 \pm 26	41 \pm 27
	(2 - 131)	(1 - 114)	(1 - 133)	(1 - 183)	(0 - 288)	(1 - 178)	(2 - 164)	(0 - 288)
Copacabana	23 \pm 14	38 \pm 18	40 \pm 24	39 \pm 25	35 \pm 16	31 \pm 17	30 \pm 16	33 \pm 19
	(3 - 112)	(3 - 153)	(4 - 115)	(3 - 229)	(3 - 171)	(3 - 103)	(4 - 116)	(3 - 229)
Tijuca	27 \pm 17	27 \pm 14	31 \pm 20	36 \pm 25	35 \pm 20	34 \pm 19	50 \pm 27	34 \pm 20
	(0 - 74)	(0 - 103)	(0 - 116)	(0 - 167)	(0 - 117)	(1 - 130)	(2 - 170)	(0 - 170)

Table 18.4 PM₁₀ monthly average concentration ± standard deviation (µg m⁻³) and data range obtained for all monitoring station between March and September of 2019 and 2020.

Monitoring station	2019							
	March	April	May	June	July	August	September	Mar - Sept
Bangu	27 ± 13	31 ± 17	41 ± 22	45 ± 21	44 ± 24	47 ± 35	56 ± 35	42 ± 24
	(2 - 125)	(2 - 272)	(4 - 149)	(3 - 133)	(3 - 154)	(1 - 108)	(7 - 217)	(1 - 272)
Campo Grande	22 ± 11	25 ± 13	37 ± 20	43 ± 22	47 ± 29	36 ± 22	32 ± 19	35 ± 19
	(2 - 81)	(2 - 145)	(5 - 180)	(9 - 163)	(4 - 112)	(1 - 104)	(2 - 162)	(1 - 180)
Centro	27 ± 12	27 ± 14	29 ± 18	30 ± 14	37 ± 24	33 ± 20	0 ± NA	31 ± 17
	(5 - 89)	(5 - 106)	(5 - 146)	(5 - 92)	(5 - 103)	(5 - 78)	(0 - 0)	(5 - 146)
Copacabana	48 ± 13	55 ± 14	54 ± 18	52 ± 20	56 ± 25	46 ± 20	57 ± 22	53 ± 19
	(26 - 105)	(11 - 171)	(9 - 175)	(4 - 202)	(16 - 138)	(18 - 111)	(21 - 143)	(4 - 202)
Tijuca	25 ± 13	26 ± 12	27 ± 15	27 ± 12	34 ± 20	28 ± 13	38 ± 23	29 ± 16
	(5 - 111)	(5 - 86)	(5 - 148)	(6 - 81)	(5 - 93)	(5 - 214)	(6 - 155)	(5 - 214)
2020								
	March	April	May	June	July	August	September	Mar - Sept
Bangu	34 ± 18	35 ± 14	36 ± 19	53 ± 30	50 ± 27	45 ± 23	51 ± 23	43 ± 22
	(3 - 105)	(6 - 174)	(3 - 175)	(8 - 196)	(1 - 114)	(2 - 141)	(1 - 132)	(1 - 196)
Campo Grande	25 ± 10	26 ± 13	30 ± 18	41 ± 28	37 ± 25	27 ± 16	34 ± 15	31 ± 18
	(3 - 92)	(1 - 91)	(1 - 144)	(1 - 161)	(2 - 117)	(1 - 117)	(1 - 92)	(1 - 161)
Centro	14 ± 10	16 ± 10	23 ± 15	32 ± 20	33 ± 18	26 ± 17	36 ± 16	26 ± 15
	(5 - 69)	(5 - 87)	(6 - 119)	(5 - 98)	(5 - 79)	(5 - 58)	(5 - 93)	(5 - 119)
Copacabana	47 ± 13	54 ± 19	44 ± 15	53 ± 20	49 ± 16	51 ± 19	74 ± 23	53 ± 18
	(7 - 143)	(16 - 124)	(19 - 115)	(13 - 131)	(15 - 172)	(10 - 147)	(23 - 180)	(7 - 180)
Tijuca	18 ± 10	19 ± 10	22 ± 11	31 ± 19	29 ± 16	25 ± 15	41 ± 18	26 ± 14
	(2 - 81)	(5 - 87)	(5 - 103)	(5 - 122)	(5 - 74)	(5 - 63)	(5 - 105)	(2 - 122)

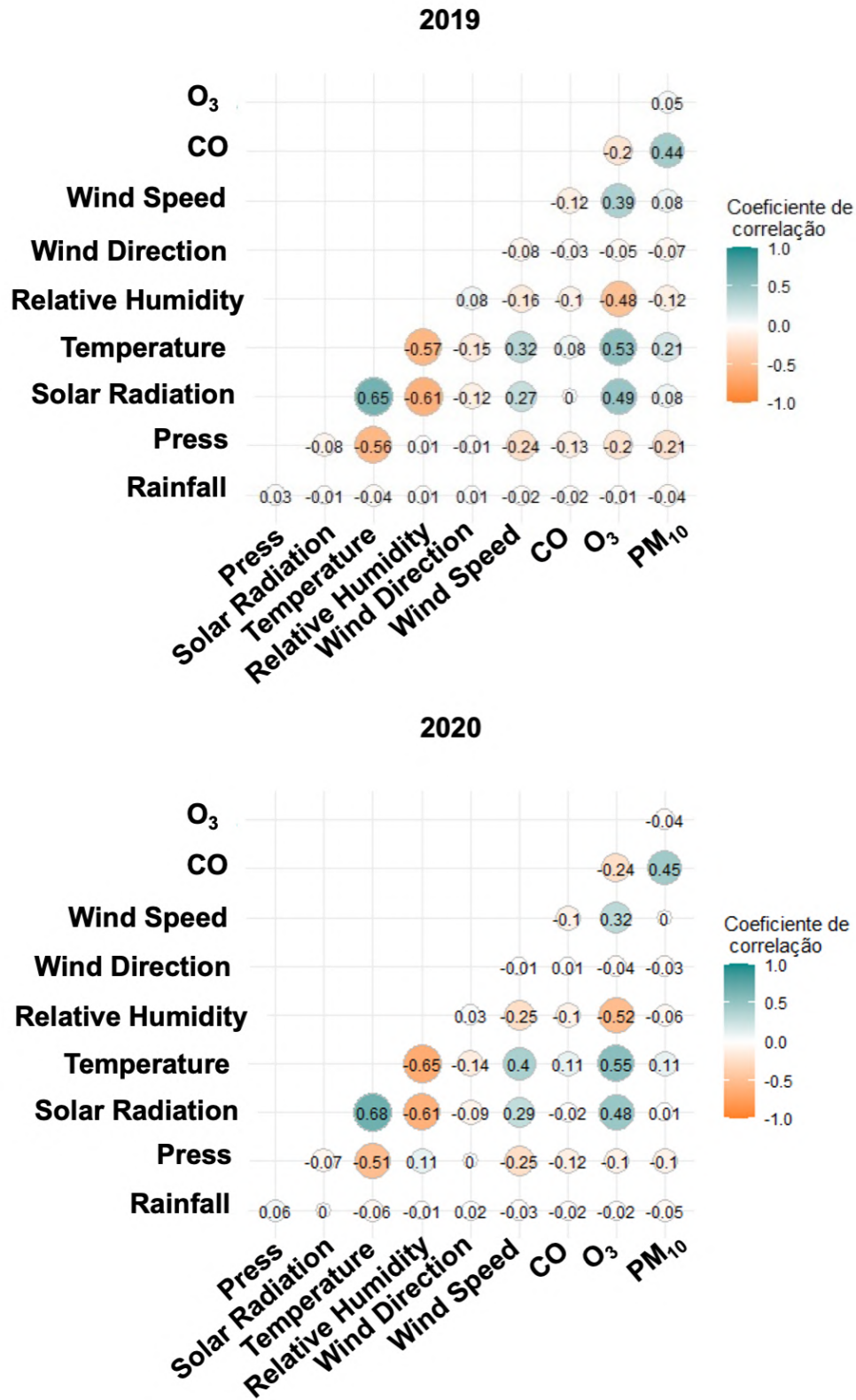


Figure 18.2 Spearman correlation between pollutants and meteorological parameter recorded from March to September, 2019 and 2020

19 Supplementary Material – 3

This material refers to paper described in Chapter 6.

PUC-Rio - Certificação Digital N° 1912855/CA



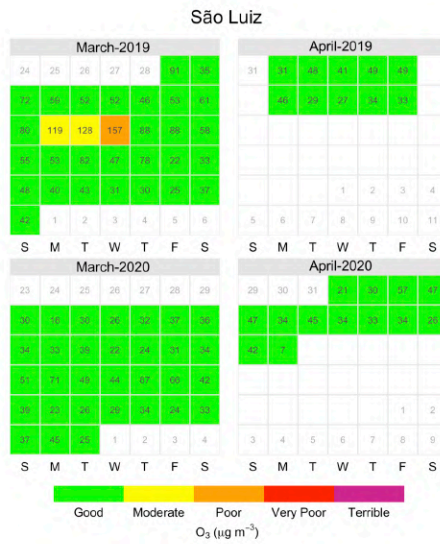
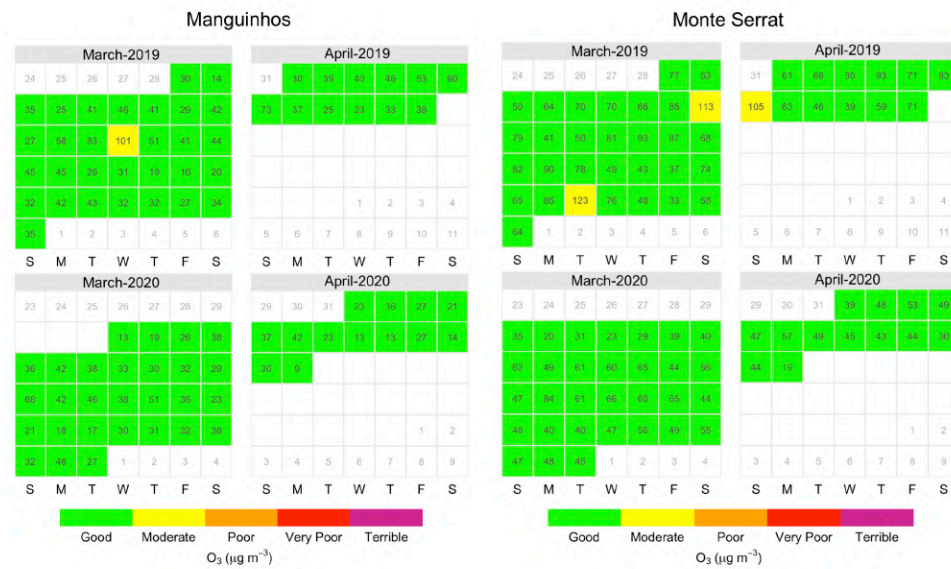


Figure 19.2 Concentrations and AQI classes comparison regarding O₃ daily average in Manguinhos, Monte Serrat and São Luiz for March and April of 2019 and 2020

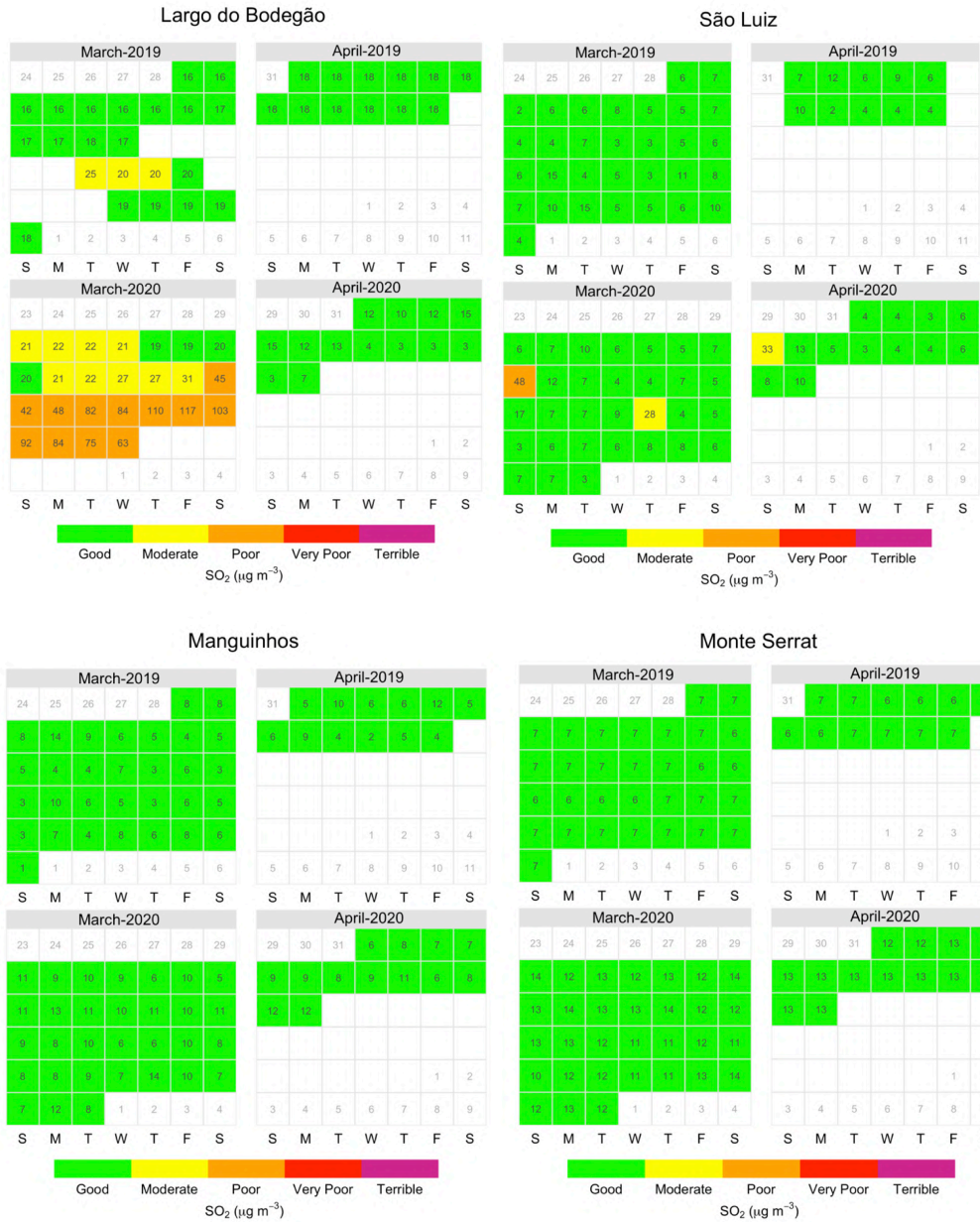


Figure 19.3 Concentrations and AQI classes comparison regarding SO₂ daily average in Manguinhos and Monte Serrat for March and April of 2019 and 2020

Table 19.1 Weekly average of meteorological parameters and Mann Withney results. Considering one site, values at each column with the same letter do not differ statistically ($p < 0.05$)

Variable	WS ($m s^{-1}$)	T ($^{\circ}C$)	SR ($W m^{-2}$)	RH (%)	AP (mbar)
Manguinhos					
Week 1	1.03 (e)	26.2 (c)	166.4 (abc)	93.1 (e)	1000.0 (b)
Week 2	0.67 (bc)	28.2 (d)	294.6 (abc)	86.8 (a)	1000.8 (a)
Week 3	0.72 (bd)	23.0 (a)	204.3 (abc)	85.0 (ab)	996.8 (c)
Week 4	0.73 (cd)	26.0 (c)	257.7 (abc)	87.6 (abc)	1002.1 (d)
Week 5	0.49 (a)	21.7 (b)	210.2 (abc)	87.1 (acd)	998.4 (e)
Week 6	0.70 (a)	23.9 (ab)	124.3 (a)	89.7 (cd)	1001.0 (a)
Vila São Luis					
Week 1	1.72 (a)	24.7 (a)	173.8 (ab)	76.3 (d)	1014.9 (a)
Week 2	2.29 (d)	27.7 (b)	275.5 (ab)	66.8 (a)	1015.9 (b)
Week 3	1.92 (b)	28.7 (c)	194.7 (ab)	68.6 (ab)	1011.9 (c)
Week 4	1.89 (abc)	25.6 (d)	246.2 (ab)	68.1 (abc)	1017.0 (d)
Week 5	2.10 (bc)	27.6 (e)	198.3 (ab)	68.0 (ac)	1013.0 (e)
Week 6	1.54 (a)	24.2 (a)	116.1 (b)	73.6 (e)	1015.3 (f)
Monte Serrat					
Week 1	0.70 (a)	23.9 (ab)			
Week 2	0.85 (b)	26.5 (c)			
Week 3	0.92 (bc)	27.2 (d)	no data	no data	no data
Week 4	0.71 (a)	24.4 (a)			
Week 5	0.84 (c)	26.1 (c)			
Week 6	0.68 (a)	23.3 (b)			
Largo do Bodegão					
Week 1	0.10 (c)	32.6 (a)			
Week 2	0.09 (a)	34.2 (b)			
Week 3	0.09 (a)	35.1 (c)	no data	no data	no data
Week 4	0.35 (d)	32.5 (a)			
Week 5	0.83 (b)	33.8 (b)			
Week 6	0.73 (b)	31.7 (d)			

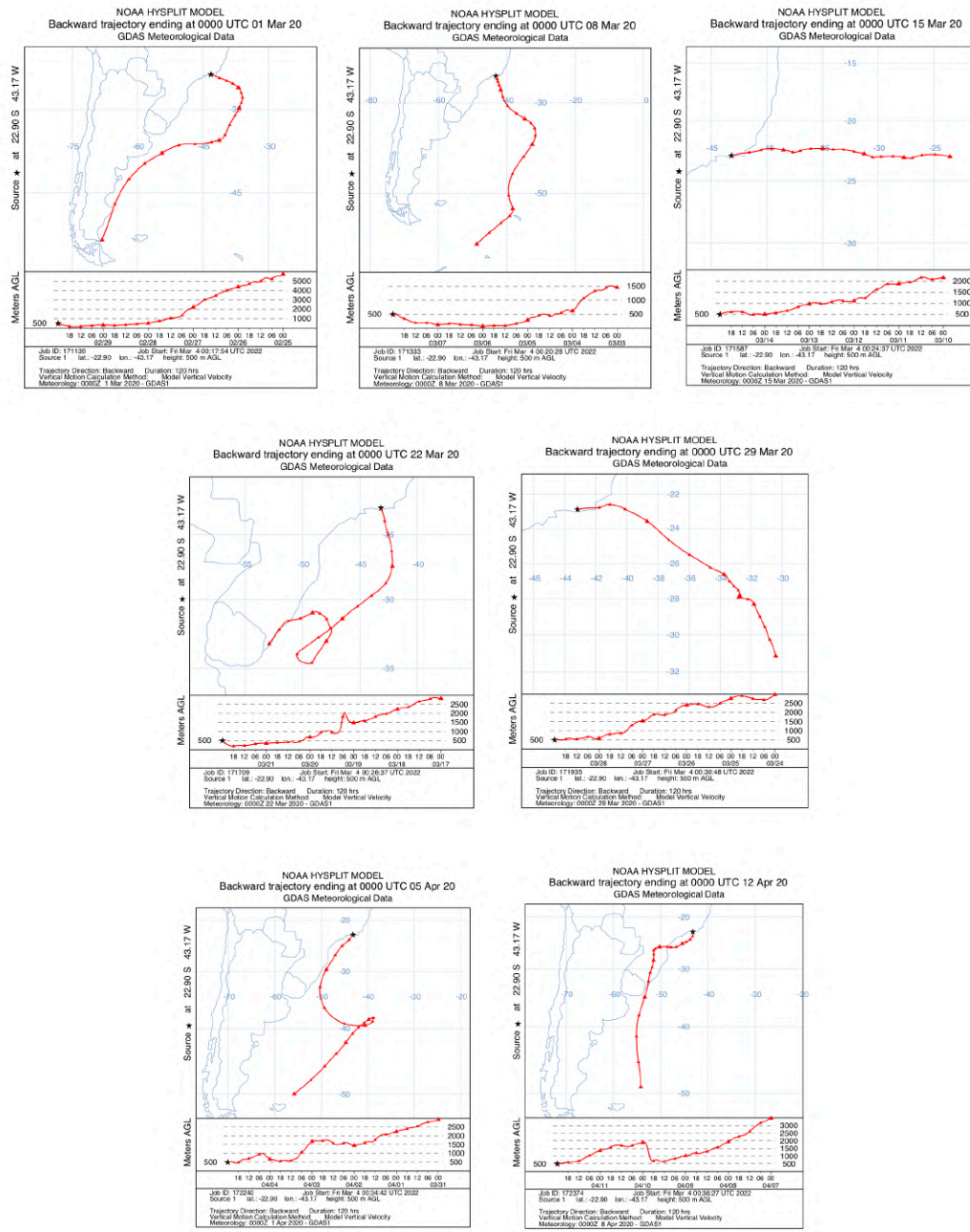


Figure 19.6 Backward trajectories calculated by Hysplit Model for the period between March 1st and April 12nd